Regulation of peripheral node addressin biosynthesis and tertiary lymphoid structures in tumors

Anthony Burt Rodriguez
New York, New York

B.S., Adelphi University, Garden City, New York, 2009
M.A., City University of New York Hunter College, New York, 2014
M.S., University of Virginia School of Medicine, Virginia, 2016

A Dissertation presented to the Graduate Faculty of the University of Virginia School of Medicine in Candidacy for the Degree of Doctor of Philosophy

Department of Microbiology, Immunology, and Cancer Biology

University of Virginia School of Medicine
August 2021

Abstract

Tumor-associated tertiary lymphoid structures (TA-TLS) are ectopic lymphoid aggregates that have considerable morphological, cellular, and molecular similarity to secondary lymphoid organs, particularly lymph nodes. Tumor vessels expressing peripheral node addressin (PNAd) are hallmark features of TA-TLS, and previously work from the lab demonstrated that development of this vasculature in murine melanoma depends on tumor necrosis factor receptor (TNFR) signaling. However, the scaffolding proteins and biosynthetic enzymes driving the biosynthesis of PNAd in tumor endothelial cells (TEC) are unknown. Also, it is unknown which of these PNAd associated components are regulated by TNFR signaling. Chapter 1 of this thesis demonstrates that scaffolding proteins and biosynthetic enzymes driving PNAd biosynthesis in lymph node high endothelial venules are expressed in TECs displaying PNAd. On the tumor vasculature, PNAd is displayed at low levels and this was associated with reduced expression of some PNAd components in TECs, including GST2, which is an important sulfotransferase for PNAd synthesis in lymph node high endothelial venules. Also, loss of PNAd on TECs in the absence of TNFR signaling is associated with reduced expression of scaffolding proteins podocalyxin and nepmucin, and sulfotransferase GST1. Lastly, checkpoint immunotherapy augments both the fraction of TECs expressing PNAd and their surface level of this ligand.

TA-TLS are found in a variety of primary and metastatic human tumors, where they are usually associated with enhanced survival and a favorable response to cancer therapies.

In mice, tumors growing in the peritoneal cavity, lungs, and liver, but not those growing subcutaneously, develop TA-TLS in juxtaposition to vessels expressing PNAd. However, the cellular and molecular mediators governing TA-TLS development were unknown. Chapter 2 of this thesis demonstrates that a discrete population of cancer-associated fibroblasts (CAF) that express high levels of B-cell chemokine CXCL13, and B-cell survival factors BAFF and APRIL orchestrate TA-TLS formation in murine melanoma. These lymphoid tissue organizer molecules in CAFs are induced by TNFR signaling mediated by an unknown cell that is neither an adaptive nor innate immune lymphoid cell. CAFs form reticular networks that are co-extensive with B- and T-cell aggregates of TA-TLS. Initial organization of CAFs into these structures is mediated by CD8 T-cells, while robust CAF accumulation and the expansion of TA-TLS-associated reticular networks depends on CXCL13-mediated recruitment of B-cells expressing lymphotoxin-$\alpha_1\beta_2$. Some of these cellular and molecular elements are also evident in TA-TLS associated with human melanoma. Lastly, immunotherapy induces more and larger TA-TLS that are more often organized with discrete T- and B-cell zones, and TA-TLS presence, number, and size are correlated with reduced tumor size and overall response to checkpoint immunotherapy. This work provides a platform for the development of novel strategies that manipulate PNAd expression on tumor vasculature and the formation of TA-TLS as a form of cancer immunotherapy.

Table of contents

List of models

List of tables

List of figures

Abbreviations

αSMA	α-smooth muscle actin
APRIL	A proliferation-inducing ligand
B3GNT3	Beta-1,3-*N*-acetylglucosaminyltransferase-3
B4GALT	Beta-1,4-galactosyltransferase
BAFF	B-cell activating factor
BCMA	B-cell maturation antigen
BEC	Blood endothelial cell
Breg	Regulatory B-cells
C1GALT1	glycoprotein-*N*-acetylgalactosamine 3-beta-galactosyltransferase-1
CAF	Cancer-associated fibroblasts
CD (i.e. CD8)	Cluster of differentiation
Col Type I	Collagen Type I
CTLA4	Cytotoxic T-lymphocyte-associated protein 4
DC	Dendritic cell
DNA-PK	DNA-dependent protein kinase
DTR	Diphtheria toxin receptor
FALC	Fat-associated lymphoid clusters
FAP	Fibroblasts activation protein
FDC	Follicular dendritic cell
FDR	False discovery rate

FMO	Fluorescence minus one
FRC	Fibroblastic reticular cell
FUT	Alpha-(1,3)-fucosyltransferase
Gal	Galactose
GalNAc	*N*-acetylgalactosamine
GALNT1	Polypeptide *N*-acetylgalactosaminyltransferase 1
GCNT1	Core 2 Beta1,6 *N*-Acetylglucosaminyltransferase 1
GlcNAc	*N*-acetylglucosamine
gMFI	Geometric mean fluorescence intensity
GST	*N*-acetylglucosamine 6-O-sulfotransferase
HER2	Human epidermal growth factor receptor 2
HEV	High endothelial venule
HR	Homing receptor
ICAM-1	Intracellular adhesion molecule-1
IF	Immunofluorescence
IFNγ	Interferon-γ
IFNγR1	Interferon gamma receptor 1
Ig (i.e., IgM)	Immunoglobulin
IHC	Immunohistochemistry
IL (i.e., IL-36)	Interleukin
Il2rg	Interleukin 2 receptor gamma
ILC	Innate lymphoid cells

Interferon alpha receptor	IFNAR
IP	Intraperitoneal
IQR	Interquartile range
LAG-3	Lymphocyte-activation gene 3
LAMP	Lysosome-associated membrane glycoprotein
LN	Lymph node
LTα	Lymphotoxin-α
LTβ	Lymphotoxin-β
$LT\alpha_1\beta_2$	Lymphotoxin-$\alpha_1\beta_2$
LTβR	Lymphotoxin-β receptor
LTi	Lymphoid tissue inducer
LTo	Lymphoid tissue organizer
MDSC	Myeloid-derived suppressor cells
MHC	Major histocompatibility complex
NeuAc	*N*-acetylneuraminic acid
NK	Natural killer
NKT	Natural killer T-cells
NSCLC	Non-small cell lung cancer
OVA	Ovalbumin
PD1	Programmed cell death protein 1
PDGFR	Platelet-derived growth factor receptor
PDL1	Programmed death-ligand 1

PDPN	Podoplanin
PNA	Peanut agglutinin
PNAd	Peripheral node addressin
qPCR	Quantitative reverse transcription polymerase chain reaction
RA	Rheumatoid arthritis
Rag	Recombination activating gene
SC	Subcutaneous
SD	Standard deviation
SLO	Secondary lymphoid organ
ST3GAL	CMP-N-acetylneuraminate-beta-galactosamide-alpha-2,3-sialyltransferase
TA-TLS	Tumor-associated tertiary lymphoid structures
TCR	T-cell receptor
TEC	Tumor endothelial cell
T_{FH}	Follicular helper T-cell
TGFβ	Transforming growth factor-β
T_H (i.e., T_H17)	T helper type cell
TIL	Tumor infiltrating lymphocytes
TIM-3	T-cell immunoglobulin and mucin domain-3
TLS	Tertiary lymphoid structures
TNFα	Tumor necrosis factor-α
TNFR	Tumor necrosis factor receptor
TNFR-related apoptosis-inducing ligand	TRAIL

Treg	Regulatory T-cell
UBS	Human ubiquitin C
USPHS	United States Public Health Service
UVA	University of Virginia
VCAM-1	Vascular cell adhesion molecule-1
WT	Wild type

Acknowledgements

This dissertation is dedicated to the family, friends, and colleagues who have supported and encouraged me, both before and throughout graduate school. First, sincere gratitude goes to the late Dr. Ralph M. Steinman of the Rockefeller University for providing me with a platform to fuel my scientific curiosity. I met Ralph as a summer undergraduate research intern at Memorial Sloan Kettering Cancer Center, where he took a special interest in me after I bombarded him with questions during one of his lectures. He felt that my scientific curiosity is a defining feature of a prominent scientist, and he believed it was his responsibility to nurture this trait. Unfortunately, I never had the opportunity to thank him for his mentorship nor was I able to congratulate him on winning the Nobel Prize in Medicine. In his honor, I dedicate this cumulative dissertation.

Secondly, I offer my sincere thanks to my current mentor, Dr. Victor H. Engelhard. When I was applying to graduate schools, I was looking for a laboratory where I would have the opportunity to apply my knowledge of immunology to a cancer setting. After learning more about Vic's research, I knew immediately that his laboratory was where I wanted to be as a developing scientist. Vic taught me to approach any problem, in life or in science, logically and to always "*think outside the box*". He encouraged me to pursue my scientific curiosity and to demand the most of myself, which I will strive to do beyond graduate school. My success in my future scientific endeavors will be a direct result of his mentorship. I leave his laboratory with so much gained and a promising future, as an adept cancer immunologist.

I am grateful to my thesis committee, Dr. Melanie Rutkowski, Dr. Timothy Bender, Dr. Loren Erickson, and Dr. Timothy Bullock, for their support and guidance. Most especially, thank you to Dr. Melanie Rutkowski for serving as chair for my committee and providing helpful commentary on this dissertation. My appreciation also goes to Dr. Craig L. Slingluff, Jr. and his laboratory for their significant contributions. I am also grateful to Dr. Kara Cummings for laboratory support, and to the past and current members of the Engelhard laboratory for their insightful advice. Additionally, I thank the faculty, staff, and students of the Beirne B. Carter Center for Immunology Research and the Department of Microbiology, Immunology, and Cancer Biology for their support and encouragement. This work was supported by the United States Public Health Service (USPHS) Grants CA78400 and CA181794, the University of Virginia (UVA) Cancer Center Schiff Foundation Grant, USPHS Immunology Training Grant AI007496, USPHS Cancer Center Support Grant P30 CA44579, and the Robert Wagner Fellowship from the University of Virginia School of Medicine.

This dissertation would not have been possible without the love and support of my family and friends. A special thank you to the following: the Grande family, Wendy, Joseph, and Peter, for their encouragement and for welcoming me into their family; and my mother and father, Maria and David Rodriguez, for always pushing me to better myself despite the limitations that a Latino American faces in this country; my brother, sister, brother in-law, and nephew for picking me up at times when I felt defeated; the many lifelong friends that I have made at UVA and CrossFit Charlottesville; and my longtime

friend Marc Gatchalian for always being a familiar face when I return home. I am indebted to you all, and I hope to continue to make you proud in the future.

Finally, I am sincerely grateful to my love, Elizabeth Marie Grande, and our dog child Oliver. Without the two of you in my life, I strongly believe that I would not have accomplished this great accolade. I greatly appreciate the sacrifices Liz has made for me throughout this journey, and I promise that they will not go disregarded. For your love, support, encouragement, and friendship through the good and bad times, I am eternally grateful. In your honor (and Oliver's), I dedicate myself and this dissertation.

Introduction

The immune system's impact on tumor development

Historically, surgical removal of a patient's tumor was the only treatment option available. However, surgery then involved the removal of tumor tissue and an extensive amount of healthy peripheral tissue. In some cases, a radical type of surgery involving the amputation of a major body part was necessary to prevent the dissemination of a malignant tumor to healthy peripheral tissue and distal organs. For example, in 1894, William Halsted routinely performed radical mastectomies to treat breast cancer (Plesca, Bordea, El Houcheimi, Ichim, & Blidaru, 2016). Although radical surgery was the standard treatment for many tumor types, some patients still developed secondary tumors after the primary mass had been surgically removed. Thus, new therapeutic strategies were needed to overcome the pitfalls associated with surgery and extend patient survival.

In 1725, Antoine Deidier described low tumor incidence and spontaneous remission in patients with chronic syphilis (Deidier, 1725). In 1868, Wilhelm Busch reported a similar observation in patients with erysipelas, a skin infection causes by *Streptococcus pyogenes* (Busch, W., 1868). Similarly, in 1893, William Coley published that cancer patients who contracted erysipelas occasionally showed signs of spontaneous tumor remission (Coley, 1893). Importantly, he showed that the inoculation of patients with live or inactive *Streptococcus pyogenes* and *Serratia marcescens* occasionally led to durable remission of inoperable tumors. Despite this significant finding, the lack of a known mechanism of action for Coley's treatment and the risk of deliberately infecting

cancer patients with pathogenic bacteria caused oncologists to adopt new surgical techniques and radiotherapy as standard treatments for tumors in the early 20th century.

The findings made by William Coley led Paul Ehrlich to hypothesize that immune responses against "Coley's toxin" were inadvertently responsible for tumor remission in these patients (Ehrlich, 1909). He also suggested that the immune system prevented nascent neoplastic cells from developing into tumors. Later, Lewis Thomas and Francis Macfarlane Burnet formalized Paul Ehrlich's theory and proposed the "cancer immunosurveillance hypothesis" (Burnet, 1957; Thomas, 1959). However, this hypothesis was not well received due to inconclusive experimental evidence. For example, early experiments involving thymectomized (G. A. Grant & Miller, 1965; Nishizuka, Nakakuki, & Usui, 1965; Trainin, Linker-Israeli, Small, & Boiato-Chen, 1967; Burstein & Law, 1971; Sanford, Kohn, Daly, & Soo, 1973) and nude mice on a CBA/H background (Stutman, 1974; Rygaard & Povlsen, 1974; Outzen, Custer, Eaton, & Prehn, 1975; Stutman, 1979), both of which contained a reduced number of mature T-cells, demonstrated that the incidence of carcinogen induced and spontaneous tumors in these mice were similar to those with an intact immune system. In contrast, nude mice on a BALB/c background developed more chemically induced tumors than their wild-type (WT) counterparts (Engel et al., 1996). Similar results were obtained with immunodeficient CB-17 severe-combined immunodeficiency (SCID) mice, which lack both mature T- and B-cells (Engel, Svane, Rygaard, & Werdelin, 1997). However, SCID mice lack a DNA-dependent protein kinase (DNA-PK) enzyme that aids antigen receptor gene rearrangement in adaptive immune cells and DNA repair in all other cell types (Featherstone & Jackson, 1999). Thus, it was suggested that SCID mice were

more susceptible to the formation of carcinogen induced tumors due to their inability to repair damaged DNA in transformed cells rather than their immune defects. Collectively, these studies failed to either prove or disprove this idea, leading to the abandonment of the cancer immunosurveillance hypothesis.

The availability of mice deficient for cellular and/or molecular components of the immune system subsequently led to two key findings that resurrected the cancer immunosurveillance concept. First, it was demonstrated that mice deficient for component associated with interferon gamma (IFNγ) signaling developed more carcinogen induced tumors than WT mice (Kaplan et al., 1998). Similar observations were reproduced in subsequent reports (Smyth, Thia, Street, MacGregor, et al., 2000; Street, Cretney, & Smyth, 2001). Second, definitive studies supporting the cancer immunosurveillance hypothesis used mice deficient for recombination activating genes (Rag) 1 or 2. Similar to DNA-PK, these enzymes aid in antigen receptor gene rearrangement in adaptive immune cells. Thus, mice deficient for either of these genes lack mature T- and B-cells (Shinkai et al., 1992). However, unlike DNA-PK, Rag1 and 2 are exclusively expressed in adaptive lymphocytes. Using Rag2 deficient mice, it was demonstrated that these mice develop more carcinogen-induced tumors than WT mice (Shankaran et al., 2001). Interestingly, the same study also showed that chemically induced tumors derived from Rag2 deficient mice were rejected after transplantation onto WT recipient mice. On the other hand, carcinogen-induced WT mouse tumors grew progressively when they were transplanted onto WT mice. This demonstrated that carcinogen induced tumors derived from immunodeficient mice are more immunogenic than those arising in mice with a functional immune system. This

observation formed the basis for the "cancer immunoediting" concept, which is a refinement of "cancer immunosurveillance" hypothesis. Cancer immunoediting is the result of three distinct phases (elimination, equilibrium, and escape) that function either independently or in sequence to control the development of tumors. The cellular and molecular mechanisms involved in each phase have been extensively reviewed elsewhere (Dunn, Old, & Schreiber, 2004; Schreiber, Old, & Smyth, 2011; Vesely, Kershaw, Schreiber, & Smyth, 2011). Collectively, these studies have conclusively demonstrated that the immune system significantly influences tumor development and progression.

Immunological and prognostic significance of intratumoral immune cells

To date, a variety of innate and adaptive immune cells have been shown to be involved in the elimination phase of cancer immunoediting. This includes natural killer T-cells (NKT) (Smyth, Thia, Street, Cretney, et al., 2000), γδ T-cell (M. Girardi et al., 2001), natural killer (NK) cells (Smyth, Crowe, & Godfrey, 2001), αβ (CD4 and CD8) T-cells (Michael Girardi et al., 2003), eosinophils (Simson et al., 2007), and CD1d-restricted T-cells (Swann et al., 2009). In addition to these immune cells, several effector molecules and signaling recognition pathways also contribute to the elimination phase. This includes interferon gamma receptor type 1 (IFNγR1) (Kaplan et al., 1998), perforin (Smyth, Thia, Street, MacGregor, et al., 2000), interleukin (IL)-12 (Smyth, Taniguchi, & Street, 2000), INFγ (Street et al., 2001), TNF-related apoptosis-inducing ligand (TRAIL) (Cretney et al., 2002; Takeda et al., 2002), interferon alpha receptor type 1 and 2 (IFNAR1/2) (Dunn et al., 2005; Swann et al., 2007, 2008), and tumor necrosis factor alpha (TNFα) (Swann et al.,

2008). Thus, the elimination phase of cancer immunoediting is best described as the cooperative efforts of the innate and adaptive immune systems to detect and destroy nascent tumor cells before they become clinically apparent. The mechanisms by which the immune system detects and eliminates nascent tumor cells before they become clinically apparent have been extensively reviewed (Dunn et al., 2004; Schreiber et al., 2011; Vesely et al., 2011).

In contrast to the above, a variety of immunosuppressive cells and molecules have been shown to shown to facilitate immune escape and tumor progression. For example, regulatory T-cells (Treg) (Terabe & Berzofsky, 2004) and myeloid-derived suppressor cells (MDSC) (Gabrilovich & Nagaraj, 2009) promote an immunosuppressive microenvironment that dampen anti-tumor responses. Immunosuppressive cytokines, such as IL-10 (Aruga et al., 1997) and transforming growth factor beta (TGFβ) (Wrzesinski, Wan, & Flavell, 2007), also promote tumor progression by inhibiting effector responses. IL-10 can be produced by Tregs (Terabe & Berzofsky, 2004), whereas TGFβ can be expressed by MDSC (Hequan Li, Han, Guo, Zhang, & Cao, 2009, p. 1) and tumor cells (Wrzesinski et al., 2007). Immune checkpoints, such as programmed cell death protein 1 (PD1) and cytotoxic T-lymphocyte-associated protein 4 (CTLA4), have gained considerable attraction because treatment with monoclonal antibodies against these molecules in tumor-bearing mice led to enhanced tumor control (Leach, Krummel, & Allison, 1996; Iwai, Terawaki, & Honjo, 2005). Also, the administration of humanized monoclonal antibodies against either PD1 (Brahmer et al., 2010) or CTLA4 (Ku et al., 2010) correlated with enhanced patient survival and lower risk of disease relapse.

Importantly, preclinical (Curran, Montalvo, Yagita, & Allison, 2010) and clinical (Larkin et al., 2015) studies concluded that combination therapy with antibodies against PD1 and CTLA4 was more therapeutically advantageous than monotherapy. Since these reports, additional checkpoint molecules are currently being explored as potential immunotherapeutic targets (Pardoll, 2012). Despite these significant findings, only a subset of patients responds to checkpoint immunotherapy, suggesting that additional barriers are present in the tumor microenvironment of unresponsive tumors. Collectively, these findings demonstrate that cancer immunoediting, which includes the elimination and escape phase, is accomplished by a variety of cellular and molecular components of the immune system.

A fundamental question is whether the immune system play a role against tumor development and progression in humans. Two early comprehensive studies concluded that patients with primary genetic immunodeficiencies (Gatti & Good, 1971) and chronically immunosuppressed organ transplant recipients (Penn & Starzl, 1972) were more susceptible to developing malignant tumors than uncompromised immune individuals. These early studies indicate that the elimination phase of cancer immunoediting exists in humans. The presence of tumor-infiltrating lymphocytes (TIL) in human immune escaped tumors is also considered a significant prognostic indicator for patient survival. For example, it was shown that a high density of TILs correlated with longer patient survival and lower risk of disease relapse. This observation was confirmed for a variety of tumor types, including those associated with the nerve (Lauder & Aherne, 1972), prostate (Epstein & Fatti, 1976), brain (Palma, Di Lorenzo, & Guidetti, 1978), colon (Nacopoulou,

Azaris, Papacharalampous, & Davaris, 1981), ovary (Deligdisch, Jacobs, & Cohen, 1982), rectal (Jass, 1986), breast (Rilke et al., 1991), and bladder (Lipponen, Eskelinen, Jauhiainen, Harju, & Terho, 1992). With the use of cell surface markers to distinguish different immune subpopulations, it was initially demonstrated that a high density of intratumoral NK cells expressing CD57 predicted better prognosis (Coca et al., 1997). However, the expression of CD57 is not restricted to NK cells, as it is also expressed by activated T cells. In that regard, subsequent studies in colorectal (Naito et al., 1998), esophageal (Schumacher, Haensch, Roefzaad, & Schlag, 2001), and ovarian (Zhang et al., 2003) tumors showed that a high density of intratumoral CD8 T-cells correlated with enhanced survival. CD4 T-cells have also been implicated in tumor progression and patient survival. For example, these cells can act as helper cells that support the activation and differentiation of CD8 T-cells into effectors that suppress tumor outgrowth (Mandic et al., 2003). In contrast, CD4 T-cells can differentiate into immunosuppressive Tregs and promote tumor outgrowth by preventing that activation of CD8 T-cells (Javia & Rosenberg, 2003). Thus, CD4 T-cells have dichotomous roles in CD8 T-cell activation and tumor progression, which are most likely governed by factors in the tumor microenvironment. Elegant studies in colorectal tumors have also demonstrated that a dense accumulation of intratumoral CD8 T-cells with an activated cytotoxic immune profile correlated strongly with enhanced patient survival and lower risk of metastatic spread (Galon et al., 2006; Pagès et al., 2009). Importantly, the subset of patients who respond favorably to new generation immunotherapies, particularly checkpoint immunotherapy, are those in which an immunological infiltrate is evident prior to treatment (Gajewski, Louahed, & Brichard,

2010; Gajewski, Schreiber, & Fu, 2013; Herbst et al., 2014; Ji et al., 2012; Ulloa-Montoya et al., 2013, p.). These studies demonstrate that the number and activation status of CD8 T-cells are significant components that must be considered when determining prognosis and response to immunotherapy.

The studies above demonstrate that a tumor enriched for CD8 T-cells have a positive prognostic value, whereas those enriched for myeloid cells, such as monocytes, neutrophils, and M2 macrophages, have a negative value (Gentles et al., 2015; Thorsson et al., 2018). Interestingly, the location of CD8 T-cells in relation to the tumor also impacts the prognostic significance of these cells. For example, in colorectal tumors, CD8 T-cells present at both the center of the tumor and at the invasive margins were associated with better clinical outcomes than those present at a single location (Galon et al., 2006; Pagès et al., 2009). Also, CD8 T-cells disseminated throughout the tumor parenchyma of metastatic melanoma have a stronger prognostic value than those confined to the perivascular space surrounding intratumoral blood vessels (Erdag et al., 2012). In contrast, CD8 T-cells that are exclusively found at the tumor invasive margin correlated with worse clinical outcomes and a higher rate of disease reoccurrence. This observation has been confirmed for Hodgkin lymphoma (Scott et al., 2013), clear cell renal carcinoma (Becht et al., 2015; Giraldo et al., 2017), and prostate cancer (Petitprez et al., 2019). On the other hand, immune infiltrates, including CD8 T-cells, that are organized into tumor-associated tertiary lymphoid structures (TA-TLS) also have significant positive prognostic value (Engelhard et al., 2018; Sautès-Fridman, Petitprez, Calderaro, & Fridman, 2019; Anthony B. Rodriguez & Engelhard, 2020). These structures and their immunological impact are

discussed in greater detail below. All of these studies demonstrate that there is remarkable heterogeneity in overall CD8 T-cell representation, activation state, and intratumoral distribution between different tumor types. Thus, the field as a whole must account for this heterogeneity when applying CD8 T-cells for prognostic purposes.

The multifaceted role of B-cells in anti-tumor immunity

It is now appreciated that B-cells represent a major proportion of TILs in many tumor types. However, these cells can either promote or inhibit tumor development and progression. For example, the depletion of B-cells through the humanized monoclonal antibody Rituximab improved the prognosis of patients with advanced colorectal cancer (E. Barbera-Guillem et al., 2000). A preclinical murine study also demonstrated that B-cells produced tumor-specific antibodies that supported tumor outgrowth (Emilio Barbera-Guillem, May, Nyhus, & Nelson, 1999). Mechanistically, tumor-specific antibodies activated granulocytes and macrophages that drove extracellular matrix degradation and angiogenesis in tumors. Consistent with this, the detection of large amounts of tumor specific antibodies in the serum or in the tumor of breast cancer patients correlated with poor clinical outcomes (DeNardo & Coussens, 2007). Similar to Tregs, B-cells can also adopt an immunosuppressive regulatory phenotype (Breg) after they have been activated (B. Peng, Ming, & Yang, 2018). However, the factors that cause the differentiation of B-cells into Bregs are not fully understood yet. Despite this, B-cells have been shown to promote tumor outgrowth by inhibiting cytotoxic CD8 T-cell responses (Shah et al., 2005). It has been suggested that differentiated Bregs do this through their production of immunosuppressive cytokines IL-10 (Horikawa, Minard-Colin, Matsushita, & Tedder, 2011) and TGFβ

(Olkhanud et al., 2011). Thus, B-cells promote tumor growth through a variety of mechanisms. However, the elements that drive pro-tumor characteristics in B-cells remain unknown and should be explored further.

On the other hand, B-cells have been shown to act as supportive elements for anti-tumor immunity. In a transplantable murine model of melanoma, depletion of B-cells led to enhanced subcutaneous tumor outgrowth and a higher density of metastatic lung nodules (DiLillo, Yanaba, & Tedder, 2010). Also, clinical studies involving breast (Simsa, Teillaud, Stott, Tóth, & Kotlan, 2005; Schmidt et al., 2008), lung (Al-Shibli et al., 2008), skin (Ladányi et al., 2011), and ovarian (Nielsen et al., 2012) cancer reported a positive correlation between the density of intratumoral B-cells and patient survival. Multivariate analysis in breast cancer established that the prognostic value of intratumoral B-cells is independent of the number of infiltrating CD8 T-cells (Mahmoud et al., 2011). It has been proposed that B-cells support anti-tumor immunity through their production of either tumor specific antibodies, antigen presentation, or pro-inflammatory cytokines (Guo & Cui, 2019). For example, immunohistochemistry and gene expression studies in breast cancer showed that the expression of plasma cell markers among intratumoral B-cells correlated with enhanced patient survival (Schmidt et al., 2008; Fan et al., 2011; Schmidt et al., 2012). Also, ovarian intratumoral B-cells that are found in close proximity to activated CD8 T-cells often express high levels of markers associated with antigen presentation, such as major histocompatibility complex (MHC) I and II, and T-cell co-stimulatory molecules CD80 and CD86 (Nielsen et al., 2012). *In vitro* studies have also concluded that B-cells directly kill tumor cells via their expression TRAIL (Kemp et al., 2004). Similarly, the

presence of B-cells producing TRAIL, IFNγ, IL-12p40, or granzyme B was a favorable prognostic indicator for patients with hepatocellular carcinoma (Shi et al., 2013). Altogether, these studies show that B-cells either support or inhibit anti-tumor immune responses through a variety of mechanisms. However, they also suggest that tumor microenvironmental factors and anatomical location influence the immunological impact and prognostic value of these cells. Yet the factors that contribute to this functional dichotomy are unknown. Moreover, it is also unknown whether B-cells support anti-tumor immune responses through alternative undescribed mechanisms. Learning more about how these cells are polarized into anti- or pro-tumor elements would provide therapeutic options for modulating anti-tumor immunity.

Anti- and pro-tumor properties of cancer-associated fibroblasts

Fibroblasts found in tumors are termed cancer-associated fibroblasts (CAF). These cells are abundant in the tumor microenvironment. Vimentin, podoplanin (PDPN), α-smooth muscle actin (αSMA), fibroblast activating protein (FAP), platelet-derived growth factor receptor alpha (PDGFRα) and beta (PDGFRβ) are sometimes used to define CAFs because these markers are highly expressed on these cells relative to non-tumor fibroblasts (Kalluri & Zeisberg, 2006). However, since CAFs are an extremely heterogenous population, special consideration must be taken when applying these markers to conclusively identify CAFs. For example, some populations of CAFs express a subset of these markers, making it difficult to identify these cells in tumors. Also, PDPN is found on T_H17 CD4 T-cells (Peters et al., 2015), while FAP is expressed on a minor population of tumor-associated M2 macrophages (Kraman et al., 2010; Arnold, Magiera, Kraman, & Fearon, 2014). Also,

a discrete population of CAFs expressing αSMA and PDGFRβ, but negative for FAP, were identified in breast cancer (Costa et al., 2018). Single-cell RNA sequencing of head and neck (Puram et al., 2017), breast (Bartoschek et al., 2018), and lung (Lambrechts et al., 2018) tumor suspensions revealed the existence of multiple CAF populations that vary in marker expression and functionality. Due to their heterogeneity, additional criteria are often used to define CAFs, such as cellular morphology, tissue positioning, and the lack of epithelial, endothelial, and immune lineage markers. CAF heterogeneity also creates difficulty for determining the origins of these cells. Single-cell RNA sequencing, adoptive transfer of bone marrow-derived mesenchymal stem cells, and lineage tracing mice have been used to shed light on CAF origins. Through these approaches, it was shown that CAFs can originate from multiple sources, including tumor, endothelial, and tissue resident $PDPN^+$ mesothelial cells (LeBleu & Kalluri, 2018; T. Liu et al., 2019). CAFs in human and murine peritoneal carcinomas have been shown to arise from $PDPN^+$ mesothelial cells lining the peritoneal cavity (Rynne-Vidal, Jiménez-Heffernan, Fernández-Chacón, López-Cabrera, & Sandoval, 2015). Also, there is evidence suggesting that CAFs are derived from adipocytes (Bochet et al., 2013), hematopoietic stem cells (L. T. McDonald et al., 2015), tissue-resident fibroblasts (Arina et al., 2016), pericytes (Hosaka et al., 2016), and adipose-derived mesenchymal stem cells (Strong et al., 2017; Huijuan Tang, Chu, Huang, Cai, & Wang, 2020). The distinct tissues in which CAFs arise from may contribute to the vast heterogeneity associated with these cells. Importantly, the tissue origins of CAFs may also contribute to the functionality of these cells and their impact on tumor progression, which is described in more detail below.

CAFs are generally viewed as cells that support tumor growth. Using a mouse model that expresses the diphtheria toxin receptor (DTR) under the control of the FAP promoter, it was demonstrated that the depletion of FAP^+ cells after diphtheria toxin administration led to reduced tumor outgrowth (Kraman et al., 2010). However, as described above, immunosuppressive M2 macrophages express FAP. Using reciprocal bone marrow chimera mice involving WT and FAP-DTR mice, it was demonstrated that the depletion of either FAP^+ hematopoietic or FAP^+ non-hematopoietic cells led to reduced outgrowth of a transplantable murine model of lung carcinoma (Arnold et al., 2014). Although these results confirm an immunosuppressive role for M2 macrophages in this tumor model, they also demonstrate that non-hematopoietic FAP^+ cells, which are likely CAFs, support tumor outgrowth. The depletion of FAP^+ CAFs in an autochthonous murine model of pancreatic ductal adenocarcinoma also led to reduced tumor outgrowth and enhanced response to checkpoint immunotherapy anti-PDL1 (Feig et al., 2013). Similarly, high densities of CAFs expressing high levels of leucine-rich repeating containing 15 protein in human pancreatic ductal adenocarcinoma correlated with poor response to anti-PDL1 (Dominguez et al., 2020). Also, a large representation of FAP^+ CAFs in colorectal cancer (Calon et al., 2015) and αSMA^+ CAFs in pancreatic ductal adenocarcinoma (Ireland et al., 2016; Franco-Barraza et al., n.d.) correlated with a worse prognosis and resistance to chemotherapy. Thus, in some tumors, CAFs are pro-tumor elements that diminish patient survival, and promote resistance to immunotherapy and chemotherapy.

Despite the overwhelming evidence indicating that CAFs have a pro-tumor role, there are some studies suggesting that these cells are involved in tumor suppression. For

example, the depletion of αSMA$^+$ CAFs in the early development of a murine model of pancreatic ductal adenocarcinoma resulted in greater tumor outgrowth (Özdemir et al., 2014). This observation suggests that αSMA$^+$ CAFs have a protective role in nascent tumor development, but this role changes as the tumor matures. Disruption of sonic hedgehog signaling in murine desmoplastic pancreatic tumors also led to reduced numbers of αSMA$^+$ CAFs and enhanced disease progression (Rhim et al., 2014). In contrast, overexpression of sonic hedgehog signaling components in murine colorectal carcinoma led to larger numbers of CAFs expressing collagen type 1 and reduced tumor outgrowth (Gerling et al., 2016). Lastly, the presence of CAFs expressing CD146 in estrogen receptor positive breast cancer is associated with enhanced patient survival and response to anti-endocrine therapy (Brechbuhl et al., 2017). Thus, special consideration must be taken when targeting CAFs for therapeutic purposes, since in some cases they are anti-tumor elements that support survival and sensitivity to cancer therapies.

CAFs contribute to tumor growth through a variety of mechanisms. This includes extracellular matrix remodeling that increases tumor stiffness (X. Tang et al., 2016; Nguyen et al., 2019), secreting soluble factors that support tumor growth (Erdogan & Webb, 2017), inducing angiogenesis (F.-T. Wang, Sun, Zhang, & Fan, 2019), and immunosuppression (Monteran & Erez, 2019). However, the anti-tumor properties of CAFs remain largely uncharacterized. One study found that αSMA$^+$ CAFs in breast cancer expressed large amounts of TGFβ inhibitor asporin, and the abundant representation of these cells correlated with better clinical outcomes (Maris et al., 2015). In a murine model of prostate cancer, FAP$^+$ CAFs are a large source of homeostatic chemokine CXCL13 and

the depletion of the cells significantly inhibits B-cell recruitment into tumors (Ammirante, Shalapour, Kang, Jamieson, & Karin, 2014). $PDPN^+$ CAFs have been documented in tertiary lymphoid structures (TLS) associated with a murine model of pancreatic carcinoma (Link et al., 2011), suggesting that that these cells drive the formation of these structures. However, this remains to be shown. Determining this will identify a new role for CAFs as immune organizers of TLS in tumors, and point to the importance of continuing to understand the heterogeneity of CAF populations in different tumor types.

Role of endothelial cells in lymphocyte trafficking and tumor development

Blood endothelial cells (BEC) form a continuous layer that line several organs and the blood endothelium. BECs perform several critical functions, including regulating the flow of blood, and the passage of nutrients, oxygen, and other solutes from the bloodstream to peripheral tissues (Krüger-Genge, Blocki, Franke, & Jung, 2019). BEC also regulate the trafficking of leukocytes into and out of tissues. Trafficking of leukocytes, including T- and B-cells, into secondary lymphoid organs (SLO) and inflamed non-lymphoid tissues involves sequential interactions of a set of homing receptors (HR) on leukocytes with cognate ligands on BECs (Ley, Laudanna, Cybulsky, & Nourshargh, 2007). For example, antigen inexperienced naïve T-cells enter lymph nodes (LN) based on their expression of L-selectin and CCR7, which bind to peripheral node addressin (PNAd) and the chemokines CCL19/CCL21, respectively. These HR ligands are normally expressed on specialized LN blood vessels called high endothelial venules (HEV) (Girard, Moussion, & Förster, 2012). During differentiation, effector T-cells downregulate L-selectin and CCR7, and acquire the ability to enter peripheral tissues by upregulating HRs that bind to cognate ligands

expressed on inflamed vasculature. HR expression on activated T-cells is determined by the SLO in which priming occurs (Mora et al., 2003, 2005; Johansson-Lindbom & Agace, 2007; Sigmundsdottir & Butcher, 2008; Ferguson & Engelhard, 2010). Tissue-specific and inflammation-induced expression of different HR ligands, in conjunction with the patterns of HRs expressed by T-cells, determines which tissues are infiltrated.

BECs that line the vasculature of tumors are termed tumor-associated endothelial cells (TEC) and these cells largely influence the trafficking of immune cells into tumors. While the requirements for entry of effector T-cells and other leukocytes into inflamed peripheral tissues, particularly skin and gut, have been well-established (Ley et al., 2007), the requirements for entry into tumors remain inadequately defined. Several studies have unambiguously identified individual HRs that mediate T-cell infiltration into some tumors (Yamada et al., 2006; Sasaki et al., 2007; Buckanovich et al., 2008; D. T. Fisher et al., 2011; Bose et al., 2011; Mikucki et al., 2015), while others have shown correlations between individual HRs or HR ligands and T-cell infiltrates (Kunz et al., 1999; Garbi, Arnold, Gordon, Hämmerling, & Ganss, 2004; Hensbergen et al., 2005; Musha et al., 2005; Clark et al., 2008; Quezada et al., 2008; Lohr et al., 2011). A comprehensive analysis of the HRs that mediate entry of CD8 T-cell effectors into B16 melanoma and Lewis lung carcinoma was recently completed, and demonstrated that HR ligand expression on the tumor vasculature varies with the anatomical location of the tumor (Woods et al., 2017). This also determines the ability of T-cells activated in different SLOs to enter tumors growing in different locations. Consistent with other work (Clark et al., 2008; Dengel et al., 2010; Weishaupt, Munoz, Buzney, Kupper, & Fuhlbrigge, 2007), HR ligand expression

on the tumor vasculature is often low. This is consistent with the low infiltration of adoptively transferred effector T-cells observed in several studies (Economou et al., 1996; B. Fisher et al., 1989; Griffith et al., 1989; Kershaw et al., 2006). Thus, one opportunity to improve cancer immunotherapy is to identify and manipulate the expression of HRs and HR ligands to enhance infiltration of CD8 T-cell effectors into tumors. This approach has been explored by transducing adoptively transferred T cells to express various chemokine receptors, and has resulted in enhanced infiltration and tumor control (Craddock et al., 2010; Di Stasi et al., 2009; W. Peng et al., 2010; Moon et al., 2011).

Since naïve T-cells do not generally enter peripheral tissue, it had been assumed that all intratumoral lymphocytes are effectors that differentiate in tumor-draining LN and home to the tumor thereafter. However, naïve T-cells were shown to infiltrate tumors that had been genetically modified to secrete lymphotoxin-α (LTα) (Schrama et al., 2001, 2008) or LIGHT (P. Yu et al., 2004). Tumors expressing LTα accumulated activated T-cells in the absence of SLOs (Schrama et al., 2008). Similar results were obtained by intratumoral injection of CCL21 or CCL21 transduced dendritic cells (DC) (Kirk, Hartigan-O'Connor, Nickoloff, et al., 2001; Kirk, Hartigan-O'Connor, & Mule, 2001; Turnquist et al., 2007). It was suggested that naïve T cells infiltrated through a LN-like vasculature based on the expression of CCL21 (P. Yu et al., 2004), or expression of CCL21 and PNAd and the accumulation of T cells expressing L-selectin (Schrama et al., 2001), although this was not shown. In all of these models, the infiltration of naïve T-cells, in conjunction with their differentiation to become effectors, was shown to promote tumor destruction. These studies established that tumors could be engineered to serve as a

surrogate site for naïve T cells recruitment and their activation to become mediators of improved anti-tumor immunity.

More recently, work from the lab demonstrated that adoptively transferred naïve CD8 T-cells can enter unmanipulated tumors and subsequently differentiate into functional effectors (Peske et al., 2015; Thompson, Enriquez, Fu, & Engelhard, 2010). This also occurs in the absence of SLOs (Thompson et al., 2010). Also, naïve CD8 T-cell entry into tumors was entirely dependent on L-selectin and CCR7, and on the development of a tumor vasculature expressing PNAd and CCL21 (Peske et al., 2015). PNAd and CCL21 were co-expressed on a small fraction of blood vessels in tumors growing in multiple anatomical locations (Peske et al., 2015). The primary source of CCL21 was CAFs, and to a lesser extent, TECs. It was also shown that preventing this influx of naïve T-cells diminished tumor control, indicating that the development of intratumoral $PNAd^+$ $CCL21^+$ LN-like vasculature is important component of the immune response in unmanipulated tumors.

Regulation of PNAd on lymph node high endothelial venules and tumor vasculature

In adult LNs, HEV morphology and expression of genes required for the biosynthesis of PNAd is maintained by continuous engagement of lymphotoxin-$\alpha_1\beta_2$ ($LT\alpha_1\beta_2$) expressed on DCs with the lymphotoxin-β receptor (LTβR) expressed on BECs (Browning et al., 2005; Moussion & Girard, 2011). However, the genes for PNAd biosynthesis can also be induced in cultured endothelial cells and monocytes by TNFα (Pablos et al., 2005; Tjew, Brown, Kannagi, & Johnson, 2005). LTβR signaling does not control expression of CCL21 in adult LNs (Browning et al., 2005; Ngo et al., 1999). Developmentally, CCL21

expression depends upon signals from $LT\alpha_1\beta_2$ or soluble $LT\alpha_3$, which engages tumor necrosis factor receptors 1 and 2 (TNFR) but not LTβR (Sacca, Cuff, Lesslauer, & Ruddle, 1998; Cuff et al., 1998; Cuff, Sacca, & Ruddle, 1999; Drayton, Ying, Lee, Lesslauer, & Ruddle, 2003); TNFα (Johnson & Jackson, 2010; Wiede, Vana, Sedger, Lechner, & Körner, 2007); and another TNFR family member, CD30 (Bekiaris et al., 2009). However, it is not clear whether these signals regulate the expression of CCL21 directly, or the development of CCL21 expressing cells. Overall, these results point to the central importance of $LT\alpha_1\beta_2$-LTβR engagement in driving development and maintenance of PNAd expression on BECs, while control of CCL21 expression remains uncertain.

In tumors, the density of intratumoral DCs (Martinet et al., 2013) and Treg depletion (Hindley et al., 2012) were correlated with development of $PNAd^+$ $CCL21^+$ vasculature, but a cause and effect relationship was not established. Indeed, in murine models of melanoma and lung carcinoma, development of $PNAd^+$ $CCL21^+$ vasculature was not induced by either DCs or LTβR signaling (Peske et al., 2015). Instead, induction of both molecules depended on CD8 T-cell effectors that had infiltrated tumors at an earlier point. In intraperitoneal tumors, PNAd expression depended on CD8 T-cell effectors secreting $LT\alpha_3$, which acted through TNFR expressed on TECs and CAFs. CCL21, but not PNAd, also depended on IFNγ secreted by CD8 T-cell effectors, which acted through IFNγ receptors on CAFs and TECs. Control of PNAd and CCL21 in subcutaneous tumors was more complex, in that both CD8 T-cell effectors and NK cells could independently induce expression of these molecules. While expression depends on signaling through TNFR,

IFNγ seems to act redundantly with another as yet unidentified modulator to induce CCL21. These results demonstrate that the mechanisms controlling development of $PNAd^+$ $CCL21^+$ vasculature in tumors are distinct from those identified in SLO, and also differ between subcutaneous and intraperitoneal tumors. It remains to be determined whether these or additional mechanisms operate in human tumors growing in different anatomical locations.

Tertiary lymphoid structures in chronic inflammation-associated tissues

The ectopic expression of PNAd on non-lymphoid blood vessels is often associated with tertiary lymphoid structures (TLS). These structures are lymphoid aggregates that frequently develop at sites of chronic infection, autoimmune disease, and allograft rejection (Drayton, Liao, Mounzer, & Ruddle, 2006; Carragher, Rangel-Moreno, & Randall, 2008; GeurtsvanKessel et al., 2009; Halle et al., 2009; Hayasaka, Taniguchi, Fukai, & Miyasaka, 2010; van de Pavert & Mebius, 2010; Link et al., 2011; Huang & Luther, 2012; Neyt, Perros, GeurtsvanKessel, Hammad, & Lambrecht, 2012; Stranford & Ruddle, 2012). These structures have considerable morphological, cellular, and molecular similarity to SLOs, particularly LNs. Inflammation-associated TLS are associated with blood vascular endothelial cells that express PNAd and CCL21 that often have a characteristic “puffy” morphology. TLS contain B-cells, T-cells, and DCs, which are typically organized into distinct functional compartments: a B-cell follicle mainly composed of naïve B cells, surrounding a germinal center composed of highly proliferative B cells; and a T-cell area mainly composed of T-cells and DCs (Jones, Hill, & Jones, 2016; Neyt et al., 2012). In SLOs, this microarchitecture is orchestrated by the homeostatic chemokines CCL19,

CCL21, CXCL13, and CXCL12 (Legler et al., 1998; Ansel et al., 2000; Sanjiv A. Luther, Tang, Hyman, Farr, & Cyster, 2000; Allen et al., 2004). These chemokines are also found in TLS (Barone et al., 2015; Fleige et al., 2014; Pikor et al., 2015; Rangel-Moreno et al., 2011; Rangel-Moreno, Moyron-Quiroz, Hartson, Kusser, & Randall, 2007). Cells resembling fibroblastic reticular cells (FRC) and follicular dendritic cells (FDC) have also been reported in well-developed TLS (Barone et al., 2015; Drayton et al., 2003; Fleige et al., 2014; Link et al., 2011; Rangel-Moreno et al., 2007), suggesting that these cells may be the source of these chemokines and function as organizers of TLS. However, this remains to be directly demonstrated.

In addition to their cellular and molecular characteristics, TLS have also been shown to have functional capabilities that can influence disease progression. In acute influenza infection, TLS that develop in the lungs are commonly associated with viral clearance (Moyron-Quiroz et al., 2004). Mechanistically, DCs in lung TLS present viral antigens to newly entering naïve T-cells and promote the generation of antiviral effector cells (Halle et al., 2009). Interestingly, SLOs are dispensable for the generation of antiviral effectors and viral clearance (Moyron-Quiroz et al., 2006, 2004). TLS and B-cells have also been shown to have a protective role against *Mycobacterium tuberculosis* infection (Maglione, Xu, & Chan, 2007; Khader et al., 2009). In these structures, B-cells express markers associated with germinal center activity, such as peanut agglutinin (PNA) and GL7. This suggests that TLS promote the generation of protective B-cells that produce antibodies against *Mycobacterium tuberculosis*. However, this has not been determined.

Nonetheless, these observations demonstrate that TLS in the lungs are beneficial structures that drive clearance of acute bacterial and viral infections.

In contrast to above, TLS have also been described in the synovial lymphoid tissue of patients with rheumatoid arthritis (RA). In these patients, TLS-associated B-cells often express markers associated with activation, germinal center activity, and antibody producing plasma cells (Manzo et al., 2005). Consistent with this, high levels of anticitrullinated protein specific antibodies in the serum and synovial fluid of RA patients is associated with a more severe disease pathology (van der Helm-van Mil, Verpoort, Breedveld, Toes, & Huizinga, 2005), suggesting that TLS perpetuate RA severity. TLS have also been identified in a variety of rejected transplanted organ, particularly those involving lung, heart, and kidney (W. Li et al., 2012; Hsao, Li, Gelman, Krupnick, & Kreisel, 2015; Koenig & Thaunat, 2016). It has been suggested that the rejection of these organs is a consequence of alloreactive T-cells generated in these structure (Nasr et al., 2007; Hsao et al., 2015). However, this remains to be determined. Nonetheless, TLS show functional capabilities that are similar to SLOs, but their impact over disease severity depends on the anatomical location in which these structures form in.

Regulation of TLS in chronic inflammation-associated tissues

The development of conventional LNs depends on interaction between $CD4^{+}CD3^{neg}$ lymphoid tissue inducer (LTi) cells expressing $LT\alpha_1\beta_2$ and RANKL (now known to be innate lymphoid cells (ILC) 3) (Sawa et al., 2010), and mesenchymal lymphoid tissue organizer (LTo) cells expressing LTβR (D. Kim et al., 2000; Mebius, 2003; Randall, Carragher, & Rangel-Moreno, 2008; Withers, 2011; Lane, Gaspal, McConnell, Withers, &

Anderson, 2012; Fletcher, Acton, & Knoblich, 2015). This leads to expression of CCL19, CCL21, and CXCL13, which attract additional LTi cells, and the recruitment and positioning of T- and B-cells (Ansel et al., 2000; Nakano & Gunn, 2001; Ohl et al., 2003; Sanjiv A. Luther, Ansel, & Cyster, 2003). In keeping with this, mice deficient in LTα, LTβ, or LTβR fail to develop all or most LNs (De Togni et al., 1994; Alimzhanov et al., 1997; Koni et al., 1997; Fütterer, Mink, Luz, Kosco-Vilbois, & Pfeffer, 1998). The formation of FDC networks and germinal centers as an element of LN development depends on engagement of TNFR as well as LTβR (Kuprash et al., 1999). LTβR signaling does not control expression of CCL21 in adult LNs (Browning et al., 2005; Ngo et al., 1999), although it does maintain CXCL13 expression in adult spleen (Ngo et al., 1999) presumably through interaction of $LT\alpha_1\beta_2$-expressing B-cells with $LT\beta R^+$ FDCs (A. V. Tumanov et al., 2010; Alexei V. Tumanov et al., 2002).

A key question is whether the development and formation of TLS occurs through pathways analogous to those controlling conventional LN development. Transgenic expression of LTα or LTβ in various organs leads to the formation of organized lymphoid aggregates typically identified as TLS, although they are not driven by an immune response (Sacca et al., 1998; Cuff et al., 1998, 1999; Drayton et al., 2003). Transgenic expression of CCL21 also leads to formation of such structures, although PNAd expression still depends on LTβR signaling (S. A. Luther, Lopez, Bai, Hanahan, & Cyster, 2000; Sanjiv A. Luther et al., 2002), and this operates through mature CD4 T-cells rather than LTi cells (Marinkovic et al., 2006). Importantly, blockade of LTβR signaling prevents immune response-driven TLS formation in thyroid, lung, salivary gland, aorta, and heart (Glaucia

C Furtado et al., 2007; Gatumu et al., 2009; Gräbner et al., 2009; GeurtsvanKessel et al., 2009; Rangel-Moreno et al., 2011; Motallebzadeh et al., 2012). These studies suggest that development of LNs and TLS are mechanistically similar.

On the other hand, TLS have been shown to depend on TNFα in aorta, fat, and intestine (Bénézech et al., 2015; G. C. Furtado et al., 2014; Guedj et al., 2014), IL22 in salivary gland (Barone et al., 2015), and IL17A in lung and meninges (Peters et al., 2011; Rangel-Moreno et al., 2011; Pikor et al., 2015). IL6 and IL23 also contribute to TLS development through IL-17A dependent and independent pathways (Cañete et al., 2015; Khader et al., 2011; Goya et al., 2003). While the exact mechanisms of action remain to be fully defined, TNFα induces CCL21 (Johnson & Jackson, 2010; Wiede et al., 2007), CXCL13 (Ngo et al., 1999), and enzymes necessary for PNAd biosynthesis (Pablos et al., 2005; Tjew et al., 2005). Also, IL22 and IL17A induces CXCL12 and CXCL13 in TLS-associated stromal cells (Hsu et al., 2008; Gopal et al., 2013; Fleige et al., 2014; Rangel-Moreno et al., 2011; Barone et al., 2015). These cytokines sometimes induce TLS independent of LTβR signaling (Bénézech et al., 2015; Guedj et al., 2014), but in other instances act cooperatively, either by inducing distinct aspects of TLS structure (Barone et al., 2015; Pikor et al., 2015), or by acting at either the TLS induction or maintenance phases (Rangel-Moreno et al., 2011). Importantly, different pathogens can induce lung-associated TLS by distinct cellular and molecular pathways (Fleige et al., 2014). The involvement of additional cytokines in formation and/or maintenance of many LTβR-dependent TLS remains to be evaluated.

Aside from the involvement of distinct molecular signaling pathways in TLS formation, a variety of different inducing cells, in lieu of LTi cells, have been identified. This includes DCs (GeurtsvanKessel et al., 2009; Halle et al., 2009; Muniz, Pacer, Lira, & Furtado, 2011) and naïve B-cells (K. G. McDonald, McDonough, & Newberry, 2005), both expressing $LT\alpha_1\beta_2$; macrophages (Bénézech et al., 2015; G. C. Furtado et al., 2014; Guedj et al., 2014), T_H17 (Peters et al., 2011; Rangel-Moreno et al., 2011; Pikor et al., 2015), NKT (Bénézech et al., 2015), γδ T-cells (Fleige et al., 2014), and multiple populations of IL22-secreting adaptive and innate lymphoid cells (Barone et al., 2015). Overall, it should be expected that distinct molecular signals, conveyed by immune cells with pleiotropic regulatory signatures, will induce TLS with important differences in the immune responses that they support.

Identification and characterization of tumor-associated tertiary lymphoid structures

TLS are also associated with a variety of tumor types. TA-TLS were initially described in melanoma (Ladanyi et al., 2007) and in non-small cell lung cancer (NSCLC) (Dieu-Nosjean et al., 2008). Since then, they have now been documented in a variety of primary and metastatic tumor types (Engelhard et al., 2018; Sautès-Fridman et al., 2019; Anthony B. Rodriguez & Engelhard, 2020). Histological elements most frequently used to identify human TA-TLS include one or more of the following: tumor vessels expressing PNAd, mature DCs expressing lysosome-associated membrane glycoprotein (DC-LAMP), dense aggregates of T- and/or B-cells, follicular helper T-cells (T_{FH}), and cells resembling FDC (Engelhard et al., 2018; Sautès-Fridman et al., 2019; Anthony B. Rodriguez & Engelhard, 2020) (Table 1). Most TA-TLS are organized “classically”, with distinct T-cell/DC and B-

cell/FDC compartments (Table 1), and one or more of the homeostatic chemokines CCL19, CCL21, CXCL12, and CXCL13, which organize the SLO microarchitecture, are documented in TA-TLS by immunohistochemistry (Engelhard et al., 2018; Sautès-Fridman et al., 2019; Anthony B. Rodriguez & Engelhard, 2020) (Model Fig. 1). Composite gene signatures are used for the detection of TA-TLS (Table 1). Expression of the plasma cell specific marker B-cell maturation antigen (BCMA) is associated with the presence of TA-TLS in ovarian cancer (Kroeger, Milne, & Nelson, 2016). A more comprehensive 19-gene signature identifying B-cells and T_H1 T-cells is associated with the presence of TA-TLS in gastric cancer (Hennequin et al., 2016), and an 8-gene signature identifying T_{FH} cells is predictive of the presence of TA-TLS in breast cancer (Gu-Trantien et al., 2013). A 12-chemokine gene signature is also predictive of the presence of TA-TLS in colorectal (Coppola et al., 2011), melanoma (Coppola et al., 2011), breast (Prabhakaran et al., 2017), and hepatocellular carcinoma (Finkin et al., 2015). Finally, a 9-gene signature has been identified by comparing $CD8^+/CD20^+$ and $CD8^+/CD20^{neg}$ melanomas (Cabrita et al., 2020). Collectively, these components provide a baseline for identifying TA-TLS. However, most human studies have relied on only one or a small number of these markers (Engelhard et al., 2018; Sautès-Fridman et al., 2019; Anthony B. Rodriguez & Engelhard, 2020). Additionally, the criteria typically used are largely oriented towards elements that support anti-tumor immunity, although Treg have occasionally been reported (García-Hernández et al., 2017; Schweiger et al., 2016). A particularly interesting study demonstrates distinct Treg, T_H1, and T_H17 biased profiles in TA-TLS associated with response or lack of response to a mesothelin vaccine (Lutz et al., 2014). However, it is still

Model 1: Cellular, organization, and location heterogeneity associated with tumor-associated tertiary lymphoid structures

TA-TLS are aggregates of T-cells, B-cells, dendritic cells (DC), and fibroblastic reticular cells (FRC)-/follicular dendritic cells (FDC)-like that are in juxtaposition to a tumor vessel expressing peripheral node addressin (PNAd). They can be found either intratumorally (A) or peritumorally (B). Limited evidence suggests that intratumoral structures may have greater prognostic significance, but this remains to be widely established. It is also unknown whether the peritumoral location limits infiltration of APC and/or effector cells. TA-TLS can exhibit either a classical organization that contains discrete T-cell/DC and B-cell/FDC compartments (C) or a non-classical organization (D). Non-classical TA-TLS usually contain B-cells that are less activated than those in classical structures. Evidence suggests that classical TA-TLS have greater prognostic value than non-classical structures, and classical structures containing germinal centers may have the greatest value. While CAF support TA-TLS formation in murine melanoma, the role of CAF and of associated FRC-/FDC-like cells in supporting formation of non-classical and classical TA-TLS in other murine and human tumors remains to be determined. Similarly, it is unknown whether the lack of compartmentalization in non-classical TA-TLS limits tumor-antigen presentation and T-cell activation relative to classical structures, and whether any of these variables alter effector T-cell differentiation. Addressing these unknowns will determine how heterogeneity in TA-TLS cellular composition, structural organization, and anatomical location influences their functionality and prognostic impact. ***Image created with BioRender.com***.

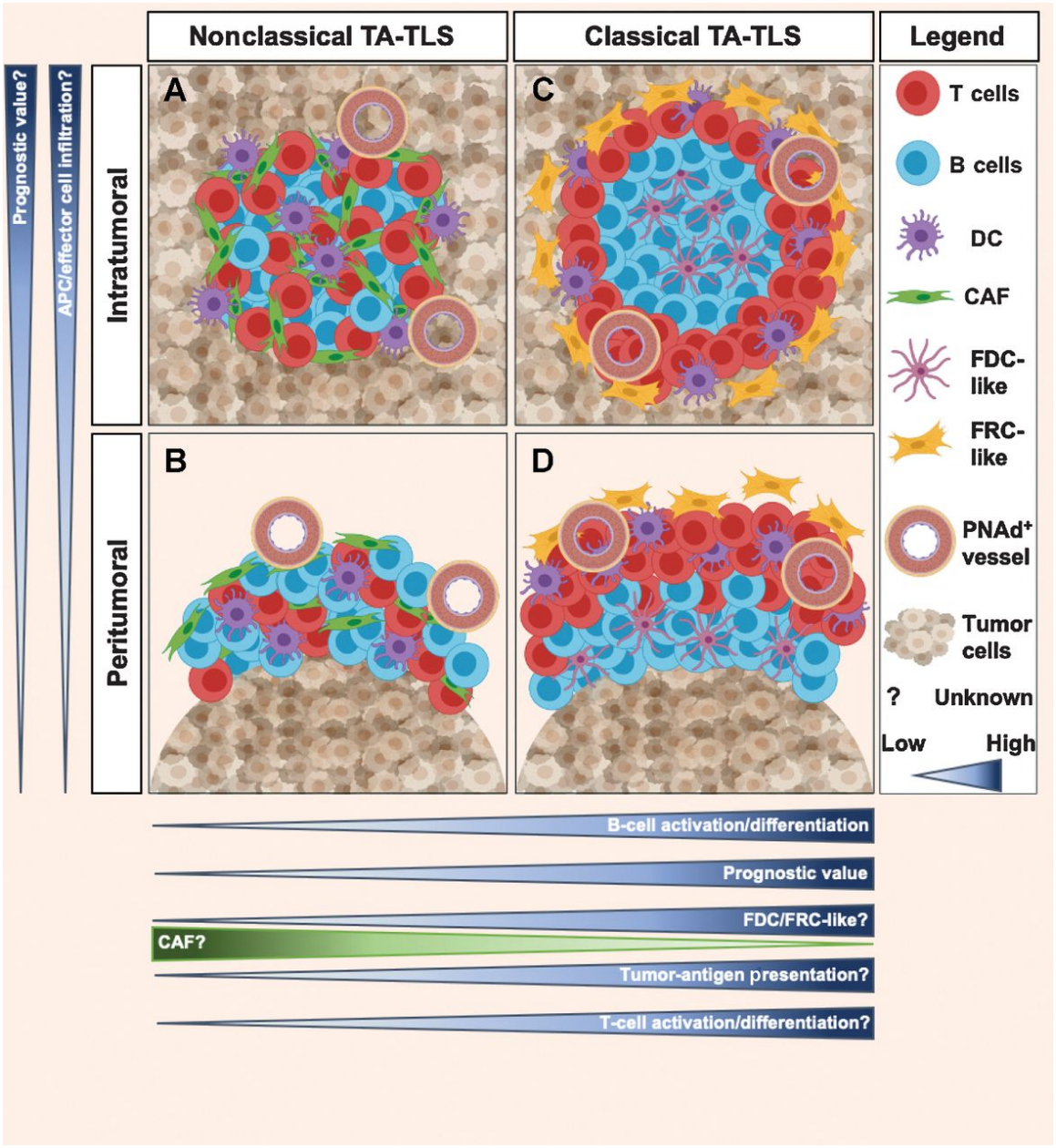
Nonclassical TA-TLS
Classical TA-TLS
Legend
Prognostic value?
APC/effector cell infiltration?
Intratumoral
Peritumoral
A
B
C
D
T cells
B cells
DC
CAF
FDC-like
FRC-like
PNAd+ vessel
Tumor cells
? Unknown
Low High
B-cell activation/differentiation
Prognostic value
FDC/FRC-like?
CAF?
Tumor-antigen presentation?
T-cell activation/differentiation?

Table 1: Characteristics of TA-TLS in human tumors and their prognostic value

Tumor Type	TA-TLS markers by IHC[a]	TA-TLS gene signatures	TA-TLS location	TA-TLS organization	# patients	TA-TLS association	Ref.
Bladder, primary	T- and B-cells, CD21 (FDC), PNAd, DC-LAMP	-	Peritumoral	Classical	28	Higher tumor grade	(Koti et al., 2017)
Breast, primary	PNAd, DC-LAMP	-	Peritumoral and intratumoral	Classical	146	Favorable overall survival	(Martinet et al., 2011, 2013)
	T- and B-cells, T_{FH}, GC B-cells	T_{FH}	Peritumoral and intratumoral	Classical	794	Favorable overall survival and response to chemotherapy	(Gu-Trantien et al., 2013)
	T- and B-cells, GC B-cells, CD21 (FDC), PNAd, DC-LAMP	-	Peritumoral	Classical	290	Higher tumor grade	(Figenschau, Fismen, Fenton, Fenton, & Mortensen, 2015)
	Mononuclear aggregates	-	Peritumoral	ND	796	Favorable overall survival	(H. J. Lee, Park, et al., 2015)
	Mononuclear aggregates	-	Peritumoral	ND	447	Favorable overall survival and response to adjuvant Trastuzumab in patients with $HER2^+$ tumors	(H. J. Lee, Kim, et al., 2015)
	T- and B-cells, CD21 (FDC)	-	Peritumoral	Classical	248	Favorable overall survival in patients with $HER2^+$ tumors	(X. Liu et al., 2017)
	Mononuclear aggregates, T- and B-cells, PNAd	-	Peritumoral	Non-classical	108	Favorable response to neoadjuvant chemotherapy	(Song et al., 2017)
	Mononuclear aggregates	-	Peritumoral	ND	769	Favorable overall survival	(Miseon Lee et al., 2019)
Cervical, primary	Mononuclear aggregates, T- and B-cells, Ki67, PNAd	-	Peritumoral	Non-classical	12	Found in only vaccinated patients	(Maldonado et al., 2014)
Colorectal, primary	T- and B-cells, GC B-cells, CD21 (FDC)	12-chemokine	Peritumoral and intratumoral	Classical	21	Favorable overall survival	(Coppola et al., 2011)
	T- and B-cells, CD21 (FDC), PNAd, CCL21, CXCL13	-	Peritumoral	Classical	351	Favorable overall survival	(Di Caro et al., 2014)
	Mononuclear aggregates, T- and B-cells	12-chemokine	Peritumoral	Classical	39	Favorable overall survival	(Prabhakaran et al., 2017)
Colorectal, lung metastatic	T- and B-cells, PNAd, DC-LAMP	-	Intratumoral	Classical	192	Favorable overall survival	(Remark et al., 2013)

	Mononuclear aggregates, T-cells, CD45RO^{+} T-cells, Foxp3^{+} cells	-	Peritumoral and intratumoral	ND	57	No evaluation	(Schweiger et al., 2016)
Colorectal, liver metastatic	Mononuclear aggregates, B-cells, GC B-cells, macrophages	-	Peritumoral (Non-tumor liver tissue)	ND	65	Favorable overall survival	(Meshcheryakova et al., 2014)
Gastric, metastatic	Mononuclear aggregates, T- and B-cells, DC-LAMP, PNAd	T_H1 and B-cell	Intratumoral	Classical	365	Favorable overall survival	(Hennequin et al., 2016)
	Mononuclear aggregates, T- and B-cells, GC B-cells, CD21 (FDC), DC-LAMP, PNAd, CCL21 and CXCL13	-	Intratumoral	Classical	176	Advanced clinical disease; no impact on overall survival	(Hill et al., 2018)
Liver, primary	Mononuclear aggregates	-	Intratumoral	ND	273	Favorable overall survival	(Calderaro et al., 2019)
	Mononuclear aggregates	12-chemokine	Intratumoral	ND	221	Favorable overall survival	(Calderaro et al., 2019)
	Mononuclear aggregates	-	Peritumoral (Non-tumor liver tissue)	ND	217	No impact on overall survival	(Calderaro et al., 2019)
	Mononuclear aggregates, T- and B-cells, CD68 (macrophages), Ly6G (neutrophils), Foxp3, CD21 (FDC)	12-chemokine	Peritumoral (Non-tumor liver tissue)	Non-classical	82	Unfavorable overall survival	(Finkin et al., 2015)
	Mononuclear aggregates, T- and B-cells, macrophages, Foxp3, CD21 (FDC)	-	Intratumoral	Non-classical	462	Favorable overall survival	(Hui Li et al., 2020)
Lung, primary	Mononuclear aggregates, T- and B-cells, CD68 (macrophages), CD21 (FDC)	-	Peritumoral	Classical	74	Favorable overall survival	(Germain et al., 2014)
	Mononuclear aggregates, T- and B-cells, CD21 (FDC), PNAd	-	Peritumoral	Classical	151	Favorable overall survival only after neoadjuvant chemotherapy	(Remark et al., 2016)
	Mononuclear aggregates, T- and B-cells, CD21 (FDC), DC-LAMP	-	Intratumoral	Classical	74	Favorable overall survival	(Dieu-Nosjean et al., 2008)
	Mononuclear aggregates, T- and B-cells, CD21 (FDC), DC-LAMP	T_H1/cytotoxic	Peritumoral and intratumoral	Classical	362	Favorable overall survival	(Goc et al., 2014)
	Mononuclear aggregates, T- and B-cells, GC B-cells, CD21	-	Peritumoral	Classical and non-classical	138	Favorable overall survival	(Siliņa et al., 2018)

	(FDC), DC-LAMP, PNAd, CCL21, CXCL13						
Renal clear-cell, lung metastatic	T- and B-cells, PNAd, DC-LAMP	-	Peritumoral	Classical	57	Unfavorable overall survival	(Remark et al., 2013)
Melanoma, primary	Mononuclear aggregates, T-cells, DC-LAMP	-	Peritumoral	ND	82	Favorable overall survival	(Ladanyi et al., 2007)
	$CD45RO^+$ T-cells, B-cells, CD21 (FDC), PNAd	-	Peritumoral	ND	39	No impact on overall survival	(Ladányi et al., 2014)
	T- and B-cells, PNAd	-	Peritumoral	Non-classical	225	No impact on overall survival	(Martinet et al., 2012)
Melanoma, metastatic	T- and B-cells, GC B-cells, CD21 (FDC), DC-LAMP, PNAd	FDC	Peritumoral	Classical	29	No impact on overall survival	(Cipponi et al., 2012)
	Mononuclear aggregates, T- and B-cells, macrophages, $Foxp3^+$ cells	12-chemokine	Peritumoral	Classical	10	Favorable overall survival	(Messina et al., 2012)
	T- and B-cells, GC B-cells	$CD20^+$ and $CD8^+$ associated	Peritumoral	Classical	177	Favorable overall survival and response to checkpoint immunotherapy	(Cabrita et al., 2020)
	Mononuclear aggregates, T- and B-cells, CD21 (FDC), $Foxp3^+$ cells	$CD20^+$ B-cell	Peritumoral	Non-classical	127	Favorable overall survival and response to checkpoint immunotherapy	(Helmink et al., 2020)
	Mononuclear aggregates, T- and B-cells, naïve & activated B-cells, $Foxp3^+$ cells	B-cell plasmablast-like	Peritumoral	Non-classical	10	Favorable response to checkpoint immunotherapy	(Griss et al., 2019)
Oral, primary	Mononuclear aggregates, T- and B-cells, macrophages, DC-LAMP, PNAd	12-chemokine	Peritumoral	Classical	80	Favorable overall survival	(Anna Maria Wirsing et al., 2018)
Ovarian, metastatic	Mononuclear aggregates, T- and B-cells, GC B-cells, CD21 (FDC), DC-LAMP, PNAd	BCMA	Peritumoral and intratumoral	Non-classical	172	Favorable overall survival	(Kroeger et al., 2016)
	Mononuclear aggregates, DC-LAMP	-	Peritumoral and intratumoral	ND	147	Favorable overall survival	(Truxova et al., 2018)
Pancreatic, primary	Mononuclear aggregates	-	Intratumoral	ND	308	Favorable overall survival	(Hiraoka et al., 2015)
	Mononuclear aggregates, T- and B-cells, DC-LAMP, PNAd, CCL21, CXCL13	-	Intratumoral	Classical	104	Favorable overall survival	(Castino et al., 2015)

	Mononuclear aggregates, T- and B-cells, $CD45RO^+$ T-cells, DC-LAMP, CD21 (FDC), Ki67, CD68 (macrophages), $Foxp3^+$ cells, $Tbet^+$ cells, PD-L1, CCL21	-	Intratumoral	Classical	93	Found in only vaccinated patients	(Lutz et al., 2014)
Soft-tissue, primary	T- and B-cells, CD21 (FDC), DC-LAMP, PNAd	12-chemokine	Intratumoral	Classical and non-classical	47	Favorable response to checkpoint immunotherapy	(Petitprez et al., 2020)
Prostate, primary	Mononuclear aggregates, T- and B-cells, CD21 (FDC), DC-LAMP, PNAd, CD68 (macrophages)	-	Peritumoral	Non-classical	17	No impact on overall survival	(García-Hernández et al., 2017)

[a] GC, germinal center; ND, not determined. Other abbreviations are defined in the text.

unknown whether other immunosuppressive cells (MDSC, some populations of innate lymphocytes or NKT cells) are present in TA-TLS. Thus, there is likely to be significant unappreciated heterogeneity in TA-TLS cellular composition. Also, some reports have identified loose aggregates of lymphocytes as TA-TLS (Finkin et al., 2015; Stowman et al., 2018), although they are typically tightly aggregated structures. Whether these are nascent or senescent TA-TLS, or something altogether different, remains unclear. Nonetheless, the field as a whole should move to utilize a more comprehensive set of markers to identify these structures to ensure that their heterogeneity, function, and prognostic value can be more thoroughly evaluated.

Composition, organization, and heterogeneity of TA-TLS

Despite the limited characterization in many studies, TA-TLS from different tumor types vary in cellular composition and organization. B-cells with immature, naïve, activated, memory, and plasma cell phenotypes are evident to varying extents in different TA-TLS (Engelhard et al., 2018; Sautès-Fridman et al., 2019; Anthony B. Rodriguez & Engelhard, 2020). In NSCLC, TA-TLS contain large numbers of mature DC-LAMP$^+$ DCs (Dieu-Nosjean et al., 2008; Goc et al., 2014), but these cells are absent in those associated with lung metastatic renal cell carcinoma (Giraldo et al., 2015). T_{FH} cells are common features of breast cancer TA-TLS (Gu-Trantien et al., 2017), whereas those associated with prostate (García-Hernández et al., 2017) and lung metastatic colorectal cancer (Schweiger et al., 2016) contain large numbers of Tregs. While this could indicate that TA-TLS in different tumor types or anatomical locations contain different T-cell subpopulations, none of these studies evaluated both. The majority of studies have identified human TA-TLS as having

a peritumoral location, whereas a smaller number have identified TA-TLS as intratumoral, usually in addition to peritumoral structures (Engelhard et al., 2018; Sautès-Fridman et al., 2019; Anthony B. Rodriguez & Engelhard, 2020) (Table 1, Model Fig. 1). However, in germ cell tumors (Willis et al., 2009), hepatocellular carcinoma (Finkin et al., 2015), and lung metastatic renal cell carcinoma (Remark et al., 2013), TA-TLS are largely intratumoral, and exhibit a non-classical organization lacking discrete T- and B-cell compartments. However, peritumoral TA-TLS are sometimes inside the tumor albeit near the tumor-invasive margin and sometimes fully outside the margin (Munoz-Erazo, Rhodes, Marion, & Kemp, 2020). This distinction may have important consequences for TA-TLS function. In addition, there is concern that the peritumoral TA-TLS identified in lymph node metastases may represent residual lymphoid follicles (Cabrita et al., 2020). In human melanoma, TLS frequently develop in metastatic lesions, but are largely absent from primary tumors, despite the presence of a $PNAd^+$ vasculature (Cipponi et al., 2012). Similarly, TA-TLS are found in intraperitoneal, but not in subcutaneous murine tumors (Peske et al., 2015; A.B. Rodriguez, Peske, & Engelhard, 2018), and are observed frequently in primary breast tumors but largely absent in metastatic brain lesions (Miseon Lee et al., 2019). Thus, TA-TLS presence and structural organization are associated with tumor microenvironment and anatomical location, although the factors responsible, and the overall impact on TA-TLS functionality remains to be determined.

Functional characteristics of TA-TLS

It has been suggested that TA-TLS serve as sites for sustained generation of *in situ* immune responses that are focused towards tumor antigens (Engelhard et al., 2018; Sautès-Fridman

et al., 2019; Anthony B. Rodriguez & Engelhard, 2020), but evidence for this remains somewhat limited. Previous work from the lab demonstrated that tumor vessels expressing PNAd, a hallmark of TA-TLS, supported infiltration of naïve T- and B-cells (Peske et al., 2015), and TA-TLS in NSCLC contain large accumulations of naïve T- and B-cells (de Chaisemartin et al., 2011; Germain et al., 2014; Goc et al., 2014). Thus, TA-TLS could promote a continual influx of naïve cells for sustaining immunity. Whereas TA-TLS vary in the number of mature DCs they contain, larger numbers of mature DCs are associated with larger numbers of T-cells with a T_H1/cytotoxic immune profile (Dieu-Nosjean et al., 2008; Goc et al., 2014), suggesting active antigen presentation to T-cells in TA-TLS. A linear relationship between the density of TA-TLS and the levels of intratumoral activated T- and/or B-cells has also been described (Engelhard et al., 2018; Sautès-Fridman et al., 2019; Anthony B. Rodriguez & Engelhard, 2020). While this observation may suggest that TA-TLS support TIL development, work described in this thesis demonstrates that TILs support TA-TLS development.

Aggregation of tumor-associated B-cells into a follicle-like structure is one of the most dramatic and defining features of TA-TLS. Although B-cells can be positive or negative mediators of anti-tumor immunity (Guo & Cui, 2019), B-cells in classically organized TA-TLS often express markers associated with germinal center activity (Nielsen et al., 2012; Germain et al., 2014; Posch et al., 2018; Siliņa et al., 2018), and show higher degrees of clonal amplification, rearranged immunoglobulins, somatic hypermutations, and isotype switching than those in tumor parenchyma (Cipponi et al., 2012; Selitsky et al., 2019), suggesting active anti-tumor humoral responses in these structures. T_{FH} cells are

also commonly found in the B-cell compartment of TA-TLS (Gu-Trantien & Willard-Gallo, 2013). These observations suggest that TA-TLS support the activation and differentiation of B-cells into antibody producing cells, and they are consistent with the idea that TA-TLS promote the *in situ* generation of tumor-specific antibody that augments anti-tumor immunity.

Despite these intriguing observations, there are a number of unaddressed issues that may limit the contribution of TA-TLS to producing effective anti-tumor immunity. Lymphatic vessels are rarely reported in TA-TLS, leading to uncertainties about tumor-antigen and cellular transport to these structures. Given the relatively small size of TA-TLS, it is unclear what fraction of the resident naïve T- and B-cells are tumor-antigen specific, and how frequently they turn over. Also, it is unclear whether DCs in TA-TLS come from tumor parenchyma, adjacent tissue, or blood-derived inflammatory monocytes. Similarly, it is unclear whether and how these cells acquire tumor antigen, and if DCs in TA-TLS are more mature than those in tumor parenchyma or tumor-draining SLO. It is unknown how the effector and exhaustion marker profiles of T-cells in TA-TLS compare to those in the surrounding tumor parenchyma and tumor-draining SLOs. Also, it remains unknown whether immunosuppressive elements in the tumor microenvironment, such as hypoxia, indoleamine 2, 3-dioxygenase, nitric oxide, arginase, TGFβ, and immune checkpoint ligands, impact immune responses that occur in TA-TLS. Finally, it is unknown whether B-cells in TA-TLS support anti-tumor immunity through tumor-antigen presentation to T-cells, secretion of pro-inflammatory cytokines (Guo & Cui, 2019), or the direct action of *in situ* produced antibody, or whether regulatory B-cells, which can

enhance tumor development by suppressing anti-tumor immunity (Guo & Cui, 2019), exist in TA-TLS. Since B-cells are a major component of TA-TLS, it is particularly important to have a more comprehensive understanding of the function(s) of these cells in these structures.

Prognostic significance and immunological impact of TA-TLS

The prognostic impact of TA-TLS has been extensively evaluated. Several studies have pointed to a significant relationship between the densities of TA-TLS and overall patient survival (Engelhard et al., 2018; Sautès-Fridman et al., 2019; Anthony B. Rodriguez & Engelhard, 2020), although there are exceptions (Bento et al., 2015; Figenschau et al., 2015; Finkin et al., 2015) (Table 1). Because TA-TLS are associated with higher densities of $CD8^+$ TILs, it remains possible that TA-TLS are simply proxies for more robust intratumoral T-cell effector activity. However, multivariate studies in NSCLC (Goc et al., 2014) and colorectal cancer (Di Caro et al., 2014) have established that the prognostic value of TA-TLS independent of TIL density. Intratumoral TA-TLS are more significantly associated with enhanced patient survival than peritumoral TA-TLS in pancreatic cancer (Hiraoka et al., 2015) and early-stage hepatocellular carcinoma (Hui Li et al., 2020). Also, oral squamous cell carcinoma patients whose tumors contained higher proportions of classically organized TA-TLS tended to survive longer, although this was not statistically significant (Anna M. Wirsing, Rikardsen, Steigen, Uhlin-Hansen, & Hadler-Olsen, 2014). Two studies show that germinal centers within TA-TLS determine their prognostic value in colorectal (Posch et al., 2018) and lung squamous cell carcinoma (Siliņa et al., 2018). However, it is important to establish more generally whether peritumoral and intratumoral,

or classically and non-classically organized TA-TLS differ in their association with patient survival (Model Fig. 1).

An area of immense interest is whether TA-TLS are associated with patient responsiveness to cancer therapies (Table 1). Interestingly, the presence of TA-TLS was initially associated with a favorable response to neoadjuvant chemotherapy in breast cancer (Gu-Trantien et al., 2013; Song et al., 2017). Similarly, densities of TA-TLS in human epidermal growth factor receptor 2 positive ($HER2^+$) breast cancer strongly correlate with disease-free survival and responsiveness to adjuvant Trastuzumab (H. J. Lee, Kim, et al., 2015). The presence of B-cells and/or TA-TLS prior to treatment is associated with favorable responses to checkpoint blockade immunotherapies in melanoma (Cabrita et al., 2020; Griss et al., 2019; Helmink et al., 2020) and soft-tissue sarcoma (Petitprez et al., 2020), and one of these studies presented evidence suggesting that immunotherapy might increase TLS density (Helmink et al., 2020). These observations establish that TA-TLS may be important predictors of patient response to chemotherapy and immunotherapy, along with overall intratumoral $CD8^+$ TIL, mutational burden, and PDL1 expression. At the same time, there is a suggestion that TA-TLS may be the site at which these therapies act. However, the range of tumors in which TA-TLS are identified is larger than the range that responds to immune checkpoint blockade. Whether this is a consequence of additional regulatory mechanisms, and whether these operate within the TA-TLS, remains to be determined. As above, it is important to establish more generally whether peritumoral and intratumoral, or classically and non-classically organized TA-TLS, differ in their association with treatment responses.

Cellular and molecular mechanisms potentially regulating TA-TLS development

Given the considerations above, it is highly attractive to develop immunotherapeutic approaches that induce or augment TA-TLS formation. Interestingly, vaccination induce TLS formation in association with pancreatic tumors (Lutz et al., 2014) and human papilloma virus-driven cervical intraepithelial neoplasia (Maldonado et al., 2014). Transgenic overexpression of LTβR ligands (Haidong Tang, Zhu, Qiao, & Fu, 2017), injection of recombinant LIGHT (Johansson-Percival et al., 2017), intratumoral administration of CCL21 (Turnquist et al., 2007), and intratumoral injection of DCs engineered to overexpress T-bet (Chen et al., 2013), IL-36 (Weinstein et al., 2017), or CCL21 (Kirk, Hartigan-O'Connor, & Mule, 2001; S.-C. Yang et al., 2006, p. 21) all induce TA-TLS in murine tumors. However, there are limited reports of spontaneous TA-TLS development in murine tumors (Di Caro et al., 2014; Finkin et al., 2015; Joshi et al., 2015; Peske et al., 2015; A.B. Rodriguez et al., 2018), and the mechanisms driving their formation have mostly remained unknown.

Abundant CXCL13 expression in TA-TLS suggest that this chemokine aids in development of these structures or long-term maintenance. However, its cellular source varies between tumor types. For example, T_{FH} cells are reported as a source of CXCL13 in breast tumors (Gu-Trantien et al., 2013). TA-TLS in late-stage NSCLC are associated with a distinct population of CXCL13 producing $CD8^+$ T-cells (Thommen et al., 2018). Conversely, TA-TLS associated with early-stage NSCLC contain a population of type 3 innate lymphocytes (Carrega et al., 2015). This suggests that the cells responsible for initiating and maintaining TA-TLS in NSCLC may evolve over time, although the direct

activity of these cell populations has not yet been demonstrated. However, it is unknown whether these cells exist in TA-TLS from other tumor types, and whether different anatomical compartments contain cellular populations that are reminiscent of LTo cells. In addition, it is unknown whether cellular populations resembling FDC and FRC exist in these structures, and promote the formation of classical TA-TLS with distinct T- and B-cell compartments. Also, it is entirely unknown what promotes the development of TA-TLS in peritumoral and intratumoral locations. Overall, while suggesting some general molecular mechanisms may operate to promote TA-TLS development and maintenance, these results also suggest that the cellular sources of these molecules may vary based on tumor type, anatomical location, and/or tumor evolution. Regardless, the preponderance of evidence suggests that the induction and/or augmentation of TA-TLS development could serve as a new aspect of cancer immunotherapy, either alone or in combination with immunotherapy or chemotherapy.

Portions of the introduction were adapted from:

Engelhard, V. H., Rodriguez, A. B., Mauldin, I. S., Woods, A. N., Peske, J. D., & Slingluff, C. L. (2018). Immune Cell Infiltration and Tertiary Lymphoid Structures as Determinants of Antitumor Immunity. The Journal of Immunology, 200(2), 432–442. https://doi.org/10.4049/jimmunol.1701269

Rodriguez, A. B., & Engelhard, V. H. (2020). Insights into Tumor-Associated Tertiary Lymphoid Structures: Novel Targets for Antitumor Immunity and Cancer Immunotherapy. Cancer Immunology Research, 8(11), 1338–1345. https://doi.org/10.1158/2326-6066.cir-20-0432

Thesis rationale

PNAd expression on intratumoral vasculature of murine melanoma is controlled by the engagement of $LT\alpha_3$ secreted by effector CD8 T cells with TNFR on TECs. PNAd expression on the tumor vasculature is substantially lower than that on LN BECs, suggesting that factors controlling the biosynthesis of this HR ligand in TECs are distinct. Thus, **Aim 1 of this thesis was to identify the differences in expression of genes associated with PNAd biosynthesis in TECs and LN BEC, and to determine which of these was also TNFR-dependent.**

Tumor vessels expressing PNAd are hallmark features of TA-TLS, and previous work from the lab demonstrated that murine melanoma growing in the subcutaneous and intraperitoneal compartments develop this vasculature. However, only the latter tumor type contains TA-TLS adjacent to vessels expressing PNAd. This suggests that the mechanisms driving TA-TLS development are different than those regulating PNAd expression on the tumor vasculature. Therefore, **Aim 2 of this thesis is to determine the cellular and molecular mechanisms regulating TA-TLS development in murine melanoma.**

The presence of TA-TLS in human tumors is usually associated with enhanced patient survival and a favorable response to cancer therapies, particularly checkpoint immunotherapy. It has been suggested that TA-TLS serve as sites for sustained generation of *in situ* antitumor immune responses that mediate tumor control, but evidence for this remains somewhat limited. Thus, **Aim 3 of this thesis is to determine whether TA- TLS support tumor control and response to checkpoint immunotherapy.**

Materials & methods

Mice

Female C57BL/6 mice were from the National Cancer Institute. Rag1$^{-/-}$, μMT$^{-/-}$, LTα$^{-/-}$, TNFR1/2$^{-/-}$, human ubiquitin C (UBC)-mCherry, and CXCR5$^{-/-}$ mice were from the Jackson Laboratory. Rag2$^{-/-}$Il2rg$^{-/-}$ mice were from Taconic Biosciences. All mice were bred and maintained on a C57BL/6 background, and kept in specific pathogen-free conditions. All experiments were carried out on female mice that were ~8-12 weeks of age. All protocols and experiments were approved by the University of Virginia Institutional Animal Care and Use Committee.

Tumor cell lines and injections

B16-F1 mouse melanoma and MC38 murine colon adenocarcinoma cells were obtained from American Type Culture Collection. The generation of B16-OVA and MC38-OVA has previously been described (Hargadon et al., 2006). B16-F1 and B16-OVA tumor cells were cultured in RPMI-1640 (Corning) supplemented to a final concentration of 10% (v/v) fetal bovine serum, 2 mM L-glutamine (ThermoFisher Scientific), and 15 mM HEPES (ThermoFisher Scientific). MC38-OVA were cultured in DMEM (Corning) supplemented to a final concentration of 10% (v/v) FBS, 2 mM L-glutamine (ThermoFisher Scientific), and 15 mM HEPES (ThermoFisher Scientific). Lewis lung carcinoma transfected to express ovalbumin (LLC-OVA) was a gift of Dr. E. Podack (University of Miami). These cells were cultured in IMDM (ThermoFisher Scientific) supplemented to a final concentration of 10% (v/v) fetal bovine serum, 2 mM L-glutamine (ThermoFisher

Scientific), and 15 mM HEPES (ThermoFisher Scientific). All cells were cultured and maintained at 37°C and 5% carbon dioxide. For tumor studies, approximately 4 x 10^5 tumor cells were I.P. or S.C. (loose neck scruff) injected into recipient mice. Both tumor types were allowed to establish for 14 days prior to harvesting.

Treatment of tumor-bearing mice

For LTβR blocking experiments, LTβR-Ig fusion protein (100 μg per injection, gift from Dr. Yang-Xin Fu, University of Texas Southwestern Medical Center) was injected I.P. into tumor-bearing mice one day prior and one day after tumor implantation, and then every four days until tumor harvest. For checkpoint immunotherapy experiments, either monotherapy anti-PDL1 (250 μg per injection, 10F.9G2, BioXcell) or dual therapy anti-PD1 (250 μg per injection, RMP1-14, BioXcell) and anti-CTLA4 (250 μg per injection, 9D9, BioXcell) was injected I.P. into tumor-bearing mice three days after tumor implantation and then every three days until tumor harvest.

Adoptive transfer of CD8 T-cells and CD19 B-cells

Lymph nodes and/or spleen were resected from either C57BL/6 or LTα$^{-/-}$ mice. Single-cell suspensions of resected lymphoid organs were prepared via Dounce homogenization. Bulk CD8 T-cells and CD19 B-cells were purified from pooled lymph nodes and/or spleen suspensions by magnetic bead isolation kits (Miltenyi Biotec) on an AutoMACS Pro Separator (Miltenyi Biotec) according to manufactures instructions. CD8 T-cells (5 x 10^6), or CD19 B-cells (5 x 10^6), or the combination were injected intravenously into Rag1$^{-/-}$ recipient mice 3 days prior to tumor implantation.

Digestion of resected tissues

For flow cytometry/cell sorting experiments, resected lymph nodes, spleen, omentum, lung, pancreas, skin, and tumors were minced and digested with a solution containing 0.1 mg/ml DNase I (Sigma), 0.8 mg/ml Collagenase Dispase (Sigma), and 0.2 mg/ml Collagenase P (Sigma) for 30 minutes at 37°C. Every 5 minutes, tissue suspensions were pipetted up-and-down several times. Digested tissues were then depleted of red blood cells by RBC Lysing Buffer Hybri-Max (Sigma) according to manufactures instructions. The concentrations specified for these digestion enzymes yield a high number of endothelial cells and fibroblasts from all tissues described above, and a high number of hematopoietic cells from tumors. Also, theses concentrations are optimized to minimize inadvertent cleaving of cell surface marker.

Enrichment of cells from digested tissues

Hematopoietic cells from digested tumor suspensions were enriched by CD45 magnetic beads (Miltenyi Biotec) on an AutoMACS Pro Separator (Miltenyi Biotec) according to manufactures instructions. A typical cell yield of $CD45^+$ cells from a B16-OVA tumor is ~1 x 10^7 per gram of tumor. In some cases, $CD45^+$ depleted suspensions were stained with α-gp38 (0.5 μg/mL) and α-CD31 (0.5 μg/mL) biotinylated antibodies for 15 minutes at 4°C. Then, endothelial cells and fibroblasts were enriched from stained $CD45^+$ depleted suspensions by anti-biotin magnetic beads (Miltenyi Biotec) on an AutoMACS Pro Separator (Miltenyi Biotec) according to manufactures instructions. A typical cell yield of TECs from S.C. and I.P. B16-OVA tumors are ~4.0 x 10^4 and ~1.5 x 10^4 per gram of tumor,

respectively. A typical cell yield of CAFs from S.C. and I.P. B16-OVA tumors are ~1.0 x 10^4 and ~5.0 x 10^4 per gram of tumor, respectively.

Flow cytometry and cell sorting

Cell surface staining was done in PBS containing 2% FBS, 2 mM EDTA (Sigma), and 2 mM NaN_3 (Sigma) for 30 minutes at 4°C. For the detection of intracellular proteins, Cytofix/Cytoperm Fixation/Permeabilization kit (BD Bioscience) or Transcription Factor Buffer Set (BD Bioscience) was used according to manufacturer's instructions. Live/Dead Aqua (Invitrogen) or 4,6-diamidino-2-phenylindole (Sigma) were used to exclude dead cells from analysis. Fibroblasts were defined as live, singlet, $Ter119^{neg}$, $CD45^{neg}$, $CD31^{neg}$, $PDPN^{hi}$ cells and endothelial cells were defined as live, singlet, $Ter119^{neg}$, $CD45^{neg}$, $PDPN^{neg}$, $CD31^{+}$. B16 tumor cells express ten-fold lower levels of PDPN. Thus, only $PDPN^{hi}$ cells were analyzed as CAFs in all experiments. Samples were run on a FACSCanto II (BD) or Attune NxT (ThermoFisher/Invitrogen) and analyzed using FlowJo Software (BD Bioscience). For qPCR experiments, pre-enriched fibroblast and/or endothelial cell populations were sorted to high purity on an Influx Cell Sorter (BD) directly into RNAlater Stabilization Solution (ThermoFischer Scientific) or PBS.

Antibodies for flow cytometry

Antibody	Vendor	Clone
eFluor 450 anti-mouse CD4	ThermoFisher	RM4-5
Brilliant Violet 605 anti-mouse PD1	Biolegend	29F.1A12
Brilliant Violet 650 anti-mouse CD62L	Biolegend	MEL-14
Brilliant Violet 785 anti-mouse CD45	Biolegend	30-F11
FITC anti-mouse TIM-3	ThermoFisher	RMT3-23
PerCP-eFluor 710 anti-mouse CD8 alpha	ThermoFisher	53-6.7

PE anti-mouse LAG-3	Biolegend	C9B7W
PE/Dazzle 594 anti-mouse CD44	Biolegend	IM7
PE-Cy7 anti-mouse Ki67	ThermoFisher	SolA15
Alexa Fluor 647 anti-mouse CD3	Biolegend	17A2
APC-Cy7 anti-mouse CD19	Biolegend	6D5
eFlour 450 anti-mouse IgM	ThermoFisher	eB121-15F9
PE/Dazzle 594 anti-mouse IgD	Biolegend	11-26c.2a
PerCP-Cy5.5 anti-mouse CD11c	Biolegend	N418
PE anti-mouse I-A/I-E (MHC II)	Biolegend	M5/114.15.2
Pacific Blue anti-mouse ICAM-1 (CD54)	Biolegend	YN1/1.7.4
Brilliant Violet 605 anti-mouse VCAM-1 (CD106)	BD Bioscience	429
Alexa Fluor 488 polyclonal Collagen Type I	SoutherBiotech	Poly
PerCP-eFlour 710 anti-mouse CD31	ThermoFisher	390
Unconjugated anti-mouse alpha smooth muscle actin	ThermoFisher	1A4
PE anti-mouse IgG2a	Biolegend	RMG2a-62
PE/Dazzle 594 anti-mouse CD140 alpha	Biolegend	APA5
PE-Cy7 anti-mouse podoplanin (gp38)	Biolegend	8.1.1
eFlour 660 anti-mouse Ki67	ThermoFisher	SolA15
Unconjugated anti-mouse FAP	Millipore	73.3
APC-Cy7 anti-mouse IgG1	Biolegend	RMG1-1
PE/Dazzle 594 anti-mouse PD-L1	Biolegend	10F.9G2
APC anti-mouse CD120 alpha (TNF R Type I/p55)	Biolegend	55R-286
Brilliant Violet 421 anti-mouse CD120 beta (TNF R Type II/p75)	BD Bioscience	TR75-89
PE/Dazzle 594 anti-mouse CD90.2 (Thy-1.2)	Biolegend	53-2.1
APC anti-mouse lymphotoxin beta receptor (LTβR)	Biolegend	5G11

S.C. tumor model with exogenous fibroblasts

B16-OVA cells were S.C. or I.P. injected into female C57BL/6 or UBC-mCherry recipient mice and allowed to establish for 14 days. Preparation of single cell suspensions from resected tumor masses is described above. Live, singlet, $Ter119^-$, $CD45^-$, $CD31^-$, $PDPN^{hi}$ CAFs from pre-enriched suspensions of bulk $PDPN^+$ CAFs/$CD31^+$ TECs were sorted to high purity on Influx Cell Sorter (BD) directly into DMEM (Corning) supplemented to a

final concentration of 10% (v/v) FBS, 2 mM L-glutamine (ThermoFisher Scientific) and 15 mM HEPES (ThermoFisher Scientific). In some cases, FAP^{+} $PDPN^{hi}$ and FAP^{neg} $PDPN^{hi}$ CAFs were purified from a pre-enriched suspension of bulk $PDPN^{+}$ CAFs/$CD31^{+}$ TECs were sorted to high purity on Influx Cell Sorter (BD) directly into DMEM (Corning) supplemented to a final concentration of 10% (v/v) FBS, 2 mM L-glutamine (ThermoFisher Scientific) and 15 mM HEPES (ThermoFisher Scientific). In all cases, B16-OVA cells (4×10^5) and purified CAFs (5×10^4) or mouse embryonic fibroblasts (5×10^4) were S.C. injected into female C57BL/6 mice. Tumor were allowed to establish for 14 days prior to harvesting.

Four-color immunofluorescence microscopy

Preparation of tumor tissue for immunofluorescence microscopy has previously been described (A.B. Rodriguez et al., 2018). Formalin fixation of tumors and cutting frozen tumor blocks on a -20°C cryostat preserves tissue morphology with few sectioning artifacts. Tumor sections were incubated in 100% methanol for 10 minutes at -20°C. Then, slides were immersed in PBS for 10 minutes at room temperature. For Fc blocking, tumor sections were incubated with 0.5 μg/mL α-CD16/32 (BioXcell; Clone:2.4G2) unconjugated antibody in PBS containing 5% BSA (Sigma) and 0.3% Triton X-100 (Sigma) for 15 minutes at room temperature. Endogenous biotin in tumor sections was blocked using the Avidin/Biotin Blocking kit (Vector Laboratories) according to manufactures instructions. Endogenous peroxidases in tumor sections were quenched with PBS containing 3% hydrogen peroxide and 0.1% (w/v) sodium azide for 45 minutes at room temperature. Tumor sections were incubated overnight at 4°C with primary

antibodies in either PBS containing 3% hydrogen peroxide and 0.1% (w/v) sodium azide or TNB Blocking Buffer (PerkinElmer) if performing tyramide signal amplification. The TSA Biotin Kit (Perkin Elmer) was used according to manufactures instructions to amplify biotinylated labelled tumor sections. Tumor sections are counterstained with fluorescently conjugated secondary antibodies and/or streptavidin in PBS containing 3% hydrogen peroxide and 0.1% (w/v) sodium azide for 2 hours at room temperature. Prior to imaging, tumor sections are mounted with ProLong Gold Antifade Mountant with or without DAPI (ThermoFisher Scientific).

Reagents for four-color immunofluorescence microscopy

Antibody	Vendor	Clone
Alexa Fluor 647 anti-mouse CD3	Biolegend	17A2
DyLight 550 Anti-Mouse/Human CD45R (B220)	Leinco Technologies (Discontinued)	RA3-6B2
Alexa Fluor 647 anti-mouse CD31	Biolegend	MEC13.3
Unconjugated anti-mouse Podoplanin (gp38)	Biolegend	8.1.1
Biotin anti-mouse/human PNAd	Biolegend	MECA-79
Alexa Fluor 488 anti-mouse CD45	Biolegend	30-F11
Biotin anti-mouse ICAM-1 (CD54)	Biolegend	YN1/1.7.4
Unconjugated anti-mouse FAP	Millipore Sigma	73.3
Alexa Fluor 647 anti-mouse VCAM-1 (CD106)	Biolegend	429
Alexa Fluor 488 AffiniPure Goat Anti-Syrian Hamster IgG	Jackson Labs	Poly
Rhodamine (TRITC) AffiniPure Goat Anti-Syrian Hamster IgG	Jackson Labs	Poly
Rhodamine (TRITC) AffiniPure Donkey Anti-Mouse IgG (H+L)	Jackson Labs	Poly
Alexa Fluor 350 Streptavidin	ThermoFisher	N/A

Four-color immunofluorescence image acquisition

For image acquisition, one section per tumor was used and all images were captured on an AxioImager with Apotome (Zeiss). Fluorescence minus one (FMO) or isotype staining controls were used to establish thresholds and exposure times to visualize positive signals while minimizing background fluorescence. B16 tumors cells express low levels of PDPN. Thus, thresholds and exposure times were set to visualize bright $PDPN^+$ cells located in the tumor parenchyma and TA-TLS regions. For tumor studies, 15-20 low magnification images per tumor section were captured and stitched together by ImageJ Software (NIH) to create an image of the entire tumor section. In these stitched images, the number and area of TA-TLS and $CD45^+PDPN^+$ clusters/aggregates were measured by ImageJ (NIH). CAF density inside and outside of TA-TLS was also measured in these stitched images by either ImageJ (NIH) or Imaris image analysis software (Bitplane). For the analysis of CAF and LTo markers on intratumoral $PDPN^+$ cells, 5 tumor parenchyma and 5 TA-TLS high powered images per a single tumor section were used, and the intensity and percentage of markers co-stained on $PDPN^+$ cells were calculated by Imaris image analysis software (Bitplane). Values across the 5 respective regional images were averaged together for each tumor section. For checkpoint immunotherapy experiments, stitched images were used to calculated the density of parenchymal T- and B-cells by ImageJ software (NIH). For image presentation, brightness and contrast were linearly adjusted and color-merged images were generated using Photoshop CS6 Software (Adobe).

Seven-color multispectral imaging

Staining of murine and human melanoma for multispectral imaging has previously been described (Mauldin, Sheybani, Young, Price, & Slingluff, 2020). In brief, 4-µm thick sections were cut from formalin fixed paraffin embedded murine tumor specimens or human melanoma biopsies, and murine spleen and human lymph node biopsies was used as a positive control. Antigen retrieval was performed using AR9 buffer (PerkinElmer) was performed according to the manufacturer's instructions. OPAL Multiplex IHC Staining (PerkinElmer) was performed according to the manufacturer's instructions. Prior to imaging, slides were mounted using prolong diamond antifade (Life Technologies).

Antibodies for seven-color multispectral imaging

Antibody	Vendor	Clone
Unconjugated anti-mouse/human Lymphotoxin alpha (LTA)	Abcam	AT15A3
Unconjugated anti-human VCAM-1	Nordic Biosite	1.4C3
Unconjugated anti-human CXCL13	Novus Biological	Poly
Unconjugated anti-human/Rat/Mouse APRIL	Abcam	EPR14588
Unconjugated anti-human gp36	Abcam	EPR22182
Unconjugated anti-human CD20	Agilent	L26
Unconjugated anti-mouse CD4	Abcam	EPR19514
Unconjugated anti-mouse CD8	Abcam	CAL38
Unconjugated anti-mouse CD19	Cell Signaling Technology	D4V4B
Unconjugated anti-human/rat/mouse CD34	Abcam	EP373Y
Unconjugated anti-mouse CD11c	Abcam	EPR21826

Seven-color multispectral image acquisition

For image acquisition, one section per human and mouse tumor was used and all images were captured on the Vectra 3.0 Automated Quantitative Pathology Imaging system

(PerkinElmer). Tumor sections were tiled scanned at low magnification, stitched together to create a whole tumor section image, and spectrally unmixed through the InForm software (PerkinElmer). Single stain positive controls were used during the spectrally unmixing process. The number and area of TA-TLS in spectrally unmixed stitched images were quantified using HALO software (Indica Labs, Albuquerque, NM). For human studies, regions of interest were identified in Phenochart Whole Slide Viewer (Akoya Bioscience), and the density of indicated populations was calculated by InForm software (PerkinElmer). For image presentation, brightness and contrast were linearly adjusted and color-merged images were generated using Photoshop CS6 Software (Adobe).

Definition of TA-TLS by immunofluorescence imaging

In I.P. tumors grown in C57BL/6, CXCR5$^{-/-}$, LTβR-Ig and checkpoint immunotherapy treated mice, and in S.C. tumors containing exogenous fibroblast populations, intratumoral TA-TLS were defined as tight aggregates of 50 or more B-cells in juxtaposition to PNAd^{+} vasculature and associated with a reticular network of elongated PDPN^{+} CAFs that are not tightly apposed to tumor endothelium (A.B. Rodriguez et al., 2018). Classical TA-TLS are defined as structures that contain tight and distinct T- and B-cells compartments. Non-classical TA-TLS are defined as structures that contain a tightly compacted B-cell compartment, but T-cells are scattered throughout the B-cell aggregate. In all cases, B-cell aggregates were used to identify the boundary of a TA-TLS.

In I.P. tumors grown in μMT$^{-/-}$, TNFR1/2$^{-/-}$, or in I.P. tumors grown in Rag1$^{-/-}$ mice repleted with bulk CD8 T-cells and/or B-cells, which lacked one or more components of TA-TLS, we identified tight aggregates of 50 or more CD45^{+} cells associated with a

network of elongated PDPN$^+$ CAFs that were not tightly apposed to tumor endothelium as evidence of TA-TLS development. In some cases, CAFs that did not form into reticular networks and were found in small, loosely organized clusters of CD45$^+$ cells were defined as non-TA-TLS structures. In both of these cases, CD45$^+$ aggregates and clusters were used to identify the boundaries of these structures.

Quantitative RT-PCR

RNA was purified from whole tumor or sorted cells using RNEasy kits (Qiagen). High-Capacity cDNA Reverse Transcription Kit (Applied Biosystems) and purified RNA was used to generate cDNA. Amplification was performed using TaqMan Fast Advanced Master Mix (Applied Biosystems) and QuantStudio 6 Flex Real-Time PCR system (Applied Biosystems) with the following program: 50°C for 2 minutes; 95°C for 2 minutes; 40 cycles of 95°C for 1 second, 60°C for 20 seconds.

Probes for quantitative RT-PCR

Probe	Vendor	Assay ID
CCL21a	ThermoFischer	Mm03646971_gH
CXCL12	ThermoFischer	Mm00445552_m1
CXCL13	ThermoFischer	Mm00444533_m1
TNFSF13 (APRIL)	ThermoFischer	Mm03809849_s1
TNFSF13b (BAFF)	ThermoFischer	Mm01218923_g1
Podocalyxin	ThermoFischer	Mm00628472_m1
CD34	ThermoFischer	Mm00519283_m1
Endomucin	ThermoFischer	Mm00497495_m1
Glycam-1	ThermoFischer	Mm00801716_m1
Nepmucin	ThermoFischer	Mm01266006_m1
GST1	ThermoFischer	Mm00490018_g1

GST2	ThermoFischer	Mm00488783_s1
GCNT1	ThermoFischer	Mm02010556_s1
B3GNT3	ThermoFischer	Mm00472247_g1
FUT7	ThermoFischer	Mm04242850_m1

Statistical Analyses

Statistical details of each experiment in this work are reported in the main and supplementary figure legends. Normality of data distribution was determined by D'Agostino-Pearson omnibus normality test and variance between groups was assessed by the *F*-test. P-values for the comparison between two or more independent groups were calculated by Welch's t-test and Kruskal-Wallis *h*-test with Dunn's post-test, respectively. For human box plot data, the Wilcoxon rank-sum test was used for non-parametric comparison of two independent groups, and P-values were corrected by controlling the False Discovery Rate (FDR) according to the method of Benjamini and Hochberg. For human correlation analysis, a linear mixed-models approach available in the R package *Correlations* (Makowski, Ben-Shachar, Patil, & Lüdecke, 2020) was used in order to account for the nested data structure (multiple data points taken from an independent tumor). For murine checkpoint immunotherapy correlation analysis, a Spearman correlation analysis with 95% confidence intervals was used for the non-parametric comparison of two independent groups. In most cases, error bars shown in graphical data represents mean ± standard deviation (S.D.) for normally distributed data or median ± IQR for non-normal data. For human box plots, error bars in data were generated using Tukey's method. $P<0.05$ was considered statistically significant. All statistics were calculated using Graph Pad Prism version 7.0, R version 4, and the SAS software suite version 9.4.

Tumor necrosis factor receptor regulation of peripheral node addressin biosynthetic components in tumor endothelial cells

Introduction

Trafficking of leukocytes, including T- and B-cells, into lymphoid and inflamed non-lymphoid tissues involves sequential interactions of a set of homing receptors (HR) on leukocytes with cognate ligands on blood endothelial cells (BEC) (Ley et al., 2007). During an immune response, effector T-cells acquire the ability to enter inflamed tissues by upregulating HRs that bind to ligands that are upregulated on activated BECs. HRs and HR ligands that are utilized for T-cell infiltration into tumors have been identified (Yamada et al., 2006; Sasaki et al., 2007; Buckanovich et al., 2008; D. T. Fisher et al., 2011; Bose et al., 2011; Mikucki et al., 2015). However, tumor endothelial cells (TEC) express HR ligands at low levels (Weishaupt et al., 2007; Clark et al., 2008; Dengel et al., 2010), and a number of studies have showed a correlation between the levels of HR ligands on the tumor vasculature and the numbers of intratumoral T-cells (Kunz et al., 1999; Garbi et al., 2004; Hensbergen et al., 2005; Musha et al., 2005; Clark et al., 2008; Quezada et al., 2008; Lohr et al., 2011). Having a better understanding of how HR ligands are regulated in TECs may provide significant opportunities to increase the number of intratumoral T-cells.

It is generally assumed that all intratumoral T-cells are effectors that differentiate in tumor-draining lymph node (LN) prior to trafficking. However, some studies have shown that naïve T-cells can directly infiltrate murine tumors that have been genetically modified to secrete homotrimeric lymphotoxin-α ($LT\alpha_3$) (Schrama et al., 2001, 2008) or

LIGHT (P. Yu et al., 2004). Similar results were also obtained through the intratumoral injection of either homeostatic chemokine CCL21 (Turnquist et al., 2007) or DCs genetically modified to express this molecule (Kirk, Hartigan-O'Connor, Nickoloff, et al., 2001). Naïve T-cells enter LNs based on their expression of L-selectin and CCR7, which bind to peripheral node addressin (PNAd) and the chemokines CCL19/CCL21, respectively. These HR ligands are normally expressed on specialized LN blood vessels called high endothelial venules (HEV). However, they have been detected in a variety of human tumors, and their presence is associated with a positive prognosis (de Chaisemartin et al., 2011; Coppola et al., 2011; Martinet et al., 2011; Cipponi et al., 2012; Martinet et al., 2012; Messina et al., 2012; Sakai, Hoshino, Kitazawa, & Kobayashi, 2014). Recently, it was demonstrated that $PNAd^+$ $CCL21^+$ vessels develop spontaneously in murine melanomas and lung carcinomas (Peske et al., 2015), and this vasculature supported the infiltration of naive T cells that significantly delayed tumor outgrowth after intratumoral activation and differentiation into functional effectors (Thompson et al., 2010; Peske et al., 2015). Thus, $PNAd^+$ $CCL21^+$ intratumoral vessels contribute to anti-tumor immunity by generating a self-sustaining infiltration of naïve T cells into the tumor mass.

PNAd is not a single protein, but refers to a multitude of mucin-domain containing scaffolding proteins, including GlyCAM-1, CD34, sgp200, podocalyxin, endomucin, and nepmucin. The crucial carbohydrate structure for L-selectin recognition is 6-sulpho sialyl Lewis X (Girard et al., 2012). This tetrasaccharide is displayed on *O*-linked glycans that primarily decorate scaffolding proteins (Rosen, 2004; Umemoto et al., 2006). Generation of 6-sulpho sialyl Lewis X involves a series of post-translational

modifications mediated by biosynthetic enzymes (Model Figure 2). Polypeptide *N*-acetylgalactosaminyltransferase 1 (GALNT1) initiates formation of the *O*-linked glycan by attaching a *N*-acetylgalactosamine (GalNAc) residue to serine and/or threonine (Ten Hagen, Fritz, & Tabak, 2003). *O*-glycans are biannternary structures consisting of Core 1 and Core 2 branches. Core 1 synthase, glycoprotein-*N*-acetylgalactosamine 3-beta-galactosyltransferase-1 (C1GALT1) creates the core 1 branch by attaching a galactose (Gal) residue to the O-linked GalNAc residue (Amado, Almeida, Schwientek, & Clausen, 1999; Yeh et al., 2001), and this branch is extended by the addition of *N*-acetylglucosamine (GlcNAc) by beta-1,3-*N*-acetylglucosaminyltransferase-3 (B3GNT3) (Yeh et al., 2001). The Core 2 branch is created by Core 2 Beta1,6 *N*-Acetylglucosaminyltransferase 1 (GCNT1), which attaches a GlcNAc residue to the *O*-linked GalNAc (L. G. Ellies et al., 1998).

The GlcNAc residues of the Core 1 and Core 2 branches are each modified in 3 additional ways. *N*-acetylglucosamine 6-O-sulfotransferase-1 (GST1) and -2 (GST2) attach sulfate onto the Core 1 and Core 2 GlcNAc, although the former sulfotransferase catalyzes this modification more efficiently than the latter (Hemmerich et al., 2001; Uchimura et al., 2004; H. Kawashima et al., 2005; Uchimura et al., 2005). Alpha-(1,3)-fucosyltransferase-4 (FUT4) (Homeister et al., 2001) and -7 (FUT7) (Malý et al., 1996) attach fucose to both Core 1 and Core 2 GlcNAcs. Finally, beta-1,4-galactosyltransferase (B4GALT) attaches Gal residues to GlcNAc in both branches (Asano et al., 2003), which are then further modified by CMP-N-acetylneuraminate-beta-galactosamide-alpha-2,3-sialyltransferase 1 (ST3GAL1) (Priatel et al., 2000), 4 (ST3GAL4) (Lesley G. Ellies et al.,

Model 2: Biosynthesis of peripheral node addressin in lymph node blood endothelial cells

PNAd is not a single protein, but refers to a multitude of mucin-domain containing scaffolding proteins, including GlyCAM-1, CD34, sgp200, podocalyxin, endomucin, and nepmucin. The crucial carbohydrate structure for L-selectin recognition is 6-sulpho sialyl Lewis X. Scaffolding proteins undergo as series of post-translational modification for the biosynthesis of this structure. Biosynthetic enzyme GALNT1 initiates *O*-glycan carbohydrate by adding a GalNAc to serine/threonine resides in scaffolding proteins. C1GALT1 extends the Core 1 branch by adding a Gal to GalNAc. GCNT1 construct the Core 2 branch by adding a GlcNAc to GalNAc. Likewise, GlcNAc is added to Gal in the Core 1 branch by B3GNT3. In both branches, GST1 and GST2 adds a sulfate to GlcNAc, although the former is more efficient at doing this than the latter. FUT4 and FUT7 also adds fucose to GlcNAc. B4GALT adds a Gal to GlcNAc in both branches, and ST3GAL1, ST3GAL4, ST3GAL6 adds a NeuAc to cap Gal in both branches. This final construct is not capable of engaging with L-selectin on naïve lymphocytes. ***Image created with BioRender.com***.

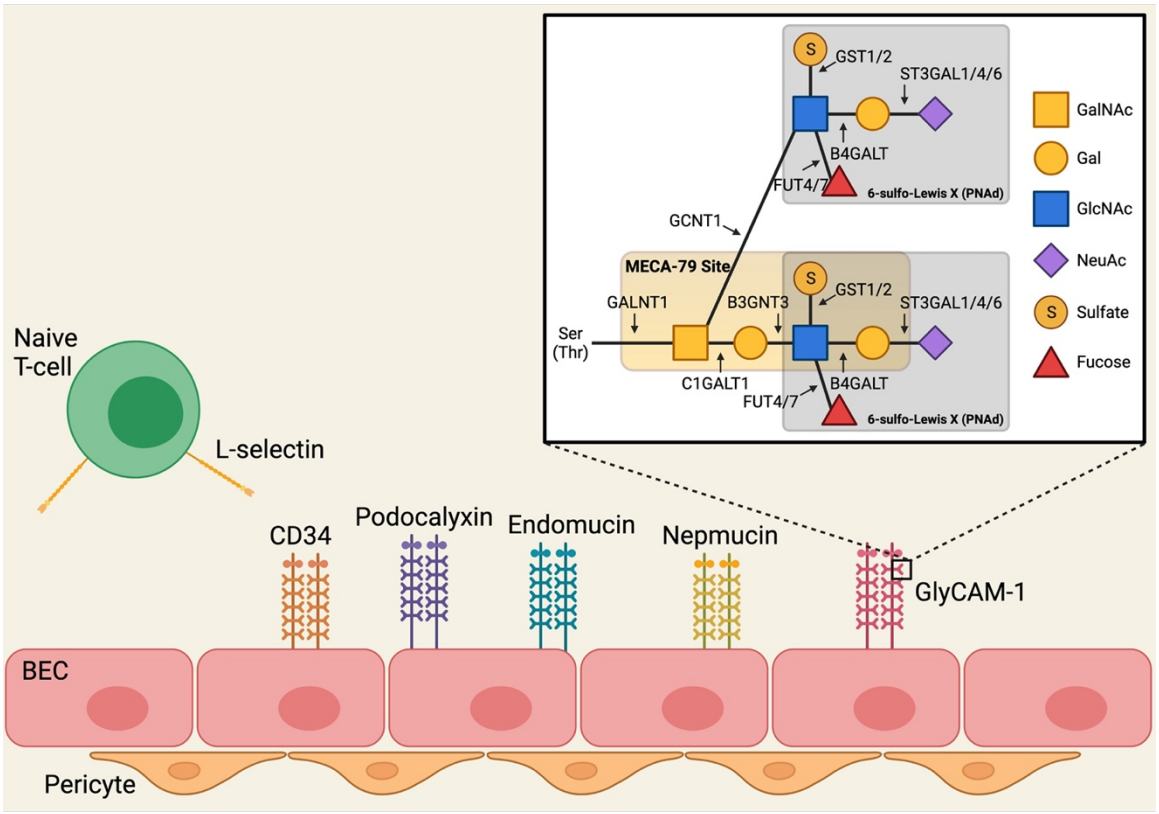
S
GST1/2
ST3GAL1/4/6
B4GALT
FUT4/7
6-sulfo-Lewis X (PNAd)
GCNT1
MECA-79 Site
GALNT1
B3GNT3
Ser
(Thr)
C1GALT1
GalNAc
Gal
GlcNAc
NeuAc
Sulfate
Fucose
Naive
T-cell
L-selectin
CD34
Podocalyxin
Endomucin
Nepmucin
GlyCAM-1
BEC
Pericyte

2002), and 6 (ST3GAL6) (W. H. Yang, Nussbaum, Grewal, Marth, & Sperandio, 2012), which attach *N*-acetylneuraminic acid (NeuAc) to Gal. This completes formation of the 6-sulpho sialyl Lewis X structure.

In adult LNs, transcript levels for scaffolding protein GlyCAM-1, and post-translational modification enzymes GST1, GST2, FUT7, GCNT1, and B3GNT3 are highly expressed in $PNAd^+$ BECs than in those lacking PNAd, while CD34, podocalyxin, endomucin, and nepmucin are expressed comparably between the two populations (Mike Lee et al., 2014; Veerman, Tardiveau, Martins, Coudert, & Girard, 2019). Expression of GlyCAM-1, GST1, GST2, FUT7, and GCNT1 is also dependent on continuous engagement of the lymphotoxin-β receptor (LTβR) expressed on LN BECs with lymphotoxin-$\alpha_1\beta_2$ ($LT\alpha_1\beta_2$) expressed on DCs (Browning et al., 2005; Moussion & Girard, 2011; Veerman et al., 2019). GST1 (Tjew et al., 2005) and GST2 (Pablos et al., 2005) can also be induced respectively in cultured monocytes and endothelial cells by TNFα. However, CD34, podocalyxin, endomucin, nepmucin and B3GNT3 in LN BECs are regulated independently of LTβR signaling through an unknown pathway (Veerman et al., 2019).

Previous work from this lab demonstrated that PNAd expression on TECs in murine melanoma was not mediated by LTβR signaling, and was instead controlled by effector CD8 T cells secreting $LT\alpha_3$, which signaled through TNF receptors (TNFR) expressed on TECs (Peske et al., 2015). In this report, it was determined that TECs expressed key PNAd biosynthetic enzymes and scaffolding proteins normally found in LN BECs, albeit at lower levels. We also determined the mechanisms by which TNFR regulated their expression and

that checkpoint immunotherapy augments PNAd expression on the tumor vasculature. These findings provide significant insight into the basis for PNAd biosynthesis in TECs.

Results

PNAd is expressed at substantially lower levels on tumor endothelial cells than on lymph node blood endothelial cells

Previous work from the lab demonstrated by immunofluorescence microscopy (IF) that transplantable murine tumors growing intraperitoneally (I.P.) and subcutaneously (S.C.) develop $CD31^+$ blood vessels that express PNAd (Peske et al., 2015). Tyramide signal amplification is a highly sensitive method enabling the detection of low-abundance targets in IF, such as PNAd on the tumor vasculature. For example, in unamplified LN sections, ~30% of $CD31^+$ BEC pixels co-stained with PNAd. In contrast, less than 2% of $CD31^+$ TEC pixels in unamplified tumor sections stained for PNAd. Staining intensity of PNAd on TECs was also significantly lower compared to PNAd intensity on $CD31^+$ BECs in unamplified LN sections, suggesting the protein levels of this HR ligand on the tumor vasculature is substantially lower compared to that on LN HEVs (Figure 1A-B). I.P. tumors contained a significantly larger fraction of TECs that stained for PNAd than S.C. tumors, and PNAd staining intensity was also significantly higher. In tyramide signal amplified sections, ~50% of $CD31^+$ BEC pixels in LNs co-stained for PNAd, while ~4% and ~1.6% of $CD31^+$ TEC pixels in I.P. and S.C. tumors stained for PNAd, respectively (Figure 1A-1B). Similar to unamplified sections, PNAd staining intensity on TECs in tyramide signal amplified tumor sections was significantly lower relative to PNAd on $CD31^+$ BEC in LN amplified sections, although PNAd intensity on $CD31^+$ TECs was significantly higher in

Figure 1: PNAd expression is significantly lower on tumor-associated endothelium than on lymph node endothelium

Wild-type (WT) mice were subcutaneously (S.C.) or intraperitoneally (I.P.) injected with B16-OVA cells. Tumors were harvested 14 days after tumor implantation. Lymph nodes (LNs) were harvested from non-tumor-bearing mice. Resected tissues were prepared for immunofluorescence microscopy (IF) (A-B) or flow cytometry (C) as described in Methods. (A) Representative images of unamplified and tyramide signal amplified LN and tumor sections stained with indicated markers. Scale bar = 100 μm. (B) Quantitative image summary data for unamplified and amplified tissue sections. PNAd percentages and pixel intensities were calculated on a $CD31^{+}$ mask. Data represents two experiments, n = 8 sections per group. (C) Representative flow cytometry plot, percentages, and geometric mean fluorescence (gMFI) intensities of PNAd on $CD45^{neg}$ $Ter119^{neg}$ $PDPN^{neg}$ $CD31^{+}$ endothelial cells in $CD45^{+}$ depleted LN and I.P. tumors suspensions. PNAd gMFIs were calculated on cells gated above the fluorescence minus one (FMO) control. Data represents one experiment, n = 5 LNs or tumors per group. (B-C) Results are mean ± standard deviation (SD) analyzed by unpaired Welch's t-test. ns: $p>0.05$, *$p<0.05$, **$p<0.01$, ***$p<0.001$, and ****$p<0.0001$.

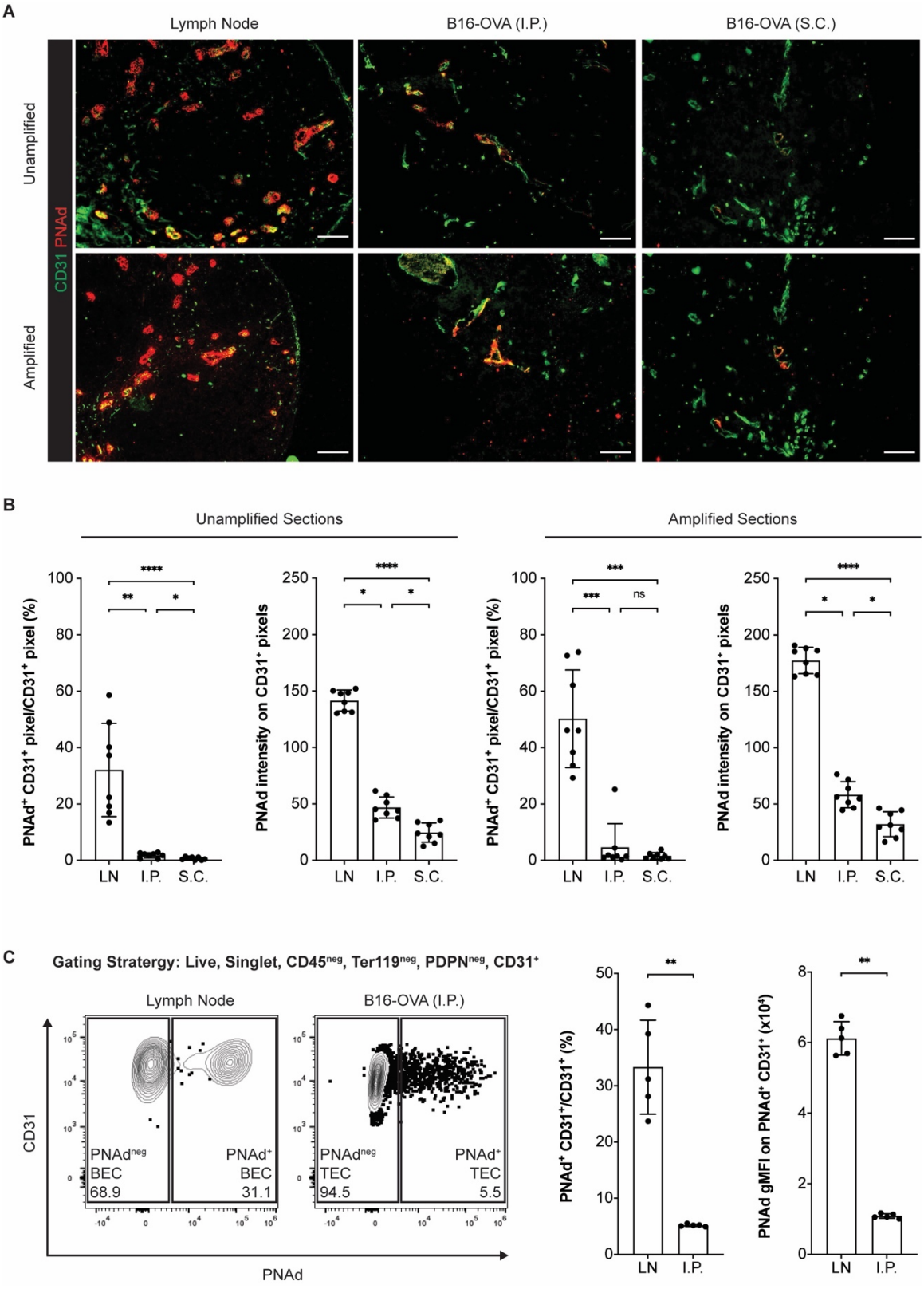
A
Lymph Node
B16-OVA (I.P.)
B16-OVA (S.C.)
Unamplified
Amplified
CD31 PNAd
B
Unamplified Sections
Amplified Sections
PNAd+ CD31+ pixel/CD31+ pixel (%)
PNAd intensity on CD31+ pixels
LN
I.P.
S.C.
ns
C
Gating Stratergy: Live, Singlet, CD45neg, Ter119neg, PDPNneg, CD31+
Lymph Node
B16-OVA (I.P.)
CD31
PNAd
PNAdneg BEC 68.9
PNAd+ BEC 31.1
PNAdneg TEC 94.5
PNAd+ TEC 5.5
PNAd+ CD31+/CD31+ (%)
PNAd gMFI on PNAd+ CD31+ (x10⁴)

I.P. amplified sections than in S.C. amplified sections (Figure 1A-1B). Flow cytometry has the capacity to detect low-abundant targets on cells without tyramide signal amplification. Thus, this approach was utilized to determine the relative protein levels of PNAd on TECs compared to LN BECs. The expression of PNAd on I.P. TECs depends on CD8 T-cells and TNFR signaling, while its expression on S.C. TECs is more complex. Thus, I.P. TECs were used to determine the relative levels of PNAd on these cells compared to LN BECs. By flow cytometry, PNAd was expressed at a uniformly high levels on ~30% of LN $CD31^+$ BECs. In contrast, ~5% of I.P. $CD31^+$ TECs stained for PNAd, and the geometric mean fluorescence intensity (gMFI) of PNAd on these cells was significantly lower and more variable relative to LN $PNAd^+$ BECs (Figure 1C). Overall, the production of PNAd in TECs from I.P. tumors is greater than those in S.C. tumors, but TECs in general express PNAd at substantially lower levels relative to LN BECs.

Low expression of PNAd on tumor endothelial cells is associated with low expression of both biosynthetic enzymes and scaffolding proteins

The low level of PNAd on tumor vasculature suggests that TECs might express low levels of PNAd biosynthetic enzymes or scaffolding proteins. We flow sorted $PNAd^+$ and $PNAd^{neg}$ cells from I.P. tumors and LNs, and evaluated expression of these molecules by quantitative PCR (qPCR). Consistent with other work (Mike Lee et al., 2014; Veerman et al., 2019), GCNT1, B3GNT3, GST1, GST2, and FUT7 were expressed at significantly higher levels in $PNAd^+$ LN BEC than in those lacking PNAd (Figure 2A). All of these enzymes were similarly expressed at higher levels in $PNAd^+$ TECs than in $PNAd^{neg}$ TECs. With the exception of FUT7, which was expressed ~17-fold lower in $PNAd^{neg}$ TEC relative

to PNAd^{neg} LN BEC, the expression levels of the remaining biosynthetic enzymes were insignificantly different between the two endothelial types (Figure 2B). However, the expression of biosynthetic enzymes in PNAd^{+} TEC was significantly lower than in PNAd^{+} LN BEC. GCNT1, B3GNT3, GST1, and FUT7 were expressed ~2-7-fold lower in PNAd^{+} TECs than in PNAd^{+} BEC, consistent with the 6-fold lower gMFI of surface PNAd on PNAd^{+} TECs (Figure 1C). However, GST2 expression was ~42-fold lower in PNAd^{+} TECs relative to PNAd^{+} BECs. GST2 is a significant sulfotransferase for the generation of 6-sulpho sialyl Lewis X on *O*-glycan structures in LN HEVs (Hemmerich et al., 2001; Uchimura et al., 2004; H. Kawashima et al., 2005; Uchimura et al., 2005). Based on these reports, this suggests that there is limited sulfonation on the Core 1 GlcNAc residue in *O*-glycans attached to TECs, which may further limit the number of the 6-sulpho sialyl Lewis X for L-selectin binding.

Transcript levels for scaffolding proteins CD34 and endomucin were comparable between LN BECs and TECs, regardless of whether they expressed PNAd (Figure 3A-B). Similarly, podocalyxin was comparably expressed between PNAd^{neg} and PNAd^{+} cells from LNs and I.P. tumors, although the transcript levels for this molecule were significantly less in TECs relative to LN BECs. On the other hand, GlyCAM-1 and nepmucin were more highly expressed in PNAd^{+} cells than in PNAd^{neg} cells in both LN BECs and TECs, although they were expressed at significantly lower levels in TECs than in LN BEC (Figure 3A-B). The 2-7-fold relative differences in expression of podocalyxin, GlyCAM-1, and nepmucin between PNAd^{+} LN BECs and PNAd^{+} TECs is again consistent with the lower cell surface expression of PNAd. Collectively, these results suggest that the low level of

Figure 2: Biosynthetic enzymes are expressed at significantly lower levels in PNAd$^+$ TECs than in LN PNAd$^+$ BECs

WT mice were I.P. injected with B16-OVA cells and tumors were harvested 14 days after implantation. LNs were harvested from non-tumor-bearing mice. (A-B) Purification of endothelial cells from CD45$^+$ depleted LN and I.P. tumors suspensions, and the expression levels of indicated RNA transcripts were determined by quantitative PCR (qPCR) as described in Methods. Data from one experiment presented as $2^{-\Delta CT}$ relative to *Hprt*, n=5 LNs or I.P. tumors per group. (A-B) Results are mean ± SD analyzed by unpaired Welch's t-test. ns: $p>0.05$, *$p<0.05$, **$p<0.01$, ***$p<0.001$, and ****$p<0.0001$.

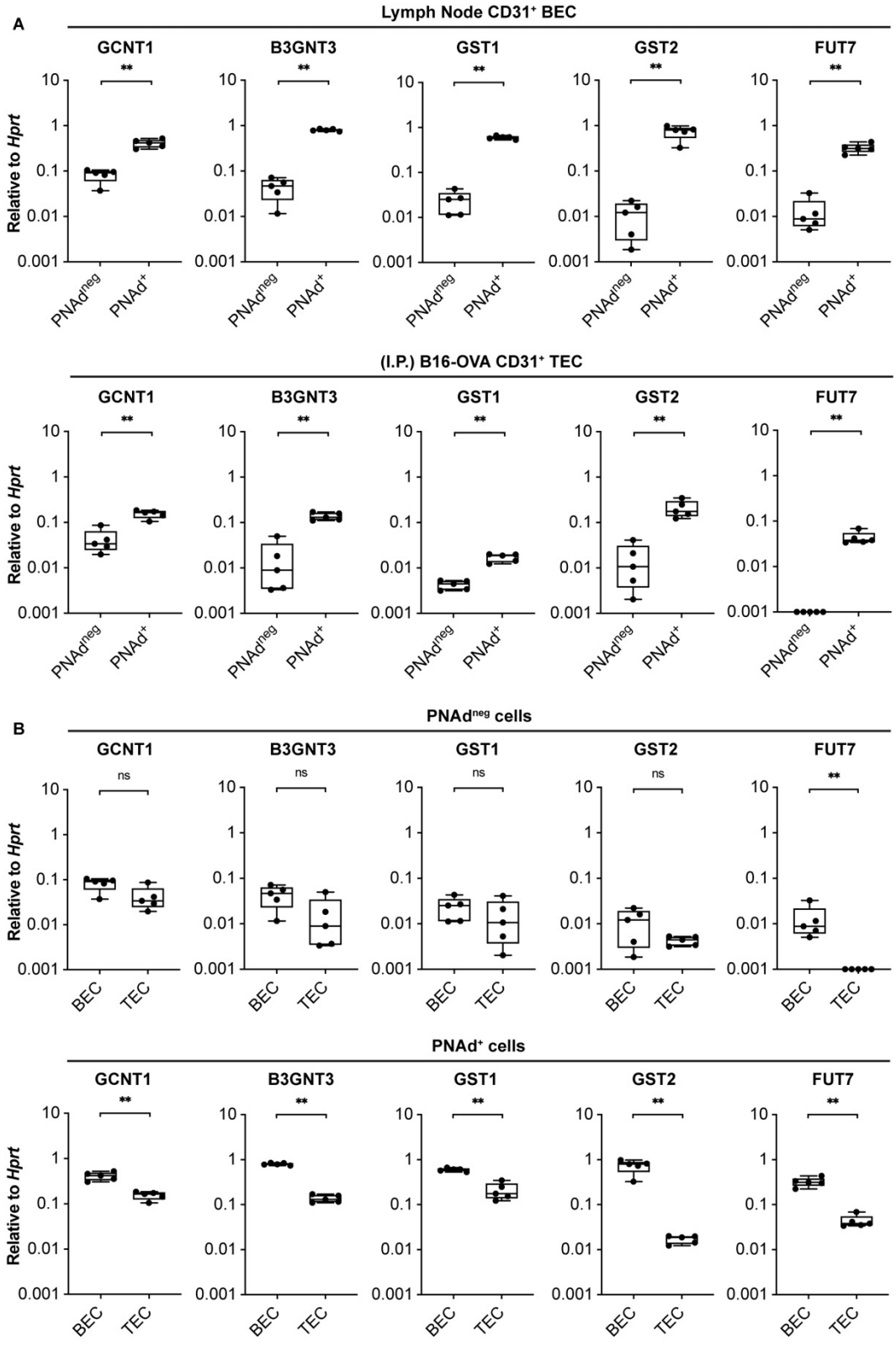
A
Lymph Node CD31+ BEC
GCNT1
B3GNT3
GST1
GST2
FUT7
**
Relative to Hprt
10
1
0.1
0.01
0.001
PNAdneg
PNAd+
(I.P.) B16-OVA CD31+ TEC
B
PNAdneg cells
ns
BEC
TEC
PNAd+ cells

Figure 3: Scaffolding proteins are expressed at significantly lower levels in PNAd$^+$ TECs than in LN PNAd$^+$ BECs

WT mice were I.P. injected with B16-OVA cells and tumors were harvested 14 days after implantation. LNs were harvested from non-tumor-bearing mice. (A-B) Purification of endothelial cells from CD45$^+$ depleted LN and I.P. tumors suspensions, and the expression levels of indicated RNA transcripts were determined by qPCR as described in Methods. Data from one experiment presented as $2^{-\Delta CT}$ relative to *Hprt*, n=5 LNs or I.P. tumors per group. (A-B) Results are mean ± SD analyzed by unpaired Welch's t-test. ns: $p>0.05$, *$p<0.05$, **$p<0.01$, ***$p<0.001$, and ****$p<0.0001$.

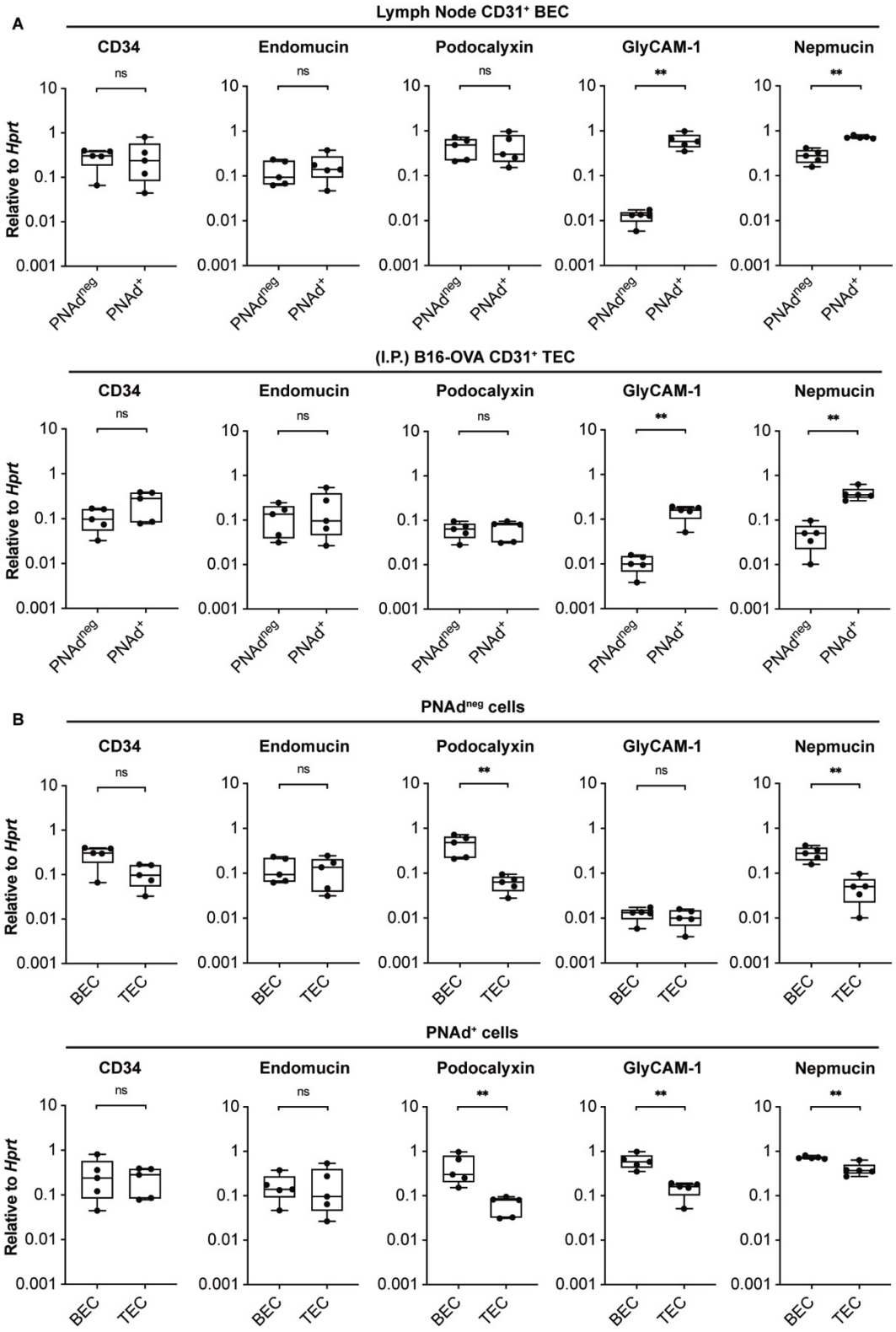
A
Lymph Node CD31+ BEC
CD34
Endomucin
Podocalyxin
GlyCAM-1
Nepmucin
ns
**
Relative to Hprt
10
1
0.1
0.01
0.001
PNAdneg
PNAd+
(I.P.) B16-OVA CD31+ TEC
B
PNAdneg cells
BEC
TEC
PNAd+ cells

expression of PNAd on TECs is a consequence of low-level expression of multiple scaffolding proteins and biosynthetic enzymes, and the substantial differential reduction in GST2 expression could also affect PNAd structure development.

Tumor necrosis factor receptor signaling regulates the transcript levels of some scaffolding proteins and biosynthetic enzymes in tumor endothelial cells.

PNAd expression on LN BECs depends on signaling through LTβR (Browning et al., 2005; Moussion & Girard, 2011; Peske et al., 2015) but not TNFR (Figure 4). In contrast, PNAd is not detected on the vasculature of I.P. tumors grown in TNFR1/2$^{-/-}$ mice, and its expression does not depend on LTβR signaling (Peske et al., 2015). However, by flow cytometry, a small percentage of TECs from I.P. tumors grown in TNFR1/2$^{-/-}$ mice retained PNAd, although their surface expression level was lower than that of TEC from wild-type (WT) mice (Figure 4). This suggests that PNAd expression in a majority of TECs depends on TNFR signaling, while a small subset of TECs depend on an alternative signaling pathway for PNAd expression. Using these cells, we determined how the loss of TNFR signaling altered expression of genes involved in PNAd biosynthesis. As expected from Figure 5, this did not alter expression of either biosynthetic enzymes (Figure 5A) or scaffolding proteins (Figure 6A) in PNAd^{neg} and PNAd^{+} LN BEC. Similarly, PNAd^{neg} TECs from I.P. tumors grown in TNFR1/2$^{-/-}$ mice did not show a reduction in the expression in either biosynthetic enzymes (Figure 5A) or scaffolding proteins (Figure 6A), although the expression of GCNT1 increased. In the small subset of PNAd^{+} TECs from I.P. tumors grown in TNFR1/2$^{-/-}$ mice, GST1 was 7-fold lower, while no other biosynthetic enzyme, including GST2, was significantly changed (Figure 5B). Also, podocalyxin and

Figure 4: Tumor necrosis factor receptor signaling controls PNAd expression in a large subset of TECs but not in LN BECs

WT or TNFR1/2$^{-/-}$ mice were I.P. injected with B16-OVA cells and tumors were harvested 14 days after implantation. LNs were harvested from non-tumor-bearing mice. Resected tissues were prepared for flow cytometry as described in Methods. Representative flow cytometry plot, percentages, and gMFI of PNAd on CD45^{neg} Ter119^{neg} PDPN^{neg} CD31^{+} endothelial cells in CD45^{+} depleted LN and I.P. tumors suspensions. PNAd gMFIs were calculated on cells gated above FMO control. Data represents one experiment, n = 5 LNs or tumors per group. Results are mean ± SD analyzed by unpaired Welch's t-test. ns: $p>0.05$, *$p<0.05$, **$p<0.01$, ***$p<0.001$, and ****$p<0.0001$.

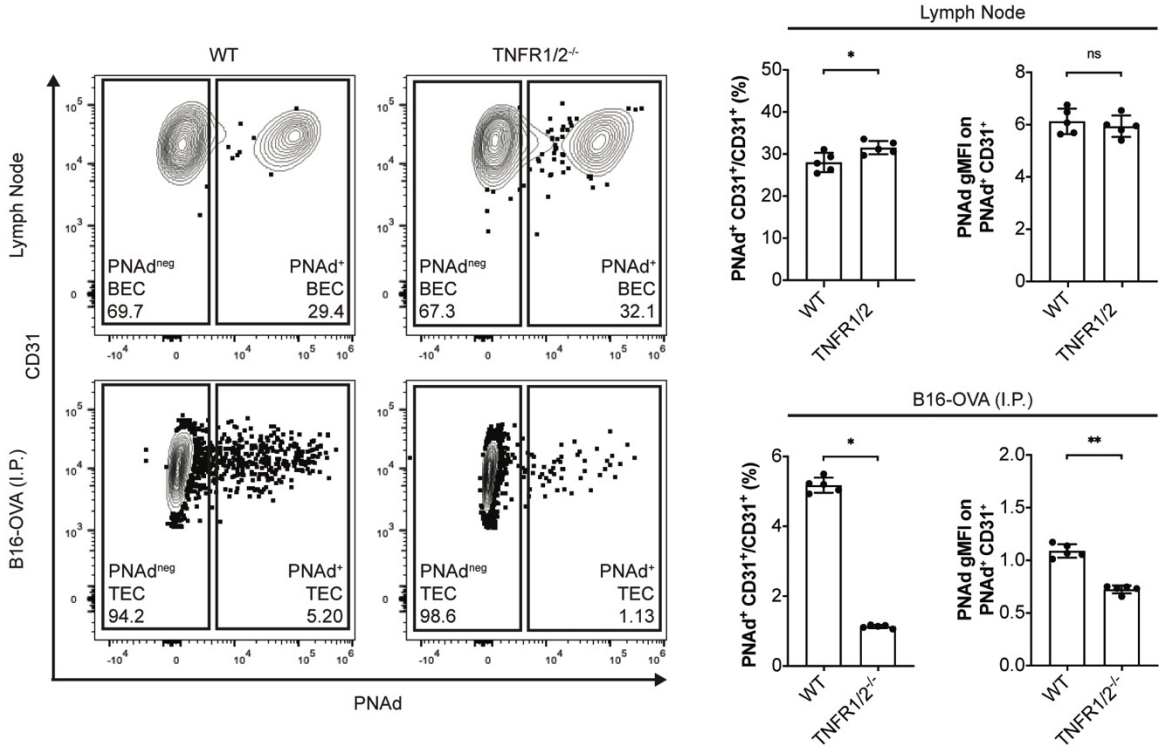
WT
TNFR1/2-/-
Lymph Node
B16-OVA (I.P.)
CD31
PNAd
PNAdneg BEC 69.7
PNAd+ BEC 29.4
PNAdneg BEC 67.3
PNAd+ BEC 32.1
PNAdneg TEC 94.2
PNAd+ TEC 5.20
PNAdneg TEC 98.6
PNAd+ TEC 1.13
Lymph Node
PNAd+ CD31+/CD31+ (%)
PNAd gMFI on PNAd+ CD31+
ns
WT
TNFR1/2
B16-OVA (I.P.)
TNFR1/2-/-

Figure 5: Tumor necrosis factor receptor signaling regulates GST1 expression in PNAd^{+} TECs

WT or TNFR1/2$^{-/-}$ mice were I.P. injected with B16-OVA cells and tumors were harvested 14 days after implantation. LNs were harvested from non-tumor-bearing mice. (A-B) Purification of endothelial cells from CD45^{+} depleted LN and I.P. tumors suspensions, and the expression levels of indicated RNA transcripts were determined by qPCR as described in Methods. Data from one experiment presented as $2^{-\Delta CT}$ relative to *Hprt*, n=5 LNs or I.P. tumors per group. (A-B) Results are mean ± SD analyzed by unpaired Welch's t-test. ns: $p>0.05$, *$p<0.05$, **$p<0.01$, ***$p<0.001$, and ****$p<0.0001$.

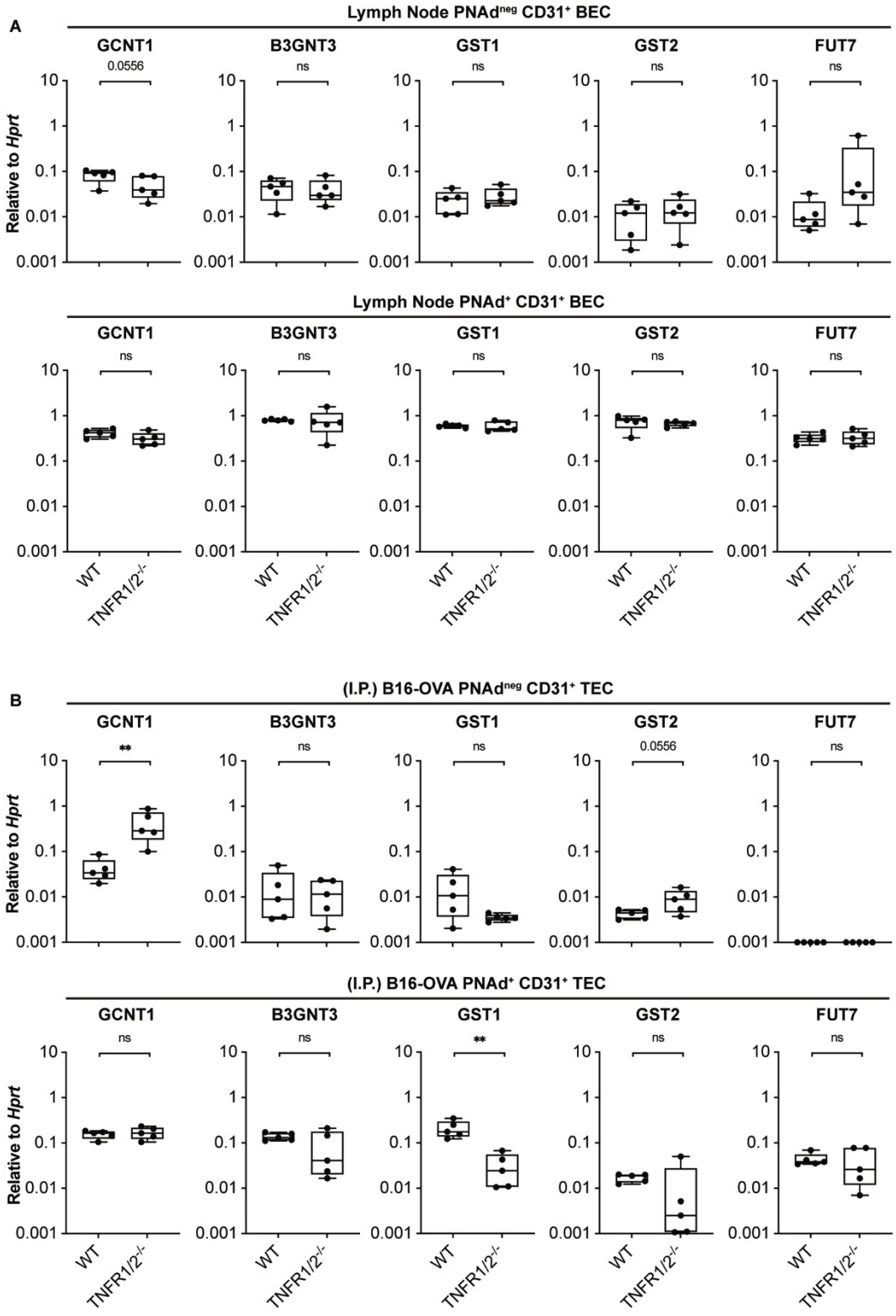
A
Lymph Node PNAd^neg CD31^+ BEC
GCNT1
B3GNT3
GST1
GST2
FUT7
0.0556
ns
Relative to Hprt
10
1
0.1
0.01
0.001
Lymph Node PNAd^+ CD31^+ BEC
WT
TNFR1/2^-/-
B
(I.P.) B16-OVA PNAd^neg CD31^+ TEC
**
(I.P.) B16-OVA PNAd^+ CD31^+ TEC

Figure 6: Tumor necrosis factor receptor signaling regulates podocalyxin and nepmucin expression in PNAd^{+} TECs

WT or TNFR1/2$^{-/-}$ mice were I.P. injected with B16-OVA cells and tumors were harvested 14 days after implantation. LNs were harvested from non-tumor-bearing mice. (A-B) Purification of endothelial cells from CD45^{+} depleted LN and I.P. tumors suspensions, and the expression levels of indicated RNA transcripts were determined by qPCR as described in Methods. Data from one experiment presented as $2^{-\Delta CT}$ relative to *Hprt*, n=5 LNs or I.P. tumors per group. (A-B) Results are mean ± SD analyzed by unpaired Welch's t-test. ns: $p>0.05$, *$p<0.05$, **$p<0.01$, ***$p<0.001$, and ****$p<0.0001$.

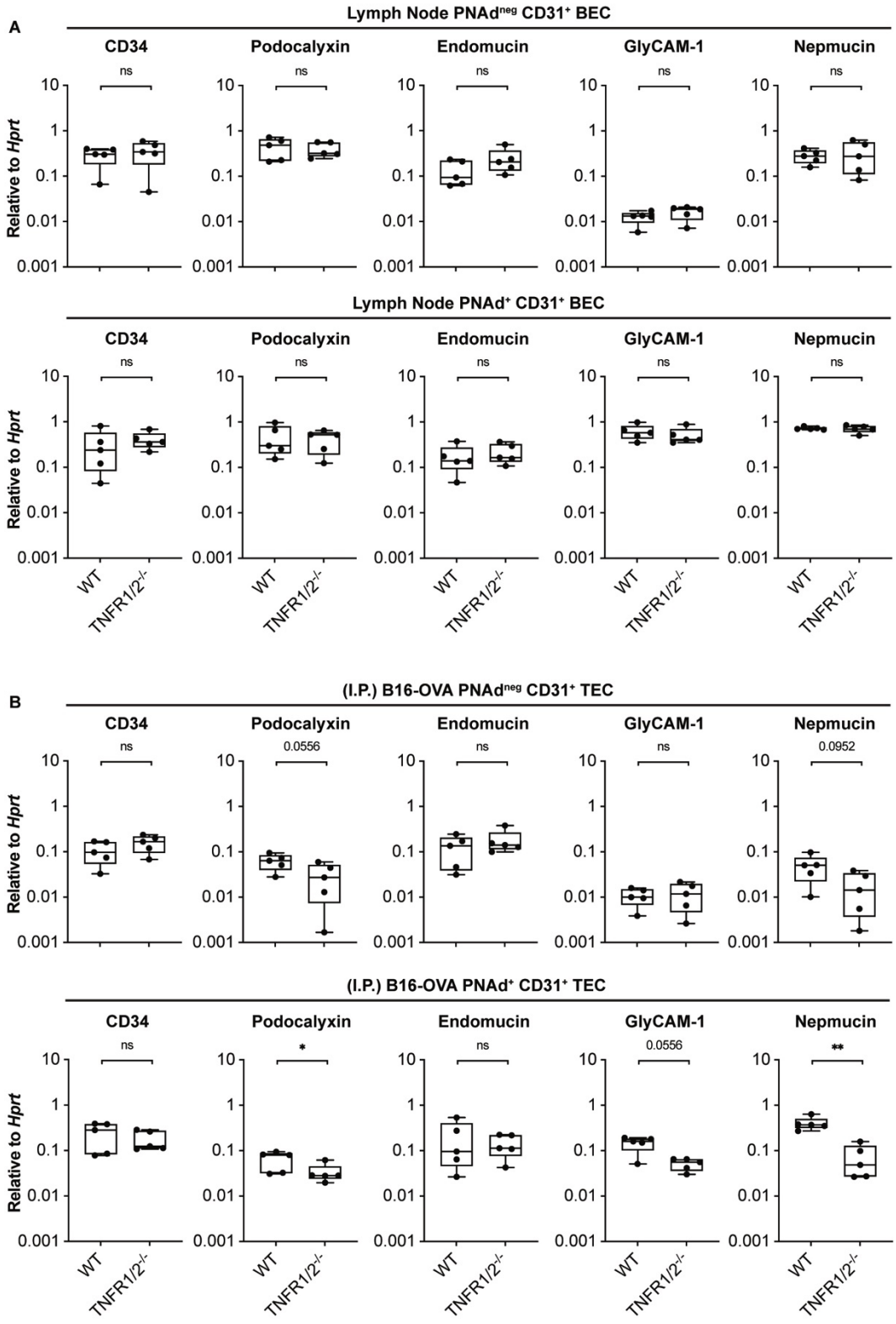
A
Lymph Node PNAd^neg CD31+ BEC
CD34
Podocalyxin
Endomucin
GlyCAM-1
Nepmucin
ns
Relative to Hprt
10
1
0.1
0.01
0.001
Lymph Node PNAd+ CD31+ BEC
WT
TNFR1/2-/-
B
(I.P.) B16-OVA PNAd^neg CD31+ TEC
0.0556
0.0952
(I.P.) B16-OVA PNAd+ CD31+ TEC
*
**

nepmucin expression was lower by 2- and 6-fold, respectively (Figure 6B). These results demonstrate that TNFR signaling selectively upregulates podocalyxin, nepmucin, and GST1, all of which are also elevated in $PNAd^{+}$ cells vs $PNAd^{neg}$ cells from WT mouse tumors. GST1 has been shown to synthesize the PNAd antibody bindings site in the Core 1 *O*-glycan branch, although this sulfotransferase does this less efficiently than GST2 (Hemmerich et al., 2001; Uchimura et al., 2004; H. Kawashima et al., 2005; Uchimura et al., 2005). This suggests the reduced surface levels of PNAd on TECs derived from $TNFR1/2^{-/-}$ mouse tumors is likely due to the reduced levels of GST1 or other biosynthetic enzymes that contribute to the formation of the MECA-79 binding site.

Checkpoint immunotherapy augments PNAd expression on I.P. tumor vasculature

Checkpoint immunotherapy has achieved impressive success in the treatment of different cancer types. This therapy type has also been associated with enhanced expression of HR ligands on the tumor vasculature, such as ICAM-1 and VCAM-1 (Hailemichael et al., 2018; Taggart et al., 2018). Thus, we determined whether checkpoint immunotherapy altered the expression of PNAd on the tumor vasculature. We treated I.P. tumor-bearing WT mice with either anti-PDL1 monotherapy or the combination of anti-CTLA4 and anti-PD1, and analyzed PNAd expression on the tumor vasculature after 14 days of outgrowth. Both treatments significantly increased the percentage of $CD31^{+}$ TEC pixels co-stained with PNAd (Figure 7A-B). Also, the staining intensity of PNAd on $CD31^{+}$ TEC pixels was significantly higher in treated tumors relative to control tumors. Since PNAd expression in I.P. tumors depend on effector CD8 T-cells secreting $LT\alpha^{3}$ (Peske et al., 2015), these

Figure 7: Checkpoint immunotherapy augments PNAd expression on I.P. tumor vasculature

WT mice were I.P. injected with B16-OVA cells and tumor-bearing mice were treated with control IgG, anti-PDL1, or anti-CTLA4/PD1 beginning 3 days after implantation. Tumors were harvested 14 days after implantation and prepared for IF as described in Methods. (A) Representative images of tyramide signal amplified tumor sections stained with indicated markers. Scale bar = 100 μm. (B) Quantitative image summary data for amplified tissue sections. PNAd percentages and pixel intensities were calculated on a $CD31^+$ mask. Data represents three experiments, n = 15 individual sections per group. (B) Results are mean ± SD analyzed by unpaired Welch's t-test. ns: $p>0.05$, *$p<0.05$, **$p<0.01$, ***$p<0.001$, and ****$p<0.0001$.

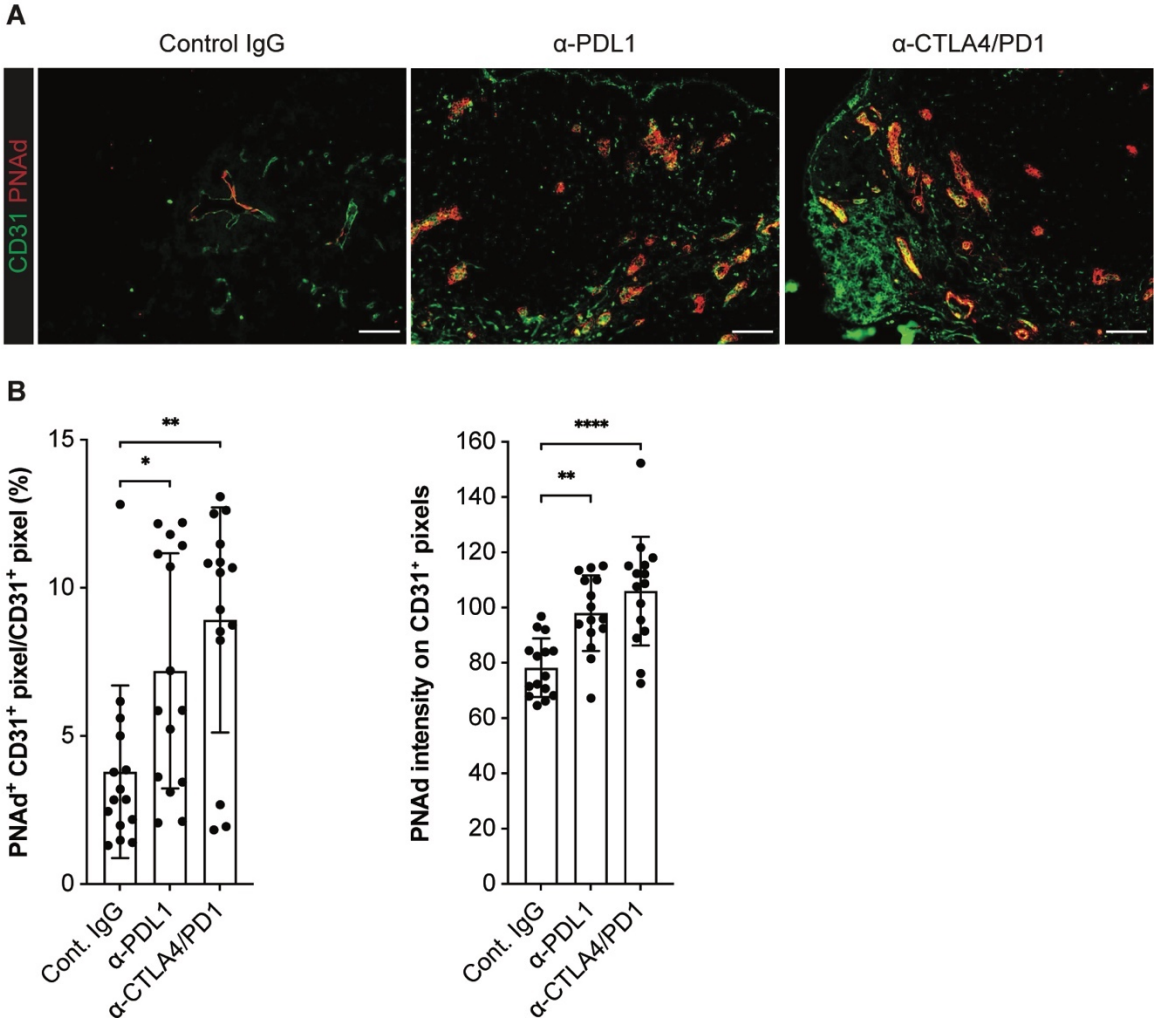
A
Control IgG
α-PDL1
α-CTLA4/PD1
CD31 PNAd
B
PNAd+ CD31+ pixel/CD31+ pixel (%)
15
10
5
0
*
**
Cont. IgG
α-PDL1
α-CTLA4/PD1
PNAd intensity on CD31+ pixels
160
140
120
100
80
60
40
20
0
**
****
Cont. IgG
α-PDL1
α-CTLA4/PD1

results suggest that checkpoint immunotherapy augments the representation of these cells in tumors, which in turn enhances the expression of PNAd associated components.

Discussion

In this report, we identified both scaffolding proteins and post-translational modification enzymes potentially used for the biosynthesis of PNAd in TECs. We showed that the expression profile of these molecules in $PNAd^+$ TECs is similar to that in LN $PNAd^+$ BECs, albeit at significantly lower levels. This observation is consistent with the low-level detection of PNAd on the tumor endothelium. Previously, we demonstrated that PNAd expression on the tumor vasculature was controlled by a mechanism involving intratumoral effector CD8 T-cells secreting $LT\alpha_3$, which in turn signaled through TNFR on TECs (Peske et al., 2015). Here, we showed that TNFR signaling controls the expression of scaffolding proteins podocalyxin and nepmucin, and post-translational modification enzyme GST1. Finally, we showed that the percentage of $PNAd^+$ TECs and their surface expression level were increased by checkpoint immunotherapy treatment. This work provides insight into the mechanisms regulating PNAd biosynthesis in TECs, and provides a platform to enhance its expression to support a continual influx of naïve cells, sustaining anti-tumor immunity.

Our results provide mechanistic insight into biosynthesis of 6-sulfo-sialyl Lewis X on TECs. We found that B3GNT3, GCNT1, GST1, GST2, and FUT7 were all are expressed at higher levels in $PNAd^+$ TECs relative to their $PNAd^{neg}$ counterpart. This is consistent with their elevated expression in $PNAd^+$ LN BECs previously reported (Mike Lee et al., 2014; Veerman et al., 2019), and their essential roles in PNAd biosynthesis in

these cells (Rosen, 2004). However, while GST1 and GST2 were comparably expressed in PNAd^{+} LN BECs, GST2 was significantly under expressed relative to GST1 in PNAd^{+} TECs. This suggests that GST1 is largely responsible for synthesizing 6-sulfo-sialyl Lewis X in TECs. Previous studies using knockout mice have established that GST1 and GST2 play complementary and partially redundant roles in PNAd expression in LNs. However, GST2 knockout mice have a more significant effect relative to GST1, at least in part because it promotes luminal rather than abluminal expression of PNAd on HEVs (Hemmerich et al., 2001; Uchimura et al., 2004). Work from the lab has previously demonstrated that PNAd is detected at both the luminal and abluminal surfaces of the tumor vasculature (Peske et al., 2015), suggesting that GST2 is driving luminal PNAd expression despite its substantially low levels in TECs. The MECA-79 antibody used in this work detects 6-sulfo-sialyl Lewis X in the Core 1, but not Core 2, *O*-glycan biantennary branch (Yeh et al., 2001). Since GST2 mediates GlcNAc sulfation only on the core 2 branch (Rosen, 2004; Uchimura & Rosen, 2006), this suggests that the levels of 6-sulfo-sialyl Lewis X on TECs is underrepresented with the MECA-79 antibody. This also suggest that some PNAd structures on TECs may be "single-armed" with respect to 6-sulfo-sialyl Lewis X. Nonetheless, PNAd expression on Peyer's Patch endothelium is entirely dependent on GST1 (Hemmerich et al., 2001; Uchimura et al., 2004), demonstrating its sufficiency, and the ability of such structures to support lymphocyte entry.

We also found that PNAd^{+} TECs and LN BECs express similar scaffolding proteins that are involved in PNAd biosynthesis. CD34 and endomucin were expressed comparably between PNAd^{+} and PNAd^{neg} cells from both LNs and I.P. tumors. These molecules were

also comparably expressed between LN BEC and TEC populations. In contrast, Glycam-1 and nepmucin were expressed at higher levels in $PNAd^{+}$ than in $PNAd^{neg}$ cells from both LNs and I.P. tumors, although transcript levels for these molecules were significantly less in TECs relative to LN BECs. It seems likely that these scaffolding proteins are redundant with one another in promoting L-selectin engagement with PNAd, as mice deficient in CD34 (Suzuki et al., 1996) or Glycam-1 (Rosen, 2004) show no impaired trafficking of naïve T-cells to peripheral LNs. Thus, the low levels of PNAd on the tumor vasculature is likely not due to the low expression levels of these scaffolding proteins. Instead, is more likely due to the low expression levels of biosynthetic enzymes, particularly GST2, that drive the synthesis of 6-sulfo-sialyl Lewis X.

This report also identified components of the PNAd biosynthesis pathway in TECs that are regulated by TNFR signaling. While PNAd is not detected on vasculature in tumors from $TNFR1/2^{-/-}$ mice by IF (Peske et al., 2015), a small percentage of TECs from these tumors maintain PNAd by flow cytometry, albeit at a lower level of surface expression. These results indicate that a majority of TECs in I.P. tumors depend on TNFR signaling for the expression PNAd, while a small fraction of cells depend on an alternative pathway for PNAd development. These residual $PNAd^{+}$ TECs expressed lower levels of podocalyxin, nepmucin, and GST1. In $PNAd^{+}$ LN BEC, LTβR signaling upregulates GST1, along with GlyCAM-1, GST2, FUT7, and GCNT1 but not podocalyxin and nepmucin (Browning et al., 2005; Moussion & Girard, 2011). It is entirely possible that TECs that retain PNAd in the absence of TNFR signaling utilize LTβR as an alternative. $PNAd^{neg}$ TECs from I.P. $TNFR1/2^{-/-}$ mouse tumors showed no reduction in any evaluated

biosynthetic enzymes or scaffolding proteins. Given the relatively small fraction of TECs that express PNAd in tumors from WT mice, it is possible that analysis of these cells would show that the same or additional PNAd components are regulated by TNFR signaling, but this small subset of $PNAd^{neg}$ TECs cannot be directly identified. Nonetheless, these results demonstrate a distinct regulation of PNAd biosynthetic components by TNFR1/2 and LTβR, or differences in endothelial cell gene expression that reflect microenvironmental influences associated with anatomic location.

Aside from differential regulation by TNFR or LTβR, the reasons that all evaluated PNAd biosynthetic enzymes and several scaffolding proteins are expressed at significantly lower levels in $PNAd^{+}$ TECs than in LN $PNAd^{+}$ BEC are also not clear. One possibility, is that TEC and LN BECs differentially regulate TNFR1, TNFR2, and LTβR or the downstream signaling components of these pathways are not functioning properly. Alternatively, since there are two TNFR isoforms that vary in their signaling pathways (MacEwan, 2002; Wajant & Siegmund, 2019) and their engagement with TNFα and $LT\alpha_3$ (Medvedev, Espevik, Ranges, & Sundan, 1996), it is entirely possible that variations in how these molecules signal through TECs would result in low PNAd expression on these cells. Several studies have also shown that the epigenetic profile of BECs is different from TECs (Reviewed in Ciesielski et al., 2020). Two studies has demonstrated that human umbilical vein endothelial cells cultured with conditioned tumor media led to epigenetic modifications in these cells that resulted in reduced VCAM-1 and ICAM-1 expression (Hellebrekers et al., 2006, 2007). This suggests that a similar mechanism is operating in TECs that consequentially causes the reduce expression of PNAd associated components

in these cells. However, this remains to be determined. Determining the factors that limit the expression of PNAd scaffolding proteins and biosynthetic enzymes would provide targets for enhancing the expression of these molecules for sustained anti-tumor immunity.

Checkpoint immunotherapy has been associated with enhanced expression of HR ligands on the tumor vasculature, such as ICAM-1 and VCAM-1 (Hailemichael et al., 2018; Taggart et al., 2018). Similarly, anti-PDL1 monotherapy or the combination of anti-CTLA4 and anti-PD1 enhanced the fraction of $CD31^+$ TECs expressing PNAd and their surface levels of PNAd. In a murine model of melanoma, PNAd expression on the tumor vasculature depends on the presence of effector CD8 T-cells secreting $LT\alpha_3$ (Peske et al., 2015). Thus, checkpoint immunotherapy is likely enhancing the number of CD8 T-cells producing $LT\alpha_3$. Despite this, the fraction of $PNAd^+$ $CD31^+$ TECs and their surface intensity of PNAd did not reach a level that was consistent with that in LNs. In murine methylcholanthrene-induced fibrosarcoma, regulatory T-cells restricted PNAd expression on tumor vessels (Hindley et al., 2012; Colbeck et al., 2017). However, the mechanism of action in which these cells mediate this inhibition is unknown. B16 tumors are known to contain regulatory T-cells (Quatromoni et al., 2011), thus the elimination of these cells would potentially further enhance PNAd expression on the tumor vasculature in checkpoint treated tumor-bearing mice. Collectively, these findings provide significant insight into the basis for PNAd biosynthesis in TECs, and how they are altered in response to checkpoint immunotherapy.

Immune mechanisms orchestrate tertiary lymphoid structures in tumors via cancer-associated fibroblasts

Introduction

Tertiary lymphoid structures (TLS) are ectopic aggregates with morphological, cellular, and molecular similarities to secondary lymphoid organs (SLO), and commonly found with chronic infection, autoimmunity, and organ transplantation (Neyt et al., 2012; Koenig & Thaunat, 2016). TLS are found in human tumors (TA-TLS), and are usually associated with higher representations of tumor infiltrating lymphocytes (TIL), enhanced patient survival, and clinical responses to chemo- and immunotherapies (Engelhard et al., 2018; Sautès-Fridman et al., 2019; Anthony B. Rodriguez & Engelhard, 2020). It has been suggested that TA-TLS are sites for sustained antitumor immunity, and that TA-TLS augmentation could be a new strategy for cancer immunotherapy. This depends on understanding the mechanisms driving TA-TLS development.

Mechanisms governing development of SLO are well-established (reviewed in (Onder & Ludewig, 2018; Mueller, Nayar, Campos, & Barone, 2018). SLO development depends on interaction between innate lymphoid type 3 (ILC3) lymphoid tissue inducer (LTi) cells expressing surface lymphotoxin-$\alpha_1\beta_2$ ($LT\alpha_1\beta_2$), and mesenchymal lymphoid tissue organizer (LTo) cells expressing lymphotoxin-β receptor (LTβR). LTo cells mature into CXCL13-producing follicular dendritic cells (FDC) and CCL19/21 producing fibroblastic reticular cells (FRC), which facilitate recruitment and compartmentalization of T- and B-cells. While some chronic inflammation-associated TLS also depend on LTβR

signaling (Glaucia C Furtado et al., 2007; Gatumu et al., 2009; GeurtsvanKessel et al., 2009; Gräbner et al., 2009; Motallebzadeh et al., 2012; Pikor et al., 2015), others depend on IL-5, IL-6, IL-17, IL-22, IL-23, and/or TNFα, either in conjunction with (Lötzer et al., 2010; Rangel-Moreno et al., 2011; Pikor et al., 2015) or independent of (J. J. Lee et al., 1997; Goya et al., 2003; Khader et al., 2011; Peters et al., 2011; G. C. Furtado et al., 2014; Guedj et al., 2014; Barone et al., 2015; Bénézech et al., 2015; Cañete et al., 2015) LTβR signaling. CCL19, CCL21, CXCL12, and CXCL13 are found in TLS (Rangel-Moreno et al., 2007; Fleige et al., 2014; Barone et al., 2015; Sato et al., 2016), along with cells expressing FRC (Peduto et al., 2009; Link et al., 2011) or FDC (Drayton et al., 2003; Bombardieri et al., 2007) surface markers, and some of the inflammatory cytokines identified above can upregulate chemokine expression in cultured smooth muscle cells (Lötzer et al., 2010; Guedj et al., 2014) and fibroblasts purified from inflamed tissues containing TLS (Khader et al., 2011; Rangel-Moreno et al., 2011; Barone et al., 2015). However, only one report has directly demonstrated that LTo-like fibroblasts could support TLS development (Nayar et al., 2019). Inflammatory TLS development can also depend on a variety of LTi cells, including dendritic cells (DC) (GeurtsvanKessel et al., 2009; Halle et al., 2009; Muniz et al., 2011), B-cells (K. G. McDonald et al., 2005; Dubey et al., 2016), macrophages (G. C. Furtado et al., 2014; Guedj et al., 2014; Bénézech et al., 2015), T_H17 cells (Peters et al., 2011; Rangel-Moreno et al., 2011; Pikor et al., 2015), natural killer T-cells (Bénézech et al., 2015), γδ T-cells (Fleige et al., 2014), and multiple populations of IL-22-secreting adaptive and innate lymphoid cells (Barone et al., 2015). The

heterogeneous drivers of TLS development likely depend on microenvironmental context. However, the cellular and molecular drivers of TA-TLS are undefined.

Vaccination can induce TA-TLS development in pancreatic tumors (Lutz et al., 2014) and cervical neoplastic lesions (Maldonado et al., 2014). TA-TLS development in murine tumors has been induced by transgenic overexpression of LTβR ligands (Schrama et al., 2001; H.-J. Kim et al., 2004; P. Yu et al., 2004, 2007), injection of recombinant LIGHT (Johansson-Percival et al., 2017), and intratumoral administration of CCL21 (Kirk, Hartigan-O'Connor, & Mule, 2001; Turnquist et al., 2007). However, there are few reports of spontaneous TA-TLS development in murine tumors (Finkin et al., 2015; Joshi et al., 2015; Peske et al., 2015; A.B. Rodriguez et al., 2018). We previously demonstrated that naïve T-cells infiltrated murine tumors, underwent *in situ* activation, and augmented tumor control (Thompson et al., 2010; Peske et al., 2015). Naïve T-cell entry depended on tumor endothelial cells expressing peripheral node addressin (PNAd) and CCL21, which in turn depended on effector CD8 T-cells and natural killer (NK) cells secreting $LT\alpha_3$ and IFNγ (Peske et al., 2015). We subsequently showed that tumors growing in the peritoneal cavity (I.P.), but not those growing subcutaneously (S.C.), had TA-TLS adjacent to $PNAd^+$ vasculature (Peske et al., 2015; A.B. Rodriguez et al., 2018). Here, we identify the cellular and molecular mechanisms driving TA-TLS development. Our results highlight the pivotal role of cancer-associated fibroblasts (CAF) as surrogate LTo cells, and multiple cell types, including intratumoral CD8 T-cells and $LT\alpha_1\beta_2^+$ B-cells, that synergistically act as LTi cells. They also demonstrate that TA-TLS development and organization are augmented by checkpoint blockade immunotherapy and associated with reduced tumor size.

Results

TA-TLS in I.P. tumors are associated with altered distributions of activated T-cells and naïve B-cells

By 7-color immunofluorescence (IF), we observed dense multicellular structures adjacent to $PNAd^+$ vessels in I.P. B16-OVA tumors (Figure 8A-C). However, these structures never formed in S.C. tumors. TA-TLS were dominated by a dense aggregate of B-cells. In most cases, CD4 T-cells were scattered throughout the B-cell aggregate, while CD8 T-cells and DC were found predominantly on the periphery, and also were not well-organized (Figure 8D-G). These structures resemble "*non-classical*" TA-TLS seen in murine and human hepatocellular carcinoma (Finkin et al., 2015). I.P. tumors also contained less frequent "*classical*" TA-TLS with distinct T- and B-cell compartments (Figure 9A). TA-TLS were also present in parental B16-F1 I.P. tumors, although they were smaller and fewer (Figure 8D-I). TA-TLS were also present in B16-OVA tumors grown in lung, and in I.P., but not S.C., MC38 and LLC OVA expressing tumors (Figure 10A-B). Thus, TA-TLS quantity and quality are associated with antigen strength, but their presence is due to tumor microenvironmental factors that depend on anatomical location.

I.P. B16 tumors grow as single pigmented masses, not ascites, juxtaposed to stomach, cecum, spleen, pancreas, and omentum (Figure 11A-B). They are connected by a blood vessel to the spleen, and superficially associated with the omentum, but not other surrounding organs, and easily removed intact with forceps (Figure 11C). Human melanoma frequently metastasizes to visceral organs (A. Kawashima, Fishman, Kuhlman, & Schuchter, 1991; Trout, Rabinowitz, Platt, & Elsayes, 2013). TA-TLS frequently

Figure 8: Tumor-associated tertiary lymphoid structures spontaneous develop in I.P. tumors, but not S.C. tumors

WT mice were S.C. or I.P. injected with B16-OVA cells. Tumors were harvested on day 14 and prepared and stained for multispectral imaging as described in Methods. (A-C) Representative uncompensated multispectral image of S.C. and I.P. B16-OVA and B16-F1 tumors. (D-G) Representative compensated merged and single channel multispectral images of TA-TLS in B16-OVA and B16-F1 I.P. tumors. (H-I) Quantitative image summary data for TA-TLS in in B16-OVA and B16-F1 I.P. tumors. Data represents one experiment, n=3-4 tumor sections per group. (A-E, F-G) scale bars = 100 μm. Results shown as mean ± SD. (H & I) Unpaired Welch's t-test. *$p<0.05$ and ****$p<0.0001$.

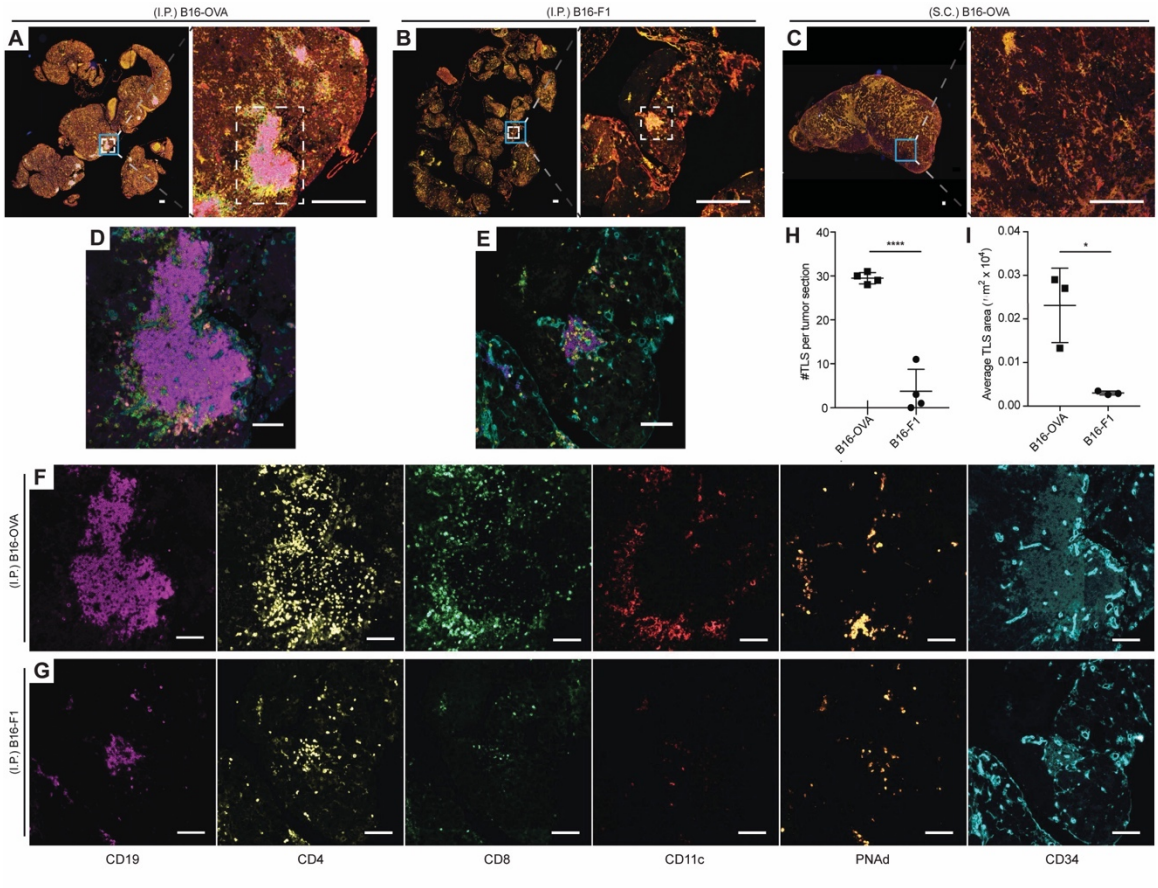
(I.P.) B16-OVA
(I.P.) B16-F1
(S.C.) B16-OVA
A
B
C
D
E
H
I
#TLS per tumor section
Average TLS area (mm² x 10⁴)
****
*
B16-OVA
B16-F1
F
G
(I.P.) B16-OVA
(I.P.) B16-F1
CD19
CD4
CD8
CD11c
PNAd
CD34

Figure 9: TA-TLS in I.P. tumors are associated with enhanced representations of distinctly differentiated T-cells and naïve B-cells

Day 14 S.C. or I.P. B16-OVA tumors from C57BL/6 (WT) mice were prepared for IF (A) or flow cytometry (B-F) as described in Methods. (A) Representative images and summary data for TA-TLS organizational types in I.P. tumors. Scale bar = 100 μm. Data from 5 experiments, n=25 tumors. (B-F) $CD45^{+}$ single cell suspensions were stained with the indicated markers to define subpopulations (DC = $CD3^{neg}$ $CD19^{neg}$ $CD11c^{+}$ MHC II^{+}; T-cells = $CD19^{neg}$ $CD3^{+}$ $CD8^{+}$ or $CD4^{+}$; B-cells = $CD3^{neg}$ $CD19^{+}$ $CD5^{+}$ or $CD5^{neg}$) and activation state, and quantitated by flow cytometry. Data from 2-5 experiments, n=8-18 tumors per group. Results are mean ± SD, analyzed by unpaired Welch's t-test. ns: $p>0.05$, *$p<0.05$, **$p<0.01$, ***$p<0.001$, and ****$p<0.0001$.

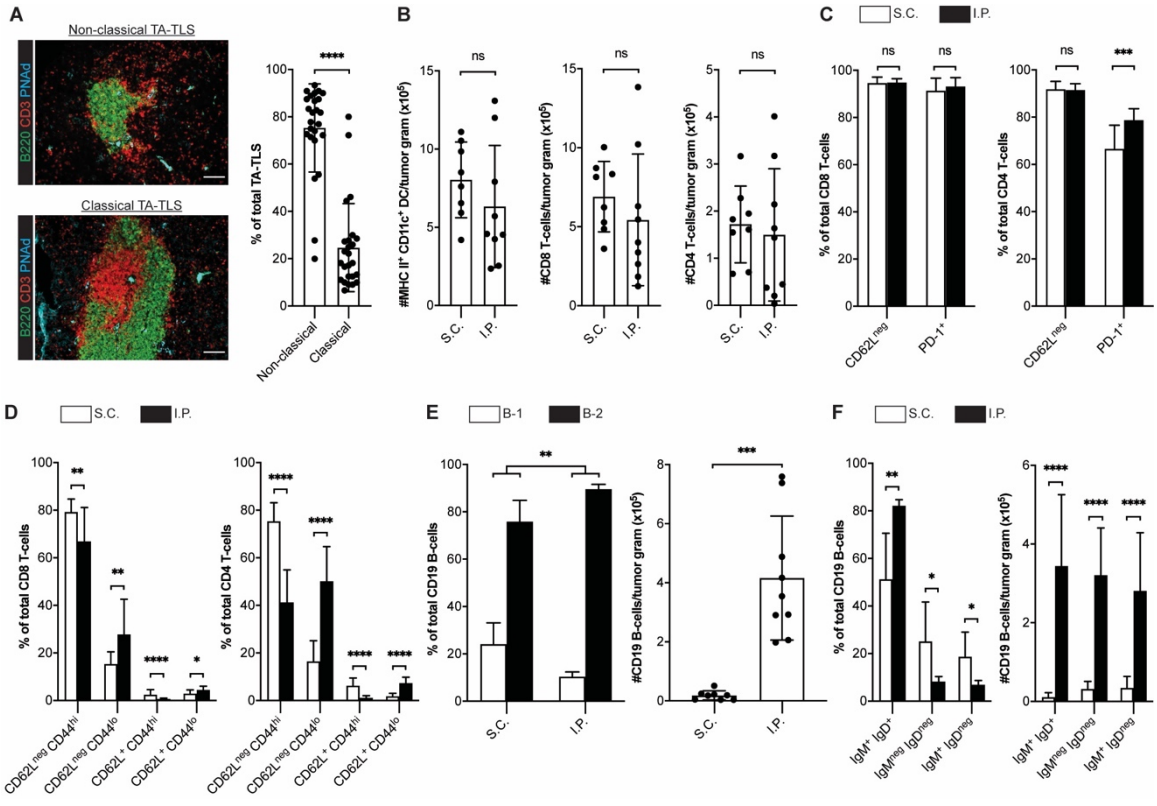
A
Non-classical TA-TLS
B220 CD3 PNAd
Classical TA-TLS
B220 CD3 PNAd
% of total TA-TLS
****
Non-classical
Classical
B
#MHC II+ CD11c+ DC/tumor gram (x10^5)
#CD8 T-cells/tumor gram (x10^5)
#CD4 T-cells/tumor gram (x10^5)
ns
S.C.
I.P.
C
S.C.
I.P.
% of total CD8 T-cells
% of total CD4 T-cells
CD62L neg
PD-1+
***
D
S.C.
I.P.
% of total CD8 T-cells
% of total CD4 T-cells
CD62L neg CD44 hi
CD62L neg CD44 lo
CD62L + CD44 hi
CD62L + CD44 lo
E
B-1
B-2
% of total CD19 B-cells
#CD19 B-cells/tumor gram (x10^5)
F
S.C.
I.P.
% of total CD19 B-cells
#CD19 B-cells/tumor gram (x10^5)
IgM+ IgD+
IgM neg IgD neg
IgM+ IgD neg

Figure 10: Spontaneously development of TA-TLS is a consequence of anatomical location and not tumor model

WT mice were S.C., intravenously (I.V.), or I.P. injected with B16-OVA cells. Tumors were harvested on day 14 and stained for immunofluorescence microscopy are described in methods. (A) Representative immunofluorescence images of TA-TLS in the lung. (B) Representative images of S.C. and I.P. tumors and image summary data. Scale bars = 100 μm. Data represents one experiment, n=5 tumors per group. Results shown as mean ± SD. (B) Unpaired Welch's t-test. ns: $p>0.05$.

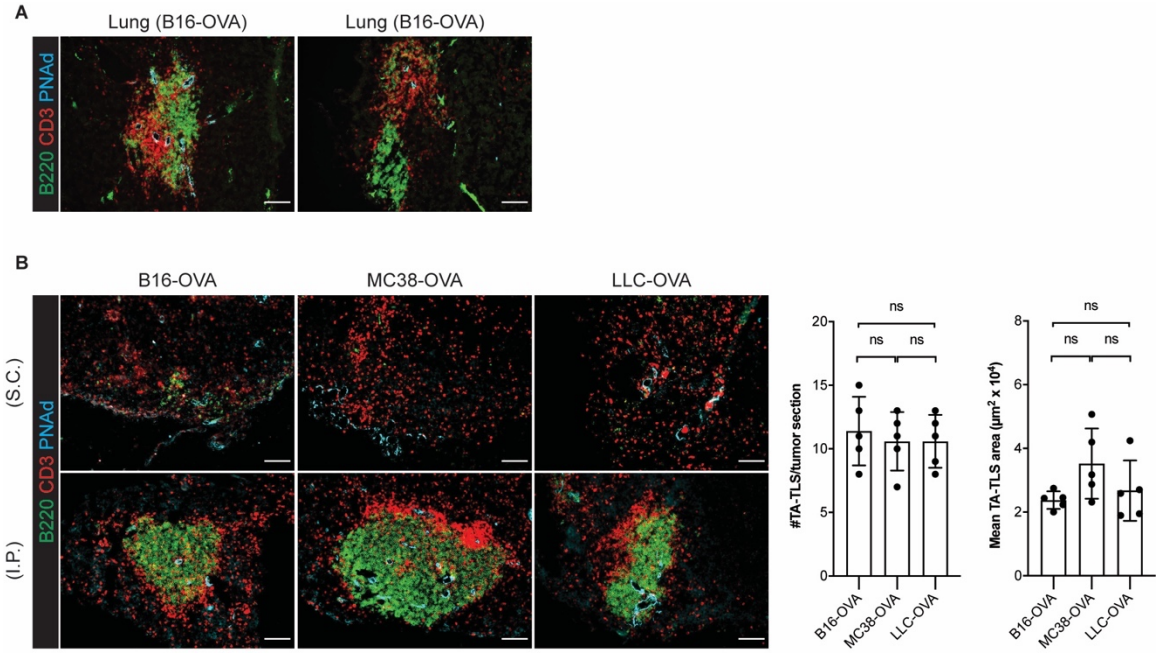
A
Lung (B16-OVA)
Lung (B16-OVA)
B220 CD3 PNAd
B
B16-OVA
MC38-OVA
LLC-OVA
(S.C.)
(I.P.)
B220 CD3 PNAd
ns
ns
ns
#TA-TLS/tumor section
Mean TA-TLS area (μm² x 10⁴)
B16-OVA
MC38-OVA
LLC-OVA

Figure 11: I.P. tumors form as solid pigmented masses with minimal attachment to visceral organs

WT mouse was I.P. injected with B16-OVA cells and euthanized 14 days after implantation. (A-B) Representative images of an I.P. tumor in the peritoneal cavity. T, tumor; Lv, liver; St, stomach; Si, small intestines; Li, large intestines; Ce, cecum; Pa, pancreas; Om, omentum; Sp, spleen. (C) Representative images of an I.P. tumor removed from the peritoneal cavity.

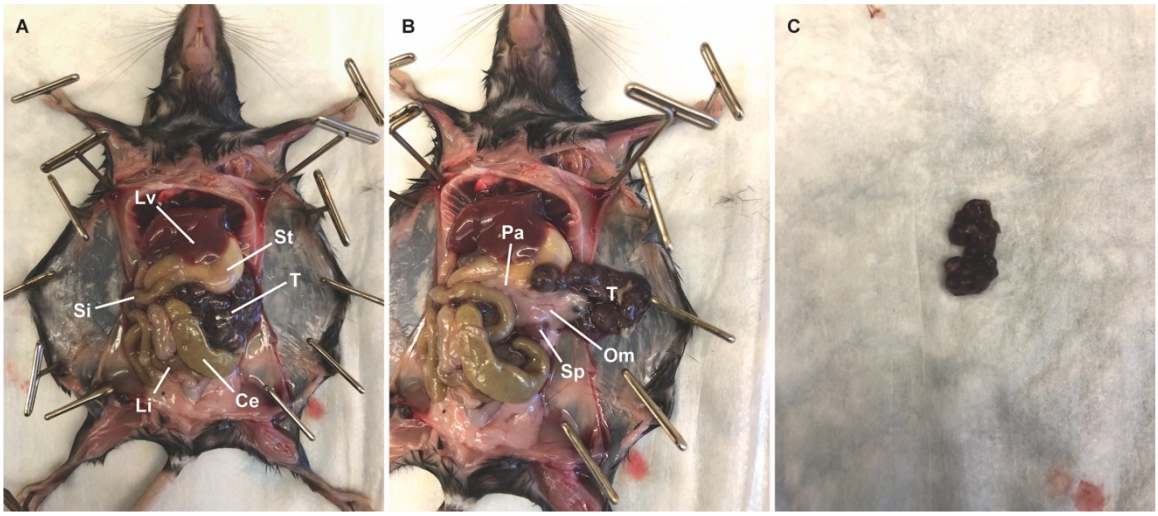
A
Lv
St
T
Si
Li
Ce
B
Pa
T
Om
Sp
C

Figure 12: S.C. and I.P. tumors contain distinctly differentiated T-cell populations

WT mice were injected S.C. or I.P. with B16-OVA cells and tumors were harvested on day 14 and prepared for flow cytometry as described in Methods. Representative histogram plots including gMFI of positive population above FMO of indicated markers on effector ($CD62L^{neg}$ $CD44^{hi}$), activated ($CD62L^{neg}$ $CD44^{lo}$), central memory ($CD62L^{+}$ $CD44^{hi}$), and naïve ($CD62L^{+}$ $CD44^{lo}$) T-cells from S.C. and I.P tumors.

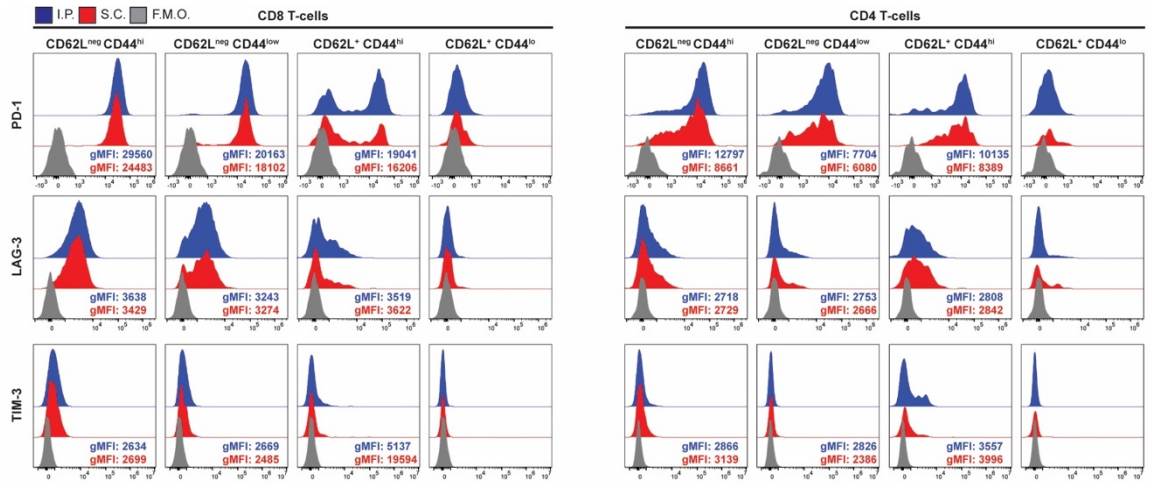
I.P.
S.C.
F.M.O.
CD8 T-cells
CD4 T-cells
CD62L^neg CD44^hi
CD62L^neg CD44^low
CD62L^+ CD44^hi
CD62L^+ CD44^lo
PD-1
LAG-3
TIM-3
gMFI: 29560
gMFI: 24483
gMFI: 20163
gMFI: 18102
gMFI: 19041
gMFI: 16206
gMFI: 12797
gMFI: 8661
gMFI: 7704
gMFI: 6080
gMFI: 10135
gMFI: 8389
gMFI: 3638
gMFI: 3429
gMFI: 3243
gMFI: 3274
gMFI: 3519
gMFI: 3622
gMFI: 2718
gMFI: 2729
gMFI: 2753
gMFI: 2666
gMFI: 2808
gMFI: 2842
gMFI: 2634
gMFI: 2699
gMFI: 2669
gMFI: 2485
gMFI: 5137
gMFI: 19594
gMFI: 2866
gMFI: 3139
gMFI: 2826
gMFI: 2386
gMFI: 3557
gMFI: 3996

develop in gut melanoma metastases, but are infrequent in primary cutaneous tumors (Cipponi et al., 2012). Thus, I.P. B16 tumors are relevant models to study TA-TLS development.

To assess the impact of TA-TLS on intratumoral immune cell composition, we compared $CD45^{+}$ cells from S.C. and I.P. tumors by flow cytometry. When normalized for tumor size, the numbers of DC, and CD8 and CD4 T-cells, were not significantly different (Figure 9B). In both tumor types, 92-95% of CD8 and CD4 T-cells were $CD62L^{neg}$, and thus antigen experienced (Figure 9C). Supporting this, 91-94% of CD8 T-cells and 65-80% of CD4 T-cells were PD-1^{+}. Most $CD62L^{neg}$ CD8 and CD4 T-cells were also $CD44^{hi}$, again in keeping with an antigen experienced phenotype (Figure 9D). However, I.P. tumors contained a larger fraction of $CD62L^{neg}$ $CD44^{lo}$ T-cells, particularly in the CD4 compartment. These cells in both tumor types were largely PD-1^{+}, although this was more variable on S.C. $CD4^{+}$ T-cells (Figure 12). Thus, despite being $CD44^{lo}$, they seem activated. Both tumors also contained small populations of $CD62L^{+}$ $CD44^{hi}$ presumptive central memory and $CD62L^{+}$ $CD44^{lo}$ naïve cells (Figure 9D), and their expression of PD-1, LAG-3, and TIM-3 was consistent with this classification (Figure 12). However, I.P. tumors contained more naïve and fewer central memory CD8 T-cells than S.C. tumors, and this was more pronounced in the CD4 compartment (Figure 9D). These results suggest that TA-TLS in I.P. tumors enhance representation of naïve and distinctly differentiated T-cells, particularly CD4 T-cells.

B-cells from both tumor types were mainly B-2, and this was significantly enriched in I.P. relative to S.C. tumors (Figure 9E). This contrasts with the dominance of B-1 cells

in the peritoneal cavity (Hayakawa, Hardy, Herzenberg, & Herzenberg, 1985) and omental fat-associated lymphoid clusters (FALCs) (Cruz-Migoni & Caamaño, 2016), and suggests that the origin of B-cells in TA-TLS and/or the factors driving their accumulation are distinct from those of these two peritoneal sites. Consistent with the large aggregates observed by IF, I.P. tumors contained ~20x more B-cells than S.C. tumors. In both tumor types, the largest population was IgM^{+} IgD^{+} and presumptively naïve (Figure 9F), and this population was significantly elevated in I.P. tumors. When normalized for size, I.P. tumors contained ~30x more naïve, ~10x more presumptive class-switched (IgM^{neg} IgD^{neg}), and 8x more memory (IgM^{+} IgD^{neg}) B-cells (Figure 9F). Thus, TA-TLS presence in I.P. tumors is associated with more robust B-cell immunity and enhanced naïve B-cell representation.

A CAF population acts as lymphoid tissue organizer cells to orchestrate TA-TLS formation

When analyzed by flow cytometry, $CD45^{+}$ depleted tumor suspensions contained many cells that were $CD31^{neg}$ and podoplanin (PDPN) positive. PDPN is a conventional CAF marker (Pula, Witkiewicz, Dziegiel, & Podhorska-Okolow, 2013), but B16 tumor cells express it at a low level (Figure 13A). However, only $PDPN^{hi}$ cells expressed canonical CAF markers, particularly platelet-derived growth factor receptor alpha (CD140α), Thy1, and fibroblast activating protein (FAP) (Figure 13B), and these were analyzed as CAFs in subsequent experiments. Thy1, FAP, and intracellular collagen type I (Col Type I) were all elevated on CAFs from S.C. compared to I.P. tumors (Figure 13B and 14A), while α-smooth muscle actin (αSMA) expression was comparable (Figure 15A). I.P. tumors contained substantially more CAFs than S.C. tumors, and a larger percentage expressed the proliferation marker $Ki67^{+}$ (Figure 14B). Interestingly, the absolute number of FAP^{+} CAFs

Figure 13: PDPN^{hi} cells represent cancer-associated fibroblasts

WT mice were injected S.C. or I.P. with B16-OVA cells and tumors were harvested on day 14. (A) Representative flow cytometry plots and gating strategy for the identification of PDPN^{lo} and PDPN^{hi} cells in CD45^{+} depleted S.C. and I.P. tumors suspensions. (B) Representative histogram plots of PDPN^{lo} and PDPN^{hi} cells in CD45^{+} depleted S.C. and I.P. tumors suspensions stained for indicated antibodies. (C) Representative immunofluorescence images of an I.P. tumor stained for indicated antibodies at different exposure times. Scale bar = 100 μm.

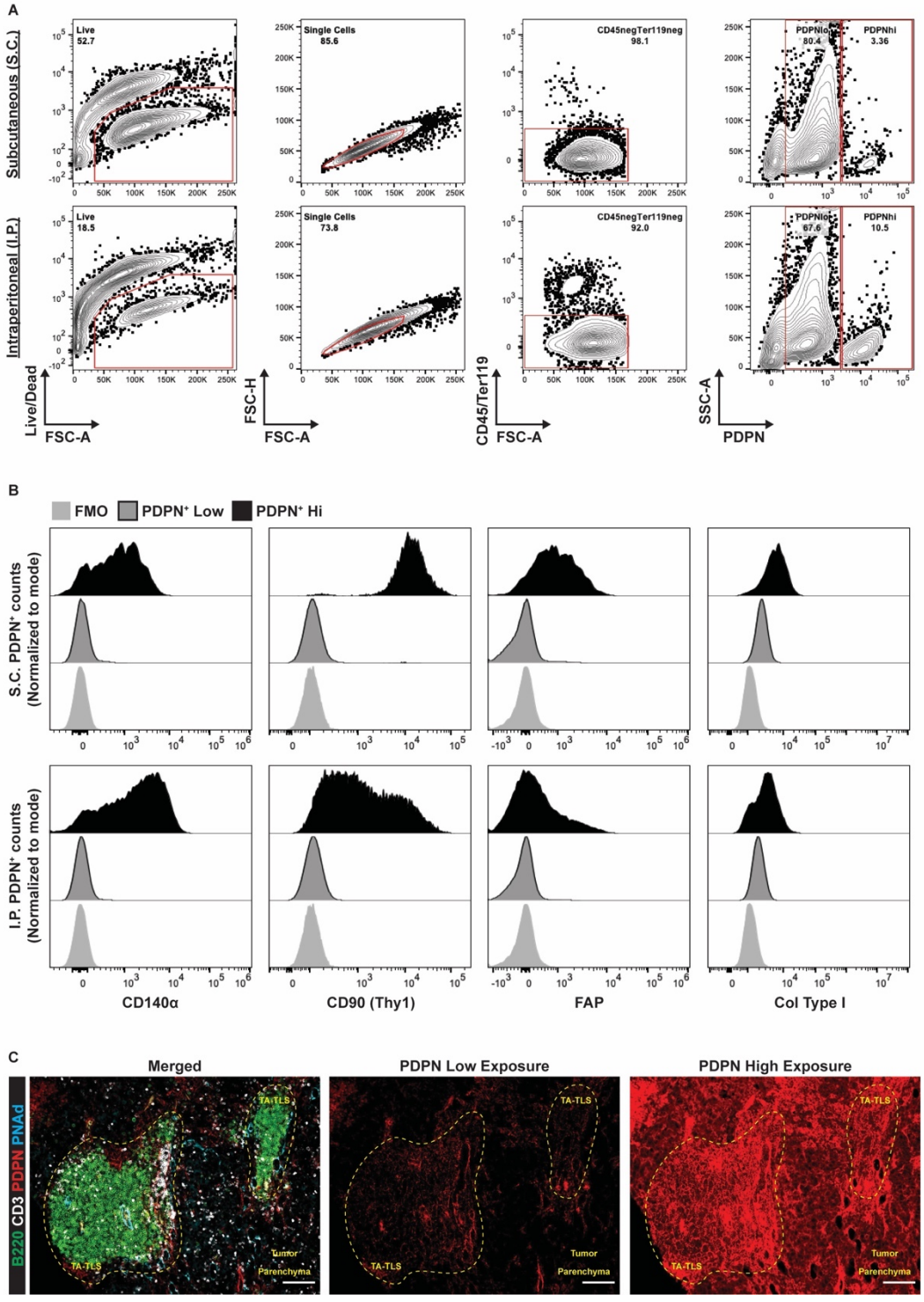
A
Subcutaneous (S.C.)
Intraperitoneal (I.P.)
Live
52.7
Live
18.5
Single Cells
85.6
Single Cells
73.8
CD45negTer119neg
98.1
CD45negTer119neg
92.0
PDPNlo
80.4
PDPNhi
3.36
PDPNlo
67.6
PDPNhi
10.5
Live/Dead
FSC-A
FSC-H
FSC-A
CD45/Ter119
FSC-A
SSC-A
PDPN
B
FMO
PDPN+ Low
PDPN+ Hi
S.C. PDPN+ counts (Normalized to mode)
I.P. PDPN+ counts (Normalized to mode)
CD140α
CD90 (Thy1)
FAP
Col Type I
C
Merged
PDPN Low Exposure
PDPN High Exposure
B220 CD3 PDPN PNAd
TA-TLS
Tumor
Parenchyma

Figure 14: A population CAFs from I.P. tumors exhibit lymphoid tissue organizer cell characteristics

Day 14 S.C. or I.P. B16-OVA tumors from WT mice were prepared for flow cytometry (A, B, D, E) or IF (C, G-H) as described in Methods. (A, D) Left, representative histograms and geometric mean fluorescence (gMFI) intensities of indicated markers on $PDPN^{hi}$ $CD31^{neg}$ $CD45^{neg}$ $Ter119^{neg}$ CAFs. gMFIs calculated on cells gated above the fluorescence minus one (FMO) control. Right, percentage of CAFs expressing indicated markers. Data from 2-5 experiments, n=11-45 tumors per group. (B, E, F) CAF subpopulations were quantitated by flow cytometry. Data from 2-3 experiments, n=8-11 tumors per group. (C, G, H) Left, representative images of tumors stained with indicated markers. Yellow dashes delimit TA-TLS area. Scale bar = 100 μm. Right, summary data of $PDPN^{+}$ CAF densities (C) and marker expression in parenchymal and TA-TLS regions (G, H) from 1 experiment, n=5 tumors per group. Pixel intensities were calculated using a PDPN mask. Results are mean ± SD analyzed by unpaired Welch's t-test. ns: $p>0.05$, $^{**}p<0.01$, $^{***}p<0.001$, and $^{****}p<0.0001$.

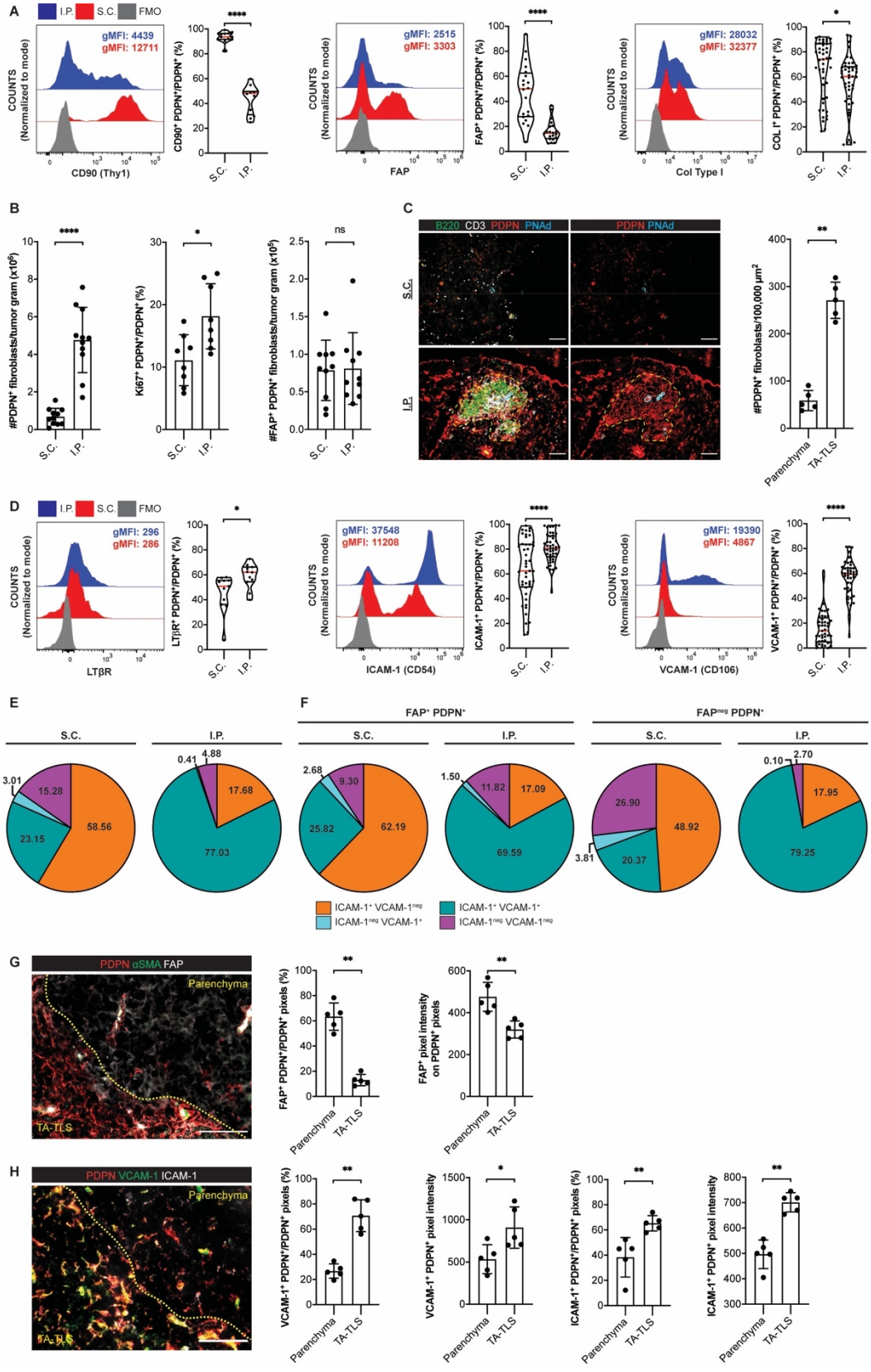
A
I.P.
S.C.
FMO
gMFI: 4439
gMFI: 12711
COUNTS (Normalized to mode)
CD90 (Thy1)
CD90+ PDPN+/PDPN+ (%)
gMFI: 2515
gMFI: 3303
FAP
FAP+ PDPN+/PDPN+ (%)
gMFI: 28032
gMFI: 32377
Col Type I
COL I+ PDPN+/PDPN+ (%)
B
#PDPN+ fibroblasts/tumor gram (x10^6)
Ki67+ PDPN+/PDPN+ (%)
#FAP+ PDPN+ fibroblasts/tumor gram (x10^6)
ns
C
B220 CD3 PDPN PNAd
PDPN PNAd
S.C.
I.P.
#PDPN+ fibroblasts/100,000 µm2
Parenchyma
TA-TLS
D
gMFI: 296
gMFI: 286
LTβR
LTβR+ PDPN+/PDPN+ (%)
gMFI: 37548
gMFI: 11208
ICAM-1 (CD54)
ICAM-1+ PDPN+/PDPN+ (%)
gMFI: 19390
gMFI: 4867
VCAM-1 (CD106)
VCAM-1+ PDPN+/PDPN+ (%)
E
S.C.
I.P.
3.01
15.28
23.15
58.56
0.41
4.88
17.68
77.03
F
FAP+ PDPN+
FAPneg PDPN+
2.68
9.30
25.82
62.19
1.50
11.82
17.09
69.59
0.10
2.70
17.95
79.25
26.90
48.92
3.81
20.37
ICAM-1+ VCAM-1neg
ICAM-1+ VCAM-1+
ICAM-1neg VCAM-1+
ICAM-1neg VCAM-1neg
G
PDPN αSMA FAP
Parenchyma
TA-TLS
FAP+ PDPN+/PDPN+ pixels (%)
FAP+ pixel intensity on PDPN+ pixels
H
PDPN VCAM-1 ICAM-1
VCAM-1+ PDPN+/PDPN+ pixels (%)
VCAM-1+ PDPN+ pixel intensity
ICAM-1+ PDPN+/PDPN+ pixels (%)
ICAM-1+ PDPN+ pixel intensity

Figure 15: S.C. and I.P. tumor-associated fibroblasts express α-smooth muscle actin and tumor necrosis factor receptor type I & II but not FDC marker CD35

WT mice were injected S.C. or I.P. with B16-OVA cells and tumors were harvested on day 14. (A-C) Representative flow cytometry histogram plots including gMFI of positive population above FMO control. Percentages of $CD45^{neg}$ $Ter119^{neg}$ $CD31^{neg}$ $PDPN^{+}$ fibroblasts expressing indicated by flow cytometry. Data represents three experiments, n=11 tumors per group. (D) Representative flow cytometry data of CD35 expression on CD45 depleted LN and I.P. tumor suspensions. Results shown as mean ± SD. (A-C) Unpaired Welch's t-test. ns:$p>0.05$ and **$p<0.01$.

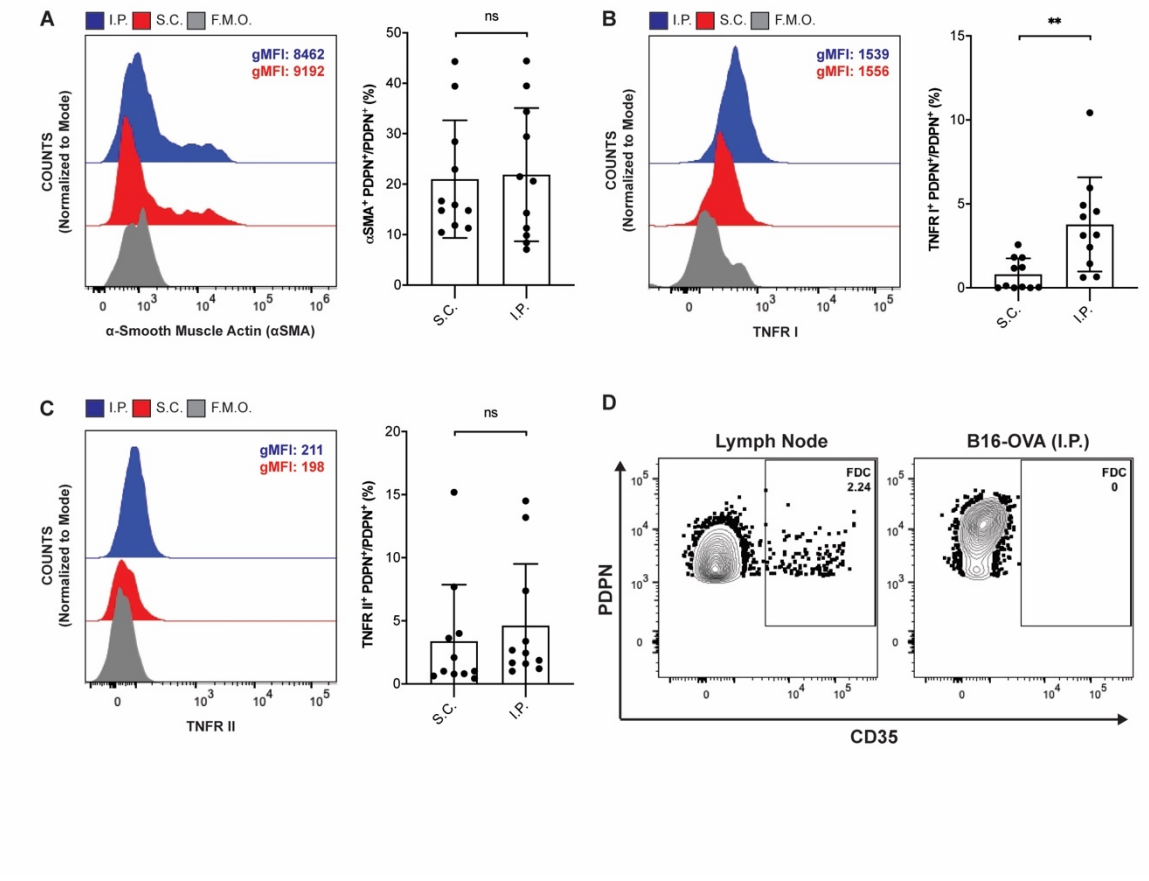
A
I.P.
S.C.
F.M.O.
gMFI: 8462
gMFI: 9192
COUNTS
(Normalized to Mode)
α-Smooth Muscle Actin (αSMA)
ns
αSMA+ PDPN+/PDPN+ (%)
S.C.
I.P.
B
gMFI: 1539
gMFI: 1556
TNFR I
**
TNFR I+ PDPN+/PDPN+ (%)
C
gMFI: 211
gMFI: 198
TNFR II
TNFR II+ PDPN+/PDPN+ (%)
D
Lymph Node
B16-OVA (I.P.)
FDC
2.24
FDC
0
PDPN
CD35

was the same between S.C. and I.P. tumors (Figure 14B). Thus, the higher number of CAFs in I.P. tumors is due to an expanded number of FAP^{neg} CAFs.

CAFs and tumor cells expressing high and low levels of PDPN, respectively, were also observed in tumor sections by IF. We established exposure times to visualize only PDPN bright CAFs (Figure 13C). In S.C. tumors, CAFs were scattered throughout the parenchyma (Figure 14C). In contrast, CAFs in I.P. tumors formed reticular networks that were co-extensive with B- and T-cell aggregates of TA-TLS. By quantitative image analysis, CAF density in TA-TLS was substantially higher than in surrounding tumor parenchyma (Figure 14C), suggesting that their overall higher number in I.P. tumors was due to TA-TLS formation.

VCAM-1, ICAM-1, LTβR, and tumor necrosis factor receptor (TNFR) I & II are canonical LTo cell markers (Mebius, 2003; Ruddle & Akirav, 2009; van de Pavert & Mebius, 2010). A larger fraction of I.P. CAFs expressed TNFR I (Figure 15B) and LTβR (Figure 14D). Also, a significantly larger fraction of I.P. CAFs expressed ICAM-1 and VCAM-1, and their surface expression levels were much higher (Figure 14D). The majority of I.P. CAFs co-expressed ICAM-1 and VCAM-1, while those from S.C. tumors mainly expressed only ICAM-1 (Figure 14E). Although FDC-like cells are often found in TA-TLS, I.P. CAFs did not express the FDC marker CD35 (Figure 15D). These results were consistent with the possibility that S.C. and I.P. tumors are dominated by mutually exclusive populations of CAFs with FAP^{+} pro-tumor (T. Liu et al., 2019) and FAP^{neg} LTo phenotypes. However, even FAP^{+} CAFs from I.P. tumors were much more likely to co-express VCAM-1 and ICAM-1 than FAP^{+} or FAP^{neg} CAFs from S.C. tumors (Figure 14F).

To provide more direct evidence for the association of these CAF populations with TA-TLS, we performed quantitative image analysis. Less than 15% of $PDPN^+$ pixels in TA-TLS co-stained with FAP, while over 60% of those in the tumor parenchyma were FAP^+, and their FAP expression was higher (Figure 14G). Conversely, 65-70% of $PDPN^+$ pixels in TA-TLS stained for VCAM-1 and ICAM-1 compared to only 25-38% in the parenchyma, and their expression level was also higher (Figure 14H). Thus, despite the presence of both FAP^+ and FAP^{neg} cells expressing ICAM-1 and VCAM-1 in I.P tumors, the latter population is enriched in TA-TLS, consistent with a role in TA-TLS development.

To directly test a role for CAFs in orchestrating TA-TLS formation, we flow-sorted these cells from resected S.C. and I.P. tumors and injected them with B16-OVA cells into a S.C. site. The resulting tumors that contained CAFs from S.C. tumors, or mouse embryonic fibroblasts, did not develop TA-TLS, lymphoid aggregates, or $PDPN^+$ reticular networks (Figure 16A-B). Conversely, S.C. tumors that contained CAFs from I.P. tumors, contained $PDPN^+$ reticular networks that were co-extensive with aggregates of $B220^+$ B-cells and $CD3^+$ T-cells and adjacent to $PNAd^+$ vasculature (Figure 16A-B). While the number of these structures and their size were significantly less than TA-TLS in I.P. tumors (Figure 16B), their composition, organization, and localization established them as TA-TLS. We also flow-sorted CAFs from I.P. tumors grown in mice that ubiquitously express mCherry. When injected with B16-OVA cells, they persisted in the resulting S.C. tumors, and were mainly found in TA-TLS (Figure 16C). Based on their association with TA-TLS, we hypothesized that only FAP^{neg} CAFs would promote TA-TLS formation. Indeed, when co-injected with B16-OVA cells, purified FAP^{neg} CAFs promoted formation of small TA-

Figure 16: CAFs act as surrogate lymphoid tissue organizer cells that orchestrate TA-TLS formation

(A-D) S.C. tumors were induced by co-injection of B16-OVA cells together with the indicated populations of fibroblasts. Day 14 S.C. or I.P tumors were prepared for IF as described in Methods. (A, C, D left) Representative images. Yellow dashed region (C) represents TA-TLS area. Scale bar = 100 μm. (B, D right) Summary data from 1-2 experiments, n=5 or 10 tumors per group. (E) CAFs from day 14 S.C. and I.P. tumors were purified and expression of the indicated RNA transcripts determined as described in Methods. Data from 2 experiments presented as $2^{-\Delta CT}$ relative to *Hprt*, n=6 tumors per group. (F-H) Day 14 I.P. tumors from WT or $CXCR5^{-/-}$ mice were prepared for IF (F) or flow cytometry (G-H) as described in Methods. (F) Left, Representative images. Scale bar = 100 μm. Right, Summary data from 1 experiment, n=5 tumors per group. (G, H) Cell populations were quantitated as outlined in Figures 1 and 2. Data represents 1 experiment, n=5 tumors per group. Results are mean ± SD, analyzed using Kruskal-Wallis h-test with Dunn's post-test (B, D) or unpaired Welch's t-test (E-H). ns: $p>0.05$, *$p<0.05$, **$p<0.01$, and ****$p<0.0001$.

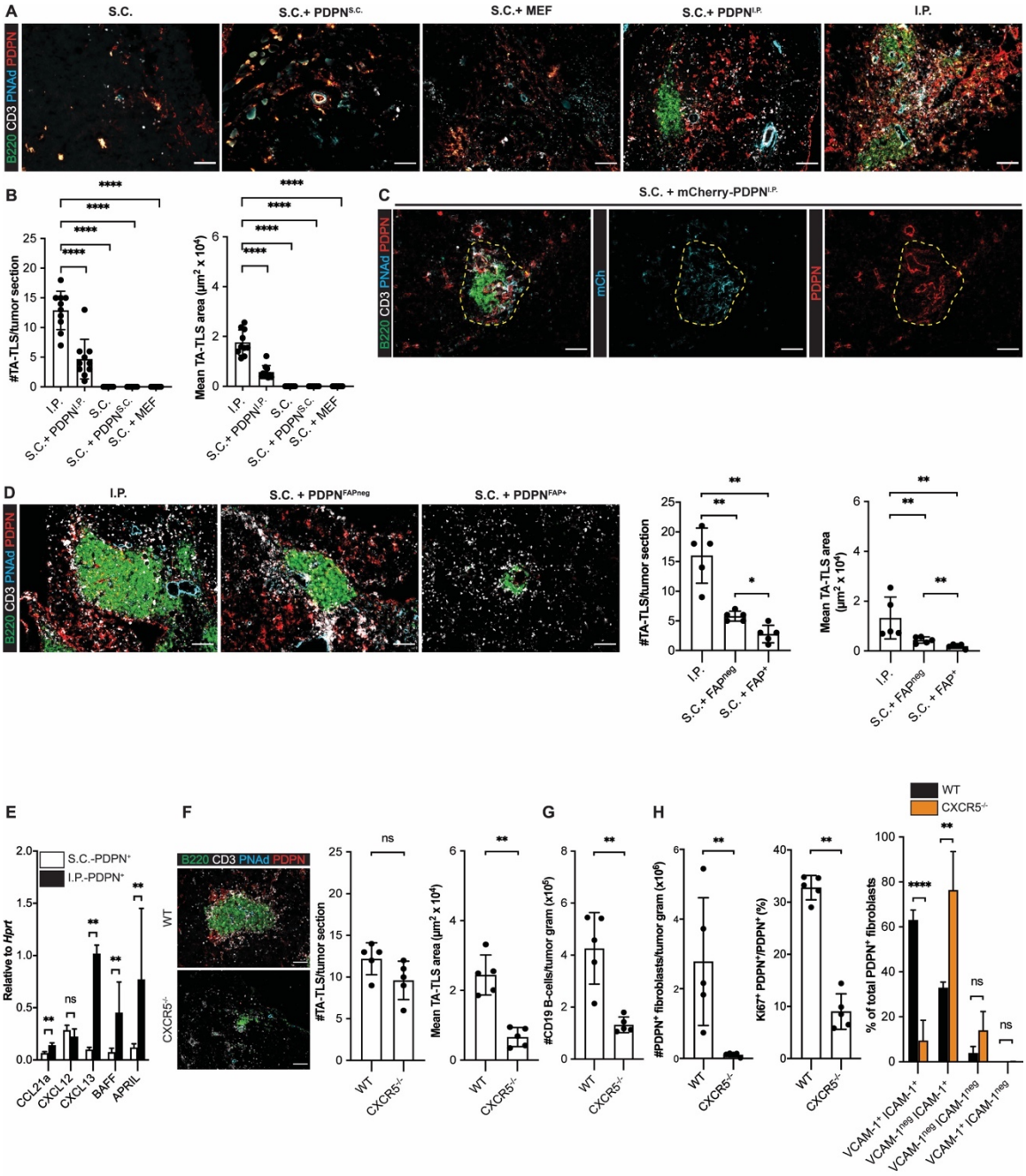
A
S.C.
S.C.+ PDPN S.C.
S.C.+ MEF
S.C.+ PDPN I.P.
I.P.
B220 CD3 PNAd PDPN
B
#TA-TLS/tumor section
Mean TA-TLS area (µm² x 10⁴)
I.P.
S.C.+ PDPN I.P.
S.C.
S.C.+ PDPN S.C.
S.C.+ MEF
C
S.C. + mCherry-PDPN I.P.
mCh
D
I.P.
S.C. + PDPN FAPneg
S.C. + PDPN FAP+
#TA-TLS/tumor section
Mean TA-TLS area (µm² x 10⁴)
S.C.+ FAPneg
S.C. + FAP+
E
S.C.-PDPN+
I.P.-PDPN+
Relative to Hprt
CCL21a
CXCL12
CXCL13
BAFF
APRIL
F
WT
CXCR5-/-
#TA-TLS/tumor section
Mean TA-TLS area (µm² x 10⁴)
G
#CD19 B-cells/tumor gram (x10⁵)
H
#PDPN+ fibroblasts/tumor gram (x10⁶)
Ki67+ PDPN+/PDPN+ (%)
% of total PDPN+ fibroblasts
VCAM-1+ ICAM-1+
VCAM-1neg ICAM-1+
VCAM-1neg ICAM-1neg
VCAM-1+ ICAM-1neg

TLS, analogous in size and number to those induced by bulk I.P. CAFs (Figure 16D). FAP^+ CAFs induced less frequent and even smaller TA-TLS-like structures that were associated with PNAd, but contained small numbers of poorly organized $PDPN^+$ cells. These results establish that FAP^{neg} CAFs from I.P. tumors act as surrogate LTo cells that promote TA-TLS formation. I.P. FAP^+ CAFs appear to have a minimal LTo capability that is nonetheless greater than that of S.C. CAFs, suggesting that this property is induced by the I.P. tumor microenvironment.

We previously showed that both S.C. and I.P. CAFs are a major source of CCL21 that recruits naïve T-cells (Peske et al., 2015). By quantitative RT-PCR (qPCR), CAFs from both tumor types expressed comparable levels of another homeostatic chemokine, CXCL12. However, I.P. CAFs expressed 5-10-fold higher levels of the B-cell organizer chemokine CXCL13, and B-cell survival factors BAFF and APRIL (Figure 16E). To provide direct evidence for the importance of CXCL13 in driving TA-TLS formation, we implanted I.P. tumors into mice lacking CXCR5, the cognate receptor for CXCL13. While the numbers of TA-TLS in these tumors were comparable to those in wild-type (WT) tumors, they were significantly smaller (Figure 16F). This was associated with a reduced number of intratumoral B-cells and CAFs (Figure 16G-H). Significantly fewer of these CAFs were proliferating, and the fraction co-expressing ICAM-1 and VCAM-1 was also reduced (Figure 16H). Thus, an intact CXCR5-CXCL13 chemotactic axis supports the proliferation of CAFs with LTo characteristics and normal TA-TLS development.

Intratumoral CD8 T-cells and B-cells act coordinately as lymphoid tissue inducer cells driving TA-TLS development

We next investigated the roles of adaptive immune cells in TA-TLS development. I.P. tumors grown in $Rag1^{-/-}$ mice lack $PNAd^{+}$ vasculature (Peske et al., 2015). These tumors also contained a smaller number of CAFs than I.P. tumors from WT mice, which was similar to that of S.C. tumors (Figure 17A). These CAFs were sometimes found in a low number of small, loosely organized clusters with $CD45^{+}$ cells (Figure 17A and 18A), which were not observed in WT S.C. tumors, but did not form $PDPN^{+}$ reticular networks. Per cell expression of CCL21 and CXCL12 in CAFs from these tumors was reduced by 11- and 6-fold, respectively, but that of CXCL13, BAFF and APRIL was unchanged (Figure 17B). Per-cell expression of CXCL13, BAFF, and APRIL in CAFs from I.P. tumors grown in $Rag2^{-/-}$ $IL2R\gamma^{-/-}$ mice, which lack mature NK and ILC, was also comparable to that of CAFs from WT mouse tumors (Figure 18B). Thus, CAF expression of molecules known to drive B-cell accumulation and survival is controlled by a non-adaptive, non-NK, non-ILC element in the I.P. tumor microenvironment, but their accumulation and organization into reticular networks is controlled by adaptive immune cells.

To identify the adaptive immune cells driving CAF accumulation and organization, we utilized I.P. tumors grown in B-cell deficient $\mu MT^{-/-}$ mice and in $Rag1^{-/-}$ mice that had been repleted with bulk resting lymphocyte subpopulations prior to tumor implantation. Since these mice lack some TA-TLS elements, we evaluated tumors for $PDPN^{+}$ reticular networks co-extensive with tightly organized aggregates of $CD45^{+}$ cells. Tumors from $\mu MT^{-/-}$ mice contained such organized $CD45^{+}/PDPN^{+}$ aggregates in numbers comparable

Figure 17: CD8 T-cells and B-cells act coordinately as lymphoid tissue inducer cells driving TA-TLS development

(A, C, D) Day 14 I.P. B16-OVA tumors from WT, $\mu MT^{-/-}$, $Rag1^{-/-}$ and $Rag1^{-/-}$ mice repleted with CD8 T-cells and/or B-cells 3 days prior to tumor implantation were prepared for and analyzed by flow cytometry or IF as described in Methods. Scale bars = 100 μm. Data from 1-2 experiments, n=3-10 tumors per group. (B) CAFs from day 14 I.P. tumors from WT or $Rag1^{-/-}$ mice were purified and expression of the indicated RNA transcripts determined as described in Methods. Data from 2 experiments presented as $2^{-\Delta CT}$ relative to *Hprt*, n=6 tumors per group. Results are mean ± SD analyzed using Kruskal-Wallis h-test with Dunn's post-test (A, D) or unpaired Welch's t-test (B-C). ns: $p>0.05$, *$p<0.05$, **$p<0.01$, and ****$p<0.0001$.

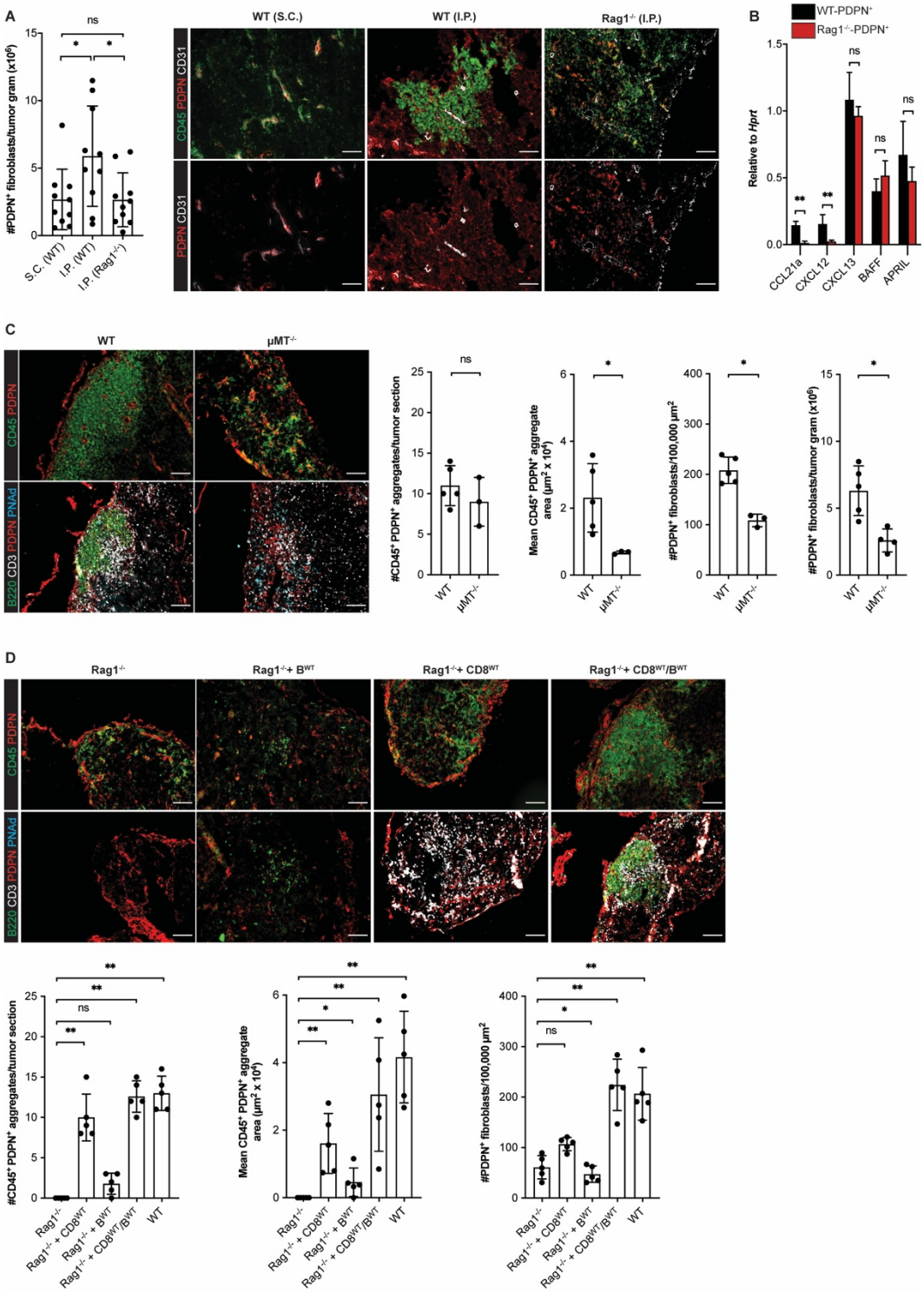
A
ns
#PDPN+ fibroblasts/tumor gram (x10^6)
S.C. (WT)
I.P. (WT)
I.P. (Rag1-/-)
WT (S.C.)
WT (I.P.)
Rag1-/- (I.P.)
CD45 PDPN CD31
PDPN CD31
B
WT-PDPN+
Rag1-/--PDPN+
Relative to Hprt
CCL21a
CXCL12
CXCL13
BAFF
APRIL
C
WT
µMT-/-
CD45 PDPN
B220 CD3 PDPN PNAd
#CD45+ PDPN+ aggregates/tumor section
Mean CD45+ PDPN+ aggregate area (µm2 x 10^4)
#PDPN+ fibroblasts/100,000 µm2
#PDPN+ fibroblasts/tumor gram (x10^6)
D
Rag1-/-
Rag1-/-+ BWT
Rag1-/-+ CD8WT
Rag1-/-+ CD8WT/BWT
#CD45+ PDPN+ aggregates/tumor section
Mean CD45+ PDPN+ aggregate area (µm2 x 10^4)
#PDPN+ fibroblasts/100,000 µm2
Rag1-/-
Rag1-/- + CD8WT
Rag1-/- + BWT
Rag1-/- + CD8WT/BWT
WT

Figure 18: CXCL13, BAFF, and APRIL are regulated independently of adaptive immunity, natural killer cells, and innate lymphoid cells

WT Rag1$^{-/-}$, Rag2$^{-/-}\gamma c^{-/-}$, and μMT$^{-/-}$ mice were injected I.P. with B16-OVA cells and tumors were harvested on day 14 and prepared for IF (A, C), qPCR (B), and flow cytometry (C) as described in Methods. (A) Summary data for loosely organized CD45^{+}/PDPN^{+} clusters in indicated tumors. Data from one experiment, n=3-5 tumor sections per group. (B) Expression of *Cxcl13, TNFSF13B* (BAFF), and *TNFS13* (APRIL) in CAFs from indicated I.P. tumors. Data presented as $2^{-\Delta CT}$ relative to *Hprt*. Data from one experiment, n=3-5 tumors per group. Left, summary data of the number of T-cells. Right, quantitative image summary data of the CD45^{+}/PDPN^{+} cluster number and size. Data represents one experiment, n=4-5 tumors per group. (A-C) Results shown as mean ± SD analyzed by unpaired Welch's t-test or (B) Kruskal-Wallis h-test with Dunn's post-test (H). ns: p>0.05, *P<0.05, **p<0.01, ***p<0.001, and ****p<0.0001.

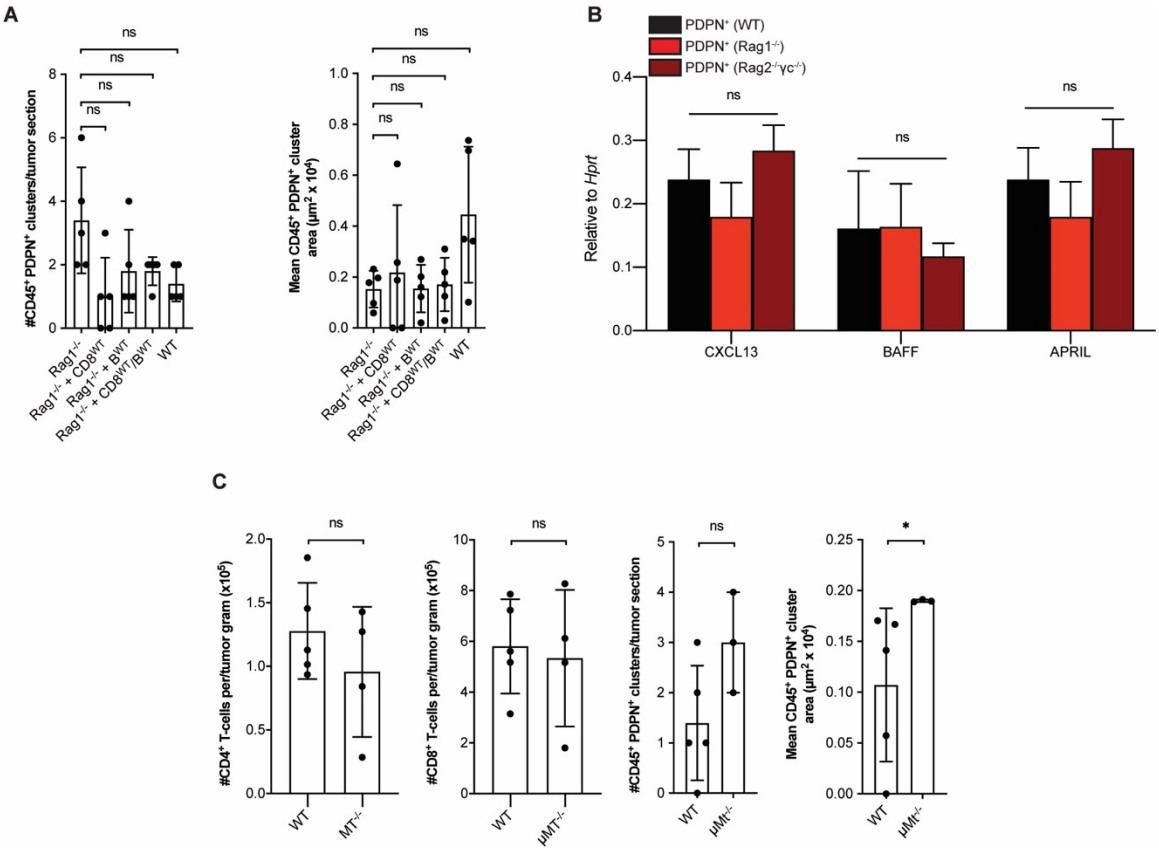
A
#CD45+ PDPN+ clusters/tumor section
Mean CD45+ PDPN+ cluster area (µm² x 10⁴)
ns
Rag1-/-
Rag1-/- + CD8WT
Rag1-/- + BWT
Rag1-/- + CD8WT/BWT
WT
B
PDPN+ (WT)
PDPN+ (Rag1-/-)
PDPN+ (Rag2-/-γc-/-)
Relative to Hprt
CXCL13
BAFF
APRIL
C
#CD4+ T-cells per/tumor gram (x10⁵)
#CD8+ T-cells per/tumor gram (x10⁵)
#CD45+ PDPN+ clusters/tumor section
Mean CD45+ PDPN+ cluster area (µm² x 10⁴)
WT
MT-/-
µMT-/-
*

to TA-TLS in WT mouse tumors, but they were significantly smaller (Figure 17C). Consistent with this, tumors from $\mu MT^{-/-}$ mice had a lower density of CAFs by IF and significantly fewer CAFs by flow cytometry (Figure 17C). However, tumors from $\mu MT^{-/-}$ and WT mice contained similar number of T-cells and the small loosely organized $CD45^+/PDPN^+$ clusters (Figure 18C). I.P. tumors from $Rag1^{-/-}$ mice repleted with $CD8^+$ T-cells contained organized $CD45^+/PDPN^+$ aggregates similar in size and number to those in $\mu MT^{-/-}$ mouse tumors (Figure 17D). Tumors from $Rag1^{-/-}$ mice repleted with B-cells contained an insignificantly different number of aggregates relative to tumors from unrepleted $Rag1^{-/-}$ mice, although there was a slight increase in aggregate area. Importantly, tumors from $Rag1^{-/-}$ mice repleted with both CD8 T-cells and B-cells resulted in structures comparable in number, size, and cellular composition and organization to TA-TLS in WT mouse tumors. The area per section of the structures in tumors from these different recipients was reflected in the density of CAFs (Figure 17D). Tumors from all of these mice contained a similar number of small loosely organized $CD45^+/PDPN^+$ clusters (Figure 18A). Thus, T-cells and B-cells act as complementary LTi cells mediating TA-TLS development: while T-cells initiate reticular network formation, B-cells drive expansion.

Intratumoral B cells drive TA-TLS expansion through LTβR signaling

LTβR signaling mediates the development of SLO and some TLS. We found that I.P. tumors expressed significantly higher transcript levels of LTβR ligands LTα, LTβ, and LIGHT than S.C. tumors (Figure 19A). To test their relevance, tumor-bearing mice were treated with an LTβR-Ig fusion protein, which binds $LT\alpha_1\beta_2$ and LIGHT and antagonizes

Figure 19: LTβR and TNFR signaling influences the representation of naïve T- and B-cell in I.P. tumors

WT or TNFR1/2$^{-/-}$ mice were S.C. or I.P. injected with B16-OVA cells, and tumors were harvested 14 days after implantation. In some cases (B-E), I.P. tumor-bearing mice were treated with a LTβR-Ig fusion protein. (A-B) whole tumor masses and inguinal LNs from tumor-bearing mice were analyzed by qPCR as described in Methods. (C-H) I.P. tumors were analyzed by flow cytometry as described in Methods. (A) Expression of *Tnfsf1* (Ltα), *Tnfsf3* (LTβ), and *Tnfsf14* (LIGHT) in whole S.C. and I.P. tumors. Data represents one experiment, n=5 tumors per group. (B) Expression of *Cxcl13* in tumor-reactive lymph node from mice treated with control IgG or LTβR-Ig. Data presented as $2^{-\Delta CT}$ relative to *Hprt*. Data represents one experiment, n=5 tumors per group. (C-D) Summary data of the total number of T-cells, and percentage of T-cells that are central memory (CD62L^{+} CD44^{hi}) and naïve (CD62L^{+} CD44^{lo}). Data represents one experiment, n=5 tumors per group. (E) Summary data of the percentage of B-cells that are naïve (IgM^{+} IgD^{+}), memory (IgM^{+} IgD^{neg}), and class-switched (IgM^{neg} IgD^{neg}). Data represents one experiment, n=5 tumors per group. (A-E, G-J) Results shown as mean ± SD analyzed by unpaired Welch's t-test or (F) Kruskal-Wallis h-test with Dunn's post-test (H). ns: $p>0.05$, *$P<0.05$, **$p<0.01$, ***$p<0.001$, and ****$p<0.0001$.

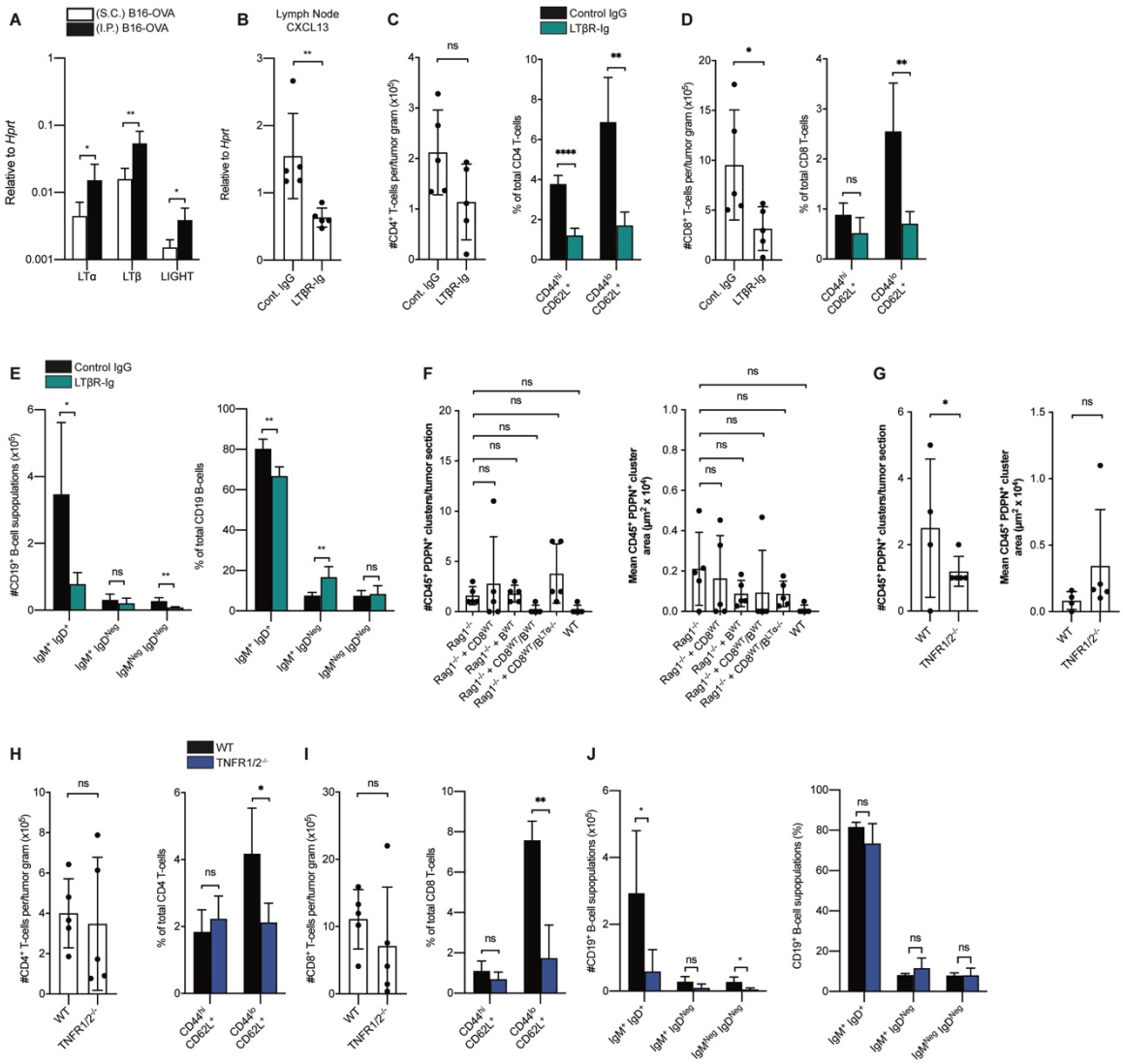
A
(S.C.) B16-OVA
(I.P.) B16-OVA
Relative to Hprt
LTα
LTβ
LIGHT
B
Lymph Node
CXCL13
Relative to Hprt
Cont. IgG
LTβR-Ig
C
Control IgG
LTβR-Ig
#CD4+ T-cells per/tumor gram (x10^5)
% of total CD4 T-cells
CD44hi CD62L+
CD44lo CD62L+
D
#CD8+ T-cells per/tumor gram (x10^5)
% of total CD8 T-cells
E
Control IgG
LTβR-Ig
#CD19+ B-cell supopulations (x10^5)
% of total CD19 B-cells
IgM+ IgD+
IgM+ IgDneg
IgMneg IgDneg
F
#CD45+ PDPN+ clusters/tumor section
Mean CD45+ PDPN+ cluster area (μm2 x 10^4)
Rag1-/-
Rag1-/- + CD8WT
Rag1-/- + BWT
Rag1-/- + CD8WT/BWT
Rag1-/- + CD8WT/BTeff-/-
WT
G
#CD45+ PDPN+ clusters/tumor section
Mean CD45+ PDPN+ cluster area (μm2 x 10^4)
WT
TNFR1/2-/-
H
WT
TNFR1/2-/-
#CD4+ T-cells per/tumor gram (x10^5)
% of total CD4 T-cells
I
#CD8+ T-cells per/tumor gram (x10^5)
% of total CD8 T-cells
J
#CD19+ B-cell supopulations (x10^5)
CD19+ B-cell supopulations (%)

LTβR signaling. Consistent with other work (Browning et al., 2005), LTβR-Ig treatment significantly reduced CXCL13 expression in tumor-reactive lymph nodes (Figure 19B). TA-TLS in I.P. tumors from LTβR-Ig treated mice were comparable in number to WT mouse tumors, but significantly smaller, and these tumors contained fewer CAFs (Figure 20A-B). Consistent with this, I.P. tumors from LTβR-Ig treated mice contained fewer CD8 T-cells and B-cells, and the fractions of naïve CD8 T-cells, naïve and central memory CD4 T-cells, and naïve B-cells were significantly reduced (Figure 19C-E and Figure 20C). However, per cell expression of CXCL13, BAFF, and APRIL in CAFs from these tumors was unaffected (Figure 20D). Thus, LTβR signaling promotes expansion of TA-TLS-associated $PDPN^+$ reticular networks, but not initial TA-TLS formation nor CAF expression of LTo molecular characteristics.

Since CAF accumulation and reticular network expansion were impaired in the absence of either B-cells or LTβR signaling, we tested whether it was mediated by $LT\alpha_1\beta_2^+$ B-cells. Tumors in $Rag1^{-/-}$ mice repleted with WT CD8 T-cells and $LT\alpha^{-/-}$ B-cells developed organized $CD45^+/PDPN^+$ aggregates comparable in size and number to those in tumors from $Rag1^{-/-}$ mice repleted with $CD8^+$ T-cells alone, and in tumors from LTβR-Ig treated mice (Figure 20E). Also, the density of CAFs in these tumor sections was comparable to I.P. tumors from $Rag1^{-/-}$ mice repleted with $CD8^+$ T-cells alone (Figure 20E). Tumors from all of these mice contained a similar number of small loosely organized $CD45^+/PDPN^+$ clusters (Figure 19F). Thus, CAF accumulation and TA-TLS expansion is mediated by intratumoral $LT\alpha_1\beta_2^+$ B-cells.

Figure 20: Induction and robust development of PDPN^{+} reticular networks in TA-TLS is regulated by TNFR and LTβR signaling, respectively

Day 14 I.P. B16-OVA tumors from WT mice, WT mice treated with LTβR-Ig fusion protein, TNFR1/2$^{-/-}$ mice, Rag1$^{-/-}$ mice, and Rag1$^{-/-}$ mice repleted with CD8 T-cells and/or B-cells 3 days prior to tumor implantation, were analyzed by IF or flow cytometry as described in Methods. (A, E, F) Scale bars = 100 μm. Data from 1 experiment, n=3-5 tumors per group. (B-C, G-H) Data from 1 experiment, n=5 tumors per group. (D, I) CAFs from day 14 I.P. tumors from WT mice, WT mice treated with LTβR-Ig, or TNFR1/2$^{-/-}$ mice were purified and expression of the indicated RNA transcripts determined as described in Methods. Data from 2 experiments presented as $2^{-\Delta CT}$ relative to *Hprt*, n=6 tumors per group. Results are mean ± SD analyzed using unpaired Welch's t-test (A-D, F-I) or Kruskal-Wallis h-test with Dunn's post-test (E). ns: $p>0.05$, *$p<0.05$, and **$p<0.01$.

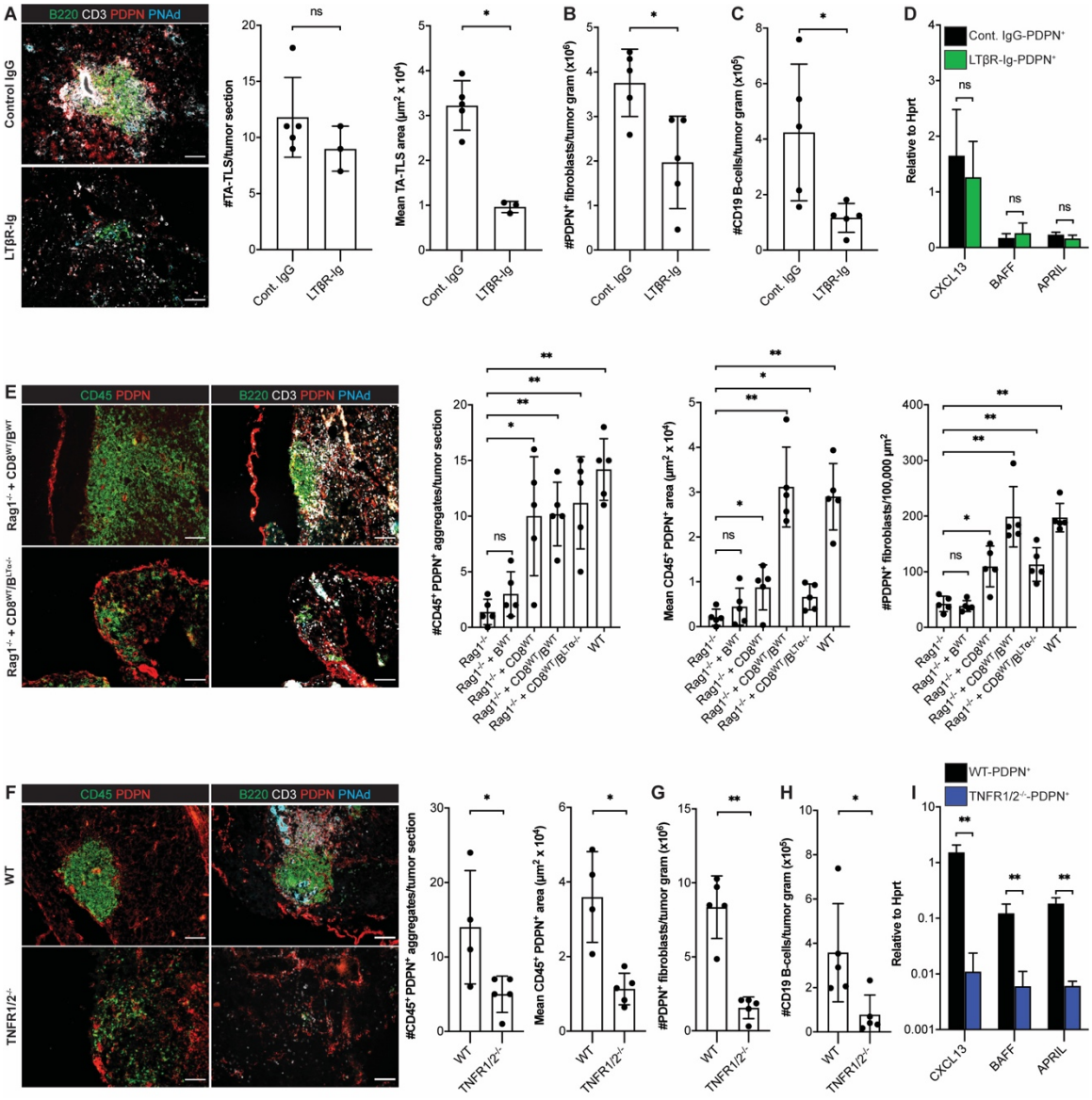
A
B220 CD3 PDPN PNAd
Control IgG
LTβR-Ig
#TA-TLS/tumor section
Mean TA-TLS area (μm² x 10⁴)
Cont. IgG
LTβR-Ig
ns
*
B
#PDPN⁺ fibroblasts/tumor gram (x10⁶)
C
#CD19 B-cells/tumor gram (x10⁵)
D
Cont. IgG-PDPN⁺
LTβR-Ig-PDPN⁺
Relative to Hprt
CXCL13
BAFF
APRIL
E
CD45 PDPN
B220 CD3 PDPN PNAd
Rag1⁻/⁻ + CD8^WT/βWT
Rag1⁻/⁻ + CD8^WT/βLTα⁻/⁻
#CD45⁺ PDPN⁺ aggregates/tumor section
Mean CD45⁺ PDPN⁺ area (μm² x 10⁴)
#PDPN⁺ fibroblasts/100,000 μm²
Rag1⁻/⁻
Rag1⁻/⁻ + BWT
Rag1⁻/⁻ + CD8WT
Rag1⁻/⁻ + CD8WT/βWT
Rag1⁻/⁻ + CD8WT/βLTα⁻/⁻
WT
F
WT
TNFR1/2⁻/⁻
G
H
I
WT-PDPN⁺
TNFR1/2⁻/⁻-PDPN⁺

TNFR signaling promotes PDPN^{+} reticular network formation and expression of LTo molecules

Next, we determined whether TNFR signaling mediates TA-TLS development. In keeping with the models described above, we observed organized CD45^{+}/PDPN^{+} aggregates in I.P. tumors grown in TNFR1/2$^{-/-}$ mice that were smaller than TA-TLS in WT mouse tumors (Figure 20F). However, they were fewer, and the number of small loosely organized CD45^{+}/PDPN^{+} clusters was also reduced (Figure 19G). As with TA-TLS in LTβR-Ig treated mice, TNFR1/2$^{-/-}$ mouse tumors contained fewer CAFs (Figure 20G), and the fractions of naïve CD4 and CD8 T-cells were reduced (Figure 19H-I). These tumors also contained fewer B-cells (Figure 20H), although the distribution of naïve, class-switched and memory B-cells was unaltered (Figure 19J). Most importantly, per cell expression of CXCL13, BAFF, and APRIL in CAFs was substantially reduced (Figure 20I). These results demonstrate that TNFR signaling promotes PDPN^{+} reticular network development and LTo molecular characteristics of CAFs.

Relationship of TA-TLS associated I.P. CAFs to peritoneal fibroblasts

The proximity of I.P. tumors to peritoneal organs suggested that CAFs with LTo characteristics might derive from them. PDPN^{hi} cells from spleen, omentum, lung, pancreas, and skin of WT mice showed varying levels of CXCL13, BAFF, and APRIL expression (Figure 21A-C). Similar to I.P. CAFs, CXCL13 expression in PDPN^{hi} cells from the omentum was significantly reduced in TNFR1/2$^{-/-}$ mice (Figure 21A), but was unaltered in cells from other organs (Figure 21A). However, in contrast to WT I.P. CAFs,

Figure 21: CXCL13 expression, but not BAFF and APRIL, in omental fibroblasts is regulated by tumor necrosis factor receptor signaling

Tissue resident fibroblasts from indicated tissues of non-tumor bearing WT and TNFR1/2$^{-/-}$ mice were analyzed by qPCR as described in Methods. (A-C) Expression of *Cxcl13, TNFSF13B* (BAFF), and *TNFS13* (APRIL) in fibroblasts from indicated tissues. Data presented as $2^{-\Delta CT}$ relative to *Hprt*. Data represents one experiment, n= 5 mice per group. Results shown as mean ± SD. (A-C) Unpaired Welch's t-test. ns: $p>0.05$, *$P<0.05$, **$p<0.01$, ***$p<0.001$, and ****$p<0.0001$.

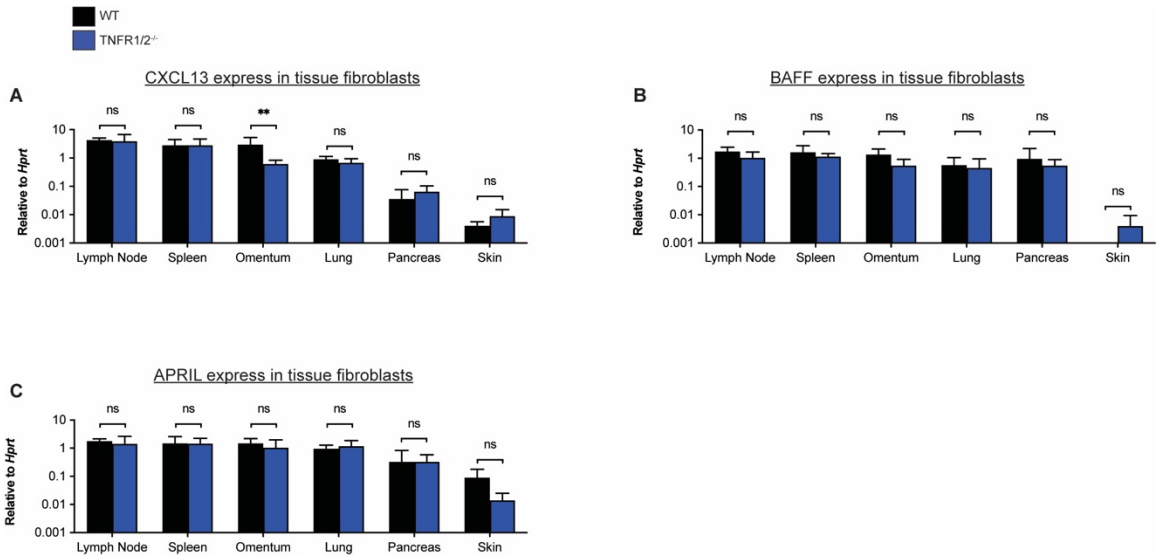
WT
TNFR1/2-/-
A
CXCL13 express in tissue fibroblasts
Relative to Hprt
10
1
0.1
0.01
0.001
ns
ns
**
ns
ns
ns
Lymph Node
Spleen
Omentum
Lung
Pancreas
Skin
B
BAFF express in tissue fibroblasts
Relative to Hprt
ns
ns
ns
ns
ns
ns
Lymph Node
Spleen
Omentum
Lung
Pancreas
Skin
C
APRIL express in tissue fibroblasts
Relative to Hprt
ns
ns
ns
ns
ns
ns
Lymph Node
Spleen
Omentum
Lung
Pancreas
Skin

BAFF and APRIL expression was not reduced in PDPN^{hi} cells from any organ in TNFR1/2$^{-/-}$ mice (Figure 21B-C). These results do not identify any peritoneal organ as the direct source of I.P. CAFs. To the extent that they do originate from a peritoneal organ, they indicate that elements within the I.P. tumor microenvironment alter their TNFR-dependent expression of BAFF, APRIL, and in some cases, CXCL13.

Human TA-TLS contain elevated densities of LT^{+} B-cells co-extensive with a reticular network of LTo-like CAFs

To establish translational relevance of mechanisms driving murine TA-TLS development, we evaluated 3 human melanomas by quantitative image analysis using 7-color IF. We identified TA-TLS as aggregates of PNAd^{+} cells, CD20^{+} B-cells, CD8^{+} T-cells, and gp36^{+} CAFs (Figure 22A-B and Figure 23A-B). TA-TLS in all samples were enriched for APRIL^{+}, VCAM-1^{+}, and LTα^{+} cells relative to the surrounding parenchyma, and TA-TLS in 2 samples showed higher densities of CXCL13^{+} cells (Figure 23B). TA-TLS in all samples were enriched for B-cells expressing LTα, and these cells represented 60-80% of the LTα^{+} population inside the TA-TLS, as opposed to 0-15% of those in the parenchyma (Figure 23C). TA-TLS in all samples also contained higher densities of CAFs expressing APRIL^{+} and VCAM-1^{+} than the tumor parenchyma. The fraction of APRIL^{+} CAFs was significantly higher in the TA-TLS of all samples, and the fraction of VCAM-1^{+} CAFs was significantly higher in TA-TLS of 2/3 samples (Figure 23C). However, only one sample showed higher densities of CXCL13^{+} CAFs in TA-TLS, and there was no enrichment of CXCL13^{+} CAFs in TA-TLS vs parenchyma (Figure 23C). The densities of B-cells in TA-TLS strongly correlated with the densities of CAFs overall, and the densities of VCAM-1^{+}

Figure 22: TA-TLS in human melanoma contain similar cellular and molecular markers found in murine TA-TLS

Human melanoma biopsies containing TA-TLS were collected, prepared, stained, and analyzed by multispectral imaging as described in Methods. (A) Representative multispectral images of three independent human melanoma biopsies stained for indicated markers. (B) Representative multispectral images of human melanoma biopsy #1 stained for indicated markers. Dashed region of interest represents TA-TLS area. Scale bar = 100

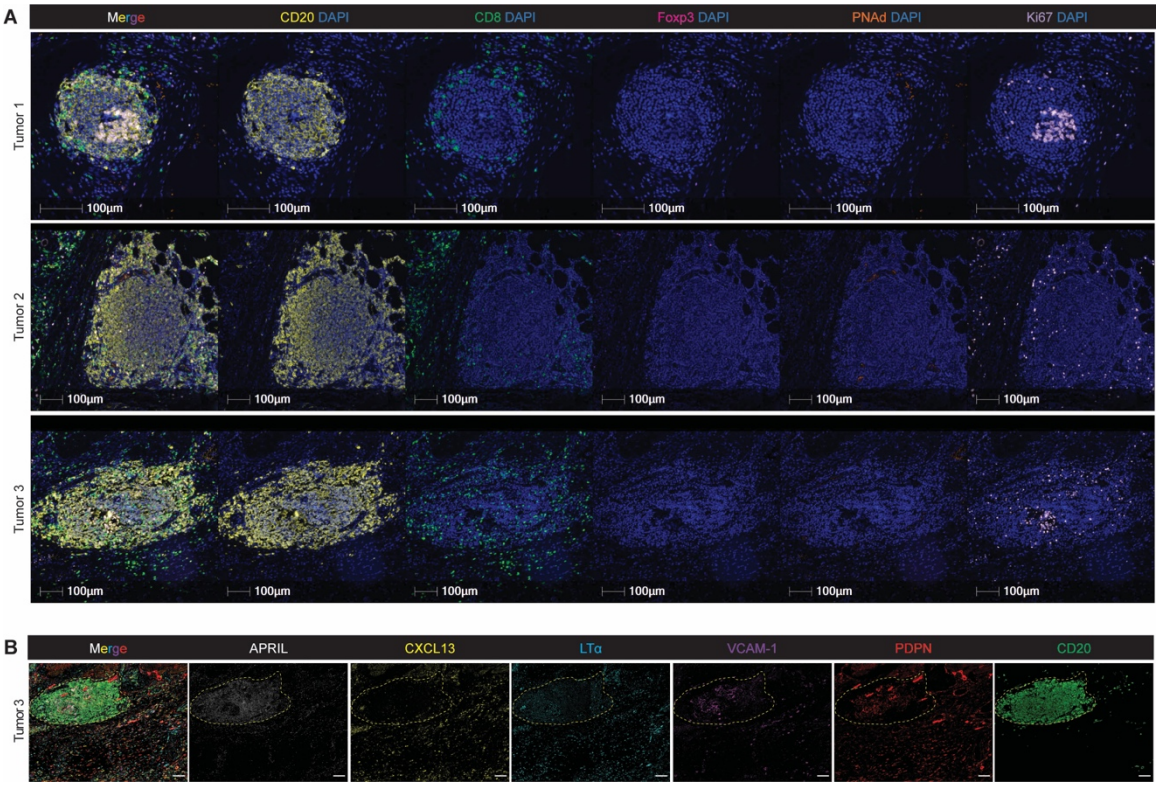
A
Merge
CD20 DAPI
CD8 DAPI
Foxp3 DAPI
PNAd DAPI
Ki67 DAPI
Tumor 1
Tumor 2
Tumor 3
100μm
B
Merge
APRIL
CXCL13
LTα
VCAM-1
PDPN
CD20
Tumor 3

Figure 23: Human TA-TLS are associated with LT^+ B-cells and a co-extensive reticular network of CAFs with lymphoid tissue organizer characteristics

Human melanoma biopsies containing TA-TLS were collected, prepared, stained and analyzed as described in Methods. (A) Representative image of a TA-TLS containing melanoma sample. Dashed yellow line represents TA-TLS area. Scale bar = 100 μm. (B, C) Densities and percentages of single (B) and dual (C) stained cell populations in parenchyma and TA-TLS regions of tumors from 3 patients (n=12-39 parenchyma and TA-TLS regions of interest). Data were analyzed by Wilcoxon Rank-Sum test, and boxplots generated according to Tukey's method. (D) Correlations between density of B-cell populations and density or fraction of fibroblast populations. Dots represent individual TA-TLS. Each line represents the correlation for an individual tumor. Rho represents the multilevel correlation coefficient for the three tumors. Spearman's linear mixed-models multilevel correlation analysis was determined for all tumors together to account for the nested data structure. ns: $p>0.05$, *$p<0.05$, **$p<0.01$, ***$p<0.001$, and ****$p<0.0001$.

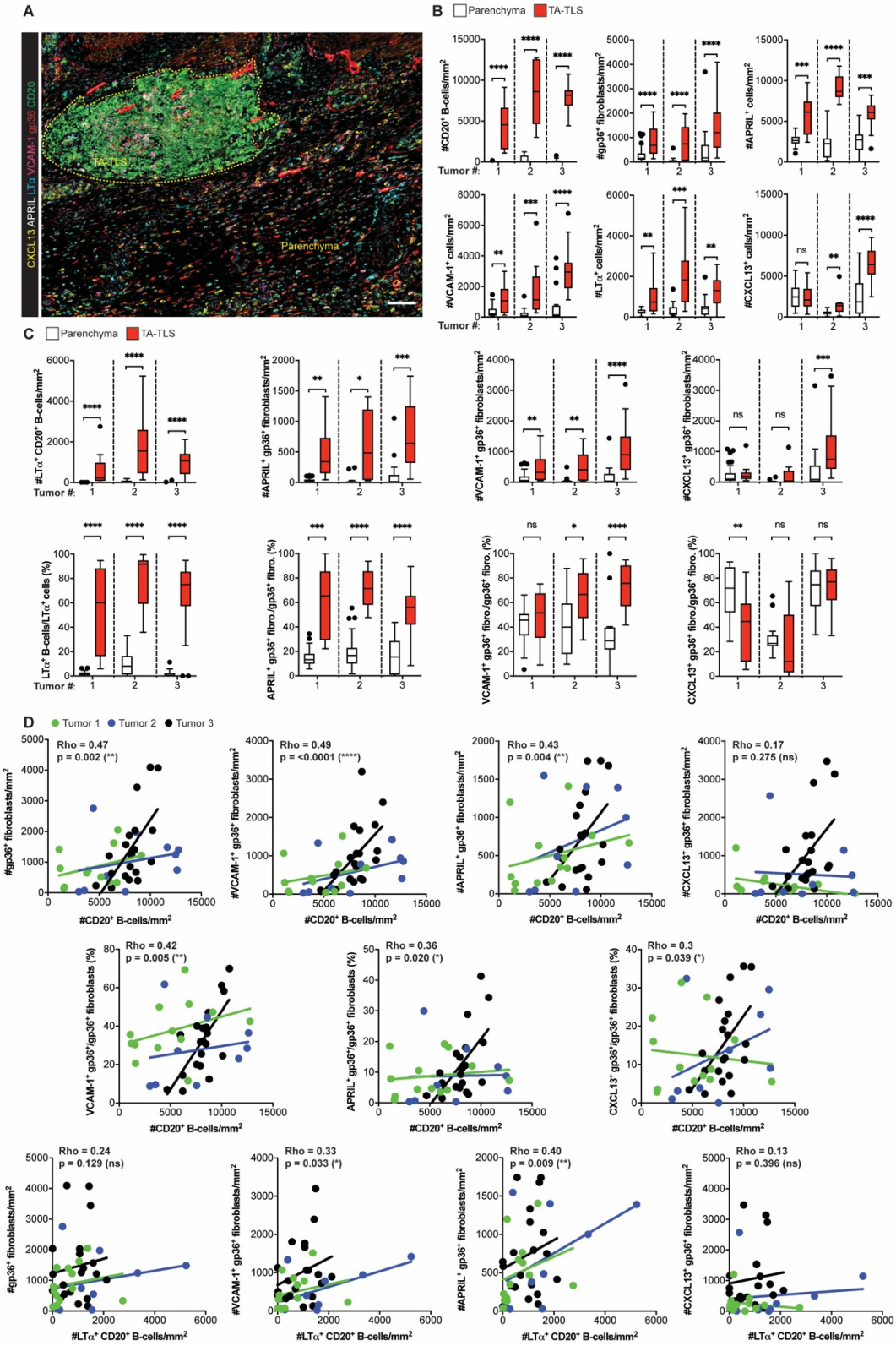
A
CXCL13 APRIL LTα VCAM-1 gp36 CD20
TA-TLS
Parenchyma
B
Parenchyma
TA-TLS
#CD20+ B-cells/mm2
#gp36+ fibroblasts/mm2
#APRIL+ cells/mm2
#VCAM-1+ cells/mm2
#LTα+ cells/mm2
#CXCL13+ cells/mm2
Tumor #:
C
Parenchyma
TA-TLS
#LTα+ CD20+ B-cells/mm2
#APRIL+ gp36+ fibroblasts/mm2
#VCAM-1+ gp36+ fibroblasts/mm2
#CXCL13+ gp36+ fibroblasts/mm2
LTα+ B-cells/LTα+ cells (%)
APRIL+ gp36+ fibro./gp36+ fibro. (%)
VCAM-1+ gp36+ fibro./gp36+ fibro. (%)
CXCL13+ gp36+ fibro./gp36+ fibro. (%)
Tumor #:
D
Tumor 1
Tumor 2
Tumor 3
Rho = 0.47
p = 0.002 (**)
Rho = 0.49
p = <0.0001 (****)
Rho = 0.43
p = 0.004 (**)
Rho = 0.17
p = 0.275 (ns)
#gp36+ fibroblasts/mm2
#VCAM-1+ gp36+ fibroblasts/mm2
#APRIL+ gp36+ fibroblasts/mm2
#CXCL13+ gp36+ fibroblasts/mm2
#CD20+ B-cells/mm2
Rho = 0.42
p = 0.005 (**)
Rho = 0.36
p = 0.020 (*)
Rho = 0.3
p = 0.039 (*)
VCAM-1+ gp36+/gp36+ fibroblasts (%)
APRIL+ gp36+/gp36+ fibroblasts (%)
CXCL13+ gp36+/gp36+ fibroblasts (%)
Rho = 0.24
p = 0.129 (ns)
Rho = 0.33
p = 0.033 (*)
Rho = 0.40
p = 0.009 (**)
Rho = 0.13
p = 0.396 (ns)
#LTα+ CD20+ B-cells/mm2

or APRIL^{+} CAFs, but not those expressing CXCL13 (Figure 23D). However, the densities of B-cells in TA-TLS also strongly correlated with the fractions of CAFs in TA-TLS expressing VCAM-1 and APRIL, as well as CXCL13. Finally, the densities of LTα^{+} B-cells in TA-TLS correlated with the densities of CAFs expressing VCAM-1 and APRIL, but not CXCL13. These results are consistent with the idea that human melanoma-associated TA-TLS are driven by similar cellular and molecular mechanisms as those driving murine TA-TLS development.

TA-TLS are associated with reduced tumor outgrowth and response to checkpoint immunotherapy

Increased number and size of TA-TLS strongly correlated with diminished I.P tumor size in WT mice (Figure 24A), and deficiencies in TA-TLS development as a result of implantation into CXCR5$^{-/-}$, μMT$^{-/-}$, LTβR-Ig treated, and TNFR1/2$^{-/-}$ mice were all associated with tumors that were significantly larger (170-235%) than tumors in WT mice (Figure 24B). Also, a larger fraction of I.P. CAFs expressed PD-L1 than their S.C. counterparts (Figure 24C). Thus, we assessed the impact of checkpoint immunotherapy on TA-TLS development and control of tumor outgrowth. We treated tumor-bearing WT mice with anti-PD-L1 monotherapy or the combination of anti-CTLA4 and anti-PD1 and analyzed tumors after 14 days of outgrowth. Both treatments increased intratumoral T-cell numbers in both S.C. and I.P. tumors, but neither increased intratumoral B-cell numbers nor promoted TA-TLS formation in S.C. tumors (Figure 25A-B). However, both treatments increased the number of intratumoral B-cells in I.P. tumors. They also induced significant increases in TA-TLS number and size, suggesting that they initiate TA-TLS

Figure 24: I.P. tumors grown in knockout and LTβR-Ig treated mice are larger than those grown in WT mice

WT, knockout, LTβR-Ig treated mice were S.C. or I.P. injected with B16-OVA cells and harvested on 14 days after implantation. (A-B) Tumors were harvest and weighed. (C) S.C. and I.P. tumors were analyzed by flow cytometry as described in Methods. (A) Correlation analysis between the number and size of TA-TLS per tumor section against tumor weight. Red lines represent 95% confident intervals. Each point represents an individual I.P. tumor. Data represents five independent experiments, n= 25 tumors. (B) Tumor weight of day 14 I.P. tumors grown in indicated mouse models. Data represents two-three independent experiments, n=8-10 tumors per group. (C) Representative histogram plots and gMFI of PD-L1 on CAFs from S.C. and I.P. tumors from WT mice. Right, summary data of the percentage of CAFs expressing PD-L1 from WT S.C. and I.P tumors. Data represents two independent experiments, n=11 tumors per group. Results shown as mean ± SD. (A) Spearman correlation analysis and (B-C) Unpaired Welch's t-test. ns: $p>0.05$, *$P<0.05$, **$p<0.01$, ***$p<0.001$, and ****$p<0.0001$.

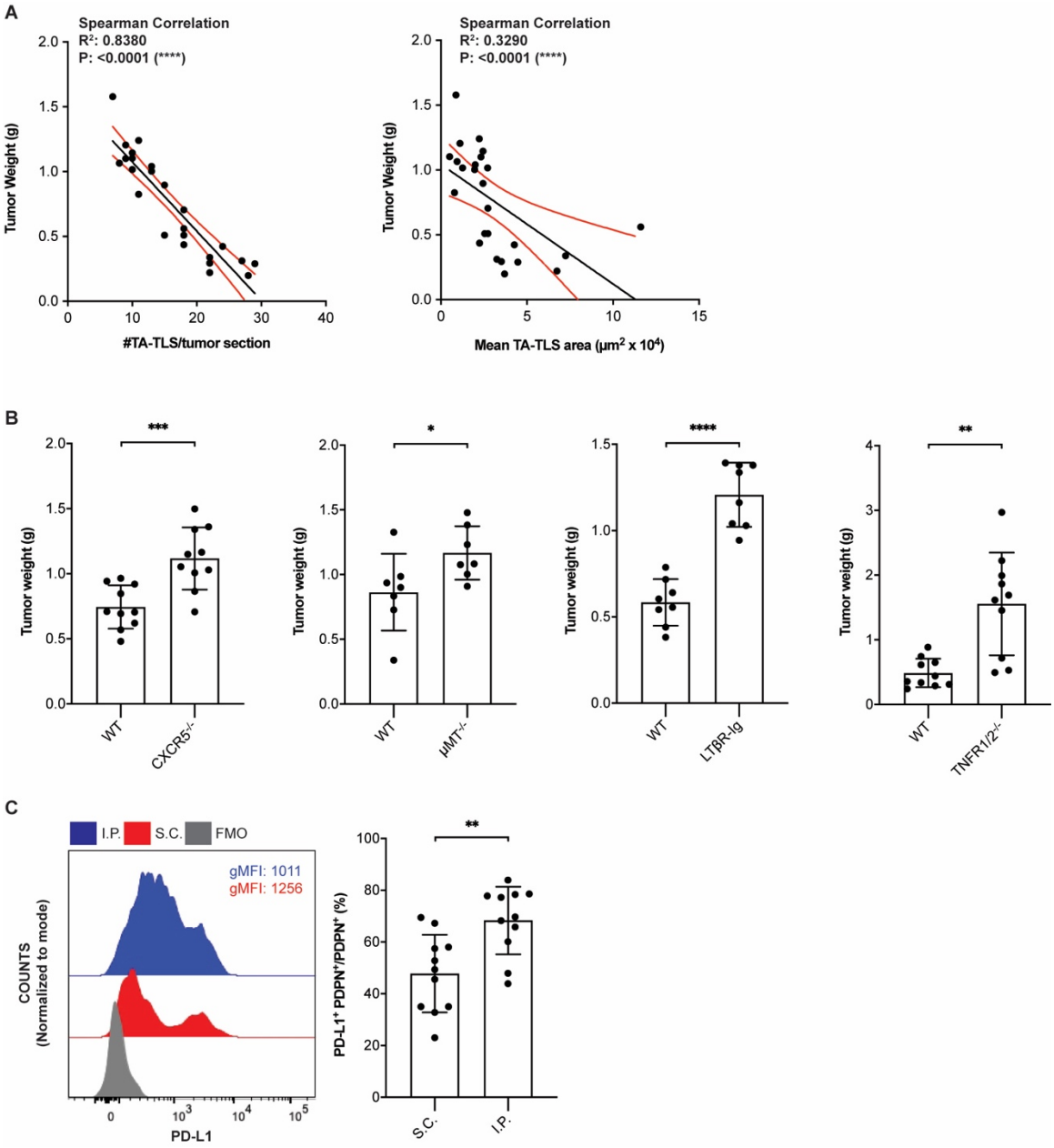
A
Spearman Correlation
R²: 0.8380
P: <0.0001 (****)
Tumor Weight (g)
#TA-TLS/tumor section
Spearman Correlation
R²: 0.3290
P: <0.0001 (****)
Tumor Weight (g)
Mean TA-TLS area (μm² x 10⁴)
B
Tumor weight (g)
WT
CXCR5-/-
μMT-/-
LTβR-Ig
TNFR1/2-/-
C
I.P.
S.C.
FMO
gMFI: 1011
gMFI: 1256
COUNTS
(Normalized to mode)
PD-L1
PD-L1+ PDPN+/PDPN+ (%)
S.C.
I.P.

Figure 25: TA-TLS number, size, and organization are augmented by checkpoint immunotherapy and correlated with tumor control

WT or TNFR1/2$^{-/-}$ mice were treated with control IgG, anti-PDL1, or anti-CTLA4/PD1 beginning 3 days after S.C. or I.P. tumor implantation. Tumors were harvested on day 14, weighed, and prepared for IF. (A-E) Data is from 2-3 experiments, n=10-15 tumors per group. (F-H) Data is from 2 experiments, n=10 tumors per group. (A) Summary data for intratumoral parenchymal (non-TA-TLS) T- and B-cell densities in WT mouse tumors. (B) Representative images showing typical TA-TLS size and organization in tumors from WT mice treated as indicated. Scale bar = 100 μm. (C) Summary data of TA-TLS characteristics in tumors from WT mice. Classical TA-TLS are distinguished from non-classical by the presence of distinct T- and B-cell compartments. (D) Tumor weights determined at harvest on day 14. (E) Spearman correlation analysis of WT mouse tumor weights with TA-TLS number, size, or densities of intratumoral parenchymal T- and B-cells. Each dot represents an individual tumor. (F) Left and middle, Summary data for intratumoral parenchymal (non-TA-TLS) T- and B-cell densities in TNFR1/2$^{-/-}$ mouse tumors. Right, Tumor weights were determined at harvest on day 14. (G) Representative intratumoral images of I.P. tumors fromTNFR1/2$^{-/-}$ mice treated as indicated. Scale bar = 100 μm. (H) Spearman correlation analysis of TNFR1/2$^{-/-}$ mouse tumor weights with densities of T- and B-cells. Each dot represents an individual tumor. Results shown as mean ± SD analyzed using Kruskal-Wallis h-test with Dunn's post-test (A, C-D, F) or Spearman's multilevel correlation analysis (E, H). ns: $p>0.05$, *$p<0.05$, and **$p<0.01$.

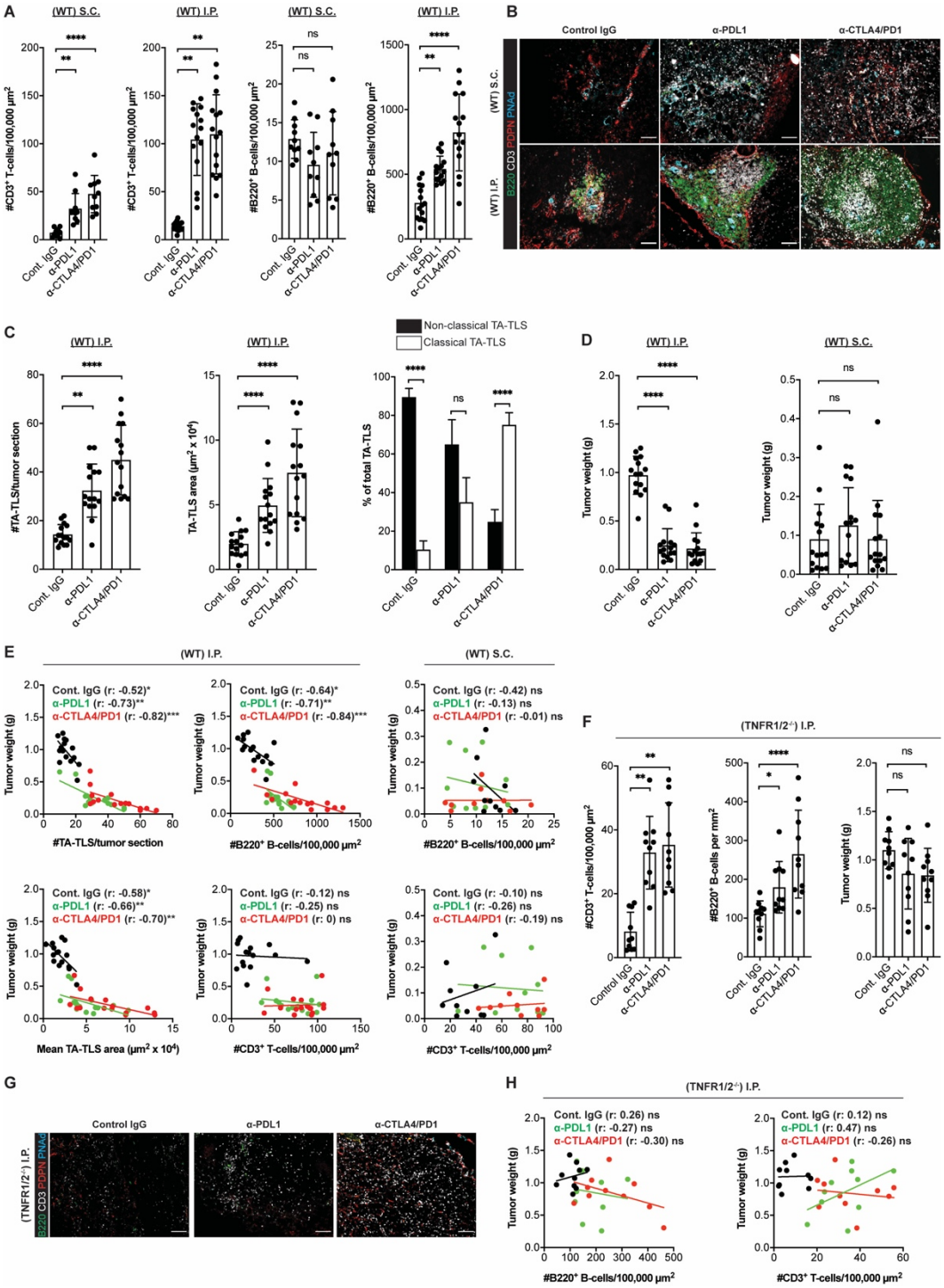
A
(WT) S.C.
(WT) I.P.
(WT) S.C.
(WT) I.P.
#CD3+ T-cells/100,000 µm2
#CD3+ T-cells/100,000 µm2
#B220+ B-cells/100,000 µm2
#B220+ B-cells/100,000 µm2
Cont. IgG
α-PDL1
α-CTLA4/PD1
B
Control IgG
α-PDL1
α-CTLA4/PD1
(WT) S.C.
(WT) I.P.
PNAd
PDPN
CD3
B220
C
Non-classical TA-TLS
Classical TA-TLS
(WT) I.P.
(WT) I.P.
#TA-TLS/tumor section
TA-TLS area (µm2 x 10⁴)
% of total TA-TLS
D
(WT) I.P.
(WT) S.C.
Tumor weight (g)
Tumor weight (g)
E
(WT) I.P.
(WT) S.C.
Cont. IgG (r: -0.52)*
α-PDL1 (r: -0.73)**
α-CTLA4/PD1 (r: -0.82)***
#TA-TLS/tumor section
Cont. IgG (r: -0.64)*
α-PDL1 (r: -0.71)**
α-CTLA4/PD1 (r: -0.84)***
#B220+ B-cells/100,000 µm2
Cont. IgG (r: -0.42) ns
α-PDL1 (r: -0.13) ns
α-CTLA4/PD1 (r: -0.01) ns
#B220+ B-cells/100,000 µm2
Cont. IgG (r: -0.58)*
α-PDL1 (r: -0.66)**
α-CTLA4/PD1 (r: -0.70)**
Mean TA-TLS area (µm2 x 10⁴)
Cont. IgG (r: -0.12) ns
α-PDL1 (r: -0.25) ns
α-CTLA4/PD1 (r: 0) ns
#CD3+ T-cells/100,000 µm2
Cont. IgG (r: -0.10) ns
α-PDL1 (r: -0.26) ns
α-CTLA4/PD1 (r: -0.19) ns
#CD3+ T-cells/100,000 µm2
F
(TNFR1/2-/-) I.P.
#CD3+ T-cells/100,000 µm2
#B220+ B-cells per mm2
Tumor weight (g)
Control IgG
α-PDL1
α-CTLA4/PD1
G
Control IgG
α-PDL1
α-CTLA4/PD1
(TNFR1/2-/-) I.P.
PNAd
PDPN
CD3
B220
H
(TNFR1/2-/-) I.P.
Cont. IgG (r: 0.26) ns
α-PDL1 (r: -0.27) ns
α-CTLA4/PD1 (r: -0.30) ns
#B220+ B-cells/100,000 µm2
Cont. IgG (r: 0.12) ns
α-PDL1 (r: 0.47) ns
α-CTLA4/PD1 (r: -0.26) ns
#CD3+ T-cells/100,000 µm2

development and also operate on existing TA-TLS (Figure 25A-C). Both treatments also promoted the development of TA-TLS with a "*classical*" (discrete T– and B-cell zones) organization (Figure 25B-C). Also, both treatments significantly reduced I.P. tumor size, but neither significantly reduced S.C. B16-OVA tumor size at this day 14 timepoint, despite the increased number of intratumoral T-cells (Figure 25D). As with untreated mice, increased TA-TLS size and number was correlated with reduced tumor size. However, this correlation was more significant in both treatment groups (Figure 25E). Similarly, B-cell density correlated with reduced I.P. tumor size in untreated mice, and this correlation was also more significant in treated mice. In contrast, neither the density of total intratumoral T-cells in S.C. or I.P. tumors, nor the density of intratumoral B-cells in S.C. tumors, correlated with day 14 tumor size under any treatment condition (Figure 25E). These results suggested that TA-TLS are an important determinant of anti-tumor activity in this model. To provide support for this hypothesis, we treated TNFR1/2$^{-/-}$ mice bearing I.P. tumors in the same way. Both treatments again increased the number of intratumoral T- and B-cells at day 14, but did not promote TA-TLS development (Figure 25F-G). In contrast to WT mouse I.P. tumors, neither treatment reduced day 14 tumor size (Figure 25F), and the correlation between intratumoral B-cell density and tumor size was lost (Figure 25H). These results demonstrate that checkpoint immunotherapy targets TA-TLS, leading to increases in their size and number. The extent of these changes is strongly correlated with tumor control. The potential importance of TA-TLS is heightened by a lack of correlation between tumor size and overall intratumoral T-cell density.

Discussion

This report identifies cellular and molecular mechanisms driving TA-TLS development in murine melanoma. A discrete population of CAFs acquire LTo molecular characteristics in response to TNFR signals from a cell that is neither an adaptive nor innate immune lymphoid cell, and respond to intratumoral CD8 T-cells and B-cells that act coordinately as LTi cells. While CD8 T-cells promote initial aggregation and reticular network formation, B-cells are recruited by CXCL13 expressing CAFs, subsequently driving CAF proliferation and TA-TLS expansion through LTβR signaling. Some of these cellular and molecular elements are overrepresented in human TA-TLS and associated with one another. Lastly, TA-TLS number, size, and organization increase in response to checkpoint immunotherapy, and these aspects of TA-TLS are strongly correlated with reduced tumor size. This work provides a platform for manipulating TA-TLS formation as a cancer immunotherapy strategy.

Our findings identify a previously undescribed role of a population of FAP^{neg} CAFs as TA-TLS organizers. CAFs that express elevated levels of FAP inversely correlate with patient survival, and their depletion results in diminished murine tumor outgrowth (Kraman et al., 2010). The numbers of FAP^{+} CAFs in both S.C. and I.P. tumors were comparable, and these cells were rarely found in TA-TLS. In contrast, FAP^{neg} CAFs were elevated in I.P. tumors and the dominant population in TA-TLS reticular networks. FAP^{neg} CAFs promoted TA-TLS development in non-TA-TLS containing S.C. tumors. The number and size of these structures was lower than in I.P tumors, and this may reflect constraints imposed by the S.C. tumor microenvironment. Both FAP^{neg} and FAP^{+} CAFs in I.P. tumors

co-expressed ICAM-1 and VCAM-1 that were significantly higher than those expressed by FAP^+ CAFs in S.C. tumors. In keeping with this, FAP^+ CAFs from I.P. tumors have a minimal LTo capability that is nonetheless greater than that of CAFs from S.C tumors. While $PDPN^+$ cells expressing elevated levels of ICAM-1 and VCAM-1 have been documented in TLS associated with chronically inflamed tissues or murine pancreatic carcinoma (Peduto et al., 2009; Link et al., 2011), only a single report has demonstrated that such fibroblasts could support TLS formation in a murine model of Sjögren's syndrome, and these cells were FAP^+ (Nayar et al., 2019). It is possible that FAP^+ CAFs from I.P. tumors express lower levels of CXCL13, BAFF, and APRIL, than their FAP^{neg} counterparts, presumably as a consequence of TNFR signaling. These FAP^+ CAFs may also be less proliferative than their FAP^{neg} counterparts. However, neither of these possibilities explains the observed differential accumulation of FAP^{neg} and FAP^+ CAFs in TA-TLS and parenchyma, respectively. Our findings point to the importance of continuing work to characterize CAF subpopulations in different human tumors.

CAFs can originate by trans-differentiation from tumor or endothelial cells, but typically from tissue resident $PDPN^+$ mesothelial cells (LeBleu & Kalluri, 2018; T. Liu et al., 2019). CAFs in human and murine peritoneal carcinomas arise from $PDPN^+$ mesothelial cells lining the peritoneal cavity (Rynne-Vidal et al., 2015). The omentum contains a substantial number of $PDPN^+$ $CXCL13^+$ mesothelial cells (Jackson-Jones et al., 2020), and we identified $PDPN^+$ $CXCL13^+$ cells in the spleen, lung, and pancreas. Any or all of these cells could contribute to CAF in I.P. tumors, but none showed the TNFR dependent regulation of BAFF and APRIL of I.P. tumor CAFs. $PDPN^+$ cells from spleen,

lung, and pancreas also did not show TNFR dependent regulation of CXCL13. This suggests either another source of I.P. tumors CAFs or changes in TNFR signaling in these populations under the influence of the tumor microenvironment. Regardless, the peritoneal cavity is a site for the growth or metastasis of many kinds of tumors, including melanoma (A. Kawashima et al., 1991; Trout et al., 2013). We also observed TA-TLS in tumors growing in lung, and $PDPN^{+}$ $CXCL13^{+}$ cells have been identified in several adipose tissues (Bénézech et al., 2015). Consequently, we believe that this I.P. tumor model reflects a physiologically relevant TA-TLS biology that should be explored further.

Our results also provided insight into the mechanisms used by the CAF population to promote TA-TLS development. CAFs from I.P. tumors expressed substantially higher levels of CXCL13, BAFF, and APRIL than those from S.C. tumors, and an intact CXCR5-CXCL13 axis promoted B-cell accumulation in tumors, increased proliferation of CAFs, and TA-TLS expansion. While B-cell follicles are disrupted in $CXCR5^{-/-}$ mice, the overall number of B-cells in SLOs is unaffected (Forster et al., 1996), making it likely that our result is due to a role for CXCL13 in promoting B-cell accumulation. It is possible that CXCL13 enhances B-cell proximity to CAFs that express BAFF and APRIL, promoting B-cell organization and/or survival in tumors. Elevated expression of CXCL13 is a common feature of TLS (Rangel-Moreno et al., 2007; Fleige et al., 2014; Barone et al., 2015; Sato et al., 2016), and fibroblasts purified from inflamed tissues containing TLS can express this molecule (Khader et al., 2011; Rangel-Moreno et al., 2011; Barone et al., 2015). The CXCR5-CXCL13 axis controls B-cell accumulation in FALCs (Bénézech et al., 2015), and B-cell organization, but not number, in TLS associated with a murine model

of type 1 diabetes (Henry & Kendall, 2010). However, neither report identified the source of CXCL13. Although the precise mechanism by which CXCL13 promotes TLS development may vary based on anatomic location and/or immune stimulus, our results point to its central importance in TA-TLS formation in melanoma.

Our results also provide insight into the molecular and cellular control of CXCL13, BAFF, and APRIL expression in CAFs. Expression of these molecules depended on signaling via TNFR, and not via LTβR, which controls them in SLO (Browning et al., 2005). Upregulation of CXCL13 in cultured smooth muscle cells from TLS-associated inflamed tissue was mediated by either LTβR or TNFR signaling alone, although the combination had a greater effect (Lötzer et al., 2010; Guedj et al., 2014). These differences point to the importance of determining the cellular sources of these LTo associated molecules, as well as the molecules that control their expression in additional TLS models and human diseases. Interestingly, we found that the expression of CXCL13, BAFF, and APRIL was not dependent on adaptive immune cells, NK cells, or ILCs. We previously showed that CCL21 expression depended on TNFR ligands expressed by effector CD8 T-cells (Peske et al., 2015). Thus, while TNFR signaling induces expression of all of these molecules, they depend on different cell types expressing TNFR ligands. The cells responsible for TNFR-induced upregulation in CAFs may be present and active only transiently during the course of tumor outgrowth, prior to the entry of CD8 effectors capable of upregulating CCL21 and PNAd. Alternatively, since there are two TNFR isoforms that vary in their signaling pathways (MacEwan, 2002; Wajant & Siegmund,

2019) and their engagement with TNFα and $LT\alpha_3$ (Medvedev et al., 1996), it is possible that these two cell types signal via distinct receptor-ligand pairs.

We found that effector CD8 T-cells and $LT\alpha_1\beta_2^+$ B-cells act as complementary LTi cells that coordinately induce TA-TLS development. While effector CD8 T-cells promoted the organization of CAFs into reticular networks, along with upregulation of PNAd and CCL21 (Peske et al., 2015), $LT\alpha_1\beta_2^+$ B-cells drove CAF accumulation and TA-TLS expansion. It has been shown that macrophages and NK cells can act as complementary LTi, although their exact roles were not defined (Bénézech et al., 2015). However, a role for effector CD8 T-cells in promoting TLS development has not been previously reported. LTβR signaling promotes TLS development in several infection/inflammation models, but $LT\alpha_1\beta_2^+$ B-cells have been shown to act as LTi only in development of isolated lymphoid follicles in small intestine, and this is independent of T-cells (K. G. McDonald et al., 2005; Dubey et al., 2016). The presence of B-cells in human tumors, particularly in association with TA-TLS, has a positive prognostic significance (Ladányi et al., 2011; Mahmoud et al., 2011; Cipponi et al., 2012; Germain et al., 2014), and it has been suggested that this is due to B-cell activation and antibody production, or enhanced antigen presenting cell function. Our results suggest that B-cells might also promote tumor immunity by acting as LTi cells to drive TA-TLS development.

The cellular and molecular elements driving murine TA-TLS development were also evident in TA-TLS of human melanoma. We identified $LT\alpha^+$ B-cells and $APRIL^+$ and VCAM-1^+ CAFs as dominant components in human melanoma TA-TLS, and these phenotypes are suggestive of surrogate LTi and LTo cells, respectively. Supporting this,

the densities LTα$^+$ B-cells in TA-TLS strongly correlated with the densities and fractions of CAFs in TA-TLS expressing VCAM-1 and APRIL. How differences in cellular densities within TA-TLS influence their organization and functionality is not yet clear. Nonetheless, these data are consistent with our model in which LTα$^+$ B-cells and LTo CAFs promote one another's accumulation. The densities of B-cells in TA-TLS strongly correlated with the fraction of CXCL13$^+$ CAFs, but not CXCL13$^+$ CAF density. Also, CXCL13$^+$ CAFs were only elevated in TA-TLS relative to parenchyma in 1 of 3 melanomas, although the TA-TLS in 2 out of 3 melanomas contained elevated densities of CXCL13$^+$ cells overall. This indicates the presence of alternative CXCL13 producing cells that are concentrated in the TA-TLS. CXCL13 expressing T_{FH} cells and CD8 T-cells have been identified in human breast tumors and non-small cell lung cancer, respectively (Gu-Trantien et al., 2017; Thommen et al., 2018), and it is likely that such cells are also found in melanoma TA-TLS. Thus, while CXCL13 is likely to be an important contributor to human TA-TLS development, its cellular source may evolve over time.

Recent publications reported that TA-TLS presence prior to treatment was associated with a favorable response to immunotherapy in patients with cancer (Griss et al., 2019; Cabrita et al., 2020; Petitprez et al., 2020; Helmink et al., 2020). While two of these papers associated TA-TLS "maturity" with measurements of activated B-cells, none correlated TA-TLS maturity and clinical responses. One paper demonstrated that checkpoint immunotherapy was associated with an increase in intratumoral B-cells, but no evident change in the number of TA-TLS. We identified a strong correlation between tumor control in response to checkpoint immunotherapy and TA-TLS development. In

several genetic models in which TA-TLS development was compromised, average I.P tumor size was significantly greater. The consistency of this observation coupled with the diversity of immune defects targeted suggests an association of tumor control with TA-TLS development. The number and size of TA-TLS in WT mice was strongly correlated with tumor size, suggesting that TA-TLS played a role in limiting tumor outgrowth. Most importantly, checkpoint immunotherapy of I.P., but not S.C. tumor-bearing mice, promoted tumor control, an increase in intratumoral B-cell number, the development of more and larger TA-TLS, and the formation of TA-TLS with discrete T- and B-cell compartments. Intratumoral B-cell number and TA-TLS size and number in checkpoint immunotherapy treated mice were even more significantly correlated with a reduction in tumor size than in control mice. While checkpoint immunotherapy also increased the overall number of intratumoral T-cells, there was no correlation between these numbers and size of either I.P or S.C. tumors. I.P. tumor control was lost in both untreated and treated TNFR1/2$^{-/-}$ mice, which lack TA-TLS, despite an increase in parenchymal T-cell accumulation similar to that of WT mice. Multivariate studies in non-small cell lung cancer (Goc et al., 2014) and colorectal cancer (Di Caro et al., 2014) have also established a beneficial prognostic value of TA-TLS independent of TIL density. While it is possible that checkpoint blockade induced tumor control in TNFR1/2$^{-/-}$ mice is compromised for other reasons, these mice develop normal SLO and have a normal immune cell distribution and number (Peschon et al., 1998). Additionally, these mice generate adequate effector T-cells (Peske et al., 2015), and total T cell infiltration into tumors in WT and TNFR1/2$^{-/-}$ mice was similar. We do not assert that S.C. B16-OVA tumors lacking TLS are entirely

unresponsive to checkpoint immunotherapy, as there is evidence of this in other studies, albeit with considerable variation (Curran et al., 2010; Binder et al., 2013; De Henau et al., 2016; Stark et al., 2017; Heidegger et al., 2019; Miller et al., 2019; Reilley et al., 2019; Perez-Ruiz et al., 2019). Their response may be delayed relative to that of I.P. tumors that contain TA-TLS, or it may be quantitatively smaller. Regardless, in our model on day 14, it is simply not evident, either as an effect on tumor size or in the association between tumor size and the number of infiltrating B and T cells. We reach a similar conclusion regarding I.P. tumors grown in TNFR1/2$^{-/-}$ mice. Collectively, our work suggests that TA-TLS are major targets of checkpoint immunotherapy, and their presence and organization may be important determinants of the antitumor immune response engendered by this treatment. This conclusion supports and extends conclusions reached in correlative studies in patients.

This chapter was adapted from:

Rodriguez, A. B., Peske, J. D., Woods, A. N., Leick, K. M., Mauldin, I. S., Young, S. J., Lindsay, R. S., Melssen, M. M., Cyranowski, S., Parriott, G., Meneveau, M. O., Conaway, M. R., Fu, Y. X., Slingluff, Jr, C. L., & Engelhard, V. H. (2021). Immune Mechanisms Orchestrate Tertiary Lymphoid Structures in Tumors Via Cancer-Associated Fibroblasts. Cell Reports, *36*(3), 109422. https://doi.org/10.1016/j.celrep.2021.109422.

Conclusions and Future Directions

The work described in this thesis supports a multistep model for the biosynthesis of PNAd in TECs (Model Figure 2) and TA-TLS development in murine melanoma (Model Figure 3): (1) $LT\alpha_3$ and/or TNFα produced by an unknown cell that is neither an adaptive nor an innate lymphoid cell signals through TNFR1 and/or TNFR2 on CAFs to upregulate the expression of CXCL13, BAFF, and APRIL; (2) $LT\alpha_3$ produced by intratumoral effector CD8 T-cells signals through TNFR1 and/or 2 on TECs (Peske et al., 2015) to upregulate the expression of scaffolding proteins podocalyxin and nepmucin, and sulfotransferase GST1; (3) The formation of biantennary *O*-glycans on scaffolding proteins in TECs is mediated by several biosynthetic enzymes; (4) One or more sulfotransferases, fucosyltransferases, and sialyltransferases generate 6-sulfo-sialyl Lewis X at the end of Core 1 and Core 2 *O*-glycan biantennary branches in TECs; (5) PNAd scaffolding proteins with 6-sulfo-sialyl Lewis X are displayed on the surface of TECs; (6) L-selectin and CCR7 on naïve lymphocytes bind respectively to PNAd and CCL21 to enter tumors; (7) Intratumoral CD8 T-cells induce the accumulation and organization of CAFs into reticular networks in I.P. but not in S.C. tumors; (8) $LT\alpha_1\beta_2$ on the surface of naïve B-cells signals through LTβR on CAFs to promote their proliferation and expansion of reticular networks; (9) In a reciprocal way, CXCL13, BAFF, and APRIL expressed by CAFs recruit, organize, and promote the survival of B-cells, which form dense aggregates that are co-extensive with CAF reticular networks; (10) Naïve and effector T-cells and DCs become associated with B-cell and CAF aggregates, likely through the action of CCL21 and CXCL12 secreted

Model 3: Working model for the development of tertiary lymphoid structures in murine melanoma

The formation of tertiary lymphoid structures is mediated by four distinct mechanisms (A-D): (A) An unidentified cell secreting TNFα or $LT\alpha_3$ upregulates CXCL13, BAFF, and APRIL via TNFR signaling in cancer-associated fibroblasts. (B) Intratumoral effector CD8 T-cells secrete $LT\alpha_3$ and interferon-γ that respectively upregulate PNAd and CCL21 on intratumoral vasculature (Peske et al., 2015), which in turn allows the entry of naïve B-cells expressing membranous $LT\alpha_1\beta_2$. (C) Through an unknown mechanism, effector CD8 T-cells drive the initial accumulation and organization of cancer-associated fibroblasts into reticular networks. (D) Cross-talk between B-cells and cancer-associated fibroblasts via $LT\alpha_1\beta_2$-LTβR signaling supports continual accumulation and survival of B-cells, which in turn promotes the robust accumulation of fibroblasts reticular network and TA-TLS. (E) Checkpoint immunotherapy augments the number and size of TA-TLS but also promotes the robust development of classical TA-TLS with distinct T- and B-cell compartments. ***Image created with BioRender.com***.

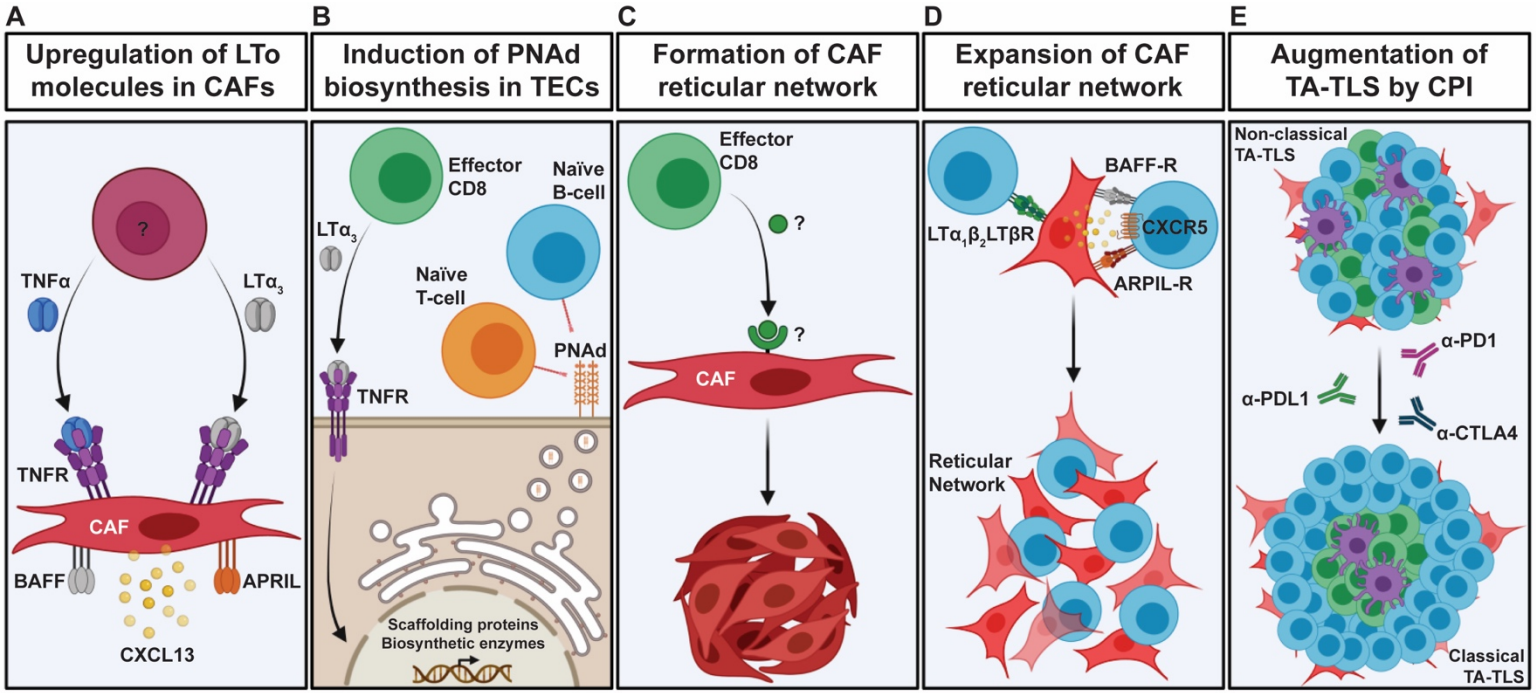
A
Upregulation of LTo molecules in CAFs
?
TNFα
LTα3
TNFR
CAF
BAFF
APRIL
CXCL13
B
Induction of PNAd biosynthesis in TECs
Effector CD8
Naïve B-cell
LTα3
Naïve T-cell
PNAd
TNFR
Scaffolding proteins
Biosynthetic enzymes
C
Formation of CAF reticular network
Effector CD8
?
?
CAF
D
Expansion of CAF reticular network
BAFF-R
LTα1β2LTβR
CXCR5
ARPIL-R
Reticular Network
E
Augmentation of TA-TLS by CPI
Non-classical TA-TLS
α-PD1
α-PDL1
α-CTLA4
Classical TA-TLS

by CAFs. This work provides a platform for manipulating PNAd expression on tumor vasculature and TA-TLS development as a new aspect of cancer immunotherapy, either alone or in combination with checkpoint immunotherapy. While this model is comprehensive, there are still some outstanding questions that remain unanswered, which are discussed in greater detail below.

Determine the absolute levels of 6-sulfo-sialyl Lewis X on TECs and its impact on L-selectin binding

GST1 and GST2 are comparably expressed in LN PNAd$^+$ BECs. In contrast, Peyer's patch BECs express GST1, but negligible levels of GST2 (Hemmerich et al., 2001; Uchimura et al., 2004; H. Kawashima et al., 2005; Uchimura et al., 2005). Consistent with this, the surface levels of 6-sulfo-sialyl Lewis X determined by immunohistochemistry and an antibody that specifically recognizes this structure are greater on peripheral and mesenteric LN HEVs than on venules in Peyer's patches (Hemmerich et al., 2001; Uchimura et al., 2004; H. Kawashima et al., 2005; Uchimura et al., 2005). PNAd$^+$ TECs express ~12-fold lower levels of GST2 relative to GST1 and at ~42-fold lower compared to GST2 in LN PNAd$^+$ BECs. However, it is unknown whether the differential loss of GST2 in PNAd$^+$ TECs affects the total surface levels of 6-sulfo-sialyl Lewis X. The PNAd (MECA-79) antibody used in this thesis largely underrepresents the number and surface levels of 6-sulfo-sialyl Lewis X on TECs because it detects this structure in the Core 1, but not Core 2, *O*-glycan branch (Yeh et al., 2001). The S2 antibody detects 6-sulfo-sialyl Lewis X on both Core 1 and Core 2 *O*-glycan branches, and has previously been used for flow cytometry (Hirakawa et al., 2010). Thus, to test the hypothesis that the reduced expression

of GST2 in TECs results in low surface levels of 6-sulfo-sialyl Lewis X, these cells would be stained with both MECA-79 and S2 antibodies for flow cytometry. BECs from peripheral and mesenteric LNs, and Peyer's patches would also be stained with these antibodies and used as comparative controls to determine the relative surface levels of 6-sulfo-sialyl Lewis X on these cells and TECs. Cells that stain double positive for MECA-79 and S2 contain 6-sulfo-sialyl Lewis X in both *O*-glycan branches, while those that are single positive for S2 contain this structure solely in the Core 2 branch. The geometric mean fluorescent staining intensity for MECA-79 and S2 on BEC and TECs would also be evaluated to determine the relative 6-sulfo-sialyl Lewis X levels on these cellular populations. Alternatively, $PNAd^{+}$ TECs would be purified from tumors, and the presence of 6-sulfo-sialyl Lewis X on Core 1 and Core 2 *O*-glycan branches would be determined by mass spectrometry. This approach is more sensitive than flow cytometry at detecting carbohydrate structures on cells. Therefore, this strategy would provide a better understanding whether the differential loss of GST2 results in lower levels of 6-sulfo-sialyl Lewis X on TECs.

Peripheral and mesenteric LN BECs, Peyer's patch BECs, and TECs would also be stained with an L-selectin-IgM fusion protein (Smith et al., 1996), then counterstained with a fluorescent anti-IgM antibody for flow cytometry. This maneuver would determine whether the low surface levels of 6-sulfo-sialyl Lewis X on TECs or whether cells with a single 6-sulfo-sialyl Lewis X affects L-selectin binding. Similarly, *in vitro* leukocyte rolling assays (Venturi et al., 2003; Sperandio, Pickard, Unnikrishnan, Acton, & Ley, 2006) involving TECs, peripheral and mesenteric LN BECs, Peyer's patch BECs, and L-selectin

positive ($CD62L^+$) T- and B-cells would be used to determine whether the number and levels of 6-sulfo-sialyl Lewis X on endothelial cells affects the binding and rolling of naïve lymphocytes. These experiments would determine whether the low surface levels of 6-sulfo-sialyl Lewis X on TECs and Peyer's patch BECs is consequentially associated with reduced L-selectin binding.

Determine whether additional PNAd biosynthetic enzymes are expressed at low levels in TECs and are controlled by TNFR signaling

GCNT1, B3GNT3, GST1, GST2, and FUT7 are are expressed at significantly lower levels in $PNAd^+$ TECs compared to $PNAd^+$ LN BECs, suggesting that the low levels of these biosynthetic enzymes may also contribute to the low surface levels of PNAd on TECs. C1GALT1 is essential for extending the Core 1 *O*-glycan branch and the formation of the glycosylated binding site for the MECA-79 antibody (Model Figure 2) (Yeh et al., 2001). FUT4, B4GALT, ST3GAL1, ST3GAL4, and ST3GAL6 are also important for the formation of 6-sulfo-sialyl Lewis X in both *O*-glycan Core branches and the proper binding of the MECA-79 antibody to these structures. C1GALT1, FUT4, B4GALT, ST3GAL1, ST3GAL4, and ST3GAL6 are highly expressed in LN $PNAd^+$ BECs than in their negative counterpart (Mike Lee et al., 2014; Veerman et al., 2019). However, these molecules were never evaluated in this thesis. Thus, it is possible that these biosynthetic enzymes are also expressed at low levels in $PNAd^+$ TECs, thereby contributing to the low levels of PNAd on TECs. To test the hypothesis that these biosynthetic enzymes are also highly expressed in $PNAd^+$ TECs than in $PNAd^{neg}$ TECs, transcript levels for C1GALT1, FUT4, B4GALT, ST3GAL1, ST3GAL4, and ST3GAL6 in these cells would be determined by qPCR. To

determine whether these biosynthetic enzymes are expressed at lower levels in PNAd^{+} TECs relative to LN PNAd^{+} BECs, transcript levels for C1GALT1, FUT4, B4GALT, ST3GAL1, ST3GAL4, and ST3GAL6 in LN PNAd^{+} BECs would also be determined by qPCR and the expression profile of these molecules in these cells would be compared to those in PNAd^{+} TECs. Determining whether additional biosynthetic enzymes in TECs are expressed at low levels similar to GST2 would provide insight into the factors that cause low surface levels of PNAd on these cells.

In I.P. tumors grown in TNFR1/2$^{-/-}$ mice, a small fraction of TECs retain PNAd, but their surface levels of this HR ligand are lower relative to PNAd^{+} TECs from WT mouse tumors. The lower surface levels of PNAd on TECs from TNFR1/2$^{-/-}$ mouse tumors is also associated with a reduced expression of GST1, suggesting that the differential loss of this sulfotransferase results in the low biosynthesis of the MECA-79 binding site. However, as described above, C1GALT1, FUT4, B4GALT, ST3GAL1, ST3GAL4, and/or ST3GAL6 are also important for the formation of the MECA-79 binding site, and it is unknown whether these molecules are reduced in PNAd^{+} TECs from TNFR1/2$^{-/-}$ mouse tumors. To test the hypothesis that the differential loss of these biosynthetic enzymes results in reduced surface levels of PNAd on TECs, transcript levels for C1GALT1, FUT4, B4GALT, ST3GAL1, ST3GAL4, and ST3GAL6 in PNAd^{+} TECs from I.P. tumors grown in TNFR1/2$^{-/-}$ mice would be determined by qPCR and the expression profile of these molecules in these cells would be compared to those in PNAd^{+} TECs from WT mouse tumors. This analysis would provide a comprehensive understanding for the factors that lead to low levels expression of PNAd on the surface of TECs from TNFR1/2$^{-/-}$ mouse

tumors. It will also determine whether additional PNAd biosynthetic enzymes in TECs are also under the control of TNFR signaling.

Determine whether the low level of PNAd on TECs is due to their low expression of GST2

GST1 and GST2 are comparably expressed in LN PNAd$^+$ BECs. In contrast, PNAd$^+$ TECs express ~12-fold lower levels of GST2 relative to GST1 and at ~42-fold lower compared to GST2 in LN PNAd$^+$ BECs. Given the relative importance of GST2 in driving PNAd expression on peripheral and mesenteric LNs HEVs, but not on those in Peyer's patches, this suggests that the low-level expression of this sulfotransferase in TECs results in reduced PNAd biosynthesis. Thus, strategies that could enhance the expression of GST2 in TECs would increase their surface levels of PNAd and the infiltration of naïve lymphocytes into tumors. Transgenic mice that overexpress GST2 are not available. Thus, to test the hypothesis that enhanced GST2 expression increases both PNAd levels on TECs and the infiltration of naïve lymphocytes, microbubbles containing either a control or GST2 overexpressing plasmid vector (Hirakawa et al., 2010; S.-Y. Yu et al., 2018) would be intravenously injected into tumor-bearing mice in combination with focused ultrasound. In this approach, microbubbles circulating in the tumor vasculature oscillate in the ultrasonic field, producing forces that act on the vessel walls that disrupt tight junctions between endothelial cells, which in turn allows efficient uptake of microbubbles with expression vectors (D. G. Fisher & Price, 2019). This technique has efficiently been used for the transport of fluorescent expression vectors across the blood-brain barrier and the transfection of endothelial cells (Mead et al., 2019; Gorick et al., 2020). In treated mice,

the number and expression levels of PNAd on TECs would be determined by flow cytometry. Since the MECA-79 antibody recognizes 6-sulfo-sialyl Lewis X in the Core 1, but not Core 2, branch, TECs from treated mice would also be stained with the S2 antibody to determine whether the enhanced GST2 expression in these cells results in greater surface levels of 6-sulfo-sialyl Lewis X. In this regard, TECs would also be stained with the L-selectin fusion protein to determine whether overexpression of GST2 in TECs results in better L-selectin binding to 6-sulfo-sialyl Lewis X. *In vitro* leukocyte rolling assays involving transfected TECs and $CD62L^+$ T- and B-cells would also be used to determine whether the enhanced expression of GST2 in TECs leads to greater binding and rolling of naïve lymphocytes. To more directly test whether enhance expression of GST2 in TECs results in greater tumor infiltration of naïve lymphocytes, $CD62L^+$ T- and B-cells expressing a congenic marker such as CD45.1 would be adoptively transferred into microbubble injected tumor-bearing mice one hour prior to harvest, and the number of infiltrating cells would be determined by flow cytometry. Previous work from the lab demonstrated that one hour is sufficient time for adoptively transferred cells to infiltrate into tumors (Thompson et al., 2010; Peske et al., 2015). The use of a congenic marker would aid in distinguishing adoptively transferred cells from endogenous CD45.2 cells in tumors. Tumor-bearing mice would also be treated with sphingosine 1-phosphate receptor modulator FTY720 at the time of transfer to prevent the egress of adoptively transferred cells that were activated in tumor-draining LNs (Cyster & Schwab, 2012). In conjunction with this, the activation status of these cells would also be determined by flow cytometry. In particular, CD44 upregulation on adoptively transferred T-cell would be evaluated to

determine whether enhanced GST2 expression in TECs results in more activated effector T-cells. Likewise, IgM and IgD expression on adoptively transferred B-cells would be evaluated by flow cytometry to determine whether GST2 overexpression results in more activated B-cells. Tumor outgrowth would also be monitored daily to determine whether GST2 overexpression correlates with tumor control. Since previous work from the lab demonstrated that naïve T-cells promoted tumor control after they differentiated into functional effectors intratumorally (Thompson et al., 2010; Peske et al., 2015), these cells would be depleted in GST2 overexpression mice via a CD8 depletion antibody. This approach would determine whether enhanced tumor control is mediated by CD8 T-cells. Overall, these experiments would determine whether the enhanced expression of GST2 in TECs results in a greater influx of naïve lymphocytes and better tumor control.

Determine why PNAd expression is differentially regulated in TECs and BECs

In adult LN, HEV morphology and the expression of genes required for the biosynthesis of PNAd is maintained by continuous engagement of $LT\alpha_1\beta_2$ expressed on DCs with LTβR expressed on BECs (Browning et al., 2005; Moussion & Girard, 2011). Consistent with this, GST2 transcripts are highly expressed in LN HEVs relative to other tissue types (Bistrup et al., 1999; Hiraoka et al., 1999), but absent in the Peyer's patches (Bistrup et al., 2004). In contrast, GST1 has a more broad expression that includes, but is not limited to, LNs and Peyer's patches (Uchimura et al., 1998, 2004; H. Kawashima et al., 2005). GST1 and GST2 can also be induced respectively in monocytes and cultured endothelial cells by TNFα (Pablos et al., 2005; Tjew et al., 2005). Similarly, PNAd scaffolding proteins podocalyxin, nepmucin, and biosynthetic enzymes GST1 are regulated by TNFR signaling

in TECs. These studies demonstrate that the expression of PNAd and its components are differentially regulated in BEC and TECs. However, it is unknown why this is.

One hypothesis to explain the discrepancy in PNAd regulation in BEC from LNs and Peyer's patches versus TECs is that these cells express different surface levels of TNFR and LTβR. To test this, BEC from peripheral and mesenteric LNs, Peyer's patches, and TECs would be stained with antibodies against TNFR1, TNFR2, and LTβR, and the number and surface levels of these receptors determined by flow cytometry. If BECs and TECs differentially express these receptors, then this could explain the difference in PNAd regulation in these cell types. However, if these cells express TNFR1, TNFR2, and LTβR at comparable levels, this would suggest that these cells respond equivalently to TNFα, $LT\alpha_3$, and $LT\alpha_1\beta_2$. To test this, purified SLO BEC and TEC would culture with increasing concentrations of recombinant TNFα, $LT\alpha_3$, or an agonist antibody for LTβR (clone 5G11). Then, the number and surface levels of PNAd on cultured cells would be determined by flow cytometry, while scaffolding and biosynthetic enzyme transcripts would be determined by qPCR.

Since a small fraction of TEC retain PNAd in the absence of TNFR, this experimental approach would provide evidence for whether a subset of TECs depend on LTβR signaling for the expression of PNAd and its components. *In vivo* approaches to determine this involves treating I.P. tumor-bearing TNFR1/2$^{-/-}$ mice with a LTβR-Ig fusion protein, whereafter the number of TECs expressing PNAd would be quantitated by flow cytometry. Chapter 2 of this thesis also showed that the number of naïve T- and B-cells in I.P. TNFR1/2$^{-/-}$ mouse tumors is reduced, but not completely abolished, suggesting that the

residual PNAd^{+} TECs in these tumors sufficiently support the infiltration of a small number of naïve lymphocytes. Thus, the number of intratumoral CD62L^{+} naïve T- and B-cells in LTβR-Ig treated TNFR1/2$^{-/-}$ mouse tumors would also be enumerated by flow cytometry. Given its importance in LN HEV, LTβR signaling may regulate the expression of PNAd in a small subset of TECs, which would add another layer of differential regulation of this HR ligand in TECs.

If BECs and TECs respond differently to TNFR and LTβR stimulation despite having comparable levels of these receptors, then this suggests that downstream elements of these signaling pathways are functionating differently between these cells. Although TNFR and LTβR are part of the same superfamily, these receptors signal through different downstream components and utilize distinct transcription factors for gene expression (Norris & Ware, 2013). For example, TNFR signaling leads to the phosphorylation and activation of the NF-κB p50-RelA transcription factor complex, while LTβR signaling phosphorylates and activates NF-κB p52-RelB. Antibodies against these transcription factors and their phosphorylated form for flow cytometry are available (Maguire, O'Loughlin, & Minderman, 2015). Thus, to test the hypothesis above, stimulated BECs and TECs would be intracellularly stained with antibodies against p50-RelA and p52-RelB, and the presence and phosphorylation status of these transcription factors would be determined by flow cytometry. If these transcription factors are present and phosphorylated equivalently in BECs and TECs, then this would suggest that the difference in PNAd regulation in these cells is at the genomic level. To test this, the promoter and gene regions of PNAd scaffolding and biosynthetic enzymes would be evaluated by ATAC-seq. This

technique would determine whether these specific gene regions are accessible for transcription. If this is the case, then strategies than can reverse these chromatin modifications can potentially enhance the expression of PNAd on the tumor vasculature.

Determining the TNFR ligand that induces LTo molecular characteristics in CAFs and its cellular source

Chapter 2 of this thesis describe an important role for TNFR signaling in inducing CXCL13, BAFF, and APRIL expression in CAFs. However, it is unknown whether $LT\alpha_3$, TNFα, or both induces the expression of LTo molecules in CAFs, since both of these molecules signal through TNFR1 and TNFR2 (Ruddle, 2014). To test the hypothesis that either or both TNFR ligands upregulate LTo molecular characteristics in CAFs, I.P. tumors would be implanted into mice deficient for LTα (De Togni et al., 1994), TNFα (Pasparakis, Alexopoulou, Episkopou, & Kollias, 1996), or both (Körner et al., 1997), and CXCL13, BAFF, and APRIL transcript levels in CAFs purified from these knockout mouse tumors would be determined by qPCR. If $LT\alpha_3$, TNFα, or both induce the expression of LTo molecules in CAFs, then it will be important to establish whether these molecules are signaling directly through TNFR1 and/or TNFR2 on CAFs. To determine this, mice expressing a tamoxifen inducible cre recombinase under the control of the PDGFRα promoter (Kang, Fukaya, Yang, Rothstein, & Bergles, 2010) would be crossed with floxed TNFR1 (Kumari et al., 2013; Van Hauwermeiren et al., 2013) and TNFR2 (Madsen, Szymkowski, Bethea, Lambertsen, & Brambilla, 2014) mice. In this mouse model, TNFR1 and TNFR2 are conditionally deleted in cells expressing PDGFRα after tamoxifen

injection, which is ~88% of the CAF population in I.P. tumors. After generating these conditional knockout mice, I.P. tumors would be implanted into them, and CXCL13, BAFF, and APRIL transcript levels in purified CAFs would be determined by qPCR. TNFR1 and TNFR2 vary in their signaling pathways (MacEwan, 2002; Wajant & Siegmund, 2019) and their engagement with TNFα and $LT\alpha_3$ (Medvedev et al., 1996). Thus, the expression of LTo molecules in CAFs could governed by a particular TNFR ligand and receptor.

CXCL13, BAFF, and APRIL expression in CAFs are induced by an unknown cell that is neither an adaptive nor innate immune lymphoid cell. Neutrophils (Foo et al., 2015), DCs (GeurtsvanKessel et al., 2009; Halle et al., 2009; Muniz et al., 2011), and macrophages (G. C. Furtado et al., 2014; Guedj et al., 2014; Bénézech et al., 2015) have been associated with the development of inflammation-associated TLS and are a source for TNFα (Hirata et al., 2010; Tecchio, Micheletti, & Cassatella, 2014; Wynn & Vannella, 2016). On the other hand, endothelial cells cultured with *Candida albicans* (Orozco, Zhou, & Filler, 2000) and idiopathic pulmonary fibroblasts (Epstein Shochet, Brook, Israeli-Shani, Edelstein, & Shitrit, 2017) have been shown to produce TNFα. Similarly and surprisingly, B16 tumors cells have been shown to be a source for both $LT\alpha_3$ (Vasilikos, Hänggi, Spilgies, & Wong, 2019, p. 1) and TNFα (P. Wang et al., 2007). Thus, the cellular source of $LT\alpha_3$ and/or TNFα in I.P. tumors could be from either a non-hematopoietic or hematopoietic cell type. To determine which compartment induces LTo molecular characteristics in CAFs via TNFR signaling, reciprocal bone marrow chimeras involving WT and LTα, TNFα, or double knockout mice would be generated. Afterwards, I.P.

tumors would be implanted into generated reciprocal bone marrow chimeras, and CXCL13, BAFF, and APRIL transcript levels in purified CAFs would be determined by qPCR. If the non-hematopoietic compartment is inducing LTo molecular characteristics in CAFs, then it will be important to determine which cell type is producing $LT\alpha_3$ and/or TNFα. The latter cytokine could easily be evaluated in the different non-hematopoietic cell types, such as TECs, CAFs, and tumor cells, by flow cytometry. However, an antibody that specifically recognizes soluble $LT\alpha_3$ is not available. Thus, single-cell RNA sequencing would be the best approach to evaluate LTα and/or TNFα expression in the different non-hematopoietic subpopulations. To distinguish tumor cells from endogenous stromal cells, I.P. tumors would be implanted into UBC-mCherry mice. In this model, tumor cells would not express mCherry, while endogenous tumor stromal cells would. Thus, stromal and tumor cells would be sorted separately from one another, and LTα and/or TNFα expression in these two separated fractions would be determine by single-cell RNA sequencing.

If a hematopoietic cell type is responsible for inducing LTo molecules in CAFs, then this would suggest that a myeloid cell regulates these molecules, since CXCL13, BAFF, and APRIL expression are maintained in CAFs in the absence of adaptive and innate lymphocytes. To test the hypothesis that neutrophils, DCs, and/or macrophages in I.P. tumors are a source for TNFR ligands, the expression levels of TNFα could easily be determined in these cells by flow cytometry. Also, these cells would be purified from I.P. tumors and their transcript levels for LTα would be determined by qPCR. If one or more of these cells are a source for LTα and/or TNFα, then it will be important to determine whether the loss of these cells results in reduced CXCL13, BAFF, and APRIL expression

in CAFs. To test this, neutrophils and macrophages would be depleted in tumor-bearing mice with an Ly6G antibody and clodronate liposome treatment, respectively. Transgenic mice that express the diphtheria toxin receptor (DTR) under the control of the Zbtb46 promoter (Zbtb46-DTR) would be used to depleted DCs in tumor-bearing mice after diphtheria toxin. In all of these models, CXCL13, BAFF, and APRIL transcript levels in CAFs purified from depleted mouse tumors would be determined by qPCR. The results from these studies will determine whether a non-hematopoietic and/or myeloid cell is acting as an additional surrogate LTi cell for the development of TA-TLS in murine melanoma. Importantly, they will determine whether LTα and/or TNFα are delivering distinct signals for the expression of CXCL13, BAFF, and APRIL in CAFs.

Determine the mechanism of action in which CD8 T-cells induce CAF reticular network formation

CD8 T-cells and TNFR signaling drives the accumulation of CAFs into reticular networks in I.P. tumors. However, it is unknown which TNFR ligand mediates this and whether it is derived from CD8 T-cells. Recently, work from the lab demonstrated that $LT\alpha_3$ produced by CD8 T-cells induce PNAd expression on the tumor vasculature (Peske et al., 2015). Although CD8 T-cells in I.P. tumors do produce low levels of TNFα, suggesting that this cytokine potentially drives the induction of small CAF reticular networks, whereas LTβR signaling mediated by B-cells expands these structures. Thus, to test the hypothesis that CD8 T-cells induce CAF reticular network formation in I.P. tumors via $LT\alpha_3$ and/or TNFα, $Rag1^{-/-}$ mice bearing I.P. tumors would be repleted with CD8 T-cells from WT, $LT\alpha^{-/-}$,

TNFα$^{-/-}$, or double knockout mice. Then, tumors would be histologically prepared, and the presence and number of CAF reticular networks would be determined by IF. In parallel, the fraction of CAFs expressing Ki67 would also be enumerated by flow cytometry to determine whether a specific TNFR ligand produced by CD8 T-cells induces CAF proliferation. If CD8 T-cells are inducing CAF reticular network formation by either LTα$_3$ and/or TNFα, then it will be important to determine whether these molecules are restricted to a specific CD8 T-cell subpopulation. To determine this, CD8 T-cells from I.P. tumors grown in WT mice would be stained with antibodies against CD44, CD62L, and TNFα, and the fraction of effector, central memory, and activated T-cells expressing TNFα would be determined by flow cytometry. These different CD8 T-cell subpopulations would also be purified from I.P. tumors, and transcript levels for LTα in these different cellular subtypes would be determined by qPCR. These experiments would determine whether a specific CD8 T-cell subpopulation is driving CAF reticular network formation.

It is still unknown whether TNFR ligands are signaling indirectly or directly through TNFR1 and/or TNFR2 on CAFs to induce reticular network formation. To determine this, reciprocal bone marrow chimera mice involving WT and TNFR$^{-/-}$ mice would be generated. Then, I.P. tumors would be implanted into reciprocal bone marrow chimeras, and the presence and number of CAF reticular networks would be determined by IF. Also, the fraction of CAFs expressing Ki67 would also be enumerated by flow cytometry. PDGFRα is a conventional CAF marker and ~88% of the CAF population in I.P. tumors express this receptor. Thus, to more directly test the hypothesis that TNFR ligands are signaling directly on CAFs, I.P. tumors would be implanted into tamoxifen

inducible PDGFRα-Cre x TNFR1 or TNFR2 floxed mice, and the formation of reticular networks and the number of $Ki67^+$ CAFs would be determined by IF and flow cytometry, respectively. Collectively, these experiments would determine whether the induction of CAF reticular networks is mediated by a distinct TNFR ligand and receptor that is different from that controlling LTo molecular characteristics in CAFs.

Determine the mechanism of action for $LT\alpha_1\beta_2$-LTβR signaling in driving TA-TLS reticular network expansion

$LT\alpha_1\beta_2^+$ B-cells and LTβR signaling drive the expansion of TA-TLS-associated reticular networks. Despite this, there are still unknowns associated with these findings. The first is whether $LT\alpha_1\beta_2$ is expressed on the surface of other cell types. Beside B-cells, $LT\alpha_1\beta_2$ is expressed on NK (Andrews, Berger, & Ware, 1990), DCs (Wu et al., 1999), and different subsets of helper CD4 T-cells (Chiang et al., 2009). To determine whether other immune cells besides B-cells express surface $LT\alpha_1\beta_2$ in I.P. tumors, $CD45^+$ tumor suspensions would be stained with LTβR-Ig and HVEM-Ig fusion proteins, and then counterstained with fluorescent secondary antibodies against corresponding IgG Fc region on these fusion proteins. LTβR binds to both $LT\alpha_1\beta_2$ and LIGHT, whereas HVEM exclusively binds to the latter (Ware, 2008). Thus, this strategy would distinguish which immune subset is expressing surface $LT\alpha_1\beta_2$ and/or LIGHT by flow cytometry. If NK, DC, and/or CD4 T-cells express $LT\alpha_1\beta_2$, then this suggests that these cells promote the expansion of TA-TLS-associated reticular networks in addition to B-cells. To determine this, Ncr1-Cre (Eckelhart et al., 2011), CD4-Cre (P. P. Lee et al., 2001), or Zbtb46-Cre (Loschko et al., 2016) mice

would be crossed to a LTβ floxed mice (Alexei V. Tumanov et al., 2002). In these conditional knockout mice, NK (Ncr), CD4 T-cells, or DCs (Zbtb46) would be unable to produce surface $LT\alpha_1\beta_2$. After these mice have been generated, I.P. tumors would be implanted into them, and the formation of reticular networks and the number of proliferating CAFs would be determined by IF and flow cytometry, respectively. These experiments would determine whether additional immune cells act as surrogate LTi cells that drive the robust expansion of TA-TLS in murine melanoma.

I.P. CAFs express substantially higher levels of CXCL13 compared to those in S.C. tumors. Relative to WT mouse tumors, I.P. tumors from $CXCR5^{-/-}$ mice contain smaller TA-TLS-associated reticular networks, and a reduced number of proliferating CAFs and intratumoral B-cells. This suggests that CXCR5 expression on $LT\alpha_1\beta_2^{+}$ B-cells is necessary for driving the expansion for reticular networks. To test this hypothesis, I.P. tumor-bearing $Rag1^{-/-}$ mice would be reconstituted with WT CD8 T-cells and CXCR5 deficient B-cells. In the resulting tumor, reticular network formation and the number of proliferating CAFs would be determined by IF and flow cytometry, respectively. This approach would determine whether the loss of CXCR5 on B-cells prevents the expansion of CAF reticular networks. Another important question that is associated with CAF reticular network expansion is whether $LT\alpha_1\beta_2$ is signaling directly through LTβR on CAFs. I.P. tumors contain a larger fraction of CAFs expressing LTβR than S.C. tumors, suggesting direct signaling by $LT\alpha_1\beta_2^{+}$ B-cells. To test this, tamoxifen inducible PDGFRα-Cre mice would be crossed with LTβR floxed mice (Y. Wang et al., 2010). Mice deficient for LTβR or its relative ligands fail to develop LNs and immune responses, including those

that drive TA-TLS development in I.P. tumors (De Togni et al., 1994; Alimzhanov et al., 1997; Koni et al., 1997). Conditionally deleting LTβR on CAFs after tumors and TA-TLS have established by tamoxifen treatment would circumvent this complexity. After generating tamoxifen inducible PDGFRα-Cre x LTβR floxed mice, I.P. tumors would be implanted into conditional knocked mice, and reticular network formation and the number of proliferating CAFs would be determined respectively by IF and flow cytometry. The outcomes from these experiments would continue to build the current model and provide a mechanism of action for $LT\alpha_1\beta_2$- LTβR mediated reticular network and TA-TLS expansion.

Determine whether TA-TLS are sites for the sustainable generation of anti-tumor immune responses

TA-TLS presence in I.P. tumors is associated with high representations of naïve T- and B-cells, and T-cells with a distinct activated phenotype. TA-TLS presence, number, and size also correlated with reduced tumor size, and this association was lost in tumors with deficiencies in TA-TLS development. Most importantly, checkpoint immunotherapy of I.P. tumor-bearing mice promoted enhanced tumor control, and the robust development of more and larger TA-TLS with discrete T- and B-cell compartments. These observations suggest that TA-TLS are sites for the sustained generation of *in situ* anti-tumor immune responses. To test this, the fraction, activation status, and cytokine production of different immune subsets in classical and non-classical TA-TLS, the tumor parenchyma surrounding TA-TLS, and S.C. tumors would be determined by IF. For this extensive analysis, the following markers would be used to identify the following immune populations in

untreated and checkpoint immunotherapy treated S.C. and I.P. tumors: CD62L for naïve and memory T-cells; CD69 for activated T- cells; Ki67 for proliferating T- and B-cells; EOMES, TOX, TCF1 for effector, exhausted, and stem-like CD8 T-cells, respectively; Tbet, GATA2, BCL6, RORγt, and FOXP3 for T_H1, T_H2, T_{FH}, T_H17, and Treg CD4 subpopulations, respectively; IgD for naïve B-cells; GL7 and CD95 for germinal center B-cells; CD138 for antibody producing plasma cells; MHC II, CD80, and CD86 for identifying and determining the maturation status of antigen-presenting cells (DCs, B-cells, and macrophages); and CD11b and Ly6G/C for myeloid-derived suppressor cells. Pro-inflammatory IFNγ and anti-inflammatory IL-10 are difficult molecules to stain by IF. Thus, S.C. and I.P. tumor would be implanted into transgenic mice that express eYFP under the control of the IFNγ (Stetson et al., 2003) or IL-10 (Calado, Paixão, Holmberg, & Haury, 2006) promoter. This maneuver would identify cytotoxic and immunosuppressive immune cells based on their expression of eYFP. These approaches would distinguish whether classical TA-TLS are sites for robust lymphocyte activation, with elevated numbers of mature DCs, cytotoxic CD8 T-cells, CD4 T-cells with a T_H1 phenotype, and antibody producing B-cells; while non-classical TA-TLS will have more immature DCs, a lower number of activated lymphocytes, and potentially, a higher regulatory contexture. They will also provide insight into elements that make TA-TLS effective targets for checkpoint immunotherapy, which are currently unknown.

If the analysis above show that TA-TLS are enriched with activated lymphocytes, then this would suggest that these structures support TIL development. To test this hypothesis, naïve T- (Hogquist et al., 1994; Barnden, Allison, Heath, & Carbone, 1998)

and B-cells (Dougan et al., 2012) that express respectively transgenic TCR and BCR specific for ovalbumin would be adoptively transferred into I.P. B16-OVA tumor-bearing WT and TNFR1/2$^{-/-}$ mice. Congenic marker CD45.1 on adoptive transferred cells would be used to distinguish them from CD45.2 endogenous cells in tumors. Also, tumor-bearing mice would be treated with sphingosine 1-phosphate receptor modulator FTY720 to prevent the egress of adoptively transferred cells that were activated in tumor-draining LNs (Cyster & Schwab, 2012). In these tumors, the number and activation status of adoptively transferred T- and B-cells would be determined by flow cytometry. Moreover, the localization and activation status of these adoptive transferred cells in tumors would be done by IF. If naïve T-cells are recruited and activated in classical TA-TLS more so than non-classical structures, and classical structures are enriched with mature DCs, then this would suggest that active antigen presentation is occurring in classical TA-TLS. To determine this, Zbtb46-DTR mice bearing established I.P. tumors would be treated with diphtheria toxin to deplete DCs. Then, congenic CD45.1^{+} naïve T-cells would be transferred into depleted tumor-bearing mice, while in the presence of FTY720. In this tumor model, the number, localization and activation status of adoptively transferred naïve T-cells would be determined by IF and flow cytometry. These experimental approaches would directly demonstrate whether TA-TLS actively recruit naïve lymphocytes into tumors, and that TA-TLS organization impacts the activation quality of these cells.

Determine whether checkpoint immunotherapy augments the cellular and molecular drivers of TA-TLS

Checkpoint immunotherapy enhances PNAd expression on the tumor vasculature, increases the number and size of TA-TLS, and promotes the robust formation of classical TA-TLS with discrete T- and B-cell compartments. However, it is still unknown how checkpoint immunotherapy promotes these enhancements. PNAd expression on the tumor vasculature is driven by $LT\alpha_3$ producing CD8 T-cells (Peske et al., 2015). In the previous sections, it was hypothesized that $LT\alpha_3$ induces CAF proliferation and reticular network formation. Since checkpoint immunotherapy also increases the density of intratumoral T-cells, this suggests that enhanced expression of PNAd on the tumor vasculature and the robust development of TA-TLS in treated tumors are due to a larger representation of $LT\alpha_3$ secreting CD8 T-cells. As stated in the previous section, an antibody that specifically recognizes this homotrimer $LT\alpha_3$ by IF or flow cytometry is not available. To test this hypothesis, bulk populations of CD8 T-cells would be purified from untreated and checkpoint treated tumors, and LTα transcript levels would be determined by qPCR. In conjunction with this, the number of proliferating CAFs in control and checkpoint treated mouse tumors would be determined by flow cytometry. It was also hypothesized in the previous section that TNFα derived from a myeloid cell upregulates CXCL13, BAFF, and APRIL expression in CAFs. Therefore, the number of TNFα producing neutrophils, DCs, and macrophages in untreated and treated tumors would be determined by flow cytometry. Checkpoint immunotherapy also increases the density of intratumoral B-cells, suggesting

that the robust expansion of TA-TLS is driven by an increased representation of $LT\alpha_1\beta_2^+$ B-cells. To determine this, untreated and treated $CD45^+$ tumor suspensions would be stained with LTβR-Ig and HVEM-Ig fusions proteins, and then counterstained with fluorescent secondary antibodies against their corresponding IgG Fc regions. Again, this strategy would distinguish which immune subset is expressing surface $LT\alpha_1\beta_2$ and/or LIGHT by flow cytometry. These strategies would determine whether the cellular and molecular mechanisms driving TA-TLS in untreated tumors persist in checkpoint immunotherapy treated tumors, just at larger quantities.

It is still unknown what promotes the robust formation of classical TA-TLS after checkpoint immunotherapy. In the LN, compartmentalization of T- and B-cells is driven by CCL21 producing FRC and CXCL13 producing FDC, respectively (S. M. Grant, Lou, Yao, Germain, & Radtke, 2020). Since checkpoint immunotherapy promotes the formation of classical TA-TLS, this suggests that the robust development of these structures is driven by bifurcated subpopulations of CAF resembling FRC and FDC. To test this, mice that express Cre under the control of the CXCL13 promoter (Onder et al., 2017) would be crossed to ROSA-eYFP mice (Srinivas et al., 2001). In these mice, CXCL13 producing cells would be identified based on their expression of eYFP. After the generation of these mice, I.P. tumors would be implanted into them, and tumor-bearing mice would be treated with control or checkpoint antibodies. For flow cytometry, $CD45^+$ depleted tumor suspensions would be stained with antibodies for CAF (PDPN, ICAM-1, VCAM-1, FAP, PDGFRα/β), FRC (CCL21, IL-7), and FDC (BAFF, APRIL, CD21) traits. Treated tumors from CXCL13-Cre x ROSA-eYFP mice would also be prepared for IF to determine

whether T- and B-cell compartments in classical TA-TLS contain cells resembling CCL21 producing FRCs and CXCL13 producing FDCs, respectively. Recognizing that CAFs are extremely heterogenous (T. Liu et al., 2019), the gene expression profile of CAFs from control and checkpoint treated mouse tumors would be determined by bulk and single cells RNAseq. The goals of this analysis are the following: (1) establish a comprehensive gene expression profile that discriminates CAFs; (2) determine differentially expressed genes between $CXCL13^{+}$ and $CXCL13^{neg}$ CAFs; (3) identify genes whose expression depends on TNFR and LTβR signaling; (4) detect changes in CAF gene expression profile after checkpoint immunotherapy. The markers that conclusively identify CAFs are lacking. However, the experiments proposed above would provide significant insight into the distinguishing qualities of CAFs, and how they change in repones to checkpoint immunotherapy.

Determine whether inducing TA-TLS formation promotes tumor control and response to checkpoint immunotherapy

Transgenic overexpression of LTβR ligands (Haidong Tang et al., 2017) and injection of recombinant LIGHT (Johansson-Percival et al., 2017) have been shown to induce TA-TLS formation in murine tumors. However, systematic injection of these cytokines into cancer patients to induce TA-TLS formation may produce off target effects and unwanted toxicity. Also, injecting CAFs with LTo characteristics into a patient's tumor may not be the best option for inducing TA-TLS formation, since a plethora of work has shown that these cells can acquire pro-tumor traits. Instead, the desired approach would be to convert existing pro-tumor CAFs into LTo-like cells that support TA-TLS formation. It was previously

shown that a murine fibrosarcoma model could be induced to support TIL infiltration by treating tumor-bearing mice with a LIGHT conjugated antibody specific for epidermal growth factor receptors (Haidong Tang et al., 2016). The authors suggested that the conjugated antibody targeted epidermal growth factor receptors on tumors cells, while LIGHT bounded to LTβR on stromal cells, thereby leading to the production of chemokines that recruit T-cells. Since PDPN is expressed on both B16 tumor cells and CAFs, a similar strategy could be used to induce TA-TLS formation in S.C. tumors. To test the hypothesis that PDPN antibodies conjugated to TNFα or $LT\alpha_3$ induce TA-TLS formation, unconjugated or conjugated antibodies would be injected into S.C. tumor-bearing mice. Tumor outgrowth would be monitor in the two arms to determine whether conjugated antibodies promote tumor control. The presence of CAF reticular networks and TA-TLS in treated mouse tumors would be determined by IF. Also, the number of proliferating CAFs, and their expression of CXCL13, BAFF, and APRIL in treated mouse tumors would also be determined by flow cytometry and qPCR, respectively. The numbers and activation status of intratumoral immune cells in treated mouse tumors would additionally be determined by flow cytometry. This strategy could serve as a therapeutic maneuver to induce TA-TLS in human tumors by converting CAFs into LTo-like cells.

If PDPN antibodies conjugated to TNFα or $LT\alpha_3$ induce TA-TLS formation and tumor control, then this would suggest that these tumors are also responsive to checkpoint immunotherapy. To test this, S.C. tumor-bearing mice would be treated with unconjugated or TNFα/$LT\alpha_3$ conjugated PDPN antibodies. After TA-TLS form in antibody conjugated treated tumors, mice would then be treated with control, monotherapy anti-PDL1, or dual

therapy anti-PD1/CTLA4, and tumor outgrowth would be monitored periodically. Checkpoint immunotherapy induces in I.P. tumors the robust formation of TA-TLS with a classical organization. Thus, treated tumors would be evaluated by IF to determine whether checkpoint immunotherapy also induces classical structures in antibody conjugated treated mouse tumors. CAF populations in the different treated mouse tumors would also be evaluated by flow cytometry to determine whether both PDPN conjugated antibodies and checkpoint immunotherapy promotes the bifurcation of CAFs that support classical TA-TLS formation. This includes staining $CD45^+$ depleted tumor suspensions antibodies for CAF (PDPN, ICAM-1, VCAM-1, FAP, PDGFRα/β), FRC (CCL21, IL-7), and FDC (BAFF, APRIL, CD21) markers. Likewise, the number and activations status of intratumoral immune cells in treated mouse tumors would be evaluated by flow cytometry to determine whether the formation of classical TA-TLS promotes TIL development. The development of antibody-cytokine conjugates could serve as a therapeutic application for inducing TA-TLS in human tumors and response to checkpoint immunotherapy. Although the work in this thesis suggests that human and murine melanoma associated TA-TLS are regulated similarly to one another, this may not be the case for alternative tumor types. Thus, further insight is needed to determine whether TA-TLS in alternative tumor types are regulated differently from those in melanoma.

Concluding remarks

Based on the preponderance of evidence, it seems highly desirable to induce and/or augment TA-TLS development as a new aspect of cancer immunotherapy, either alone or in combination with immunotherapy or chemotherapy. However, few reports have

demonstrated a negative association with the presence of TA-TLS. For example, TA-TLS in a murine model of hepatocellular carcinoma serve as sites for the generation of malignant hepatocyte progenitor cells (Finkin et al., 2015). Also, TA-TLS in a murine model of lung adenocarcinoma promote the recruitment of immunosuppressive Tregs (Joshi et al., 2015). Lastly, human breast carcinomas frequently contain TA-TLS and the presence of these structures is associated with an aggressive form of tumor (Figenschau et al., 2015). Given that TA-TLS are heterogenous in organization and functionality, special consideration should be given when applying these structures for prognostic significance. Cellular and molecular mechanisms responsible for spontaneous TA-TLS formation, and strategies to induce these structures, are described in murine models. However, much remains to be done to understand the overall heterogeneity and functionality of these structures in human tumors, and the tumor, tissue, and temporal elements that may control these properties. These in turn will enable more refined understanding of the properties of TA-TLS that are of greatest value in determining patient survival, and applicability to the widest array of different cancer types.

References

Alimzhanov, M. B., Kuprash, D. V., Kosco-Vilbois, M. H., Luz, A., Turetskaya, R. L., Tarakhovsky, A., … Pfeffer, K. (1997). Abnormal development of secondary lymphoid tissues in lymphotoxin β-deficient mice. *Proceedings of the National Academy of Sciences of the United States of America*, *94*(17), 9302–9307.

Allen, C. D. C., Ansel, K. M., Low, C., Lesley, R., Tamamura, H., Fujii, N., & Cyster, J. G. (2004). Germinal center dark and light zone organization is mediated by CXCR4 and CXCR5. *Nature Immunology*, *5*(9), 943–952. https://doi.org/10.1038/ni1100

Al-Shibli, K. I., Donnem, T., Al-Saad, S., Persson, M., Bremnes, R. M., & Busund, L.-T. (2008). Prognostic Effect of Epithelial and Stromal Lymphocyte Infiltration in Non–Small Cell Lung Cancer. *American Association for Cancer Research*, *14*(16), 5220–5227. https://doi.org/10.1158/1078-0432.CCR-08-0133

Amado, M., Almeida, R., Schwientek, T., & Clausen, H. (1999). Identification and characterization of large galactosyltransferase gene families: Galactosyltransferases for all functions1This paper is dedicated to Drs. Harry Schachter and Akira Kobata on the occasion of their 65th birthdays. This paper constitutes part of the requirement for a Ph.D. thesis for Margarida Amado.1. *Biochimica et Biophysica Acta (BBA) - General Subjects*, *1473*(1), 35–53. https://doi.org/10.1016/S0304-4165(99)00168-3

Ammirante, M., Shalapour, S., Kang, Y., Jamieson, C. A. M., & Karin, M. (2014). Tissue injury and hypoxia promote malignant progression of prostate cancer by inducing

CXCL13 expression in tumor myofibroblasts. *Proceedings of the National Academy of Sciences*, *111*(41), 14776–14781. https://doi.org/10.1073/pnas.1416498111

Andrews, J. S., Berger, A. E., & Ware, C. F. (1990). Characterization of the receptor for tumor necrosis factor (TNF) and lymphotoxin (LT) on human T lymphocytes. TNF and LT differ in their receptor binding properties and the induction of MHC class I proteins on a human CD4+ T cell hybridoma. *Journal of Immunology (Baltimore, Md.: 1950)*, *144*(7), 2582–2591.

Ansel, K. M., Ngo, V. N., Hyman, P. L., Luther, S. A., Förster, R., Sedgwick, J. D., … Cyster, J. G. (2000). A chemokine-driven positive feedback loop organizes lymphoid follicles. *Nature*, *406*(6793), 309–314. https://doi.org/10.1038/35018581

Arina, A., Idel, C., Hyjek, E. M., Alegre, M.-L., Wang, Y., Bindokas, V. P., … Schreiber, H. (2016). Tumor-associated fibroblasts predominantly come from local and not circulating precursors. *Proceedings of the National Academy of Sciences*, *113*(27), 7551–7556. https://doi.org/10.1073/pnas.1600363113

Arnold, J. N., Magiera, L., Kraman, M., & Fearon, D. T. (2014). Tumoral immune suppression by macrophages expressing fibroblast activation protein-α and heme oxygenase-1. *Cancer Immunology Research*, *2*(2), 121–126. https://doi.org/10.1158/2326-6066.CIR-13-0150

Aruga, A., Aruga, E., Tanigawa, K., Bishop, D. K., Sondak, V. K., & Chang, A. E. (1997). Type 1 versus type 2 cytokine release by Vbeta T cell subpopulations determines

in vivo antitumor reactivity: IL-10 mediates a suppressive role. *Journal of Immunology*, *159*(2), 664–673.

Asano, M., Nakae, S., Kotani, N., Shirafuji, N., Nambu, A., Hashimoto, N., … Iwakura, Y. (2003). Impaired selectin-ligand biosynthesis and reduced inflammatory responses in beta-1,4-galactosyltransferase-I-deficient mice. *Blood*, *102*(5), 1678–1685. https://doi.org/10.1182/blood-2003-03-0836

Barbera-Guillem, E., Nelson, M. B., Barr, B., Nyhus, J. K., May, K. F., Feng, L., & Sampsel, J. W. (2000). B lymphocyte pathology in human colorectal cancer. Experimental and clinical therapeutic effects of partial B cell depletion. *Cancer Immunology, Immunotherapy: CII*, *48*(10), 541–549.

Barbera-Guillem, Emilio, May, K. F., Nyhus, J. K., & Nelson, M. B. (1999). Promotion of Tumor Invasion by Cooperation of Granulocytes and Macrophages Activated by Anti-tumor Antibodies. *Neoplasia*, *1*(5), 453–460. https://doi.org/10.1038/sj.neo.7900054

Barnden, M. J., Allison, J., Heath, W. R., & Carbone, F. R. (1998). Defective TCR expression in transgenic mice constructed using cDNA-based alpha- and beta-chain genes under the control of heterologous regulatory elements. *Immunology and Cell Biology*, *76*(1), 34–40. https://doi.org/10.1046/j.1440-1711.1998.00709.x

Barone, F., Nayar, S., Campos, J., Cloake, T., Withers, D. R., Toellner, K.-M., … Buckley, C. D. (2015). IL-22 regulates lymphoid chemokine production and assembly of

tertiary lymphoid organs. *Proceedings of the National Academy of Sciences*, *112*(35), 11024–11029. https://doi.org/10.1073/pnas.1503315112

Bartoschek, M., Oskolkov, N., Bocci, M., Lövrot, J., Larsson, C., Sommarin, M., … Pietras, K. (2018). Spatially and functionally distinct subclasses of breast cancer-associated fibroblasts revealed by single cell RNA sequencing. *Nature Communications*, *9*(1), 5150. https://doi.org/10.1038/s41467-018-07582-3

Becht, E., Giraldo, N. A., Beuselinck, B., Job, S., Marisa, L., Vano, Y., … Fridman, W. H. (2015). Prognostic and theranostic impact of molecular subtypes and immune classifications in renal cell cancer (RCC) and colorectal cancer (CRC). *Oncoimmunology*, *4*(12). https://doi.org/10.1080/2162402X.2015.1049804

Bekiaris, V., Gaspal, F., Kim, M.-Y., Withers, D. R., McConnell, F. M., Anderson, G., & Lane, P. J. L. (2009). CD30 is required for CCL21 expression and CD4 T cell recruitment in the absence of lymphotoxin signals. *Journal of Immunology*, *182*(8), 4771–4775. https://doi.org/10.4049/jimmunol.0803481

Bénézech, C., Luu, N.-T., Walker, J. A., Kruglov, A. A., Loo, Y., Nakamura, K., … Caamaño, J. H. (2015). Inflammation-induced formation of fat-associated lymphoid clusters. *Nature Immunology*, *16*(8), 819–828. https://doi.org/10.1038/ni.3215

Bento, D. C., Jones, E., Junaid, S., Tull, J., Williams, G. T., Godkin, A., … Gallimore, A. (2015). High endothelial venules are rare in colorectal cancers but accumulate in

extra-tumoral areas with disease progression. *OncoImmunology*, *4*(3), e974374. https://doi.org/10.4161/2162402X.2014.974374

Binder, D. C., Engels, B., Arina, A., Yu, P., Slauch, J. M., Fu, Y.-X., … Schreiber, H. (2013). Antigen-specific bacterial vaccine combined with anti-PD-L1 rescues dysfunctional endogenous T cells to reject long-established cancer. *Cancer Immunology Research*, *1*, 123–133. https://doi.org/10.1158/2326-6066.CIR-13-0058

Bistrup, A., Bhakta, S., Lee, J. K., Belov, Y. Y., Gunn, M. D., Zuo, F. R., … Hemmerich, S. (1999). Sulfotransferases of two specificities function in the reconstitution of high endothelial cell ligands for L-selectin. *The Journal of Cell Biology*, *145*(4), 899–910. https://doi.org/10.1083/jcb.145.4.899

Bistrup, A., Tsay, D., Shenoy, P., Singer, M. S., Bangia, N., Luther, S. A., … Rosen, S. D. (2004). Detection of a sulfotransferase (HEC-GlcNAc6ST) in high endothelial venules of lymph nodes and in high endothelial venule-like vessels within ectopic lymphoid aggregates: Relationship to the MECA-79 epitope. *American Journal of Pathology*, *164*(5), 1635–1644.

Bochet, L., Lehuédé, C., Dauvillier, S., Wang, Y. Y., Dirat, B., Laurent, V., … Muller, C. (2013). Adipocyte-derived fibroblasts promote tumor progression and contribute to the desmoplastic reaction in breast cancer. *Cancer Research*, *73*(18), 5657–5668. https://doi.org/10.1158/0008-5472.CAN-13-0530

Bombardieri, M., Barone, F., Humby, F., Kelly, S., McGurk, M., Morgan, P., … Pitzalis, C. (2007). Activation-Induced Cytidine Deaminase Expression in Follicular Dendritic Cell Networks and Interfollicular Large B Cells Supports Functionality of Ectopic Lymphoid Neogenesis in Autoimmune Sialoadenitis and MALT Lymphoma in Sjögren's Syndrome. *The Journal of Immunology*, *179*(7), 4929–4938. https://doi.org/10.4049/jimmunol.179.7.4929

Bose, A., Taylor, J. L., Alber, S., Watkins, S. C., Garcia, J. A., Rini, B. I., … Storkus, W. J. (2011). Sunitinib facilitates the activation and recruitment of therapeutic anti-tumor immunity in concert with specific vaccination. *International Journal of Cancer*, *129*(9), 2158–2170.

Brahmer, J. R., Drake, C. G., Wollner, I., Powderly, J. D., Picus, J., Sharfman, W. H., … Topalian, S. L. (2010). Phase I study of single-agent anti-programmed death-1 (MDX-1106) in refractory solid tumors: Safety, clinical activity, pharmacodynamics, and immunologic correlates. *Journal of Clinical Oncology*, *28*(19), 3167–3175. https://doi.org/10.1200/jco.2009.26.7609

Brechbuhl, H. M., Finlay-Schultz, J., Yamamoto, T. M., Gillen, A. E., Cittelly, D. M., Tan, A.-C., … Kabos, P. (2017). Fibroblast Subtypes Regulate Responsiveness of Luminal Breast Cancer to Estrogen. *Clinical Cancer Research*, *23*(7), 1710–1721. https://doi.org/10.1158/1078-0432.CCR-15-2851

Browning, J. L., Allaire, N., Ngam-Ek, A., Notidis, E., Hunt, J., Perrin, S., & Fava, R. A. (2005). Lymphotoxin-beta receptor signaling is required for the homeostatic

control of HEV differentiation and function. *Immunity*, *23*(5), 539–550. https://doi.org/10.1016/j.immuni.2005.10.002

Buckanovich, R. J., Facciabene, A., Kim, S., Benencia, F., Sasaroli, D., Balint, K., … Coukos, G. (2008). Endothelin B receptor mediates the endothelial barrier to T cell homing to tumors and disables immune therapy. *Nature Medicine*, *14*(1), 28–36. https://doi.org/10.1038/nm1699

Burnet, M. (1957). Cancer—A Biological Approach. *British Medical Journal*, *1*(APR13), 841–846.

Burstein, N. A., & Law, L. W. (1971). Neonatal Thymectomy and Non-viral Mammary Tumours in Mice. *Nature*, *231*(5303), 450–452. https://doi.org/10.1038/231450a0

Busch, W. (1868). *"Aus der Sitzung der medicinischen Section vom 13*. *5*, 137.

Cabrita, R., Lauss, M., Sanna, A., Donia, M., Larsen, M. S., Mitra, S., … Jönsson, G. (2020). Tertiary lymphoid structures improve immunotherapy and survival in melanoma. *Nature*, *577*(7791), 561–565. https://doi.org/10.1038/s41586-019-1914-8

Calado, D. P., Paixão, T., Holmberg, D., & Haury, M. (2006). Stochastic monoallelic expression of IL-10 in T cells. *Journal of Immunology (Baltimore, Md.: 1950)*, *177*(8), 5358–5364. https://doi.org/10.4049/jimmunol.177.8.5358

Calderaro, J., Petitprez, F., Becht, E., Laurent, A., Hirsch, T. Z., Rousseau, B., … Sautès-Fridman, C. (2019). Intra-tumoral tertiary lymphoid structures are associated with

a low risk of early recurrence of hepatocellular carcinoma. *Journal of Hepatology*, *70*(1), 58–65. https://doi.org/10.1016/j.jhep.2018.09.003

Calon, A., Lonardo, E., Berenguer-Llergo, A., Espinet, E., Hernando-Momblona, X., Iglesias, M., … Batlle, E. (2015). Stromal gene expression defines poor-prognosis subtypes in colorectal cancer. *Nature Genetics*, *47*(4), 320–329. https://doi.org/10.1038/ng.3225

Cañete, J. D., Celis, R., Yeremenko, N., Sanmartí, R., Duivenvoorde, L. van, Ramírez, J., … Baeten, D. L. (2015). Ectopic lymphoid neogenesis is strongly associated with activation of the IL-23 pathway in rheumatoid synovitis. *Arthritis Research & Therapy*, *17*(1), 173. https://doi.org/10.1186/s13075-015-0688-0

Carragher, D. M., Rangel-Moreno, J., & Randall, T. D. (2008). Ectopic lymphoid tissues and local immunity. *Seminars in Immunology*, *20*(1), 26–42. https://doi.org/10.1016/j.smim.2007.12.004

Carrega, P., Loiacono, F., Di Carlo, E., Scaramuccia, A., Mora, M., Conte, R., … Ferlazzo, G. (2015). NCR+ILC3 concentrate in human lung cancer and associate with intratumoral lymphoid structures. *Nature Communications*, *6*, 8280. https://doi.org/10.1038/ncomms9280

Castino, G. F., Cortese, N., Capretti, G., Serio, S., Di Caro, G., Mineri, R., … Marchesi, F. (2015). Spatial distribution of B cells predicts prognosis in human pancreatic adenocarcinoma. *Oncoimmunology*, *5*(4), e1085147. https://doi.org/10.1080/2162402X.2015.1085147

Chen, L., Taylor, J. L., Sabins, N. C., Lowe, D. B., Qu, Y., You, Z., & Storkus, W. J. (2013). Extranodal induction of therapeutic immunity in the tumor microenvironment after intratumoral delivery of Tbet gene-modified dendritic cells. *Cancer Gene Therapy*, *20*(8), 469–477. https://doi.org/10.1038/cgt.2013.42

Chiang, E. Y., Kolumam, G. A., Yu, X., Francesco, M., Ivelja, S., Peng, I., … Grogan, J. L. (2009). Targeted depletion of lymphotoxin-alpha-expressing TH1 and TH17 cells inhibits autoimmune disease. *Nature Medicine*, *15*(7), 766–773. https://doi.org/10.1038/nm.1984

Ciesielski, O., Biesiekierska, M., Panthu, B., Vialichka, V., Pirola, L., & Balcerczyk, A. (2020). The Epigenetic Profile of Tumor Endothelial Cells. Effects of Combined Therapy with Antiangiogenic and Epigenetic Drugs on Cancer Progression. *International Journal of Molecular Sciences*, *21*(7). https://doi.org/10.3390/ijms21072606

Cipponi, A., Mercier, M., Seremet, T., Baurain, J.-F., Théate, I., van den Oord, J., … van Baren, N. (2012). Neogenesis of lymphoid structures and antibody responses occur in human melanoma metastases. *Cancer Research*, *72*(16), 3997–4007. https://doi.org/10.1158/0008-5472.CAN-12-1377

Clark, R. A., Huang, S. J., Murphy, G. F., Mollet, I. G., Hijnen, D., Muthukuru, M., … Kupper, T. S. (2008). Human squamous cell carcinomas evade the immune response by down-regulation of vascular E-selectin and recruitment of regulatory

T cells. *Journal of Experimental Medicine*, *205*(10), 2221–2234. https://doi.org/10.1084/jem.20071190

Coca, S., Perez-Piqueras, J., Martinez, D., Colmenarejo, A., Saez, M. A., Vallejo, C., … Moreno, M. (1997). The prognostic significance of intratumoral natural killer cells in patients with colorectal carcinoma. *Cancer*, *79*(12), 2320–2328. https://doi.org/10.1002/(sici)1097-0142(19970615)79:12<2320::aid-cncr5>3.0.co;2-p

Colbeck, E. J., Jones, E., Hindley, J. P., Smart, K., Schulz, R., Browne, M., … Gallimore, A. (2017). Treg Depletion Licenses T Cell-Driven HEV Neogenesis and Promotes Tumor Destruction. *Cancer Immunology Research*, *5*(11), 1005–1015. https://doi.org/10.1158/2326-6066.CIR-17-0131

Coley, W. (1893). The treatment of malignant tumors by repeated inoculations of erysipelas. With a report of ten original cases. *LWW*, *105*(5), 487–510.

Coppola, D., Nebozhyn, M., Khalil, F., Dai, H., Yeatman, T., Loboda, A., & Mulé, J. J. (2011). Unique ectopic lymph node-like structures present in human primary colorectal carcinoma are identified by immune gene array profiling. *American Journal of Pathology*, *179*(1), 37–45. https://doi.org/10.1016/j.ajpath.2011.03.007

Costa, A., Kieffer, Y., Scholer-Dahirel, A., Pelon, F., Bourachot, B., Cardon, M., … Mechta-Grigoriou, F. (2018). Fibroblast Heterogeneity and Immunosuppressive Environment in Human Breast Cancer. *Cancer Cell*, *33*(3), 463-479.e10. https://doi.org/10.1016/j.ccell.2018.01.011

Craddock, J. A., Lu, A., Bear, A., Pule, M., Brenner, M. K., Rooney, C. M., & Foster, A. E. (2010). Enhanced tumor trafficking of GD2 chimeric antigen receptor T cells by expression of the chemokine receptor CCR2b. *Journal of Immunotherapy (Hagerstown, Md.: 1997)*, *33*(8), 780–788. https://doi.org/10.1097/CJI.0b013e3181ee6675

Cretney, E., Takeda, K., Yagita, H., Glaccum, M., Peschon, J. J., & Smyth, M. J. (2002). Increased susceptibility to tumor initiation and metastasis in TNF-related apoptosis-inducing ligand-deficient mice. *Journal of Immunology (Baltimore, Md.: 1950)*, *168*(3), 1356–1361. https://doi.org/10.4049/jimmunol.168.3.1356

Cruz-Migoni, S., & Caamaño, J. (2016). Fat-associated lymphoid clusters in inflammation and immunity. *Frontiers in Immunology*, *7*, 612. https://doi.org/10.3389/fimmu.2016.00612

Cuff, C. A., Sacca, R., & Ruddle, N. H. (1999). Differential induction of adhesion molecule and chemokine expression by LTα3 and LTαβ in inflammation elucidates potential mechanisms of mesenteric and peripheral lymph node development. *Journal of Immunology*, *162*(10), 5965–5972.

Cuff, C. A., Schwartz, J., Bergman, C. M., Russell, K. S., Bender, J. R., & Ruddle, N. H. (1998). Lymphotoxin α3 Induces chemokines and adhesion molecules: Insight into the role of LTα in inflammation and lymphoid organ development. *Journal of Immunology*, *161*(12), 6853–6860.

Curran, M. A., Montalvo, W., Yagita, H., & Allison, J. P. (2010). PD-1 and CTLA-4 combination blockade expands infiltrating T cells and reduces regulatory T and myeloid cells within B16 melanoma tumors. *Proceedings of the National Academy of Sciences of the United States of America*, *107*(9), 4275–4280. https://doi.org/10.1073/pnas.0915174107

Cyster, J. G., & Schwab, S. R. (2012). Sphingosine-1-Phosphate and Lymphocyte Egress from Lymphoid Organs. *Annual Review of Immunology*, *30*(1), 69–94. https://doi.org/10.1146/annurev-immunol-020711-075011

de Chaisemartin, L., Goc, J., Damotte, D., Validire, P., Magdeleinat, P., Alifano, M., … Dieu-Nosjean, M.-C. (2011). Characterization of chemokines and adhesion molecules associated with T cell presence in tertiary lymphoid structures in human lung cancer. *Cancer Research*, *71*(20), 6391–6399. https://doi.org/10.1158/0008-5472.CAN-11-0952

De Henau, O., Rausch, M., Winkler, D., Campesato, L. F., Liu, C., Cymerman, D. H., … Merghoub, T. (2016). Overcoming resistance to checkpoint blockade therapy by targeting PI3Kγ in myeloid cells. *Nature*, *539*(7629), 443–447. https://doi.org/10.1038/nature20554

De Togni, P., Goellner, J., Ruddle, N. H., Streeter, P. R., Fick, A., Mariathasan, S., … Chaplin, D. D. (1994). Abnormal development of peripheral lymphoid organs in mice deficient in lymphotoxin. *Science*, *264*(5159), 703–707.

Deidier, A. (1725). *Dissertation Medecinal et Chirurgical sur les Tumeurs*.

Deligdisch, L., Jacobs, A. J., & Cohen, C. J. (1982). Histologic correlates of virulence in ovarian adenocarcinoma: II. Morphologic correlates of host response. *American Journal of Obstetrics and Gynecology*, *144*(8), 885–889. https://doi.org/10.1016/0002-9378(82)90178-8

DeNardo, D. G., & Coussens, L. M. (2007). Inflammation and breast cancer. Balancing immune response: Crosstalk between adaptive and innate immune cells during breast cancer progression. *Breast Cancer Research: BCR*, *9*(4), 212. https://doi.org/10.1186/bcr1746

Dengel, L. T., Norrod, A. G., Gregory, B. L., Clancy-Thompson, E., Burdick, M. D., Strieter, R. M., … Mullins, D. W. (2010). Interferons induce CXCR3-cognate chemokine production by human metastatic melanoma. *Journal of Immunotherapy*, *33*(9), 965–974. https://doi.org/10.1097/CJI.0b013e3181fb045d

Di Caro, G., Bergomas, F., Grizzi, F., Doni, A., Bianchi, P., Malesci, A., … Marchesi, F. (2014). Occurrence of tertiary lymphoid tissue is associated with T-cell infiltration and predicts better prognosis in early-stage colorectal cancers. *Clinical Cancer Research*, *20*(8), 2147–2158. https://doi.org/10.1158/1078-0432.CCR-13-2590

Di Stasi, A., De Angelis, B., Rooney, C. M., Zhang, L., Mahendravada, A., Foster, A. E., … Savoldo, B. (2009). T lymphocytes coexpressing CCR4 and a chimeric antigen receptor targeting CD30 have improved homing and antitumor activity in a Hodgkin tumor model. *Blood*, *113*(25), 6392. https://doi.org/10.1182/blood-2009-03-209650

Dieu-Nosjean, M.-C., Antoine, M., Danel, C., Heudes, D., Wislez, M., Poulot, V., … Cadranel, J. (2008). *Long-term survival for patients with non-small-cell lung cancer with intratumoral lymphoid structures*. *26*(27), 4410–4417. https://doi.org/10.1200/JCO.2007.15.0284

DiLillo, D. J., Yanaba, K., & Tedder, T. F. (2010). B Cells Are Required for Optimal CD4+ and CD8+ T Cell Tumor Immunity: Therapeutic B Cell Depletion Enhances B16 Melanoma Growth in Mice. *The Journal of Immunology*, *184*(7), 4006–4016. https://doi.org/10.4049/jimmunol.0903009

Dominguez, C. X., Müller, S., Keerthivasan, S., Koeppen, H., Hung, J., Gierke, S., … Turley, S. J. (2020). Single-Cell RNA Sequencing Reveals Stromal Evolution into LRRC15+ Myofibroblasts as a Determinant of Patient Response to Cancer Immunotherapy. *Cancer Discovery*, *10*(2), 232–253. https://doi.org/10.1158/2159-8290.CD-19-0644

Dougan, S. K., Ogata, S., Hu, C.-C. A., Grotenbreg, G. M., Guillen, E., Jaenisch, R., & Ploegh, H. L. (2012). IgG1+ ovalbumin-specific B-cell transnuclear mice show class switch recombination in rare allelically included B cells. *Proceedings of the National Academy of Sciences of the United States of America*, *109*(34), 13739–13744. https://doi.org/10.1073/pnas.1210273109

Drayton, D. L., Liao, S., Mounzer, R. H., & Ruddle, N. H. (2006). Lymphoid organ development: From ontogeny to neogenesis. *Nature Immunology*, *7*(4), 344–353. https://doi.org/10.1038/ni1330

Drayton, D. L., Ying, X., Lee, J., Lesslauer, W., & Ruddle, N. H. (2003). Ectopic LTαβ directs lymphoid organ neogenesis with concomitant expression of peripheral node addressin and a HEV-restricted sulfotransferase. *Journal of Experimental Medicine*, *197*(9), 1153–1163. https://doi.org/10.1084/jem.20021761

Dubey, L. K., Lebon, L., Mosconi, I., Yang, C.-Y., Scandella, E., Ludewig, B., … Harris, N. L. (2016). Lymphotoxin-Dependent B Cell-FRC Crosstalk Promotes De Novo Follicle Formation and Antibody Production following Intestinal Helminth Infection. *Cell Reports*, *15*(7), 1527–1541. https://doi.org/10.1016/j.celrep.2016.04.023

Dunn, G. P., Bruce, A. T., Sheehan, K. C. F., Shankaran, V., Uppaluri, R., Bui, J. D., … Schreiber, R. D. (2005). A critical function for type I interferons in cancer immunoediting. *Nature Immunology*, *6*(7), 722–729. https://doi.org/10.1038/ni1213

Dunn, G. P., Old, L. J., & Schreiber, R. D. (2004). The immunobiology of cancer immunosurveillance and immunoediting. *Immunity*, *21*(2), 137–148. https://doi.org/10.1016/j.immuni.2004.07.017

Eckelhart, E., Warsch, W., Zebedin, E., Simma, O., Stoiber, D., Kolbe, T., … Sexl, V. (2011). A novel Ncr1-Cre mouse reveals the essential role of STAT5 for NK-cell survival and development. *Blood*, *117*(5), 1565–1573. https://doi.org/10.1182/blood-2010-06-291633

Economou, J. S., Belldegrun, A. S., Glaspy, J., Toloza, E. M., Figlin, R., Hobbs, J., … Moen, R. C. (1996). In vivo trafficking of adoptively transferred interleukin-2 expanded tumor-infiltrating lymphocytes and peripheral blood lymphocytes. Results of a double gene marking trial. *Journal of Clinical Investigation*, *97*(2), 515–521. https://doi.org/10.1172/JCI118443

Ehrlich, P. (1909). Ueber den jetzigen stand der Karzinomforschung. *Ned. Tijdschr. Geneeskd*, *5*, 273–290.

Ellies, L. G., Tsuboi, S., Petryniak, B., Lowe, J. B., Fukuda, M., & Marth, J. D. (1998). Core 2 oligosaccharide biosynthesis distinguishes between selectin ligands essential for leukocyte homing and inflammation. *Immunity*, *9*(6), 881–890. https://doi.org/10.1016/s1074-7613(00)80653-6

Ellies, Lesley G., Sperandio, M., Underhill, G. H., Yousif, J., Smith, M., Priatel, J. J., … Marth, J. D. (2002). Sialyltransferase specificity in selectin ligand formation. *Blood*, *100*(10), 3618–3625. https://doi.org/10.1182/blood-2002-04-1007

Engel, A. M., Svane, I. M., Mouritsen, S., Rygaard, J., Clausen, J., & Werdelin, O. (1996). Methylcholanthrene-induced sarcomas in nude mice have short induction times and relatively low levels of surface MHC class I expression. *APMIS: Acta Pathologica, Microbiologica, et Immunologica Scandinavica*, *104*(9), 629–639. https://doi.org/10.1111/j.1699-0463.1996.tb04923.x

Engel, A. M., Svane, I. M., Rygaard, J., & Werdelin, O. (1997). MCA sarcomas induced in scid mice are more immunogenic than MCA sarcomas induced in congenic,

immunocompetent mice. *Scandinavian Journal of Immunology*, *45*(5), 463–470. https://doi.org/10.1046/j.1365-3083.1997.d01-419.x

Engelhard, V. H., Rodriguez, A. B., Mauldin, I. S., Woods, A. N., Peske, J. D., & Slingluff, C. L. (2018). Immune Cell Infiltration and Tertiary Lymphoid Structures as Determinants of Antitumor Immunity. *Journal of Immunology*, *200*(2), 432–442. https://doi.org/10.4049/jimmunol.1701269

Epstein, N. A., & Fatti, L. P. (1976). Prostatic carcinoma. Some morphological features affecting prognosis. *Cancer*, *37*(5), 2455–2465. https://doi.org/10.1002/1097-0142(197605)37:5<2455::AID-CNCR2820370539>3.0.CO;2-V

Epstein Shochet, G., Brook, E., Israeli-Shani, L., Edelstein, E., & Shitrit, D. (2017). Fibroblast paracrine TNF-α signaling elevates integrin A5 expression in idiopathic pulmonary fibrosis (IPF). *Respiratory Research*, *18*(1), 122. https://doi.org/10.1186/s12931-017-0606-x

Erdag, G., Schaefer, J. T., Smolkin, M. E., Deacon, D. H., Shea, S. M., Dengel, L. T., … Slingluff, C. L., Jr. (2012). Immunotype and immunohistologic characteristics of tumor-infiltrating immune cells are associated with clinical outcome in metastatic melanoma. *Cancer Research*, *72*(5), 1070–1080. https://doi.org/10.1158/0008-5472.CAN-11-3218

Erdogan, B., & Webb, D. J. (2017). Cancer-associated fibroblasts modulate growth factor signaling and extracellular matrix remodeling to regulate tumor metastasis.

Biochemical Society Transactions, *45*(1), 229–236. https://doi.org/10.1042/BST20160387

Fan, C., Prat, A., Parker, J. S., Liu, Y., Carey, L. A., Troester, M. A., & Perou, C. M. (2011). Building prognostic models for breast cancer patients using clinical variables and hundreds of gene expression signatures. *BMC Medical Genomics*, *4*, 3. https://doi.org/10.1186/1755-8794-4-3

Featherstone, C., & Jackson, S. P. (1999). DNA double-strand break repair. *Current Biology*, *9*(20), R759–R761. https://doi.org/10.1016/S0960-9822(00)80005-6

Feig, C., Jones, J. O., Kraman, M., Wells, R. J. B., Deonarine, A., Chan, D. S., … Fearon, D. T. (2013). Targeting CXCL12 from FAP-expressing carcinoma-associated fibroblasts synergizes with anti-PD-L1 immunotherapy in pancreatic cancer. *Proceedings of the National Academy of Sciences of the United States of America*, *110*(50), 20212–20217. https://doi.org/10.1073/pnas.1320318110

Ferguson, A. R., & Engelhard, V. H. (2010). CD8 T cells activated in distinct lymphoid organs differentially express adhesion proteins and coexpress multiple chemokine receptors. *Journal of Immunology*, *184*(8), 4079–4086. https://doi.org/jimmunol.0901903 [pii] 10.4049/jimmunol.0901903

Figenschau, S. L., Fismen, S., Fenton, K. A., Fenton, C., & Mortensen, E. S. (2015). Tertiary lymphoid structures are associated with higher tumor grade in primary operable breast cancer patients. *BMC Cancer*, *15*, 101. https://doi.org/10.1186/s12885-015-1116-1

Finkin, S., Yuan, D., Stein, I., Taniguchi, K., Weber, A., Unger, K., … Pikarsky, E. (2015). Ectopic lymphoid structures function as microniches for tumor progenitor cells in hepatocellular carcinoma. *Nature Immunology*, *16*(12), 1235–1244. https://doi.org/10.1038/ni.3290

Fisher, B., Packard, B. S., Read, E. J., Carrasquillo, J. A., Carter, C. S., Topalian, S. L., … Rosenberg, S. A. (1989). Tumor localization of adoptively transferred indium-111 labeled tumor infiltrating lymphocytes in patients with metastatic melanoma. *Journal of Clinical Oncology*, *7*(2), 250–261.

Fisher, D. G., & Price, R. J. (2019). Recent Advances in the Use of Focused Ultrasound for Magnetic Resonance Image-Guided Therapeutic Nanoparticle Delivery to the Central Nervous System. *Frontiers in Pharmacology*, *10*. https://doi.org/10.3389/fphar.2019.01348

Fisher, D. T., Chen, Q., Skitzki, J. J., Muhitch, J. B., Zhou, L., Appenheimer, M. M., … Evans, S. S. (2011). IL-6 trans-signaling licenses mouse and human tumor microvascular gateways for trafficking of cytotoxic T cells. *The Journal of Clinical Investigation*, *121*(10), 3846–3859. https://doi.org/10.1172/JCI44952

Fleige, H., Ravens, S., Moschovakis, G. L., Bölter, J., Willenzon, S., Sutter, G., … Förster, R. (2014). IL-17–induced CXCL12 recruits B cells and induces follicle formation in BALT in the absence of differentiated FDCs. *The Journal of Experimental Medicine*, *211*(4), 643–651. https://doi.org/10.1084/jem.20131737

Fletcher, A. L., Acton, S. E., & Knoblich, K. (2015). Lymph node fibroblastic reticular cells in health and disease. *Nature Reviews Immunology*, *15*(6), 350–361. https://doi.org/10.1038/nri3846

Foo, S. Y., Zhang, V., Lalwani, A., Lynch, J. P., Zhuang, A., Lam, C. E., … Phipps, S. (2015). Regulatory T Cells Prevent Inducible BALT Formation by Dampening Neutrophilic Inflammation. *The Journal of Immunology*, *194*(9), 4567–4576. https://doi.org/10.4049/jimmunol.1400909

Forster, R., Mattis, A. E., Kremmer, E., Wolf, E., Brem, G., & Lipp, M. (1996). A putative chemokine receptor, BLR1, directs B cell migration to defined lymphoid organs and specific anatomic compartments of the spleen. *Cell*, *87*(6), 1037–1047. https://doi.org/10.1016/s0092-8674(00)81798-5

Franco-Barraza, J., Francescone, R., Luong, T., Shah, N., Madhani, R., Cukierman, G., … Cukierman, E. (n.d.). Matrix-regulated integrin αvβ5 maintains α5β1-dependent desmoplastic traits prognostic of neoplastic recurrence. *ELife*, *6*. https://doi.org/10.7554/eLife.20600

Furtado, G. C., Pacer, M. E., Bongers, G., Bénézech, C., He, Z., Chen, L., … Lira, S. A. (2014). TNFα-dependent development of lymphoid tissue in the absence of RORγt^{+} lymphoid tissue inducer cells. *Mucosal Immunology*, *7*(3), 602–614. https://doi.org/10.1038/mi.2013.79

Furtado, Glaucia C, Marinkovic, T., Martin, A. P., Garin, A., Hoch, B., Hubner, W., … Lira, S. A. (2007). Lymphotoxin beta receptor signaling is required for

inflammatory lymphangiogenesis in the thyroid. *Proceedings of the National Academy of Sciences of the United States of America*, *104*(12), 5026–5031. https://doi.org/10.1073/pnas.0606697104

Fütterer, A., Mink, K., Luz, A., Kosco-Vilbois, M. H., & Pfeffer, K. (1998). The lymphotoxin β receptor controls organogenesis and affinity maturation in peripheral lymphoid tissues. *Immunity*, *9*(1), 59–70. https://doi.org/10.1016/S1074-7613(00)80588-9

Gabrilovich, D. I., & Nagaraj, S. (2009). Myeloid-derived suppressor cells as regulators of the immune system. *Nature Reviews Immunology*, *9*(3), 162–174. https://doi.org/10.1038/nri2506

Gajewski, T. F., Louahed, J., & Brichard, V. G. (2010). Gene signature in melanoma associated with clinical activity. *Cancer Journal*, *16*(4), 399–403. https://doi.org/10.1097/PPO.0b013e3181eacbd8

Gajewski, T. F., Schreiber, H., & Fu, Y.-X. (2013). Innate and adaptive immune cells in the tumor microenvironment. *Nature Immunology*, *14*(10), 1014–1022. https://doi.org/10.1038/ni.2703

Galon, J., Costes, A., Sanchez-Cabo, F., Kirilovsky, A., Mlecnik, B., Lagorce-Pagès, C., … Pagès, F. (2006). Type, density, and location of immune cells within human colorectal tumors predict clinical outcome. *Science*, *313*(5795), 1960–1964. https://doi.org/10.1126/science.1129139

Garbi, N., Arnold, B., Gordon, S., Hämmerling, G. J., & Ganss, R. (2004). CpG motifs as proinflammatory factors render autochthonous tumors permissive for infiltration and destruction. *The Journal of Immunology*, *172*(10), 5861–5869.

García-Hernández, M. de la L., Uribe-Uribe, N. O., Espinosa-González, R., Kast, W. M., Khader, S. A., & Rangel-Moreno, J. (2017). A Unique Cellular and Molecular Microenvironment Is Present in Tertiary Lymphoid Organs of Patients with Spontaneous Prostate Cancer Regression. *Frontiers in Immunology*, *8*, 563. https://doi.org/10.3389/fimmu.2017.00563

Gatti, R. A., & Good, R. A. (1971). Occurrence of malignancy in immunodeficiency diseases. A literature review. *Cancer*, *28*(1), 89–98. https://doi.org/10.1002/1097-0142(197107)28:1<89::aid-cncr2820280117>3.0.co;2-q

Gatumu, M. K., Skarstein, K., Papandile, A., Browning, J. L., Fava, R. A., & Bolstad, A. (2009). Blockade of lymphotoxin-beta receptor signaling reduces aspects of Sjögren syndrome in salivary glands of non-obese diabetic mice. *Arthritis Research & Therapy*, *11*(1), R24. https://doi.org/10.1186/ar2617

Gentles, A. J., Newman, A. M., Liu, C. L., Bratman, S. V., Feng, W., Kim, D., … Alizadeh, A. A. (2015). The prognostic landscape of genes and infiltrating immune cells across human cancers. *Nature Medicine*, *21*(8), 938–945. https://doi.org/10.1038/nm.3909

Gerling, M., Büller, N. V. J. A., Kirn, L. M., Joost, S., Frings, O., Englert, B., … Toftgård, R. (2016). Stromal Hedgehog signalling is downregulated in colon cancer and its

restoration restrains tumour growth. *Nature Communications*, *7*(1), 12321. https://doi.org/10.1038/ncomms12321

Germain, C., Gnjatic, S., Tamzalit, F., Knockaert, S., Remark, R., Goc, J., … Dieu-Nosjean, M.-C. (2014). Presence of B cells in tertiary lymphoid structures is associated with a protective immunity in patients with lung cancer. *American Journal of Respiratory and Critical Care Medicine*, *189*(7), 832–844. https://doi.org/10.1164/rccm.201309-1611OC

GeurtsvanKessel, C. H., Willart, M. A., Bergen, I. M., van Rijt, L. S., Muskens, F., Elewaut, D., … Lambrecht, B. N. (2009). Dendritic cells are crucial for maintenance of tertiary lymphoid structures in the lung of influenza virus-infected mice. *Journal of Experimental Medicine*, *206*(11), 2339–2349. https://doi.org/jem.20090410 [pii] 10.1084/jem.20090410

Giraldo, N. A., Becht, E., Pagès, F., Skliris, G., Verkarre, V., Vano, Y., … Sautès-Fridman, C. (2015). *Orchestration and Prognostic Significance of Immune Checkpoints in the Microenvironment of Primary and Metastatic Renal Cell Cancer*. *21*(13), 3031–3040. https://doi.org/10.1158/1078-0432.CCR-14-2926

Giraldo, N. A., Becht, E., Vano, Y., Petitprez, F., Lacroix, L., Validire, P., … Sautès-Fridman, C. (2017). Tumor-Infiltrating and Peripheral Blood T-cell Immunophenotypes Predict Early Relapse in Localized Clear Cell Renal Cell Carcinoma. *Clinical Cancer Research: An Official Journal of the American*

Association for Cancer Research, *23*(15), 4416–4428. https://doi.org/10.1158/1078-0432.CCR-16-2848

Girard, J.-P., Moussion, C., & Förster, R. (2012). HEVs, lymphatics and homeostatic immune cell trafficking in lymph nodes. *Nature Reviews Immunology*, *12*(11), 762–773. https://doi.org/10.1038/nri3298

Girardi, M., Oppenheim, D. E., Steele, C. R., Lewis, J. M., Glusac, E., Filler, R., … Hayday, A. C. (2001). Regulation of cutaneous malignancy by gammadelta T cells. *Science*, *294*(5542), 605–609.

Girardi, Michael, Glusac, E., Filler, R. B., Roberts, S. J., Propperova, I., Lewis, J., … Hayday, A. C. (2003). The Distinct Contributions of Murine T Cell Receptor (TCR)γδ+ and TCRαβ+ T Cells to Different Stages of Chemically Induced Skin Cancer. *The Journal of Experimental Medicine*, *198*(5), 747–755. https://doi.org/10.1084/jem.20021282

Goc, J., Germain, C., Vo-Bourgais, T. K. D., Lupo, A., Klein, C., Knockaert, S., … Dieu-Nosjean, M.-C. (2014). Dendritic cells in tumor-associated tertiary lymphoid structures signal a Th1 cytotoxic immune contexture and license the positive prognostic value of infiltrating CD8+ T cells. *Cancer Research*, *74*(3), 705–715. https://doi.org/10.1158/0008-5472.CAN-13-1342

Gopal, R., Rangel-Moreno, J., Slight, S., Lin, Y., Nawar, H. F., Fallert Junecko, B. A., … Khader, S. A. (2013). Interleukin-17-dependent CXCL13 mediates mucosal

vaccine–induced immunity against tuberculosis. *Mucosal Immunology*, *6*(5), 972–984. https://doi.org/10.1038/mi.2012.135

Gorick, C. M., Mathew, A. S., Garrison, W. J., Thim, E. A., Fisher, D. G., Copeland, C. A., … Price, R. J. (2020). Sonoselective transfection of cerebral vasculature without blood–brain barrier disruption. *Proceedings of the National Academy of Sciences*, *117*(11), 5644–5654. https://doi.org/10.1073/pnas.1914595117

Goya, S., Matsuoka, H., Mori, M., Morishita, H., Kida, H., Kobashi, Y., … Hayashi, S. (2003). Sustained interleukin-6 signalling leads to the development of lymphoid organ-like structures in the lung. *The Journal of Pathology*, *200*(1), 82–87. https://doi.org/10.1002/path.1321

Gräbner, R., Lötzer, K., Döpping, S., Hildner, M., Radke, D., Beer, M., … Habenicht, A. J. R. (2009). Lymphotoxin β receptor signaling promotes tertiary lymphoid organogenesis in the aorta adventitia of aged ApoE−/− mice. *Journal of Experimental Medicine*, *206*(1), 233–248. https://doi.org/10.1084/jem.20080752

Grant, G. A., & Miller, J. F. (1965). Effect of neonatal thymectomy on the induction of sarcomata in C57 BL mice. *Nature*, *205*(976), 1124–1125. https://doi.org/10.1038/2051124a0

Grant, S. M., Lou, M., Yao, L., Germain, R. N., & Radtke, A. J. (2020). The lymph node at a glance – how spatial organization optimizes the immune response. *Journal of Cell Science*, *133*(jcs241828). https://doi.org/10.1242/jcs.241828

Griffith, K. D., Read, E. J., Carrasquillo, J. A., Carter, C. S., Yang, J. C., Fisher, B., … Rosenberg, S. A. (1989). In vivo distribution of adoptively transferred indium-111-labeled tumor infiltrating lymphocytes and peripheral blood lymphocytes in patients with metastatic melanoma. *Journal of the National Cancer Institute*, *81*(22), 1709–1717.

Griss, J., Bauer, W., Wagner, C., Simon, M., Chen, M., Grabmeier-Pfistershammer, K., … Wagner, S. N. (2019). B cells sustain inflammation and predict response to immune checkpoint blockade in human melanoma. *Nature Communications*, *10*(1), 4186. https://doi.org/10.1038/s41467-019-12160-2

Guedj, K., Khallou-Laschet, J., Clement, M., Morvan, M., Gaston, A.-T., Fornasa, G., … Nicoletti, A. (2014). M1 macrophages act as LTβR-independent lymphoid tissue inducer cells during atherosclerosis-related lymphoid neogenesis. *Cardiovascular Research*, *101*(3), 434–443. https://doi.org/10.1093/cvr/cvt263

Guo, F. F., & Cui, J. W. (2019). The Role of Tumor-Infiltrating B Cells in Tumor Immunity. *Journal of Oncology*, *2019*, 2592419. https://doi.org/10.1155/2019/2592419

Gu-Trantien, C., Loi, S., Garaud, S., Equeter, C., Libin, M., de Wind, A., … Willard-Gallo, K. (2013). $CD4^+$ follicular helper T cell infiltration predicts breast cancer survival. *The Journal of Clinical Investigation*, *123*(7), 2873–2892. https://doi.org/10.1172/JCI67428

Gu-Trantien, C., Migliori, E., Buisseret, L., de Wind, A., Brohée, S., Garaud, S., … Willard-Gallo, K. (2017). CXCL13-producing T_{FH} cells link immune suppression and adaptive memory in human breast cancer. *JCI Insight*, *2*(11), e91487. https://doi.org/10.1172/jci.insight.91487

Gu-Trantien, C., & Willard-Gallo, K. (2013). Tumor-infiltrating follicular helper T cells. *Oncoimmunology*, *2*(10), e26066. https://doi.org/10.4161/onci.26066

Hailemichael, Y., Woods, A., Fu, T., He, Q., Nielsen, M. C., Hasan, F., … Overwijk, W. W. (2018). Cancer vaccine formulation dictates synergy with CTLA-4 and PD-L1 checkpoint blockade therapy. *The Journal of Clinical Investigation*, *128*(4), 1338–1354. https://doi.org/10.1172/JCI93303

Halle, S., Dujardin, H. C., Bakocevic, N., Fleige, H., Danzer, H., Willenzon, S., … Forster, R. (2009). Induced bronchus-associated lymphoid tissue serves as a general priming site for T cells and is maintained by dendritic cells. *Journal of Experimental Medicine*, *206*(12), 2593–2601. https://doi.org/jem.20091472 [pii] 10.1084/jem.20091472

Hargadon, K. M., Brinkman, C. C., Sheasley-O'Neill, S. L., Nichols, L. A., Bullock, T. N. J., & Engelhard, V. H. (2006). Incomplete differentiation of tumor-specific CD8+ T cells in tumor-draining lymph nodes. *Journal of Immunology*, *177*, 6081–6090.

Hayakawa, K., Hardy, R. R., Herzenberg, L. A., & Herzenberg, L. A. (1985). Progenitors for Ly-1 B cells are distinct from progenitors for other B cells. *Journal of*

Experimental Medicine, *161*(6), 1554–1568. https://doi.org/10.1084/jem.161.6.1554

Hayasaka, H., Taniguchi, K., Fukai, S., & Miyasaka, M. (2010). Neogenesis and development of the high endothelial venules that mediate lymphocyte trafficking. *Cancer Science*, *101*(11), 2302–2308. https://doi.org/10.1111/j.1349-7006.2010.01687.x

Heidegger, S., Wintges, A., Stritzke, F., Bek, S., Steiger, K., Koenig, P.-A., … Poeck, H. (2019). RIG-I activation is critical for responsiveness to checkpoint blockade. *Science Immunology*, *4*(39). https://doi.org/10.1126/sciimmunol.aau8943

Hellebrekers, D. M. E. I., Castermans, K., Viré, E., Dings, R. P. M., Hoebers, N. T. H., Mayo, K. H., … Griffioen, A. W. (2006). Epigenetic Regulation of Tumor Endothelial Cell Anergy: Silencing of Intercellular Adhesion Molecule-1 by Histone Modifications. *Cancer Research*, *66*(22), 10770–10777. https://doi.org/10.1158/0008-5472.CAN-06-1609

Hellebrekers, D. M. E. I., Melotte, V., Viré, E., Langenkamp, E., Molema, G., Fuks, F., … Engeland, M. van. (2007). Identification of Epigenetically Silenced Genes in Tumor Endothelial Cells. *Cancer Research*, *67*(9), 4138–4148. https://doi.org/10.1158/0008-5472.CAN-06-3032

Helmink, B. A., Reddy, S. M., Gao, J., Zhang, S., Basar, R., Thakur, R., … Wargo, J. A. (2020). B cells and tertiary lymphoid structures promote immunotherapy response. *Nature*, *577*(7791), 549–555. https://doi.org/10.1038/s41586-019-1922-8

Hemmerich, S., Bistrup, A., Singer, M. S., Zante, A. van, Lee, J. K., Tsay, D., … Rosen, S. D. (2001). Sulfation of L-Selectin Ligands by an HEV-Restricted Sulfotransferase Regulates Lymphocyte Homing to Lymph Nodes. *Immunity*, *15*(2), 237–247. https://doi.org/10.1016/S1074-7613(01)00188-1

Hennequin, A., Derangère, V., Boidot, R., Apetoh, L., Vincent, J., Orry, D., … Ladoire, S. (2016). Tumor infiltration by Tbet+ effector T cells and CD20+ B cells is associated with survival in gastric cancer patients. *Oncoimmunology*, *5*(2), e1054598. https://doi.org/10.1080/2162402X.2015.1054598

Henry, R. A., & Kendall, P. L. (2010). CXCL13 blockade disrupts B lymphocyte organization in tertiary lymphoid structures without altering B cell receptor bias or preventing diabetes in nonobese diabetic mice. *Journal of Immunology*, *185*(3), 1460–1465. https://doi.org/10.4049/jimmunol.0903710

Hensbergen, P. J., Wijnands, P. G., Schreurs, M. W., Scheper, R. J., Willemze, R., & Tensen, C. P. (2005). The CXCR3 targeting chemokine CXCL11 has potent antitumor activity in vivo involving attraction of CD8+ T lymphocytes but not inhibition of angiogenesis. *Journal of Immunotherapy*, *28*(4), 343–351.

Herbst, R. S., Soria, J.-C., Kowanetz, M., Fine, G. D., Hamid, O., Gordon, M. S., … Hodi, F. S. (2014). Predictive correlates of response to the anti-PD-L1 antibody MPDL3280A in cancer patients. *Nature*, *515*(7528), 563–567. https://doi.org/10.1038/nature14011

Hill, D. G., Yu, L., Gao, H., Balic, J. J., West, A., Oshima, H., … Jones, G. W. (2018). Hyperactive gp130/STAT3-driven gastric tumourigenesis promotes submucosal tertiary lymphoid structure development. *International Journal of Cancer*, *143*(1), 167–178. https://doi.org/10.1002/ijc.31298

Hindley, J. P., Jones, E., Smart, K., Bridgeman, H., Lauder, S. N., Ondondo, B., … Gallimore, A. M. (2012). T-cell trafficking facilitated by high endothelial venules is required for tumor control after regulatory T-cell depletion. *Cancer Research*, *72*(21), 5473–5482. https://doi.org/10.1158/0008-5472.CAN-12-1912

Hirakawa, J., Tsuboi, K., Sato, K., Kobayashi, M., Watanabe, S., Takakura, A., … Kawashima, H. (2010). Novel anti-carbohydrate antibodies reveal the cooperative function of sulfated N- and O-glycans in lymphocyte homing. *The Journal of Biological Chemistry*, *285*(52), 40864–40878. https://doi.org/10.1074/jbc.M110.167296

Hiraoka, N., Ino, Y., Yamazaki-Itoh, R., Kanai, Y., Kosuge, T., & Shimada, K. (2015). Intratumoral tertiary lymphoid organ is a favourable prognosticator in patients with pancreatic cancer. *British Journal of Cancer*, *112*(11), 1782–1790. https://doi.org/10.1038/bjc.2015.145

Hiraoka, N., Petryniak, B., Nakayama, J., Tsuboi, S., Suzuki, M., Yeh, J. C., … Fukuda, M. (1999). A novel, high endothelial venule-specific sulfotransferase expresses 6-sulfo sialyl Lewis(x), an L-selectin ligand displayed by CD34. *Immunity*, *11*(1), 79–89. https://doi.org/10.1016/s1074-7613(00)80083-7

Hirata, N., Yanagawa, Y., Satoh, M., Ogura, H., Ebihara, T., Noguchi, M., … Iwabuchi, K. (2010). Dendritic cell-derived TNF-alpha is responsible for development of IL-10-producing CD4+ T cells. *Cellular Immunology*, *261*(1), 37–41. https://doi.org/10.1016/j.cellimm.2009.10.009

Hogquist, K. A., Jameson, S. C., Heath, W. R., Howard, J. L., Bevan, M. J., & Carbone, F. R. (1994). T cell receptor antagonist peptides induce positive selection. *Cell*, *76*, 17–27.

Homeister, J. W., Thall, A. D., Petryniak, B., Malý, P., Rogers, C. E., Smith, P. L., … Lowe, J. B. (2001). The α(1,3)fucosyltransferases FucT-IV and FucT-VII Exert Collaborative Control over Selectin-Dependent Leukocyte Recruitment and Lymphocyte Homing. *Immunity*, *15*(1), 115–126. https://doi.org/10.1016/S1074-7613(01)00166-2

Horikawa, M., Minard-Colin, V., Matsushita, T., & Tedder, T. F. (2011). Regulatory B cell production of IL-10 inhibits lymphoma depletion during CD20 immunotherapy in mice. *The Journal of Clinical Investigation*, *121*(11), 4268–4280. https://doi.org/10.1172/JCI59266

Hosaka, K., Yang, Y., Seki, T., Fischer, C., Dubey, O., Fredlund, E., … Cao, Y. (2016). Pericyte-fibroblast transition promotes tumor growth and metastasis. *Proceedings of the National Academy of Sciences of the United States of America*, *113*(38), E5618-5627. https://doi.org/10.1073/pnas.1608384113

Hsao, H.-M., Li, W., Gelman, A. E., Krupnick, A. S., & Kreisel, D. (2015). The Role of Lymphoid Neogenesis in Allografts. *American Journal of Transplantation*, *16*, 1079–1085. https://doi.org/10.1111/ajt.13645

Hsu, H.-C., Yang, P., Wang, J., Wu, Q., Myers, R., Chen, J., … Mountz, J. D. (2008). Interleukin 17–producing T helper cells and interleukin 17 orchestrate autoreactive germinal center development in autoimmune BXD2 mice. *Nature Immunology*, *9*(2), 166–175. https://doi.org/10.1038/ni1552

Huang, H.-Y., & Luther, S. A. (2012). Expression and function of interleukin-7 in secondary and tertiary lymphoid organs. *Seminars in Immunology*, *24*(3), 175–189. https://doi.org/10.1016/j.smim.2012.02.008

Ireland, L., Santos, A., Ahmed, M. S., Rainer, C., Nielsen, S. R., Quaranta, V., … Mielgo, A. (2016). Chemoresistance in Pancreatic Cancer Is Driven by Stroma-Derived Insulin-Like Growth Factors. *Cancer Research*, *76*(23), 6851–6863. https://doi.org/10.1158/0008-5472.CAN-16-1201

Iwai, Y., Terawaki, S., & Honjo, T. (2005). PD-1 blockade inhibits hematogenous spread of poorly immunogenic tumor cells by enhanced recruitment of effector T cells. *International Immunology*, *17*(2), 133–144. https://doi.org/10.1093/intimm/dxh194

Jackson-Jones, L. H., Smith, P., Portman, J. R., Magalhaes, M. S., Mylonas, K. J., Vermeren, M. M., … Bénézech, C. (2020). Stromal Cells Covering Omental Fat-Associated Lymphoid Clusters Trigger Formation of Neutrophil Aggregates to

Capture Peritoneal Contaminants. *Immunity*, *52*(4), 700-715.e6. https://doi.org/10.1016/j.immuni.2020.03.011

Jass, J. R. (1986). Lymphocytic infiltration and survival in rectal cancer. *Journal of Clinical Pathology*, *39*(6), 585–589.

Javia, L. R., & Rosenberg, S. A. (2003). CD4+CD25+ suppressor lymphocytes in the circulation of patients immunized against melanoma antigens. *Journal of Immunotherapy (Hagerstown, Md.: 1997)*, *26*(1), 85–93. https://doi.org/10.1097/00002371-200301000-00009

Ji, R.-R., Chasalow, S. D., Wang, L., Hamid, O., Schmidt, H., Cogswell, J., … Shahabi, V. (2012). An immune-active tumor microenvironment favors clinical response to ipilimumab. *Cancer Immunology, Immunotherapy*, *61*(7), 1019–1031. https://doi.org/10.1007/s00262-011-1172-6

Johansson-Lindbom, B., & Agace, W. W. (2007). Generation of gut-homing T cells and their localization to the small intestinal mucosa. *Immunological Reviews*, *215*, 226–242. https://doi.org/10.1111/j.1600-065X.2006.00482.x

Johansson-Percival, A., He, B., Li, Z.-J., Kjellén, A., Russell, K., Li, J., … Ganss, R. (2017). De novo induction of intratumoral lymphoid structures and vessel normalization enhances immunotherapy in resistant tumors. *Nature Immunology*, *18*(11), 1207–1217. https://doi.org/10.1038/ni.3836

Johnson, L. A., & Jackson, D. G. (2010). Inflammation-induced secretion of CCL21 in lymphatic endothelium is a key regulator of integrin-mediated dendritic cell

transmigration. *International Immunology*, *22*(10), 839–849. https://doi.org/10.1093/intimm/dxq435

Jones, G. W., Hill, D. G., & Jones, S. A. (2016). Understanding Immune Cells in Tertiary Lymphoid Organ Development: It Is All Starting to Come Together. *Frontiers in Immunology*, 401. https://doi.org/10.3389/fimmu.2016.00401

Joshi, N. S., Akama-Garren, E. H., Lu, Y., Lee, D.-Y., Chang, G. P., Li, A., … Jacks, T. (2015). Regulatory T cells in tumor-associated tertiary lymphoid structures suppress anti-tumor T cell responses. *Immunity*, *43*(3), 579–590. https://doi.org/10.1016/j.immuni.2015.08.006

Kalluri, R., & Zeisberg, M. (2006). Fibroblasts in cancer. *Nature Reviews. Cancer*, *6*(5), 392–401. https://doi.org/10.1038/nrc1877

Kang, S. H., Fukaya, M., Yang, J. K., Rothstein, J. D., & Bergles, D. E. (2010). NG2+ CNS glial progenitors remain committed to the oligodendrocyte lineage in postnatal life and following neurodegeneration. *Neuron*, *68*(4), 668–681. https://doi.org/10.1016/j.neuron.2010.09.009

Kaplan, D. H., Shankaran, V., Dighe, A. S., Stockert, E., Aguet, M., Old, L. J., & Schreiber, R. D. (1998). Demonstration of an interferon gamma-dependent tumor surveillance system in immunocompetent mice. *Proceedings of the National Academy of Sciences of the United States of America*, *95*(13), 7556–7561.

Kawashima, A., Fishman, E. K., Kuhlman, J. E., & Schuchter, L. M. (1991). CT of malignant melanoma: Patterns of small bowel and mesenteric involvement. *Journal of Computer Assisted Tomography*, *15*(4), 570–574.

Kawashima, H., Petryniak, B., Hiraoka, N., Mitoma, J., Huckaby, V., Nakayama, J., … Fukuda, M. (2005). N-acetylglucosamine-6-O-sulfotransferases 1 and 2 cooperatively control lymphocyte homing through L-selectin ligand biosynthesis in high endothelial venules. *Nature Immunology*, *6*(11), 1096–1104. https://doi.org/10.1038/ni1259

Kemp, T. J., Moore, J. M., & Griffith, T. S. (2004). Human B Cells Express Functional TRAIL/Apo-2 Ligand after CpG-Containing Oligodeoxynucleotide Stimulation. *The Journal of Immunology*, *173*(2), 892–899. https://doi.org/10.4049/jimmunol.173.2.892

Kershaw, M. H., Westwood, J. A., Parker, L. L., Wang, G., Eshhar, Z., Mavroukakis, S. A., … Hwu, P. (2006). A phase I study on adoptive immunotherapy using gene-modified T cells for ovarian cancer. *Clinical Cancer Research*, *12*(20 Pt 1), 6106–6115. https://doi.org/10.1158/1078-0432.CCR-06-1183

Khader, S. A., Guglani, L., Rangel-Moreno, J., Gopal, R., Junecko, B. A. F., Fountain, J. J., … Cooper, A. M. (2011). IL-23 is required for long-term control of Mycobacterium tuberculosis and B cell follicle formation in the infected lung. *Journal of Immunology (Baltimore, Md.: 1950)*, *187*(10), 5402–5407. https://doi.org/10.4049/jimmunol.1101377

Khader, S. A., Rangel-Moreno, J., Fountain, J. J., Martino, C. A., Reiley, W. W., Pearl, J. E., … Cooper, A. M. (2009). In a Murine Tuberculosis Model, the Absence of Homeostatic Chemokines Delays Granuloma Formation and Protective Immunity. *The Journal of Immunology*, *183*(12), 8004–8014. https://doi.org/10.4049/jimmunol.0901937

Kim, D., Mebius, R. E., MacMicking, J. D., Jung, S., Cupedo, T., Castellanos, Y., … Choi, Y. (2000). Regulation of peripheral lymph node genesis by the tumor necrosis factor family member TRANCE. *Journal of Experimental Medicine*, *192*(10), 1467–1478.

Kim, H.-J., Kammertoens, T., Janke, M., Schmetzer, O., Qin, Z., Berek, C., & Blankenstein, T. (2004). Establishment of early lymphoid organ infrastructure in transplanted tumors mediated by local production of Lymphotoxin α and in the combined absence of functional B and T cells. *Journal of Immunology*, *172*(7), 4037–4047.

Kirk, C. J., Hartigan-O'Connor, D., & Mule, J. J. (2001). The dynamics of the T-cell antitumor response: Chemokine-secreting dendritic cells can prime tumor-reactive T cells extranodally. *Cancer Research*, *61*(24), 8794–8802.

Kirk, C. J., Hartigan-O'Connor, D., Nickoloff, B. J., Chamberlain, J. S., Giedlin, M., Aukerman, L., & Mulé, J. J. (2001). T cell-dependent antitumor immunity mediated by secondary lymphoid tissue chemokine augmentation of dendritic cell-based immunotherapy. *Cancer Research*, *61*(5), 2062–2070.

Koenig, A., & Thaunat, O. (2016). Lymphoid Neogenesis and Tertiary Lymphoid Organs in Transplanted Organs. *Frontiers in Immunology*, *7*, 646. https://doi.org/10.3389/fimmu.2016.00646

Koni, P. A., Sacca, R., Lawton, P., Browning, J. L., Ruddle, N. H., & Flavell, R. A. (1997). Distinct roles in lymphoid organogenesis for lymphotoxins alpha and beta revealed in lymphotoxin beta-deficient mice. *Immunity*, *6*(4), 491–500.

Körner, H., Cook, M., Riminton, D. S., Lemckert, F. A., Hoek, R. M., Ledermann, B., … Sedgwick, J. D. (1997). Distinct roles for lymphotoxin-alpha and tumor necrosis factor in organogenesis and spatial organization of lymphoid tissue. *European Journal of Immunology*, *27*(10), 2600–2609. https://doi.org/10.1002/eji.1830271020

Koti, M., Xu, A. S., Ren, K. Y. M., Visram, K., Ren, R., Berman, D. M., & Siemens, D. R. (2017). Tertiary Lymphoid Structures Associate with Tumour Stage in Urothelial Bladder Cancer. *Bladder Cancer (Amsterdam, Netherlands)*, *3*(4), 259–267. https://doi.org/10.3233/BLC-170120

Kraman, M., Bambrough, P. J., Arnold, J. N., Roberts, E. W., Magiera, L., Jones, J. O., … Fearon, D. T. (2010). Suppression of antitumor immunity by stromal cells expressing fibroblast activation protein-alpha. *Science (New York, N.Y.)*, *330*(6005), 827–830. https://doi.org/10.1126/science.1195300

Kroeger, D. R., Milne, K., & Nelson, B. H. (2016). Tumor-Infiltrating Plasma Cells Are Associated with Tertiary Lymphoid Structures, Cytolytic T-Cell Responses, and

Superior Prognosis in Ovarian Cancer. *Clinical Cancer Research*, *22*(12), 3005–3015. https://doi.org/10.1158/1078-0432.CCR-15-2762

Krüger-Genge, A., Blocki, A., Franke, R.-P., & Jung, F. (2019). Vascular Endothelial Cell Biology: An Update. *International Journal of Molecular Sciences*, *20*(18). https://doi.org/10.3390/ijms20184411

Ku, G. Y., Yuan, J., Page, D. B., Schroeder, S. E. A., Panageas, K. S., Carvajal, R. D., … Wolchok, J. D. (2010). Single-institution experience with ipilimumab in advanced melanoma patients in the compassionate use setting. *Cancer*, *116*(7), 1767–1775. https://doi.org/10.1002/cncr.24951

Kumari, S., Bonnet, M. C., Ulvmar, M. H., Wolk, K., Karagianni, N., Witte, E., … Haase, I. (2013). Tumor Necrosis Factor Receptor Signaling in Keratinocytes Triggers Interleukin-24-Dependent Psoriasis-like Skin Inflammation in Mice. *Immunity*, *39*(5), 899–911. https://doi.org/10.1016/j.immuni.2013.10.009

Kunz, M., Toksoy, A., Goebeler, M., Engelhardt, E., Bröcker, E., & Gillitzer, R. (1999). Strong expression of the lymphoattractant C-X-C chemokine Mig is associated with heavy infiltration of T cells in human malignant melanoma. *Journal of Pathology*, *189*(4), 552–558.

Kuprash, D. V., Alimzhanov, M. B., Tumanov, A. V., Anderson, A. O., Pfeffer, K., & Nedospasov, S. A. (1999). TNF and Lymphotoxin β Cooperate in the Maintenance of Secondary Lymphoid Tissue Microarchitecture But Not in the Development of Lymph Nodes. *Journal of Immunology*, *163*(12), 6575–6580.

Ladányi, A., Kiss, J., Mohos, A., Somlai, B., Liszkay, G., Gilde, K., … Tímár, J. (2011). Prognostic impact of B-cell density in cutaneous melanoma. *Cancer Immunology, Immunotherapy*, *60*(12), 1729–1738. https://doi.org/10.1007/s00262-011-1071-x

Ladanyi, A., Kiss, J., Somlai, B., Gilde, K., Fejos, Z., Mohos, A., … Timar, J. (2007). Density of DC-LAMP(+) mature dendritic cells in combination with activated T lymphocytes infiltrating primary cutaneous melanoma is a strong independent prognostic factor. *Cancer Immunology, Immunotherapy*, *56*, 1459–1469.

Ladányi, A., Sebestyén, T., Mohos, A., Liszkay, G., Somlai, B., Tóth, E., & Tímár, J. (2014). Ectopic lymphoid structures in primary cutaneous melanoma. *Pathology & Oncology Research*, *20*(4), 981–985. https://doi.org/10.1007/s12253-014-9784-8

Lambrechts, D., Wauters, E., Boeckx, B., Aibar, S., Nittner, D., Burton, O., … Thienpont, B. (2018). Phenotype molding of stromal cells in the lung tumor microenvironment. *Nature Medicine*, *24*(8), 1277–1289. https://doi.org/10.1038/s41591-018-0096-5

Lane, P. J. L., Gaspal, F. M., McConnell, F. M., Withers, D. R., & Anderson, G. (2012). Lymphoid tissue inducer cells: Pivotal cells in the evolution of CD4 immunity and tolerance? *Frontiers in Immunology*, *3*, 24. https://doi.org/10.3389/fimmu.2012.00024

Larkin, J., Chiarion-Sileni, V., Gonzalez, R., Grob, J. J., Cowey, C., Lao, C., … Wolchok, J. D. (2015). Combined Nivolumab and Ipilimumab versus Ipilimumab in Untreated Melanoma. *New England Journal of Medicine*, *373*, 23–34.

Lauder, I., & Aherne, W. (1972). The significance of lymphocytic infiltration in neuroblastoma. *British Journal of Cancer*, *26*(4), 321–330.

Leach, D. R., Krummel, M. F., & Allison, J. P. (1996). Enhancement of antitumor immunity by CTLA-4 blockade [see comments]. *Science*, *271*, 1734–1736.

LeBleu, V. S., & Kalluri, R. (2018). A peek into cancer-associated fibroblasts: Origins, functions and translational impact. *Disease Models & Mechanisms*, *11*(4). https://doi.org/10.1242/dmm.029447

Lee, H. J., Kim, J. Y., Park, I. A., Song, I. H., Yu, J. H., Ahn, J.-H., & Gong, G. (2015). Prognostic Significance of Tumor-Infiltrating Lymphocytes and the Tertiary Lymphoid Structures in HER2-Positive Breast Cancer Treated With Adjuvant Trastuzumab. *American Journal of Clinical Pathology*, *144*(2), 278–288. https://doi.org/10.1309/AJCPIXUYDVZ0RZ3G

Lee, H. J., Park, I. A., Song, I. H., Shin, S.-J., Kim, J. Y., Yu, J. H., & Gong, G. (2015). Tertiary lymphoid structures: Prognostic significance and relationship with tumour-infiltrating lymphocytes in triple-negative breast cancer. *Journal of Clinical Pathology*, *69*(5), 422–430. https://doi.org/10.1136/jclinpath-2015-203089

Lee, J. J., McGarry, M. P., Farmer, S. C., Denzler, K. L., Larson, K. A., Carrigan, P. E., … Lee, N. A. (1997). Interleukin-5 Expression in the Lung Epithelium of Transgenic Mice Leads to Pulmonary Changes Pathognomonic of Asthma. *Journal of Experimental Medicine*, *185*(12), 2143–2156. https://doi.org/10.1084/jem.185.12.2143

Lee, Mike, Kiefel, H., LaJevic, M. D., Macauley, M. S., Kawashima, H., O'Hara, E., … Butcher, E. C. (2014). Transcriptional programs of lymphoid tissue capillary and high endothelium reveal control mechanisms for lymphocyte homing. *Nature Immunology*, *15*(10), 982–995. https://doi.org/10.1038/ni.2983

Lee, Miseon, Heo, S.-H., Song, I. H., Rajayi, H., Park, H. S., Park, I. A., … Lee, H. J. (2019). Presence of tertiary lymphoid structures determines the level of tumor-infiltrating lymphocytes in primary breast cancer and metastasis. *Modern Pathology*, *32*(1), 70–80. https://doi.org/10.1038/s41379-018-0113-8

Lee, P. P., Fitzpatrick, D. R., Beard, C., Jessup, H. K., Lehar, S., Makar, K. W., … Wilson, C. B. (2001). A critical role for Dnmt1 and DNA methylation in T cell development, function, and survival. *Immunity*, *15*(5), 763–774. https://doi.org/10.1016/s1074-7613(01)00227-8

Legler, D. F., Loetscher, M., Roos, R. S., Clark-Lewis, I., Baggiolini, M., & Moser, B. (1998). B cell–attracting chemokine 1, a human CXC chemokine expressed in lymphoid tissues, selectively attracts B lymphocytes via BLR1/CXCR5. *The Journal of Experimental Medicine*, *187*(4), 655–660. https://doi.org/10.1084/jem.187.4.655

Ley, K., Laudanna, C., Cybulsky, M. I., & Nourshargh, S. (2007). Getting to the site of inflammation: The leukocyte adhesion cascade updated. *Nature Reviews. Immunology*, *7*(9), 678–689. PubMed (17717539). https://doi.org/10.1038/nri2156

Li, Hequan, Han, Y., Guo, Q., Zhang, M., & Cao, X. (2009). Cancer-expanded myeloid-derived suppressor cells induce anergy of NK cells through membrane-bound TGF-beta 1. *Journal of Immunology (Baltimore, Md.: 1950)*, *182*(1), 240–249. https://doi.org/10.4049/jimmunol.182.1.240

Li, Hui, Wang, J., Liu, H., Lan, T., Xu, L., Wang, G., … Wu, H. (2020). Existence of intratumoral tertiary lymphoid structures is associated with immune cells infiltration and predicts better prognosis in early-stage hepatocellular carcinoma. *Aging (Albany NY)*, *12*(4), 3451–3472. https://doi.org/10.18632/aging.102821

Li, W., Bribriesco, A. C., Nava, R. G., Brescia, A. A., Ibricevic, A., Spahn, J. H., … Kreisel, D. (2012). Lung transplant acceptance is facilitated by early events in the graft and is associated with lymphoid neogenesis. *Mucosal Immunology*, *5*(5), 544–554. https://doi.org/10.1038/mi.2012.30

Link, A., Hardie, D. L., Favre, S., Britschgi, M. R., Adams, D. H., Sixt, M., … Luther, S. A. (2011). Association of T-zone reticular networks and conduits with cctopic lymphoid tissues in mice and humans. *The American Journal of Pathology*, *178*(4), 1662–1675. https://doi.org/10.1016/j.ajpath.2010.12.039

Lipponen, P. K., Eskelinen, M. J., Jauhiainen, K., Harju, E., & Terho, R. (1992). Tumour infiltrating lymphocytes as an independent prognostic factor in transitional cell bladder cancer. *European Journal of Cancer (Oxford, England: 1990)*, *29A*(1), 69–75. https://doi.org/10.1016/0959-8049(93)90579-5

Liu, T., Han, C., Wang, S., Fang, P., Ma, Z., Xu, L., & Yin, R. (2019). *Cancer-associated fibroblasts: An emerging target of anti-cancer immunotherapy*. *12*(1), 86. https://doi.org/10.1186/s13045-019-0770-1

Liu, X., Tsang, J. Y. S., Hlaing, T., Hu, J., Ni, Y.-B., Chan, S. K., … Tse, G. M. (2017). Distinct Tertiary Lymphoid Structure Associations and Their Prognostic Relevance in HER2 Positive and Negative Breast Cancers. *The Oncologist*, *22*(11), 1316–1324. https://doi.org/10.1634/theoncologist.2017-0029

Lohr, J., Ratliff, T., Huppertz, A., Ge, Y., Dictus, C., Ahmadi, R., … Herold-Mende, C. (2011). Effector T-cell infiltration positively impacts survival of glioblastoma patients and is impaired by tumor-derived TGF-β. *Clinical Cancer Research*, *17*(13), 4296–4308. https://doi.org/10.1158/1078-0432.CCR-10-2557

Loschko, J., Schreiber, H. A., Rieke, G. J., Esterházy, D., Meredith, M. M., Pedicord, V. A., … Nussenzweig, M. C. (2016). Absence of MHC class II on cDCs results in microbial-dependent intestinal inflammation. *The Journal of Experimental Medicine*, *213*(4), 517–534. https://doi.org/10.1084/jem.20160062

Lötzer, K., Döpping, S., Connert, S., Gräbner, R., Spanbroek, R., Lemser, B., … Habenicht, A. J. R. (2010). Mouse Aorta Smooth Muscle Cells Differentiate Into Lymphoid Tissue Organizer-Like Cells on Combined Tumor Necrosis Factor Receptor-1/Lymphotoxin β-Receptor NF-κB Signaling. *Arteriosclerosis, Thrombosis, and Vascular Biology*, *30*(3), 395–402. https://doi.org/10.1161/ATVBAHA.109.191395

Luther, S. A., Lopez, T., Bai, W., Hanahan, D., & Cyster, J. G. (2000). BLC expression in pancreatic islets causes B cell recruitment and lymphotoxin-dependent lymphoid neogenesis. *Immunity*, *12*(5), 471–481.

Luther, Sanjiv A., Ansel, K. M., & Cyster, J. G. (2003). Overlapping roles of CXCL13, interleukin 7 receptor α, and CCR7 ligands in lymph node development. *The Journal of Experimental Medicine*, *197*(9), 1191–1198. https://doi.org/10.1084/jem.20021294

Luther, Sanjiv A., Bidgol, A., Hargreaves, D. C., Schmidt, A., Xu, Y., Paniyadi, J., … Cyster, J. G. (2002). Differing activities of homeostatic chemokines CCL19, CCL21, and CXCL12 in lymphocyte and dendritic cell recruitment and lymphoid neogenesis. *Journal of Immunology*, *169*(1), 424–433.

Luther, Sanjiv A., Tang, H. L., Hyman, P. L., Farr, A. G., & Cyster, J. G. (2000). Coexpression of the chemokines ELC and SLC by T zone stromal cells and deletion of the ELC gene in the plt/plt mouse. *Proceedings of the National Academy of Sciences*, *97*(23), 12694–12699. https://doi.org/10.1073/pnas.97.23.12694

Lutz, E. R., Wu, A. A., Bigelow, E., Sharma, R., Mo, G., Soares, K., … Zheng, L. (2014). Immunotherapy converts nonimmunogenic pancreatic tumors into immunogenic foci of immune regulation. *Cancer Immunology Research*, *2*(7), 616–631. https://doi.org/10.1158/2326-6066.CIR-14-0027

MacEwan, D. J. (2002). TNF receptor subtype signalling: Differences and cellular consequences. *Cellular Signalling*, *14*(6), 477–492. https://doi.org/10.1016/S0898-6568(01)00262-5

Madsen, P., Szymkowski, D., Bethea, J., Lambertsen, K., & Brambilla, R. (2014, June). *Oligodendroglial TNFR2 promotes remyelination in experimental autoimmune encephalomyelitis*. Presented at the 13th Annual OAK Meeting Danish Brain Research Laboratories Meeting. Retrieved from http://cfin.au.dk/oak-2014/oak-2014-program/

Maglione, P. J., Xu, J., & Chan, J. (2007). B Cells Moderate Inflammatory Progression and Enhance Bacterial Containment upon Pulmonary Challenge with Mycobacterium tuberculosis. *The Journal of Immunology*, *178*(11), 7222–7234. https://doi.org/10.4049/jimmunol.178.11.7222

Maguire, O., O'Loughlin, K., & Minderman, H. (2015). Simultaneous assessment of NF-κB/p65 phosphorylation and nuclear localization using imaging flow cytometry. *Journal of Immunological Methods*, *423*, 3–11. https://doi.org/10.1016/j.jim.2015.03.018

Mahmoud, S. M. A., Lee, A. H. S., Paish, E. C., Macmillan, R. D., Ellis, I. O., & Green, A. R. (2011). The prognostic significance of B lymphocytes in invasive carcinoma of the breast. *Breast Cancer Research and Treatment*, *132*(2), 545–553. https://doi.org/10.1007/s10549-011-1620-1

Makowski, D., Ben-Shachar, M. S., Patil, I., & Lüdecke, D. (2020). Methods and Algorithms for Correlation Analysis in R. *Journal of Open Source Software*, *5*(51), 2306. https://doi.org/10.21105/joss.02306

Maldonado, L., Teague, J. E., Morrow, M. P., Jotova, I., Wu, T. C., Wang, C., … Trimble, C. L. (2014). Intramuscular Therapeutic Vaccination Targeting HPV16 Induces T Cell Responses That Localize in Mucosal Lesions. *Science Translational Medicine*, *6*(221), 221ra13-221ra13. https://doi.org/10.1126/scitranslmed.3007323

Malý, P., Thall, A., Petryniak, B., Rogers, C. E., Smith, P. L., Marks, R. M., … Lowe, J. B. (1996). The alpha(1,3)fucosyltransferase Fuc-TVII controls leukocyte trafficking through an essential role in L-, E-, and P-selectin ligand biosynthesis. *Cell*, *86*(4), 643–653.

Mandic, M., Almunia, C., Vicel, S., Gillet, D., Janjic, B., Coval, K., … Zarour, H. M. (2003). The Alternative Open Reading Frame of LAGE-1 Gives Rise to Multiple Promiscuous HLA-DR-restricted Epitopes Recognized by T-helper 1-type Tumor-reactive CD4+ T Cells. *Cancer Research*, *63*(19), 6506–6515.

Manzo, A., Paoletti, S., Carulli, M., Blades, M. C., Barone, F., Yanni, G., … Pitzalis, C. (2005). Systematic microanatomical analysis of CXCL13 and CCL21 in situ production and progressive lymphoid organization in rheumatoid synovitis. *European Journal of Immunology*, *35*(5), 1347–1359. https://doi.org/10.1002/eji.200425830

Marinkovic, T., Garin, A., Yokota, Y., Fu, Y.-X., Ruddle, N. H., Furtado, G. C., & Lira, S. A. (2006). Interaction of mature CD3+ CD4+ T cells with dendritic cells triggers the development of tertiary lymphoid structures in the thyroid. *The Journal of Clinical Investigation*, *116*(10), 2622–2632. https://doi.org/10.1172/JCI28993

Maris, P., Blomme, A., Palacios, A. P., Costanza, B., Bellahcène, A., Bianchi, E., … Turtoi, A. (2015). Asporin Is a Fibroblast-Derived TGF-β1 Inhibitor and a Tumor Suppressor Associated with Good Prognosis in Breast Cancer. *PLoS Medicine*, *12*(9). https://doi.org/10.1371/journal.pmed.1001871

Martinet, L., Filleron, T., Guellec, S. L., Rochaix, P., Garrido, I., & Girard, J.-P. (2013). High endothelial venule blood vessels for tumor-infiltrating lymphocytes are associated with Lymphotoxin β–producing dendritic cells in human breast cancer. *The Journal of Immunology*, *191*(4), 2001–2008. https://doi.org/10.4049/jimmunol.1300872

Martinet, L., Garrido, I., Filleron, T., Le Guellec, S., Bellard, E., Fournie, J.-J., … Girard, J.-P. (2011). Human solid tumors contain high endothelial venules: Association with T- and B-lymphocyte infiltration and favorable prognosis in breast cancer. *Cancer Research*, *71*(17), 5678–5687. https://doi.org/10.1158/0008-5472.CAN-11-0431

Martinet, L., Le Guellec, S., Filleron, T., Lamant, L., Meyer, N., Rochaix, P., … Girard, J.-P. (2012). High endothelial venules (HEVs) in human melanoma lesions: Major

gateways for tumor-infiltrating lymphocytes. *Oncoimmunology*, *1*(6), 829–839. https://doi.org/10.4161/onci.20492

Mauldin, I. S., Sheybani, N. D., Young, S. J., Price, R. J., & Slingluff, C. L. (2020). Chapter Six—Deconvolution of the immunological contexture of mouse tumors with multiplexed immunohistochemistry. In L. Galluzzi & N.-P. Rudqvist (Eds.), *Methods in Enzymology* (pp. 81–93). Academic Press. https://doi.org/10.1016/bs.mie.2019.05.038

McDonald, K. G., McDonough, J. S., & Newberry, R. D. (2005). Adaptive immune responses are dispensable for isolated lymphoid follicle formation: Antigen-naive, lymphotoxin-sufficient B lymphocytes drive the formation of mature isolated lymphoid follicles. *The Journal of Immunology*, *174*(9), 5720–5728. https://doi.org/10.4049/jimmunol.174.9.5720

McDonald, L. T., Russell, D. L., Kelly, R. R., Xiong, Y., Motamarry, A., Patel, R. K., … LaRue, A. C. (2015). Hematopoietic stem cell-derived cancer-associated fibroblasts are novel contributors to the pro-tumorigenic microenvironment. *Neoplasia (New York, N.Y.)*, *17*(5), 434–448. https://doi.org/10.1016/j.neo.2015.04.004

Mead, B. P., Curley, C. T., Kim, N., Negron, K., Garrison, W. J., Song, J., … Price, R. J. (2019). Focused Ultrasound Preconditioning for Augmented Nanoparticle Penetration and Efficacy in the Central Nervous System. *Small*, *15*(49), 1903460. https://doi.org/10.1002/smll.201903460

Mebius, R. E. (2003). Organogenesis of lymphoid tissues. *Nature Reviews Immunology*, *3*(4), 292–303. https://doi.org/10.1038/nri1054

Medvedev, A. E., Espevik, T., Ranges, G., & Sundan, A. (1996). Distinct roles of the two tumor necrosis factor (TNF) receptors in modulating TNF and lymphotoxin alpha effects. *The Journal of Biological Chemistry*, *271*(16), 9778–9784. https://doi.org/10.1074/jbc.271.16.9778

Meshcheryakova, A., Tamandl, D., Bajna, E., Stift, J., Mittlboeck, M., Svoboda, M., … Mechtcheriakova, D. (2014). B cells and ectopic follicular structures: Novel players in anti-tumor programming with prognostic power for patients with metastatic colorectal cancer. *PloS One*, *9*(6), e99008. https://doi.org/10.1371/journal.pone.0099008

Messina, J. L., Fenstermacher, D. A., Eschrich, S., Qu, X., Berglund, A. E., Lloyd, M. C., … Mulé, J. J. (2012). 12-Chemokine gene signature identifies lymph node-like structures in melanoma: Potential for patient selection for immunotherapy? *Scientific Reports*, *2*, 765. https://doi.org/10.1038/srep00765

Mikucki, M. E., Fisher, D. T., Matsuzaki, J., Skitzki, J. J., Gaulin, N. B., Muhitch, J. B., … Evans, S. S. (2015). Non-redundant requirement for CXCR3 signaling during tumoricidal T-cell trafficking across tumour vascular checkpoints. *Nature Communications*, *6*, 7458. https://doi.org/10.1038/ncomms8458.

Miller, B. C., Sen, D. R., Al Abosy, R., Bi, K., Virkud, Y. V., LaFleur, M. W., … Haining, W. N. (2019). Subsets of exhausted CD8+ T cells differentially mediate tumor

control and respond to checkpoint blockade. *Nature Immunology*, *20*(3), 326–336. https://doi.org/10.1038/s41590-019-0312-6

Monteran, L., & Erez, N. (2019). The Dark Side of Fibroblasts: Cancer-Associated Fibroblasts as Mediators of Immunosuppression in the Tumor Microenvironment. *Frontiers in Immunology*, *10*. https://doi.org/10.3389/fimmu.2019.01835

Moon, E. K., Carpenito, C., Sun, J., Wang, L.-C. S., Kapoor, V., Predina, J., … Albelda, S. M. (2011). Expression of a Functional CCR2 Receptor Enhances Tumor Localization and Tumor Eradication by Retargeted Human T cells Expressing a Mesothelin-Specific Chimeric Antibody Receptor. *Clinical Cancer Research*, *17*(14), 4719. https://doi.org/10.1158/1078-0432.CCR-11-0351

Mora, J. R., Bono, M. R., Manjunath, N., Weninger, W., Cavanagh, L. L., Rosemblatt, M., & von Andrian, U. H. (2003). Selective imprinting of gut-homing T cells by Peyer's patch dendritic cells. *Nature*, *424*(6944), 88–93.

Mora, J. R., Cheng, G., Picarella, D., Briskin, M., Buchanan, N., & von Andrian, U. H. (2005). Reciprocal and dynamic control of CD8 T cell homing by dendritic cells from skin- and gut-associated lymphoid tissues. *Journal of Experimental Medicine*, *201*(2), 303–316.

Motallebzadeh, R., Rehakova, S., Conlon, T. M., Win, T. S., Callaghan, C. J., Goddard, M., … Pettigrew, G. J. (2012). Blocking lymphotoxin signaling abrogates the development of ectopic lymphoid tissue within cardiac allografts and inhibits

effector antibody responses. *FASEB Journal*, *26*(1), 51–62. https://doi.org/10.1096/fj.11-186973

Moussion, C., & Girard, J.-P. (2011). Dendritic cells control lymphocyte entry to lymph nodes through high endothelial venules. *Nature*, *479*(7374), 542–546. https://doi.org/10.1038/nature10540

Moyron-Quiroz, J. E., Rangel-Moreno, J., Hartson, L., Kusser, K., Tighe, M. P., Klonowski, K. D., … Randall, T. D. (2006). Persistence and Responsiveness of Immunologic Memory in the Absence of Secondary Lymphoid Organs. *Immunity*, *25*, 643–654.

Moyron-Quiroz, J. E., Rangel-Moreno, J., Kusser, K., Hartson, L., Sprague, F., Goodrich, S., … Randall, T. D. (2004). Role of inducible bronchus associated lymphoid tissue (iBALT) in respiratory immunity. *Nature Medicine*, *10*, 927–934.

Mueller, C. G., Nayar, S., Campos, J., & Barone, F. (2018). Molecular and Cellular Requirements for the Assembly of Tertiary Lymphoid Structures. *Advances in Experimental Medicine and Biology*, *1060*, 55–72. https://doi.org/10.1007/978-3-319-78127-3_4

Muniz, L. R., Pacer, M. E., Lira, S. A., & Furtado, G. C. (2011). A Critical Role for Dendritic Cells in the Formation of Lymphatic Vessels within Tertiary Lymphoid Structures. *The Journal of Immunology*, *187*(2), 828–834. https://doi.org/10.4049/jimmunol.1004233

Munoz-Erazo, L., Rhodes, J. L., Marion, V. C., & Kemp, R. A. (2020). Tertiary lymphoid structures in cancer – considerations for patient prognosis. *Cellular & Molecular Immunology*, *17*(6), 570–575. https://doi.org/10.1038/s41423-020-0457-0

Musha, H., Ohtani, H., Mizoi, T., Kinouchi, M., Nakayama, T., Shiiba, K., … Sasaki, I. (2005). Selective infiltration of CCR5(+)CXCR3(+) T lymphocytes in human colorectal carcinoma. *International Journal of Cancer*, *116*(6), 949–956.

Nacopoulou, L., Azaris, P., Papacharalampous, N., & Davaris, P. (1981). Prognostic significance of histologic host response in cancer of the large bowel. *Cancer*, *47*(5), 930–936. https://doi.org/10.1002/1097-0142(19810301)47:5<930::AID-CNCR2820470519>3.0.CO;2-1

Naito, Y., Saito, K., Shiiba, K., Ohuchi, A., Saigenji, K., Nagura, H., & Ohtani, H. (1998). CD8+ T cells infiltrated within cancer cell nests as a prognostic factor in human colorectal cancer. *Cancer Research*, *58*, 3491–3494.

Nakano, H., & Gunn, M. D. (2001). Gene duplications at the chemokine locus on mouse chromosome 4: Multiple strain-specific haplotypes and the deletion of secondary lymphoid-organ chemokine and EBI-1 ligand chemokine genes in the plt mutation. *Journal of Immunology*, *166*(1), 361–369.

Nasr, I. W., Reel, M., Oberbarnscheidt, M. H., Mounzer, R. H., Baddoura, F. K., Ruddle, N. H., & Lakkis, F. G. (2007). Tertiary Lymphoid Tissues Generate Effector and Memory T cells That Lead to Allograft Rejection. *American Journal of Transplantation*, *7*, 1071–1079.

Nayar, S., Campos, J., Smith, C. G., Iannizzotto, V., Gardner, D. H., Mourcin, F., … Barone, F. (2019). Immunofibroblasts are pivotal drivers of tertiary lymphoid structure formation and local pathology. *Proceedings of the National Academy of Sciences*, *116*(27), 13490–13497. https://doi.org/10.1073/pnas.1905301116

Neyt, K., Perros, F., GeurtsvanKessel, C. H., Hammad, H., & Lambrecht, B. N. (2012). Tertiary lymphoid organs in infection and autoimmunity. *Trends in Immunology*, *33*(6), 297–305. https://doi.org/10.1016/j.it.2012.04.006

Ngo, V. N., Korner, H., Gunn, M. D., Schmidt, K. N., Riminton, D. S., Cooper, M. D., … Cyster, J. G. (1999). Lymphotoxin alpha/beta and tumor necrosis factor are required for stromal cell expression of homing chemokines in B and T cell areas of the spleen. *Journal of Experimental Medicine*, *189*(2), 403–412.

Nguyen, E. V., Pereira, B. A., Lawrence, M. G., Ma, X., Rebello, R. J., Chan, H., … Daly, R. J. (2019). Proteomic Profiling of Human Prostate Cancer-associated Fibroblasts (CAF) Reveals LOXL2-dependent Regulation of the Tumor Microenvironment. *Molecular & Cellular Proteomics: MCP*, *18*(7), 1410–1427. https://doi.org/10.1074/mcp.RA119.001496

Nielsen, J. S., Sahota, R. A., Milne, K., Kost, S. E., Nesslinger, N. J., Watson, P. H., & Nelson, B. H. (2012). *CD20+ tumor-infiltrating lymphocytes have an atypical CD27- memory phenotype and together with CD8+ T cells promote favorable prognosis in ovarian cancer*. *18*(12), 3281–3292. https://doi.org/10.1158/1078-0432.CCR-12-0234

Nishizuka, Y., Nakakuki, K., & Usui, M. (1965). Enhancing Effect of Thymectomy on Hepatotumorigenesis in Swiss Mice following Neonatal Injection of 20-Methylcholanthrene. *Nature*, *205*(4977), 1236–1238. https://doi.org/10.1038/2051236b0

Norris, P. S., & Ware, C. F. (2013). The LTβR Signaling Pathway. In *Madame Curie Bioscience Database [Internet]*. Landes Bioscience. Retrieved from https://www.ncbi.nlm.nih.gov/books/NBK6515/

Ohl, L., Henning, G., Krautwald, S., Lipp, M., Hardtke, S., Bernhardt, G., … Förster, R. (2003). Cooperating mechanisms of CXCR5 and CCR7 in development and organization of secondary lymphoid organs. *The Journal of Experimental Medicine*, *197*(9), 1199–1204. https://doi.org/10.1084/jem.20030169

Olkhanud, P. B., Damdinsuren, B., Bodogai, M., Gress, R. E., Sen, R., Wejksza, K., … Biragyn, A. (2011). Tumor-evoked regulatory B cells promote breast cancer metastasis by converting resting $CD4^+$ T cells to T-regulatory cells. *Cancer Research*, *71*(10), 3505–3515. https://doi.org/10.1158/0008-5472.CAN-10-4316

Onder, L., & Ludewig, B. (2018). A Fresh View on Lymph Node Organogenesis. *Trends in Immunology*, *39*(10), 775–787. https://doi.org/10.1016/j.it.2018.08.003

Onder, L., Mörbe, U., Pikor, N., Novkovic, M., Cheng, H.-W., Hehlgans, T., … Ludewig, B. (2017). Lymphatic Endothelial Cells Control Initiation of Lymph Node Organogenesis. *Immunity*, *47*(1), 80-92.e4. https://doi.org/10.1016/j.immuni.2017.05.008

Orozco, A. S., Zhou, X., & Filler, S. G. (2000). Mechanisms of the Proinflammatory Response of Endothelial Cells to Candida albicans Infection. *Infection and Immunity*, *68*(3), 1134–1141.

Outzen, H. C., Custer, R. P., Eaton, G. J., & Prehn, R. T. (1975). Spontaneous and induced tumor incidence in germfree "nude" mice. *Journal of the Reticuloendothelial Society*, *17*(1), 1–9.

Özdemir, B. C., Pentcheva-Hoang, T., Carstens, J. L., Zheng, X., Wu, C.-C., Simpson, T. R., … Kalluri, R. (2014). Depletion of carcinoma-associated fibroblasts and fibrosis induces immunosuppression and accelerates pancreas cancer with reduced survival. *Cancer Cell*, *25*(6), 719–734. https://doi.org/10.1016/j.ccr.2014.04.005

Pablos, J., Santiago, B., Tsay, D., Singer, M., Palao, G., Galindo, M., & Rosen, S. (2005). A HEV-restricted sulfotransferase is expressed in rheumatoid arthritis synovium and is induced by lymphotoxin-α/β and TNF-α in cultured endothelial cells. *BMC Immunology*, *6*(1), 6. https://doi.org/10.1186/1471-2172-6-6

Pagès, F., Kirilovsky, A., Mlecnik, B., Asslaber, M., Tosolini, M., Bindea, G., … Galon, J. (2009). In situ cytotoxic and memory T cells predict outcome in patients with early-stage colorectal cancer. *Journal of Clinical Oncology*, *27*(35), 5944–5951. https://doi.org/10.1200/JCO.2008.19.6147

Palma, L., Di Lorenzo, N., & Guidetti, B. (1978). Lymphocytic infiltrates in primary glioblastomas and recidivous gliomas. Incidence, fate, and relevance to prognosis in 228 operated cases. *Journal of Neurosurgery*, *49*(6), 854–861.

Pardoll, D. M. (2012). The blockade of immune checkpoints in cancer immunotherapy. *Nature Reviews Cancer*, *12*(4), 252–264. https://doi.org/10.1038/nrc3239

Pasparakis, M., Alexopoulou, L., Episkopou, V., & Kollias, G. (1996). Immune and inflammatory responses in TNF alpha-deficient mice: A critical requirement for TNF alpha in the formation of primary B cell follicles, follicular dendritic cell networks and germinal centers, and in the maturation of the humoral immune response. *The Journal of Experimental Medicine*, *184*(4), 1397–1411. https://doi.org/10.1084/jem.184.4.1397

Peduto, L., Dulauroy, S., Lochner, M., Späth, G. F., Morales, M. A., Cumano, A., & Eberl, G. (2009). Inflammation recapitulates the ontogeny of lymphoid stromal cells. *Journal of Immunology*, *182*(9), 5789–5799. https://doi.org/10.4049/jimmunol.0803974

Peng, B., Ming, Y., & Yang, C. (2018). Regulatory B cells: The cutting edge of immune tolerance in kidney transplantation. *Cell Death & Disease*, *9*(2), 1–13. https://doi.org/10.1038/s41419-017-0152-y

Peng, W., Ye, Y., Rabinovich, B. A., Liu, C., Lou, Y., Zhang, M., … Hwu, P. (2010). Transduction of Tumor-Specific T Cells with CXCR2 Chemokine Receptor Improves Migration to Tumor and Antitumor Immune Responses. *Clinical Cancer Research*, *16*(22), 5458. https://doi.org/10.1158/1078-0432.CCR-10-0712

Penn, I., & Starzl, T. E. (1972). Malignant Tumors Arising De Novo in Immunosuppressed Organ Transplant Recipients. *Transplantation*, *14*(4), 407–417.

Perez-Ruiz, E., Minute, L., Otano, I., Alvarez, M., Ochoa, M. C., Belsue, V., … Melero, I. (2019). Prophylactic TNF blockade uncouples efficacy and toxicity in dual CTLA-4 and PD-1 immunotherapy. *Nature*, *569*(7756), 428–432. https://doi.org/10.1038/s41586-019-1162-y

Peschon, J. J., Torrance, D. S., Stocking, K. L., Glaccum, M. B., Otten, C., Willis, C. R., … Mohler, K. M. (1998). TNF Receptor-Deficient Mice Reveal Divergent Roles for p55 and p75 in Several Models of Inflammation. *The Journal of Immunology*, *160*(2), 943–952.

Peske, J. D., Thompson, E. D., Gemta, L., Baylis, R. A., Fu, Y.-X., & Engelhard, V. H. (2015). Effector lymphocyte-induced lymph node-like vasculature enables naive T-cell entry into tumours and enhanced anti-tumour immunity. *Nature Communications*, *6*, 7114. https://doi.org/10.1038/ncomms8114

Peters, A., Burkett, P. R., Sobel, R. A., Buckley, C. D., Watson, S. P., Bettelli, E., & Kuchroo, V. K. (2015). Podoplanin negatively regulates CD4+ effector T cell responses. *Journal of Clinical Investigation*, *125*(1), 129–140. https://doi.org/10.1172/JCI74685

Peters, A., Pitcher, L. A., Sullivan, J. M., Mitsdoerffer, M., Acton, S. E., Franz, B., … Kuchroo, V. K. (2011). Th17 cells induce ectopic lymphoid follicles in central nervous system tissue inflammation. *Immunity*, *35*(6), 986–996. https://doi.org/10.1016/j.immuni.2011.10.015

Petitprez, F., Fossati, N., Vano, Y., Freschi, M., Becht, E., Lucianò, R., … Bellone, M. (2019). PD-L1 Expression and CD8+ T-cell Infiltrate are Associated with Clinical Progression in Patients with Node-positive Prostate Cancer. *European Urology Focus*, *5*(2), 192–196. https://doi.org/10.1016/j.euf.2017.05.013

Petitprez, F., Reyniès, A. de, Keung, E. Z., Chen, T. W.-W., Sun, C.-M., Calderaro, J., … Fridman, W. H. (2020). B cells are associated with survival and immunotherapy response in sarcoma. *Nature*, *577*(7791), 556–560. https://doi.org/10.1038/s41586-019-1906-8

Pikor, N. B., Astarita, J. L., Summers-Deluca, L., Galicia, G., Qu, J., Ward, L. A., … Gommerman, J. L. (2015). Integration of Th17- and lymphotoxin-derived signals initiates meningeal-resident stromal cell remodeling to propagate neuroinflammation. *Immunity*, *43*(6), 1160–1173. https://doi.org/10.1016/j.immuni.2015.11.010

Plesca, M., Bordea, C., El Houcheimi, B., Ichim, E., & Blidaru, A. (2016). Evolution of radical mastectomy for breast cancer. *Journal of Medicine and Life*, *9*(2), 183–186.

Posch, F., Silina, K., Leibl, S., Mündlein, A., Moch, H., Siebenhüner, A., … Winder, T. (2018). Maturation of tertiary lymphoid structures and recurrence of stage II and III colorectal cancer. *Oncoimmunology*, *7*(2), e1378844. https://doi.org/10.1080/2162402X.2017.1378844

Prabhakaran, S., Rizk, V. T., Ma, Z., Cheng, C.-H., Berglund, A. E., Coppola, D., … Soliman, H. H. (2017). *Evaluation of invasive breast cancer samples using a 12-*

chemokine gene expression score: Correlation with clinical outcomes. *19*(1), 71. https://doi.org/10.1186/s13058-017-0864-z

Priatel, J. J., Chui, D., Hiraoka, N., Simmons, C. J. T., Richardson, K. B., Page, D. M., … Marth, J. D. (2000). The ST3Gal-I Sialyltransferase Controls CD8+ T Lymphocyte Homeostasis by Modulating O-Glycan Biosynthesis. *Immunity*, *12*(3), 273–283. https://doi.org/10.1016/S1074-7613(00)80180-6

Pula, B., Witkiewicz, W., Dziegiel, P., & Podhorska-Okolow, M. (2013). Significance of podoplanin expression in cancer-associated fibroblasts: A comprehensive review. *International Journal of Oncology*, *42*(6), 1849–1857. https://doi.org/10.3892/ijo.2013.1887

Puram, S. V., Tirosh, I., Parikh, A. S., Patel, A. P., Yizhak, K., Gillespie, S., … Bernstein, B. E. (2017). Single-Cell Transcriptomic Analysis of Primary and Metastatic Tumor Ecosystems in Head and Neck Cancer. *Cell*, *171*(7), 1611-1624.e24. https://doi.org/10.1016/j.cell.2017.10.044

Quatromoni, J. G., Morris, L. F., Donahue, T. R., Wang, Y., McBride, W., Chatila, T., & Economou, J. S. (2011). T cell receptor transgenic lymphocytes infiltrating murine tumors are not induced to express foxp3. *Journal of Hematology & Oncology*, *4*, 48. https://doi.org/10.1186/1756-8722-4-48

Quezada, S. A., Peggs, K. S., Simpson, T. R., Shen, Y., Littman, D. R., & Allison, J. P. (2008). Limited tumor infiltration by activated T effector cells restricts the therapeutic activity of regulatory T cell depletion against established melanoma.

The Journal of Experimental Medicine, *205*(9), 2125–2138. https://doi.org/10.1084/jem.20080099

Randall, T. D., Carragher, D. M., & Rangel-Moreno, J. (2008). Development of secondary lymphoid organs. *Annual Review of Immunology*, *26*, 627–650. https://doi.org/10.1146/annurev.immunol.26.021607.090257

Rangel-Moreno, J., Carragher, D. M., Garcia-Hernandez, M. de la L., Hwang, J. Y., Kusser, K., Hartson, L., … Randall, T. D. (2011). The development of inducible bronchus-associated lymphoid tissue depends on IL-17. *Nature Immunology*, *12*(7), 639–646. https://doi.org/10.1038/ni.2053

Rangel-Moreno, J., Moyron-Quiroz, J. E., Hartson, L., Kusser, K., & Randall, T. D. (2007). Pulmonary expression of CXC chemokine ligand 13, CC chemokine ligand 19, and CC chemokine ligand 21 is essential for local immunity to influenza. *Proceedings of the National Academy of Sciences*, *104*(25), 10577–10582. https://doi.org/10.1073/pnas.0700591104

Reilley, M. J., Morrow, B., Ager, C. R., Liu, A., Hong, D. S., & Curran, M. A. (2019). TLR9 activation cooperates with T cell checkpoint blockade to regress poorly immunogenic melanoma. *Journal for Immunotherapy of Cancer*, *7*(1), 323. https://doi.org/10.1186/s40425-019-0811-x

Remark, R., Alifano, M., Cremer, I., Lupo, A., Dieu-Nosjean, M.-C., Riquet, M., … Damotte, D. (2013). *Characteristics and Clinical Impacts of the Immune Environments in Colorectal and Renal Cell Carcinoma Lung Metastases: Influence*

of Tumor Origin. *19*(15), 4079–4091. https://doi.org/10.1158/1078-0432.CCR-12-3847

Remark, R., Lupo, A., Alifano, M., Biton, J., Ouakrim, H., Stefani, A., … Damotte, D. (2016). Immune contexture and histological response after neoadjuvant chemotherapy predict clinical outcome of lung cancer patients. *Oncoimmunology*, *5*(12), e1255394. https://doi.org/10.1080/2162402X.2016.1255394

Rhim, A. D., Oberstein, P. E., Thomas, D. H., Mirek, E. T., Palermo, C. F., Sastra, S. A., … Stanger, B. Z. (2014). Stromal elements act to restrain, rather than support, pancreatic ductal adenocarcinoma. *Cancer Cell*, *25*(6), 735–747. https://doi.org/10.1016/j.ccr.2014.04.021

Rilke, F., Colnaghi, M. I., Cascinelli, N., Andreola, S., Baldini, M. T., Bufalino, R., … Testori, A. (1991). Prognostic significance of HER-2/neu expression in breast cancer and its relationship to other prognostic factors. *International Journal of Cancer*, *49*(1), 44–49. https://doi.org/10.1002/ijc.2910490109

Rodriguez, A.B., Peske, J. D., & Engelhard, V. H. (2018). Identification and characterization of tertiary lymphoid structures in murine melanoma. *Methods in Molecular Biology*, *1845*, 241–257.

Rodriguez, Anthony B., & Engelhard, V. H. (2020). Insights into Tumor-Associated Tertiary Lymphoid Structures: Novel Targets for Antitumor Immunity and Cancer Immunotherapy. *Cancer Immunology Research*, *8*(11), 1338–1345. https://doi.org/10.1158/2326-6066.CIR-20-0432

Rosen, S. D. (2004). Ligands for L-selectin: Homing, inflammation, and beyond. *Annual Review of Immunology*, *22*, 129–156.

Ruddle, N. H. (2014). Lymphotoxin and TNF: How it all began- A tribute to the travelers. *Cytokine & Growth Factor Reviews*, *25*(2), 83–89. https://doi.org/10.1016/j.cytogfr.2014.02.001

Ruddle, N. H., & Akirav, E. M. (2009). Secondary Lymphoid Organs: Responding to Genetic and Environmental Cues in Ontogeny and the Immune Response. *The Journal of Immunology*, *183*(4), 2205–2212. https://doi.org/10.4049/jimmunol.0804324

Rygaard, J., & Povlsen, C. O. (1974). The mouse mutant nude does not develop spontaneous tumours. An argument against immunological surveillance. *Acta Pathologica Et Microbiologica Scandinavica. Section B: Microbiology and Immunology*, *82*(1), 99–106.

Rynne-Vidal, A., Jiménez-Heffernan, J. A., Fernández-Chacón, C., López-Cabrera, M., & Sandoval, P. (2015). The Mesothelial Origin of Carcinoma Associated-Fibroblasts in Peritoneal Metastasis. *Cancers*, *7*(4), 1994–2011. https://doi.org/10.3390/cancers7040872

Sacca, R., Cuff, C. A., Lesslauer, W., & Ruddle, N. H. (1998). Differential Activities of Secreted Lymphotoxin-α3 and Membrane Lymphotoxin-α1β2 in Lymphotoxin-Induced Inflammation: Critical Role of TNF Receptor 1 Signaling. *Journal of Immunology*, *160*(1), 485–491.

Sakai, Y., Hoshino, H., Kitazawa, R., & Kobayashi, M. (2014). High endothelial venule-like vessels and lymphocyte recruitment in testicular seminoma. *Andrology*, *2*(2), 282–289. https://doi.org/10.1111/j.2047-2927.2014.00192.x

Sanford, B. H., Kohn, H. I., Daly, J. J., & Soo, S. F. (1973). Long-term spontaneous tumor incidence in neonatally thymectomized mice. *Journal of Immunology (Baltimore, Md.: 1950)*, *110*(5), 1437–1439.

Sasaki, K., Zhu, X., Vasquez, C., Nishimura, F., Dusak, J. E., Huang, J., … Okada, H. (2007). Preferential expression of very late antigen-4 on type 1 CTL cells plays a critical role in trafficking into central nervous system tumors. *Cancer Research*, *67*(13), 6451–6458. https://doi.org/10.1158/0008-5472.CAN-06-3280

Sato, Y., Mii, A., Hamazaki, Y., Fujita, H., Nakata, H., Masuda, K., … Yanagita, M. (2016). Heterogeneous fibroblasts underlie age-dependent tertiary lymphoid tissues in the kidney. *JCI Insight*, *1*(11), e87680. https://doi.org/10.1172/jci.insight.87680

Sautès-Fridman, C., Petitprez, F., Calderaro, J., & Fridman, W. H. (2019). Tertiary lymphoid structures in the era of cancer immunotherapy. *Nature Reviews Cancer*, *19*(6), 307–325. https://doi.org/10.1038/s41568-019-0144-6

Sawa, S., Cherrier, M., Lochner, M., Satoh-Takayama, N., Fehling, H. J., Langa, F., … Eberl, G. (2010). Lineage Relationship Analysis of RORγt+ Innate Lymphoid Cells. *Science*, *330*(6004), 665–669. https://doi.org/10.1126/science.1194597

Schmidt, M., Böhm, D., Törne, C. von, Steiner, E., Puhl, A., Pilch, H., … Gehrmann, M. (2008). The Humoral Immune System Has a Key Prognostic Impact in Node-

Negative Breast Cancer. *Cancer Research*, *68*(13), 5405–5413. https://doi.org/10.1158/0008-5472.CAN-07-5206

Schmidt, M., Hellwig, B., Hammad, S., Othman, A., Lohr, M., Chen, Z., … Hengstler, J. G. (2012). A comprehensive analysis of human gene expression profiles identifies stromal immunoglobulin κ C as a compatible prognostic marker in human solid tumors. *Clinical Cancer Research: An Official Journal of the American Association for Cancer Research*, *18*(9), 2695–2703. https://doi.org/10.1158/1078-0432.CCR-11-2210

Schrama, D., thor Straten, P., Fischer, W. H., McLellan, A. D., Bröcker, E.-B., Reisfeld, R. A., & Becker, J. C. (2001). Targeting of Lymphotoxin-α to the tumor elicits an efficient immune response associated with induction of peripheral lymphoid-like tissue. *Immunity*, *14*(2), 111–121. https://doi.org/10.1016/S1074-7613(01)00094-2

Schrama, D., Voigt, H., Eggert, A. O., Xiang, R., Zhou, H., Schumacher, T. N. M., … Becker, J. C. (2008). Immunological tumor destruction in a murine melanoma model by targeted LTalpha independent of secondary lymphoid tissue. *Cancer Immunology, Immunotherapy*, *57*(1), 85–95. https://doi.org/10.1007/s00262-007-0352-x

Schreiber, R. D., Old, L. J., & Smyth, M. J. (2011). Cancer immunoediting: Integrating immunity's roles in cancer suppression and promotion. *Science (New York, N.Y.)*, *331*(6024), 1565–1570. https://doi.org/10.1126/science.1203486

Schumacher, K., Haensch, W., Roefzaad, C., & Schlag, P. M. (2001). Prognostic significance of activated CD8(+) T cell infiltrations within esophageal carcinomas. *Cancer Research*, *61*(10), 3932–3936.

Schweiger, T., Berghoff, A. S., Glogner, C., Glueck, O., Rajky, O., Traxler, D., … Hoetzenecker, K. (2016). Tumor-infiltrating lymphocyte subsets and tertiary lymphoid structures in pulmonary metastases from colorectal cancer. *Clinical & Experimental Metastasis*, *33*(7), 727–739. https://doi.org/10.1007/s10585-016-9813-y

Scott, D. W., Chan, F. C., Hong, F., Rogic, S., Tan, K. L., Meissner, B., … Gascoyne, R. D. (2013). Gene expression-based model using formalin-fixed paraffin-embedded biopsies predicts overall survival in advanced-stage classical Hodgkin lymphoma. *Journal of Clinical Oncology: Official Journal of the American Society of Clinical Oncology*, *31*(6), 692–700. https://doi.org/10.1200/JCO.2012.43.4589

Selitsky, S. R., Mose, L. E., Smith, C. C., Chai, S., Hoadley, K. A., Dittmer, D. P., … Vincent, B. G. (2019). Prognostic value of B cells in cutaneous melanoma. *Genome Medicine*, *11*(1), 36. https://doi.org/10.1186/s13073-019-0647-5

Shah, S., Divekar, A. A., Hilchey, S. P., Cho, H. M., Newman, C. L., Shin, S. U., … Rosenblatt, J. D. (2005). Increased rejection of primary tumors in mice lacking B cells: Inhibition of anti-tumor CTL and TH1 cytokine responses by B cells. *International Journal of Cancer*, *117*(4), 574–586.

Shankaran, V., Ikeda, H., Bruce, A. T., White, J. M., Swanson, P. E., Old, L. J., & Schreiber, R. D. (2001). IFNgamma and lymphocytes prevent primary tumour development and shape tumour immunogenicity. *Nature*, *410*(6832), 1107–1111.

Shi, J.-Y., Gao, Q., Wang, Z.-C., Zhou, J., Wang, X.-Y., Min, Z.-H., … Fan, J. (2013). Margin-Infiltrating CD20+ B Cells Display an Atypical Memory Phenotype and Correlate with Favorable Prognosis in Hepatocellular Carcinoma. *Clinical Cancer Research*, *19*(21), 5994–6005. https://doi.org/10.1158/1078-0432.CCR-12-3497

Shinkai, Y., Rathbun, 0Gary, Lam, K.-P., Oltz, E. M., Stewart, V., Mendelsohn, M., … Alt, F. W. (1992). RAG-2-deficient mice lack mature lymphocytes owing to inability to initiate V(D)J rearrangement. *Cell*, *68*(5), 855–867. https://doi.org/10.1016/0092-8674(92)90029-C

Sigmundsdottir, H., & Butcher, E. C. (2008). Environmental cues, dendritic cells and the programming of tissue-selective lymphocyte trafficking. *Nature Immunology*, *9*(9), 981–987.

Siliņa, K., Soltermann, A., Attar, F. M., Casanova, R., Uckeley, Z. M., Thut, H., … van den Broek, M. (2018). Germinal Centers Determine the Prognostic Relevance of Tertiary Lymphoid Structures and Are Impaired by Corticosteroids in Lung Squamous Cell Carcinoma. *Cancer Research*, *78*(5), 1308–1320. https://doi.org/10.1158/0008-5472.CAN-17-1987

Simsa, P., Teillaud, J.-L., Stott, D. I., Tóth, J., & Kotlan, B. (2005). Tumor-infiltrating B cell immunoglobulin variable region gene usage in invasive ductal breast

carcinoma. *Pathology & Oncology Research*, *11*(2), 92–97. https://doi.org/10.1007/BF02893374

Simson, L., Ellyard, J. I., Dent, L. A., Matthaei, K. I., Rothenberg, M. E., Foster, P. S., … Parish, C. R. (2007). Regulation of Carcinogenesis by IL-5 and CCL11: A Potential Role for Eosinophils in Tumor Immune Surveillance. *The Journal of Immunology*, *178*(7), 4222–4229. https://doi.org/10.4049/jimmunol.178.7.4222

Smith, P. L., Gersten, K. M., Petryniak, B., Kelly, R. J., Rogers, C., Natsuka, Y., … Lowe, J. B. (1996). Expression of the α(1,3)Fucosyltransferase Fuc-TVII in Lymphoid Aggregate High Endothelial Venules Correlates with Expression of L-Selectin Ligands (*). *Journal of Biological Chemistry*, *271*(14), 8250–8259. https://doi.org/10.1074/jbc.271.14.8250

Smyth, M. J., Crowe, N. Y., & Godfrey, D. I. (2001). NK cells and NKT cells collaborate in host protection from methylcholanthrene-induced fibrosarcoma. *International Immunology*, *13*(4), 459–463.

Smyth, M. J., Taniguchi, M., & Street, S. E. (2000). The anti-tumor activity of IL-12: Mechanisms of innate immunity that are model and dose dependent. *Journal of Immunology (Baltimore, Md.: 1950)*, *165*(5), 2665–2670. https://doi.org/10.4049/jimmunol.165.5.2665

Smyth, M. J., Thia, K. Y., Street, S. E., Cretney, E., Trapani, J. A., Taniguchi, M., … Godfrey, D. I. (2000). Differential tumor surveillance by natural killer (NK) and

NKT cells. *The Journal of Experimental Medicine*, *191*(4), 661–668. https://doi.org/10.1084/jem.191.4.661

Smyth, M. J., Thia, K. Y., Street, S. E., MacGregor, D., Godfrey, D. I., & Trapani, J. A. (2000). Perforin-mediated cytotoxicity is critical for surveillance of spontaneous lymphoma. *Journal of Experimental Medicine*, *192*(5), 755–760.

Song, I. H., Heo, S.-H., Bang, W. S., Park, H. S., Park, I. A., Kim, Y.-A., … Lee, H. J. (2017). *Predictive Value of Tertiary Lymphoid Structures Assessed by High Endothelial Venule Counts in the Neoadjuvant Setting of Triple-Negative Breast Cancer*. *49*(2), 399–407. https://doi.org/10.4143/crt.2016.215

Sperandio, M., Pickard, J., Unnikrishnan, S., Acton, S. T., & Ley, K. (2006). Analysis of Leukocyte Rolling In Vivo and In Vitro. In *Glycomics*: *Vol. 416*. *Methods in Enzymology* (pp. 346–371). Academic Press. https://doi.org/10.1016/S0076-6879(06)16023-1

Srinivas, S., Watanabe, T., Lin, C. S., William, C. M., Tanabe, Y., Jessell, T. M., & Costantini, F. (2001). Cre reporter strains produced by targeted insertion of EYFP and ECFP into the ROSA26 locus. *BMC Developmental Biology*, *1*, 4.

Stark, F. C., Weeratna, R. D., Deschatelets, L., Gurnani, K., Dudani, R., McCluskie, M. J., & Krishnan, L. (2017). An Archaeosome-Adjuvanted Vaccine and Checkpoint Inhibitor Therapy Combination Significantly Enhances Protection from Murine Melanoma. *Vaccines*, *5*(4), 38. https://doi.org/10.3390/vaccines5040038

Stetson, D. B., Mohrs, M., Reinhardt, R. L., Baron, J. L., Wang, Z.-E., Gapin, L., … Locksley, R. M. (2003). Constitutive cytokine mRNAs mark natural killer (NK) and NK T cells poised for rapid effector function. *The Journal of Experimental Medicine*, *198*(7), 1069–1076. https://doi.org/10.1084/jem.20030630

Stowman, A. M., Hickman, A. W., Mauldin, I. S., Mahmutovic, A., Gru, A. A., & Slingluff, C. L. (2018). Lymphoid aggregates in desmoplastic melanoma have features of tertiary lymphoid structures. *Melanoma Research*, *28*(3), 237–245. https://doi.org/10.1097/CMR.0000000000000439

Stranford, S., & Ruddle, N. H. (2012). Follicular dendritic cells, conduits, lymphatic vessels, and high endothelial venules in tertiary lymphoid organs: Parallels with lymph node stroma. *Frontiers in Immunology*, *3*, 350. https://doi.org/10.3389/fimmu.2012.00350

Street, S. E., Cretney, E., & Smyth, M. J. (2001). Perforin and interferon-gamma activities independently control tumor initiation, growth, and metastasis. *Blood*, *97*(1), 192–197.

Strong, A. L., Pei, D. T., Hurst, C. G., Gimble, J. M., Burow, M. E., & Bunnell, B. A. (2017). Obesity Enhances the Conversion of Adipose-Derived Stromal/Stem Cells into Carcinoma-Associated Fibroblast Leading to Cancer Cell Proliferation and Progression to an Invasive Phenotype. *Stem Cells International*, *2017*, 9216502. https://doi.org/10.1155/2017/9216502

Stutman, O. (1974). Tumor development after 3-methylcholanthrene in immunologically deficient athymic-nude mice. *Science*, *183*(124), 534–536.

Stutman, O. (1979). Chemical carcinogenesis in nude mice: Comparison between nude mice from homozygous matings and heterozygous matings and effect of age and carcinogen dose. *Journal of the National Cancer Institute*, *62*(2), 353–358.

Suzuki, A., Andrew, D. P., Gonzalo, J. A., Fukumoto, M., Spellberg, J., Hashiyama, M., … Mak, T. W. (1996). CD34-deficient mice have reduced eosinophil accumulation after allergen exposure and show a novel crossreactive 90-kD protein. *Blood*, *87*, 3550–3562.

Swann, J. B., Hayakawa, Y., Zerafa, N., Sheehan, K. C. F., Scott, B., Schreiber, R. D., … Smyth, M. J. (2007). Type I IFN contributes to NK cell homeostasis, activation, and antitumor function. *Journal of Immunology (Baltimore, Md.: 1950)*, *178*(12), 7540–7549. https://doi.org/10.4049/jimmunol.178.12.7540

Swann, J. B., Uldrich, A. P., van Dommelen, S., Sharkey, J., Murray, W. K., Godfrey, D. I., & Smyth, M. J. (2009). Type I natural killer T cells suppress tumors caused by p53 loss in mice. *Blood*, *113*(25), 6382–6385. https://doi.org/10.1182/blood-2009-01-198564

Swann, J. B., Vesely, M. D., Silva, A., Sharkey, J., Akira, S., Schreiber, R. D., & Smyth, M. J. (2008). Demonstration of inflammation-induced cancer and cancer immunoediting during primary tumorigenesis. *Proceedings of the National*

Academy of Sciences of the United States of America, *105*(2), 652–656. https://doi.org/10.1073/pnas.0708594105

Taggart, D., Andreou, T., Scott, K. J., Williams, J., Rippaus, N., Brownlie, R. J., … Lorger, M. (2018). Anti–PD-1/anti–CTLA-4 efficacy in melanoma brain metastases depends on extracranial disease and augmentation of CD8+ T cell trafficking. *Proceedings of the National Academy of Sciences*, *115*(7), E1540–E1549. https://doi.org/10.1073/pnas.1714089115

Takeda, K., Smyth, M. J., Cretney, E., Hayakawa, Y., Kayagaki, N., Yagita, H., & Okumura, K. (2002). Critical role for tumor necrosis factor-related apoptosis-inducing ligand in immune surveillance against tumor development. *The Journal of Experimental Medicine*, *195*(2), 161–169. https://doi.org/10.1084/jem.20011171

Tang, Haidong, Wang, Y., Chlewicki, L. K., Zhang, Y., Guo, J., Liang, W., … Fu, Y.-X. (2016). Facilitating T Cell Infiltration in Tumor Microenvironment Overcomes Resistance to PD-L1 Blockade. *Cancer Cell*, *29*(3), 285–296. https://doi.org/10.1016/j.ccell.2016.02.004

Tang, Haidong, Zhu, M., Qiao, J., & Fu, Y.-X. (2017). Lymphotoxin signalling in tertiary lymphoid structures and immunotherapy. *Cellular & Molecular Immunology*, *14*(10), 809–818. https://doi.org/10.1038/cmi.2017.13

Tang, Huijuan, Chu, Y., Huang, Z., Cai, J., & Wang, Z. (2020). The metastatic phenotype shift toward myofibroblast of adipose-derived mesenchymal stem cells promotes

ovarian cancer progression. *Carcinogenesis*, *41*(2), 182–193. https://doi.org/10.1093/carcin/bgz083

Tang, X., Hou, Y., Yang, G., Wang, X., Tang, S., Du, Y.-E., … Liu, M. (2016). Stromal miR-200s contribute to breast cancer cell invasion through CAF activation and ECM remodeling. *Cell Death and Differentiation*, *23*(1), 132–145. https://doi.org/10.1038/cdd.2015.78

Tecchio, C., Micheletti, A., & Cassatella, M. A. (2014). Neutrophil-Derived Cytokines: Facts Beyond Expression. *Frontiers in Immunology*, *5*. https://doi.org/10.3389/fimmu.2014.00508

Ten Hagen, K. G., Fritz, T. A., & Tabak, L. A. (2003). All in the family: The UDP-GalNAc:polypeptide N-acetylgalactosaminyltransferases. *Glycobiology*, *13*(1), 1R-16R. https://doi.org/10.1093/glycob/cwg007

Terabe, M., & Berzofsky, J. A. (2004). Immunoregulatory T cells in tumor immunity. *Current Opinion in Immunology*, *16*(2), 157–162.

Thomas, L. (1959). *Delayed hypersensitivity in health and disease. In: Cellular and humoral aspects of the hypersensitive states*. P.B. Hoeber.

Thommen, D. S., Koelzer, V. H., Herzig, P., Roller, A., Trefny, M., Dimeloe, S., … Zippelius, A. (2018). A transcriptionally and functionally distinct PD-1+ CD8+ T cell pool with predictive potential in non-small-cell lung cancer treated with PD-1 blockade. *Nature Medicine*, *24*(7), 994–1004. https://doi.org/10.1038/s41591-018-0057-z

Thompson, E. D., Enriquez, H. L., Fu, Y.-X., & Engelhard, V. H. (2010). Tumor masses support naive T cell infiltration, activation, and differentiation into effectors. *Journal of Experimental Medicine*, *207*(8), 1791–1804. https://doi.org/10.1084/jem.20092454

Thorsson, V., Gibbs, D. L., Brown, S. D., Wolf, D., Bortone, D. S., Ou Yang, T.-H., … Shmulevich, I. (2018). The Immune Landscape of Cancer. *Immunity*, *48*(4), 812-830.e14. https://doi.org/10.1016/j.immuni.2018.03.023

Tjew, S. L., Brown, K. L., Kannagi, R., & Johnson, P. (2005). Expression of N-acetylglucosamine 6-O-sulfotransferases (GlcNAc6STs)-1 and -4 in human monocytes: GlcNAc6ST-1 is implicated in the generation of the 6-sulfo N-acetyllactosamine/Lewis x epitope on CD44 and is induced by TNF-α. *Glycobiology*, *15*(7), 7C-13C. https://doi.org/10.1093/glycob/cwi050

Trainin, N., Linker-Israeli, M., Small, M., & Boiato-Chen, L. (1967). Enhancement of lung adenoma formation by neonatal thymectomy in mice treated with 7,12-dimethylbenz(a)anthracene or urethan. *International Journal of Cancer*, *2*(4), 326–336. https://doi.org/10.1002/ijc.2910020407

Trout, A. T., Rabinowitz, R. S., Platt, J. F., & Elsayes, K. M. (2013). Melanoma metastases in the abdomen and pelvis: Frequency and patterns of spread. *World Journal of Radiology*, *5*(2), 25–32. https://doi.org/10.4329/wjr.v5.i2.25

Truxova, I., Kasikova, L., Hensler, M., Skapa, P., Laco, J., Pecen, L., … Fucikova, J. (2018). Mature dendritic cells correlate with favorable immune infiltrate and

improved prognosis in ovarian carcinoma patients. *Journal for Immunotherapy of Cancer*, *6*, 139. https://doi.org/10.1186/s40425-018-0446-3

Tumanov, A. V., Grivennikov, S. I., Kruglov, A. A., Shebzukhov, Y. V., Koroleva, E. P., Piao, Y., … Nedospasov, S. A. (2010). Cellular source and molecular form of TNF specify its distinct functions in organization of secondary lymphoid organs. *Blood*, *116*(18), 3456–3464. https://doi.org/Research Support, N.I.H., Intramural Research Support, Non-U.S. Gov't

Tumanov, Alexei V., Kuprash, D. V., Lagarkova, M. A., Grivennikov, S. I., Abe, K., Shakhov, A. N., … Nedospasov, S. A. (2002). Distinct Role of Surface Lymphotoxin Expressed by B Cells in the Organization of Secondary Lymphoid Tissues. *Immunity*, *17*(3), 239–250. https://doi.org/10.1016/S1074-7613(02)00397-7

Turnquist, H. R., Lin, X., Ashour, A. E., Hollingsworth, M. A., Singh, R. K., Talmadge, J. E., & Solheim, J. C. (2007). CCL21 induces extensive intratumoral immune cell infiltration and specific anti-tumor cellular immunity. *International Journal of Oncology*, *30*(3), 631–639.

Uchimura, K., Gauguet, J.-M., Singer, M. S., Tsay, D., Kannagi, R., Muramatsu, T., … Rosen, S. D. (2005). A major class of L-selectin ligands is eliminated in mice deficient in two sulfotransferases expressed in high endothelial venules. *Nature Immunology*, *6*(11), 1105–1113. https://doi.org/10.1038/ni1258

Uchimura, K., Kadomatsu, K., El-Fasakhany, F. M., Singer, M. S., Izawa, M., Kannagi, R., … Muramatsu, T. (2004). N-Acetylglucosamine 6-O-Sulfotransferase-1 Regulates Expression of L-Selectin Ligands and Lymphocyte Homing. *Journal of Biological Chemistry*, *279*(33), 35001–35008. https://doi.org/10.1074/jbc.M404456200

Uchimura, K., Muramatsu, H., Kadomatsu, K., Fan, Q.-W., Kurosawa, N., Mitsuoka, C., … Muramatsu, T. (1998). Molecular Cloning and Characterization of anN-Acetylglucosamine-6-O-sulfotransferase *. *Journal of Biological Chemistry*, *273*(35), 22577–22583. https://doi.org/10.1074/jbc.273.35.22577

Uchimura, K., & Rosen, S. D. (2006). Sulfated L-selectin ligands as a therapeutic target in chronic inflammation. *Trends in Immunology*, *27*(12), 559–565. https://doi.org/10.1016/j.it.2006.10.007

Ulloa-Montoya, F., Louahed, J., Dizier, B., Gruselle, O., Spiessens, B., Lehmann, F. F., … Brichard, V. G. (2013). Predictive gene signature in MAGE-A3 antigen-specific cancer immunotherapy. *Journal of Clinical Oncology*, *31*(19), 2388–2395. https://doi.org/10.1200/JCO.2012.44.3762

Umemoto, E., Tanaka, T., Kanda, H., Jin, S., Tohya, K., Otani, K., … Miyasaka, M. (2006). Nepmucin, a novel HEV sialomucin, mediates L-selectin-dependent lymphocyte rolling and promotes lymphocyte adhesion under flow. *The Journal of Experimental Medicine*, *203*(6), 1603–1614. https://doi.org/10.1084/jem.20052543

van de Pavert, S. A., & Mebius, R. E. (2010). New insights into the development of lymphoid tissues. *Nature Reviews Immunology*, *10*(9), 664–674. https://doi.org/10.1038/nri2832

van der Helm-van Mil, A. H., Verpoort, K. N., Breedveld, F. C., Toes, R. E., & Huizinga, T. W. (2005). Antibodies to citrullinated proteins and differences in clinical progression of rheumatoid arthritis. *Arthritis Research & Therapy*, *7*(5), R949–R958. https://doi.org/10.1186/ar1767

Van Hauwermeiren, F., Armaka, M., Karagianni, N., Kranidioti, K., Vandenbroucke, R. E., Loges, S., … Kollias, G. (2013). Safe TNF-based antitumor therapy following p55TNFR reduction in intestinal epithelium. *The Journal of Clinical Investigation*, *123*(6), 2590–2603. https://doi.org/10.1172/JCI65624

Vasilikos, L., Hänggi, K., Spilgies, L. M., & Wong, W. W.-L. (2019). Tumor cell-derived lymphotoxin alpha triggers metastatic extravasation through TNFRs/cIAP1. *BioRxiv*, 766485. https://doi.org/10.1101/766485

Veerman, K., Tardiveau, C., Martins, F., Coudert, J., & Girard, J.-P. (2019). Single-Cell Analysis Reveals Heterogeneity of High Endothelial Venules and Different Regulation of Genes Controlling Lymphocyte Entry to Lymph Nodes. *Cell Reports*, *26*(11), 3116-3131.e5. https://doi.org/10.1016/j.celrep.2019.02.042

Venturi, G. M., Tu, L., Kadono, T., Khan, A. I., Fujimoto, Y., Oshel, P., … Tedder, T. F. (2003). Leukocyte migration is regulated by L-selectin endoproteolytic release. *Immunity*, *19*(5), 713–724. https://doi.org/10.1016/s1074-7613(03)00295-4

Vesely, M., Kershaw, M., Schreiber, R., & Smyth, M. (2011). Natural innate and adaptive immunity to cancer. *Annual Review of Immunology*, *29*, 235–271.

Wajant, H., & Siegmund, D. (2019). TNFR1 and TNFR2 in the Control of the Life and Death Balance of Macrophages. *Frontiers in Cell and Developmental Biology*, *7*. https://doi.org/10.3389/fcell.2019.00091

Wang, F.-T., Sun, W., Zhang, J.-T., & Fan, Y.-Z. (2019). Cancer-associated fibroblast regulation of tumor neo-angiogenesis as a therapeutic target in cancer. *Oncology Letters*, *17*(3), 3055–3065. https://doi.org/10.3892/ol.2019.9973

Wang, P., Yang, X., Wu, P., Zhang, J., Sato, T., Yamagata, S., & Yamagata, T. (2007). GM3 Signals Regulating TNF-Alpha Expression Are Mediated by Rictor and Arhgdib in Mouse Melanoma B16 Cells. *Oncology*, *73*(5–6), 430–438. https://doi.org/10.1159/000136801

Wang, Y., Koroleva, E. P., Kruglov, A. A., Kuprash, D. V., Nedospasov, S. A., Fu, Y.-X., & Tumanov, A. V. (2010). Lymphotoxin Beta Receptor Signaling in Intestinal Epithelial Cells Orchestrates Innate Immune Responses against Mucosal Bacterial Infection. *Immunity*, *32*(3), 403–413. https://doi.org/10.1016/j.immuni.2010.02.011

Ware, C. F. (2008). Targeting lymphocyte activation through the lymphotoxin and LIGHT pathways. *Immunological Reviews*, *223*, 186–201. https://doi.org/10.1111/j.1600-065X.2008.00629.x

Weinstein, A. M., Chen, L., Brzana, E. A., Patil, P. R., Taylor, J. L., Fabian, K. L., … Storkus, W. J. (2017). Tbet and IL-36γ cooperate in therapeutic DC-mediated promotion of ectopic lymphoid organogenesis in the tumor microenvironment. *Oncoimmunology*, *6*(6), e1322238. https://doi.org/10.1080/2162402X.2017.1322238

Weishaupt, C., Munoz, K. N., Buzney, E., Kupper, T. S., & Fuhlbrigge, R. C. (2007). T-cell distribution and adhesion receptor expression in metastatic melanoma. *Clinical Cancer Research*, *13*(9), 2549–2556. https://doi.org/10.1158/1078-0432.CCR-06-2450

Wiede, F., Vana, K., Sedger, L. M., Lechner, A., & Körner, H. (2007). TNF-dependent overexpression of CCL21 is an underlying cause of progressive lymphoaccumulation in generalized lymphoproliferative disorder. *European Journal of Immunology*, *37*(2), 351–357. https://doi.org/10.1002/eji.200636218

Willis, S. N., Mallozzi, S. S., Rodig, S. J., Cronk, K. M., McArdel, S. L., Caron, T., … O'Connor, K. C. (2009). The microenvironment of germ cell tumors harbors a prominent antigen-driven humoral response. *Journal of Immunology*, *182*(5), 3310–3317. https://doi.org/10.4049/jimmunol.0803424

Wirsing, Anna M., Rikardsen, O. G., Steigen, S. E., Uhlin-Hansen, L., & Hadler-Olsen, E. (2014). Characterisation and prognostic value of tertiary lymphoid structures in oral squamous cell carcinoma. *BMC Clinical Pathology*, *14*, 38. https://doi.org/10.1186/1472-6890-14-38

Wirsing, Anna Maria, Ervik, I. K., Seppola, M., Uhlin-Hansen, L., Steigen, S. E., & Hadler-Olsen, E. (2018). Presence of high-endothelial venules correlates with a favorable immune microenvironment in oral squamous cell carcinoma. *Modern Pathology*, *31*(6), 910–922. https://doi.org/10.1038/s41379-018-0019-5

Withers, D. R. (2011). Lymphoid tissue inducer cells. *Current Biology*, *21*(10), R381–R382. https://doi.org/10.1016/j.cub.2011.03.022

Woods, A. N., Wilson, A. L., Srivinisan, N., Zeng, J., Dutta, A. B., Peske, J. D., … Engelhard, V. H. (2017). Differential Expression of Homing Receptor Ligands on Tumor-Associated Vasculature that Control CD8 Effector T-cell Entry. *Cancer Immunology Research*, *5*(12), 1062–1073. https://doi.org/10.1158/2326-6066.CIR-17-0190

Wrzesinski, S. H., Wan, Y. Y., & Flavell, R. A. (2007). Transforming growth factor-beta and the immune response: Implications for anticancer therapy. *Clinical Cancer Research: An Official Journal of the American Association for Cancer Research*, *13*(18 Pt 1), 5262–5270. https://doi.org/10.1158/1078-0432.CCR-07-1157

Wu, Q., Wang, Y., Wang, J., Hedgeman, E. O., Browning, J. L., & Fu, Y. X. (1999). The requirement of membrane lymphotoxin for the presence of dendritic cells in lymphoid tissues. *Journal of Experimental Medicine*, *190*(5), 629–638.

Wynn, T. A., & Vannella, K. M. (2016). Macrophages in Tissue Repair, Regeneration, and Fibrosis. *Immunity*, *44*(3), 450–462. https://doi.org/10.1016/j.immuni.2016.02.015

Yamada, M., Yanaba, K., Hasegawa, M., Matsushita, Y., Horikawa, M., Komura, K., … Sato, S. (2006). Regulation of local and metastatic host-mediated anti-tumour mechanisms by l-selectin and intercellular adhesion molecule-1. *Clinical & Experimental Immunology*, *143*(2), 216–227. https://doi.org/10.1111/j.1365-2249.2005.02989.x

Yang, S.-C., Batra, R. K., Hillinger, S., Reckamp, K. L., Strieter, R. M., Dubinett, S. M., & Sharma, S. (2006). Intrapulmonary administration of CCL21 gene-modified dendritic cells reduces tumor burden in spontaneous murine bronchoalveolar cell carcinoma. *Cancer Research*, *66*(6), 3205–3213. https://doi.org/10.1158/0008-5472.CAN-05-3619

Yang, W. H., Nussbaum, C., Grewal, P. K., Marth, J. D., & Sperandio, M. (2012). Coordinated roles of ST3Gal-VI and ST3Gal-IV sialyltransferases in the synthesis of selectin ligands. *Blood*, *120*(5), 1015–1026. https://doi.org/10.1182/blood-2012-04-424366

Yeh, J. C., Hiraoka, N., Petryniak, B., Nakayama, J., Ellies, L. G., Rabuka, D., … Fukuda, M. (2001). Novel sulfated lymphocyte homing receptors and their control by a Core1 extension beta 1,3-N-acetylglucosaminyltransferase. *Cell*, *105*(7), 957–969. https://doi.org/10.1016/s0092-8674(01)00394-4

Yu, P., Lee, Y., Liu, W., Chin, R. K., Wang, J., Wang, Y., … Fu, Y. X. (2004). Priming of naive T cells inside tumors leads to eradication of established tumors. *Nature Immunology*, *5*, 141–149.

Yu, P., Lee, Y., Wang, Y., Liu, X., Auh, S., Gajewski.T.F, … Fu, Y. X. (2007). Targeting the primary tumor to generate CTL for the effective eradication of spontaneous metastases. *Journal of Immunology*, *179*, 1960–1968.

Yu, S.-Y., Hsiao, C.-T., Izawa, M., Yusa, A., Ishida, H., Nakamura, S., … Khoo, K.-H. (2018). Distinct substrate specificities of human GlcNAc-6-sulfotransferases revealed by mass spectrometry–based sulfoglycomic analysis. *The Journal of Biological Chemistry*, *293*(39), 15163–15177. https://doi.org/10.1074/jbc.RA118.001937

Zhang, L., Conejo-Garcia, J. R., Katsaros, D., Gimotty, P. A., Massobrio, M., Regnani, G., … Coukos, G. (2003). Intratumoral T cells, recurrence, and survival in epithelial ovarian cancer. *New England Journal of Medicine*, *348*(3), 203–213. https://doi.org/10.1056/NEJMoa020177 348/3/203 [pii]